

Bangor University

DOCTOR OF PHILOSOPHY

4,5-Diazafluorene-based conjugated oligomers, polymers, and iridium complexes as materials for organic electronics

Ghosh, Sanjay

Award date:
2014

Awarding institution:
Bangor University

[Link to publication](#)

General rights

Copyright and moral rights for the publications made accessible in the public portal are retained by the authors and/or other copyright owners and it is a condition of accessing publications that users recognise and abide by the legal requirements associated with these rights.

- Users may download and print one copy of any publication from the public portal for the purpose of private study or research.
- You may not further distribute the material or use it for any profit-making activity or commercial gain
- You may freely distribute the URL identifying the publication in the public portal ?

Take down policy

If you believe that this document breaches copyright please contact us providing details, and we will remove access to the work immediately and investigate your claim.

4,5-Diazafluorene-based Conjugated Oligomers, Polymers, and Iridium Complexes as Materials for Organic Electronics

A thesis presented in partial fulfilment

for the

PhD in Material Chemistry

in the

School of Chemistry

by

Sanjay Ghosh



Prifysgol Bangor • Bangor University

© November 2014



Contents

Declaration	v
Abstract	viii
Acknowledgements	ix
Abbreviations	x
Chapter 1 An Introduction to Organic Electronics	1
<i>1.1 Background of conjugated polymer for organic electronics</i>	1
<i>1.2 Application of conjugated polymers in electronic device</i>	3
<i>1.3 Organic light emitting diodes, OLEDs: basic principles</i>	4
<i>1.4 Light-emitting electrochemical cells, LECs: basic principles</i>	6
<i>References</i>	7
Chapter 2 4,5-Diazafluorene Derivatives as Materials for Optoelectronic Applications ..	8
2.1 Introduction	8
2.1.1 4,5-Diazafluorenes: structural aspects and applications.....	8
2.1.2 4,5-Diazafluorene: synthesis and properties.....	10
2.1.2.1 Reactions at C-9 position of 4,5-diazafluorene	11
2.1.2.2 Substitution at the 3,6-position of 4,5-diazafluorene	19
2.1.2.3 Functionalisation at the 2,7-position of 4,5-diazafluorene	22
2.1.3 4,5-Diazafluorenes as ligands for complex formation with transition metals.....	27
2.1.3.1 Complexes of 4,5-diazafluorene with Ru	28
2.1.3.2 Complexes of DAF with Pd	30
2.1.3.3 DAF as ancillary ligand for catalyst	31
2.1.3.4 Complexes of iridium with 4,5-diazafluorene	32
2.2 Results and Discussion	33
2.2.1 Improved method of the synthesis of 2,7-dibromo-4,5-diazafluorenone	33
2.2.2 Synthesis of 2,7-dibromo 4,5-diazafluoren-9-one through improved method	36
2.2.3 Proposed mechanism for the synthesis of 2,7-dibromo-4,5-diazafluoren-9-one	38
2.3 Conclusion	39
2.4 Experimental	40
References	47

Chapter 3 Cationic Iridium Complexes as Emissive Materials for Light-Emitting Electrochemical Cells	51
3.1 Introduction	51
3.1.1 Transition metal complexes for application in light-emitting electrochemical cells...	51
3.1.2 Development of LEC based on ionic transition metals: a brief overview.....	52
3.1.3 General method of the synthesis of iridium(III) complexes and their properties.....	54
3.1.3.1 Synthesis of neutral iridium(III) complexes.....	56
3.1.3.2 Synthesis of charge iridium(III) complexes	58
3.1.3.3 Cationic iridium complexes: colour tuning	58
3.1.3.4 Cationic iridium complexes: stability and response time.....	60
3.1.3.5 Cationic iridium complexes: white light LECs	64
3.2 Results and Discussion	69
3.2.1 Scope and rationale for synthesis of iridium(III) complexes with DAF	69
3.2.2 Synthesis of DAF-based ligands	71
3.2.3 Synthesis of Iridium Complexes	74
3.2.4 Photophysical studies of iridium(III) complexes.....	79
3.2.4.1 Absorption and emission study of iridium(III) complexes in solution state	79
3.2.4.2 Electrochemical studies of iridium(III) complexes	85
3.2.5 Computational studies of iridium(III) complexes by DFT method.....	88
3.2.6 Device test for a LEC based on the iridium(III) complex	100
3.3 Conclusion	103
3.4 Experimental	106
References	136
Chapter 4 4,5-Diazafluorene-Based Oligomers	140
4.1 Introduction	140
4.1.1 Oligofluorenes: synthesis and properties.....	141
4.1.2 Fluorene-based co-oligomers: synthesis and properties.....	151
4.2 Results and Discussion	152
4.2.1 Synthesis of 4,5-diazafluorene-based oligomers	153
4.2.2 Absorption and emission properties of 4,5-diazafluorene-based oligomers	157
4.2.2.1 Absorption	157
4.2.2.2 Emission	160
4.2.2.3 Photoluminescence quantum yields	160
4.2.3 Cyclic voltammetry study of 4,5-diazafluorene-based oligomers.....	163

4.2.4 Computational studies of 4,5-diazafluorene-based oligomers	165
4.2.4.1 Geometry of diazafluorene-based oligomers.....	166
4.2.4.2 Frontier molecular orbitals of diazafluorene-based oligomers.....	166
4.4.5 Study of FDF oligomer as optical sensor for metal ions	170
4.4.5.1 Effect of various metal ions on UV-vis and PL spectra of FDF.....	172
4.4.5.1 Effect of Hg ²⁺ concentrations on absorption and emission spectra of FDF	177
4.4.5.2 Determination of stoichiometry of the complex between FDF and Hg ²⁺ , and detection limit of Hg ²⁺	179
4.3 Conclusion	182
4.4 Experimental	184
References	200
Chapter 5 4,5-Diazafluorene-Based Polymers	203
5.1 Introduction	203
5.1.1 Synthesis and properties of polyfluorenes.....	204
5.1.2 Synthesis and properties of fluorene based copolymer	206
5.1.3 Defects in polyfluorenes: keto defects.....	207
5.2 Results and Discussion	211
5.2.1 Computational study of polyfluorene and poly(4,5-diazafluorene)	211
5.2.2 Synthesis and characteriztaion of 4,5-diazafluorene-based homopolymers.....	216
5.2.3 Synthesis and properties of 4,5-diazafluorene-based copolymers.....	219
5.2.4 Electrochemical properties of the 4,5-diazafluorene based polymers	221
5.2.5 Optical properties of the 4,5-diazafluorene based polymers	223
5.2.6 Thermal annealing studies of the 4,5-diazafluorene based polymers.....	227
5.3 Conclusion	230
5.4 Experimental	232
References	242
Appendix-NMR and MS spectra	246

Declaration and Consent

Details of the Work

I hereby agree to deposit the following item in the digital repository maintained by Bangor University and/or in any other repository authorized for use by Bangor University.

Author Name: Sanjay Ghosh

Title: 4,5-Diazafluorne-based conjugated oligomers, polymers and iridium complexes as materials for organic electronics.

Supervisor/Department: Prof. Igor F. Perepichka, School of Chemistry.

Funding body (if any): Bangor University (125th Anniversary Scholarship).

Qualification/Degree obtained: PhD

This item is a product of my own research endeavours and is covered by the agreement below in which the item is referred to as “the Work”. It is identical in content to that deposited in the Library, subject to point 4 below.

Non-exclusive Rights

Rights granted to the digital repository through this agreement are entirely non-exclusive. I am free to publish the Work in its present version or future versions elsewhere.

I agree that Bangor University may electronically store, copy or translate the Work to any approved medium or format for the purpose of future preservation and accessibility. Bangor University is not under any obligation to reproduce or display the Work in the same formats or resolutions in which it was originally deposited.

Bangor University Digital Repository

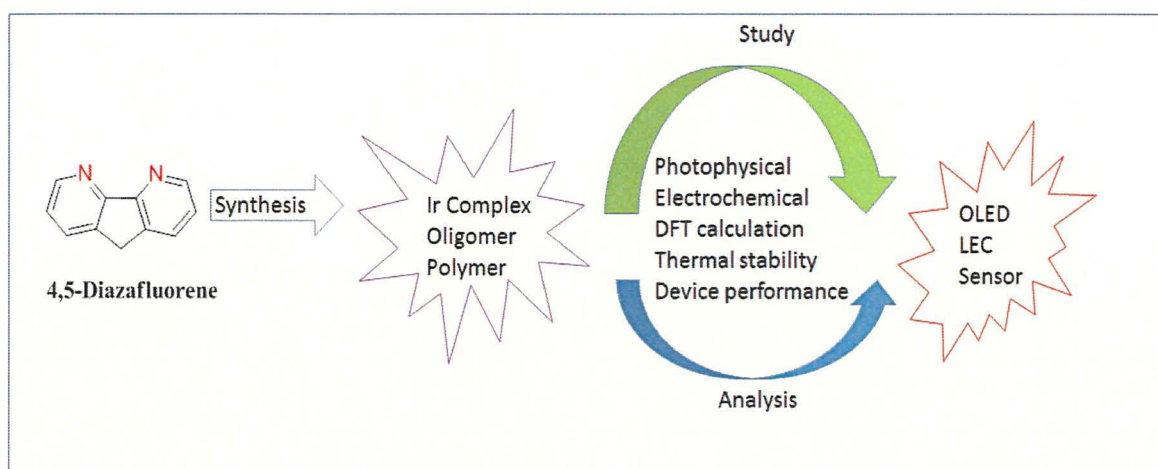
I understand that work deposited in the digital repository will be accessible to a wide variety of people and institutions, including automated agents and search engines via the World Wide Web.

I understand that once the Work is deposited, the item and its metadata may be incorporated into public access catalogues or services, national databases of electronic theses and dissertations such as the British Library’s EThOS or any service provided by the National Library of Wales.

I understand that the Work may be made available via the National Library of Wales Online Electronic Theses Service under the declared terms and conditions of use (<http://www.llgc.org.uk/index.php?id=4676>). I agree that as part of this service the National Library of Wales may electronically store, copy or convert the Work to any approved medium or format for the purpose of future preservation and accessibility. The National Library of Wales is not under any obligation to reproduce or display the Work in the same formats or resolutions in which it was originally deposited.

Abstract

This Thesis deals with the design, synthesis and study of properties of novel 4,5-diazafluorene based material for application in electronic devices. Organic conjugated polymers with semiconducting properties offer many exciting prospects in material science and nanoelectronics and attract tremendous interest from both academia and hi-tech industry. Over the last decade, polyfluorenes (PF) have emerged as leading electroluminescent materials with bright blue emission, good thermal and electrochemical stability, high charge mobility and easily tunable properties through chemical modifications and co-polymerisations. 4,5-diazafluorene is topologically similar to fluorene, however, due to presence of electron deficient nitrogen atoms it possess much lower LUMO energy level. Moreover, the two nitrogen atoms of 4,5-diazafluorene provides the binding site to form metal complexes similar to well-known ligands 1,10-phenanthroline and 2,2'-bipyridine. These advantages makes 4,5-diazafluorene an attractive object for design of novel electron deficient conjugated oligomers, polymers and metal complexes for optoelectronics applications such as organic light-emitting diodes (OLED), light-emitting electrochemical cells (LEC), photovoltaics (OPV), field-effect transistors (FET) and sensors. The Thesis is presented in the form of five chapters. In the first chapter, a brief introduction about organic electronic is described. Chapter 2 deals with the development of synthetic method for key starting material 2,7-dibromo-4,5-diazafluorene. Chapter 3 exclusively discussed 4,5-diazafluorene based iridium complexes for light emitting electrochemical cells. In chapters 4 and 5, 4,5-diazafluorene based oligomers and polymers are discussed, respectively.



Acknowledgements

I would like to acknowledge The Bangor University for 125th Anniversary Scholarship, which covered my tuition fees and living expenses. I would like to extend my acknowledgement to the Staff members of the School of Chemistry. I would also like to acknowledge my colleagues Anna Tochwin, Srikanth Kommanaboyina, and Charlotte Jones (PhD students, Bangor University) for some useful discussion and exchanging ideas. Special thanks to Dr. Michal P. Krompiec for doing some DFT calculations of metal complexes and help with cyclic voltammetry analyses during his postdoctoral fellowship in our group and Dr. Jeff Kettle for testing electroluminescence (Senior Lecturer, School of Electronic Engineering, Bangor University). I thank my friend Dr. Ranjit Thakuria (Lecturer, Gauwahati University) for helping me doing DSC analysis during his postdoctoral study at Cambridge University. I acknowledge Megan Hallett, Tom Lees, Jack Atkins (BSc students) and Addulaziz Saud Alghunaim (MSc student) for their valuable contribution as project students have had worked in my area of research. I am thankful to Dr. Courtney William (Biocomposites Centre, Staff), Dr. Deniol Pritchard (Chemistry, Staff), Dr. Sanjeev Pran Mahanta and Dr. Athanasius Justin Manji (Post doc fellow, Chemistry) for their useful tips and suggestions in writing my Thesis.

I thank Prof. Martin Taylor (School of Electronic Engineering, Bangor University) for inviting me to participate in Centre for Advanced Functional Materials and Devices Away Day (*Organic Electronics and Photonics*) seminar which was a joint event between Bangor University and Aberystwyth University. Very special thanks to my mentor Dr. Subrata Booruah (retired lecturer, B. Booruah College) for introducing me into the fascinating world of Chemistry. I thank Dr. Juma Al-Dulayymi and Dr. Viacheslav Tverezovskiy (Biocomposites Centre, Bangor) for measurement (GPC, DSC) of my PhD work compounds and providing me a part time job (three months) which helping me gaining experience in industrial project work as well as offering financial support during my write up period.

Finally and most importantly, I express deep gratitude to my supervisor Prof. Igor F. Perepichka for his expert guidance and constant encouragement throughout my journey toward my PhD. I sincerely appreciate what I learn from him in these years.

Abbreviations

acac	Acetylacetate
ACN	Acetonitrile
AcOH	Acetic acid
Ar	Aryl
B ₂ (pin) ₂	Bis(pinacolato)diboron
B3LYP	Becke's exchange and Lee, Yang, Paar's correlation functional
BCP	2,9-Dimethyl-4,7-diphenyl-1,10-phenanthroline
Bpy	2,2'-Bipyridine
BMIMPF ₆	1-Butyl-3-methylimidazolium hexafluorophosphate
COD	1,5-Cyclooctadiene
COSY	Correlation spectroscopy
DAF	4,5-Diazafluorene
DAFone	4,5-Diazafluoren-9-one
DCM	Dichloromethane
DDQ	2,3-Dichloro-5,6-dicyano-1,4-benzoquinone
DEPTQ	Distortionless enhancement by polarisation transfer to quaternary carbon
DSSC	Dye-sensitized solar cell
dfl-ppy	2,4-Difluorophenylpyridine
DFT	Density functional theory
DMF	<i>N,N</i> -Dimethylformamide
DMSO	Dimethyl sulfoxide
dppf	1,1'-Bis(diphenylphosphino)ferrocene
DSC	Differential scanning calorimetry
dye R6G	Rhodamine 6G
EA	Ethyl acetate
EI	Electron impact (mass spectrum)
EL	Emissive layer
ESI	Electrospray (mass spectrum)
ETL	Electron transport layer
FRET	Fluorescence resonance energy transfer

GC-MS	Gas chromatography – mass spectrometer
GPC	Gel permeating chromatography
HTL	Hole transport layer
Hx	Hexyl
Hz	Hertz
ICT	Intramolecular charge transfer
iTMC	Ionic transition metal complex
ITO	Indium-tin oxide
LANL2DZ	Los Alamos National Laboratory 2 double zeta functional
LEC	Light-emitting electrochemical cell
LFSE	Ligand field stabilisation energy
LUMO	Lowest unoccupied molecular orbital
LWE	Low work function electrode
<i>m</i> -CPBA	<i>meta</i> -Chloroperbenzoic acid
Me	Methyl
MeOH	Methanol
MLCT	Metal-to-ligand charge transfer
<i>m</i> -ppy	2-(<i>p</i> -Tolyl)pyridyl
MS	Mass spectrometry
NBS	<i>N</i> -bromosuccinamide
NCS	<i>N</i> -Chlorosuccinimide
NMR	Nuclear magnetic resonance
OFET	Organic field-effect transistor
OLED	Organic light-emitting diode
OPV	Organic photovoltaic
Ox	Oxidation
PCT	Photo induced charge transfer
PE	Petroleum ether (bp = 40–60 °C)
PEDOT	Poly(3,4-ethylenedioxythiophene)
PET	Photoinduced electron transfer
PFO	Poly(9,9-dioctylfluorene)
PFs	Polyfluorenes
phen	1,10-Phenanthroline
PhLi	Phenyllithium
PL	Photoluminescence

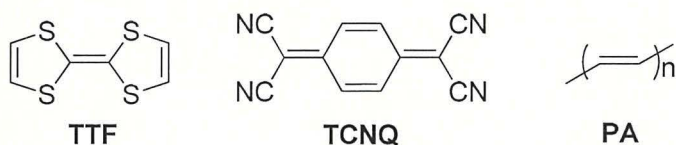
PSS	Polystyrene sulfonate
PVC	Photovoltaic cells
py	Pyridine
Red	Reduction
RT	Room temperature
S ₀	Singlet ground state
S ₁	First singlet excited state
SSL	Solid state lighting
T ₁	First triplet excited state
t-BuOK	Potassium <i>tert</i> -butoxide
TCNQ	Tetracyano- <i>p</i> -quinodimethane
TD-DFT	Time-dependent density functional theory
T _g	Glass transition temperature
TGA	Thermal gravimetric analysis
THF	Tetrahydrofuran
T _k	Crystallisation temperature
TLC	Thin layer chromatography
T _m	Crystalline melting points
TOF	time-of-flight
TTF	Tetrathiafulvalene
UV	Ultraviolet

Chapter 1

An Introduction to Organic Electronics

1.1 Background of conjugated polymer for organic electronics

A foremost criterion of materials for electronic applications is to be electrically conductive or semiconductive in nature. The majority of organic materials are insulators, i.e. bad conductors of electricity. The first organic material having metallic type of conductivity was the charge transfer complex between electron donor tetrathiafulvalene (**TTF**) and the electron acceptor tetracyano-*p*-quinodimethane (**TCNQ**) reported by Ferraris' group in 1973.¹



The story of breakthrough research of discovering metallic conductivity in a simple polymer, polyacetylene (**PA**) when doped by halogens, by Heeger, MacDiarmid and Shirakawa appeared in a Chemical Communication paper in 1977.² Their findings are considered to be the starting point of a new field in chemistry and technology. They have demonstrated that upon doping polyacetylene with halogens, the conductivity has been increased up to seven orders of magnitude (up to 100 S cm^{-1}) becoming comparable to metals, e.g. copper. The story of this breakthrough discovery in the field of organic conducting material is very exciting to learn, in the sense that scientists of different background, that is Heeger, a physicist, MacDiarmid, a polymer scientist, and Shirakova, an inorganic chemist, have discovered and developed the new field of electrically conductive organic materials that became a key point of the hi-tech field of 21st century now known as polymer electronics (or more broadly, organic electronics). After their combined breakthrough discovery there has been tremendous development into this new area of research with the set up of the new interdisciplinary field of organic electronics involving thousands of scientists in chemistry, physics, polymer science and engineering, both in academia and in industry. This resulted in

many fascinating materials based on conjugated polymers with unique electronic properties and opened the door for their wide range of innovative technological applications including organic light emitting diodes (OLED), organic field effect transistors (OFET), photovoltaic cells (PVC), electrochromics and sensors. In recognition of their work, Profs. Heeger, McDiarmid and Shirakawa have been awarded with Nobel Prize in Chemistry (2000) for their breakthrough discovery and development of conducting polymers.^{3,4,5,6}

In 1990, for the first time, the research group of Prof. Sir Richard Friend at the Cavendish Laboratory in Cambridge reported an electroluminescence (EL) from thin films of poly(*p*-phenylene vinylene) sandwiched between two electrodes⁷ that has been quickly recognised as a potential new technology for polymer organic light-emitting devices (OLED).⁸ This discovery is considered to be another breakthrough research in the field of organic electronics. A huge number of soluble and solution-processable electroluminescent polymers have been reported since then with tunable emission wavelengths through structural variations in polymers, high brightness, power efficiency and lifetime suitable for their applications in full colour displays and other OLED technologies.^{9,10} Some examples of conjugated polymers that have been successfully used in organic devices in recent times are polythiophenes, polycarbazoles, polyfluorenes and poly(*p*-phenylene vinylene) (Fig. 1.1) and their derivatives. Other well studied polymers include polypyrrole, polyaniline, poly(*p*-phenylene) and *trans*-polyacetylene (Fig. 1.1) and their derivatives.^{5,15,21}

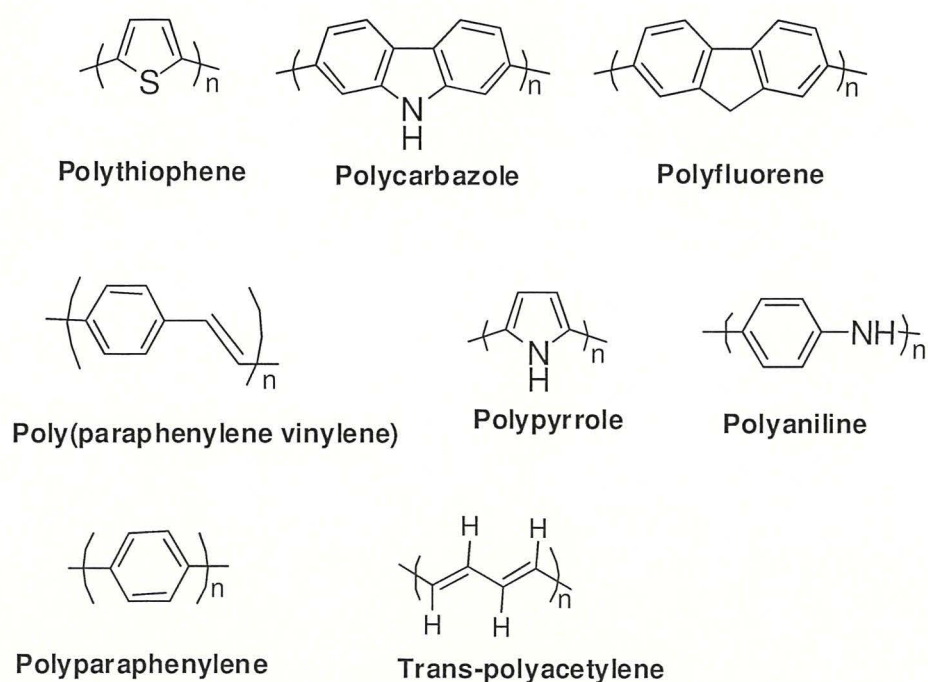


Fig. 1.1 Examples of some well known conjugated polymers.

An important criterion to develop and improve the performance of polymers in practical device is to look for optimum energies associated with the HOMO and LUMO orbital together with their ability for charge carrier mobility. Combination of electron-rich (**D**) and electron-deficient (**A**) building blocks by synthesis to construct conjugated organic polymers is the most common means of controlling or tuning the optoelectronic properties for particular application. As a result, wide range of copolymers containing **D** and **A** building blocks has been reported. Other important common strategies to improve performance of conjugated polymers include variation of substituents attached to the polymers building blocks themselves.^{11,12,13}

1.2 Application of conjugated polymers in electronic device

The last two decades have witnessed tremendous progress in development of conjugated polymers for using in electronic devices. The main advantages associated with conjugated polymers lie in their flexibility, light-weight, low cost and easy processing. Conjugated polymers-based electronic devices may prove to be cost-effective, next generation alternatives to conventional widely used silicon based material. The conjugated polymer based optoelectronic devices can be fabricated by easy processing technologies, such as spin coating and inkjet printing onto flexible substrates. Driven by robust research both from academia and industry, OLEDs based devices have already found a place in the market, the latest example being the display screen of a smart mobile phone made of OLED introduced by Samsung. Organic photovoltaic cells (OPVs) and organic field-effect transistors (OFETs) based on conjugated polymers are likely to enter the market in the near future.¹⁴ It has been predicted that efficient solid state lighting (SSL) based on OLEDs will be the next generation lighting source replacing conventional incandescence bulb and fluorescent lamps, that will not only reduce total electricity consumption but also prove to be environmental friendly.¹⁵

The development of white OLED, with focus on applications such as large space display backlight and illumination (Fig. 1.2) is a very rapidly growing field of research.^{16,17,18} The discovery of conducting polymers offer unique combination of properties which are not available in any other known materials.⁵ From trend of market data, it is predicted that the global market for organic electronics is destined to rise from the current level estimated to be £ 9 billion in 2014 to £ 44 billion in 2023.¹⁹ Research activities both in academia and industries to unearth the potential of organic compounds for application in various kinds of electronic devices are expected to increase many fold in the near future with an increase in

collaborative effort of interdisciplinary science involving chemists, physicists, engineers and others.

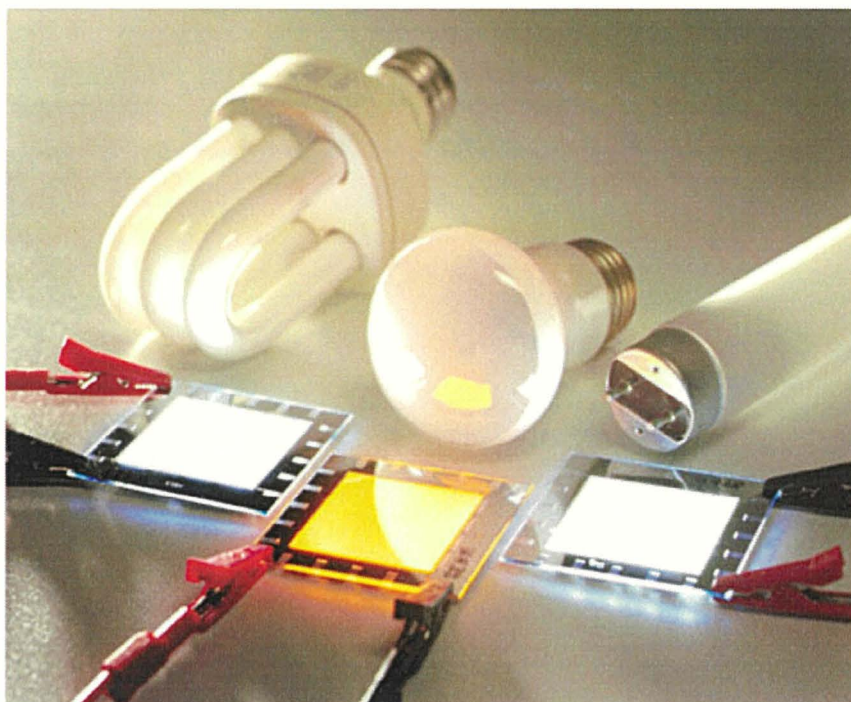


Fig. 1.2 Examples of white OLED, regarded as future replacement to incandescent light bulbs (Fig. taken from Ref. 16).

1.3 Organic light emitting diodes, OLEDs: basic principles

A typical organic light-emitting device consisting of a juxtaposed structure of light-emitting polymer between a transparent indium-tin oxide (ITO) anode and metallic cathode (such as Al, Mg or Ba) is shown on Fig. 1.3; it can also include additional hole/electron transporting and blocking layers to improve the OLED performance.^{20,21,22} Under the influence of applied voltages across the OLED, electrons tend to move from the cathode (negative charge) toward the anode (positive charge). In this process, electrons are diffused into the HOMO of the organic material and escape from the LUMO creating holes as illustrated in Fig. 1.3. As a consequence, the electrons and the holes are pulled toward each other and when they combine the excitons (excited state) are formed. The excitons formed undergo a relaxation process resulting in the emission of light ($h\nu$), which is the observed illumination of OLEDs. The additional hole/electron transporting and blocking layers facilitates the recombination process of electrons and holes to form excitons.

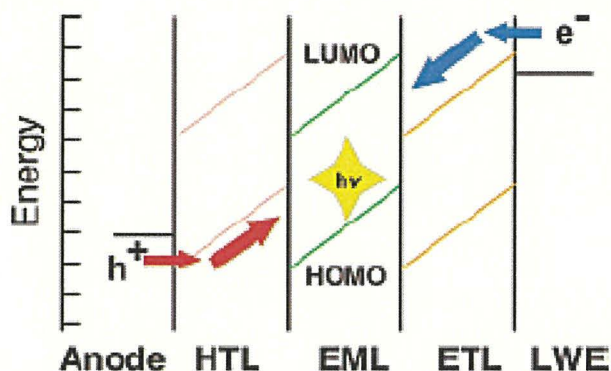
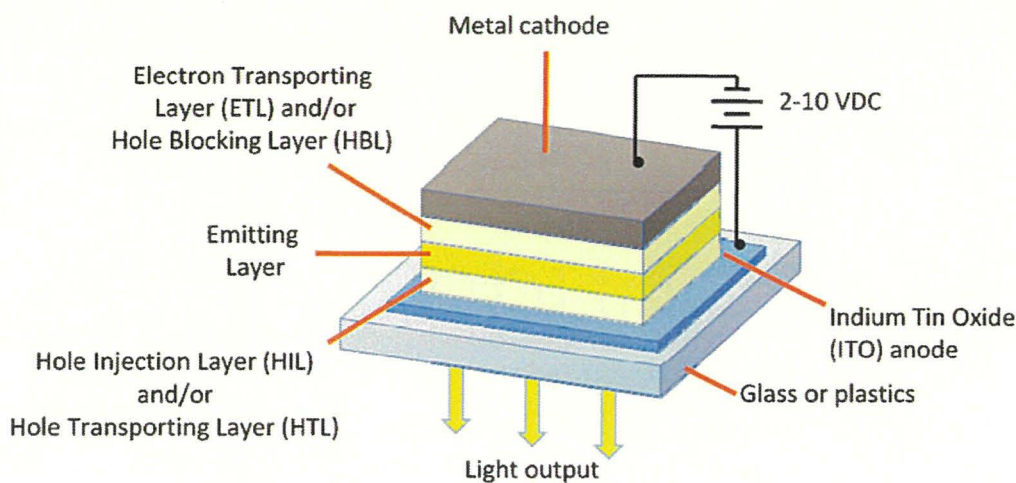


Fig. 1.3 Schematic diagram of OLED (top) and energy level diagram of a multilayer OLED (bottom). Low work function electrode (LWE), electron transport/emissive layer (ETL/EL), and hole transport layer (HTL). (Fig. taken from ref 15)

The frequency of emitted light from exciton relaxation is governed largely by the band gap or the difference in energy between the HOMO and LUMO of the organic material used. The electrons and holes are of half integer spin. As such, when an exciton is formed the spin multiplicity may either be in a singlet state or a triplet state, governed by how the spins of the electron and hole are combined. In terms of statistic, three triplet excitons will result for each singlet exciton when an electron and hole have been combined. Therefore, the maximum internal quantum yield (the number of emitted photons per injected holes/electrons) is theoretically limited to 25% because the emission from the triplet states is spin-forbidden.^{8,22,23} Phosphorescent organic light-emitting diodes based on transition metal complexes make use of spin-orbit interactions to facilitate intersystem crossing between singlet and triplet states, thus obtaining emission from both singlet and triplet states and improving the internal efficiency up to theoretical limit of 100%.²⁴

1.4 Light-emitting electrochemical cells, LECs: basic principles

In general, LECs consist of a single material with ionic charges sandwiched between two electrodes (Fig. 1.4a).²⁵ A representative mechanism of operation in LECs is depicted in Fig. 1.4.^{26,27} Under the applied voltages, ions move towards electrodes and a strong interfacial electric field is generated. The separated ions undergo oxidation and reduction processes (also called doping) near the electrodes. The p-type region is formed near the anode and n-type region near the cathode. These doping regions facilitate Ohmic contacts with the electrodes which promotes the injection of electrons and holes. Ohmic contact makes the device operation to be independent on the used electrodes and as such, low work function electrodes (such as Ag, Au) can be used in LECs and the device can operate at very low voltages. The electrons and holes recombine at junction between p-type and n-type region, forming exciton (in chemistry also called excited state) which upon relaxation emit light.

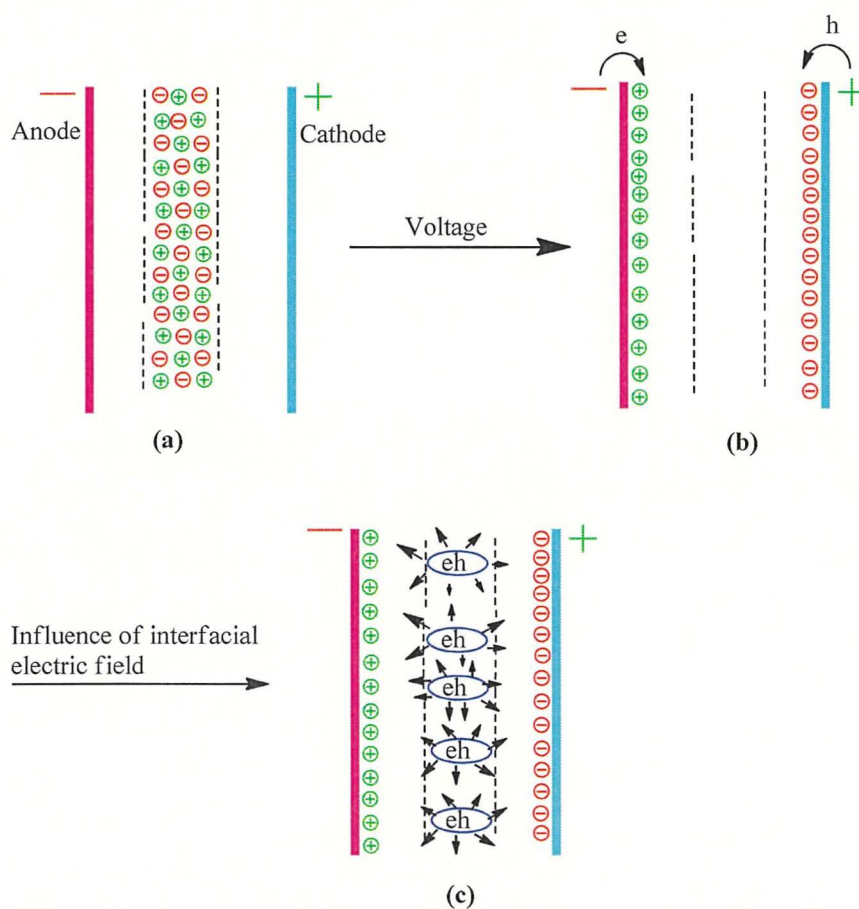


Fig. 1.4 Operating mechanism of LEC. (a) The cell before applying voltage. (b) Doping opposite sides as n-type and p-type regions near electrodes. (c) Redistribution of ions to create electric field and facilitate charge injection to form excitons.

References

- 1 J. Ferraris, D. O. Cowan, V. Walatka, J. H. Perlstein, *J. Am. Chem. Soc.*, **1973**, 7, 948.
- 2 H. Shirakawa, E. J. Louis, A. G. MacDiarmid, C. K. Chiang, and A. J. Heeger, *Chem. Commun.*, **1977**, 578.
- 3 H. Shirakawa, *Angew. Chem. Int. Ed.*, **2001**, 40, 2574.
- 4 A. G. MacDiarmid, *Angew. Chem. Int. Ed.*, **2001**, 40, 2581.
- 5 A. J. Heeger, *Chem. Soc. Rev.*, **2010**, 39, 2354.
- 6 A. J. Heeger, *Angew. Chem. Int. Ed.*, **2001**, 40, 2591.
- 7 J. H. Burroughes, D. D. C. Bradley, A. R. Brown, R. N. Marks, K. Makcay, R. H. Friend, P. L. Burn, and A. B. Holmes, *Nature*, **1990**, 347, 539.
- 8 A. Kraft, A. C. Grimsdale, and A. B. Holmes, *Angew. Chem. Int. Ed.*, **1998**, 37, 402.
- 9 D. F. Perepichka, I. F. Perepichka, H. Meng, and F. Wudl, in: *Organic Light-Emitting Materials and Devices*, Z. Li and H. Meng (Eds.), CRC Press, Boca Raton, FL, **2007**, Chapter 2, pp. 45–293
- 10 A. C. Grimsdale, K. L. Chan, R. E. Martin, P. G. Jokisz, and A. B. Holmes, *Chem. Rev.*, **2009**, 109, 897.
- 11 T. A. Skotheim and J. R. Reynolds (Eds.), *Handbook of Conducting Polymers (3rd Edition). Conjugated Polymers. Vol. 1: Theory, Synthesis, Properties and Characterization; Vol. 2: Processing and Applications*, CRC Press, Boca Raton, FL, **2007**.
- 12 Y. Chujo (Ed.), *Conjugated Polymer Synthesis*, Wiley–VCH, **2010**.
- 13 M. Leclerc and J.-F. Morin (Eds.), *Design and Synthesis of Conjugated Polymers*, Wiley-VCH, **2010**.
- 14 X. Zhaoab and X. Zhan, *Chem. Soc. Rev.*, **2011**, 40, 3728.
- 15 G. M. Farinola and R. Ragni, *Chem. Soc. Rev.*, **2011**, 40, 3467.
- 16 C. Ulbricht, B. Beyer, C. Friebe, A. Winter, and U. S. Schubert, *Adv. Mater.*, **2009**, 21, 4418.
- 17 B. W. D’Andrade and S. R. Forrest, *Adv. Mater.*, **2004**, 16, 1585.
- 18 C.-L. Ho, W.-Y. Wong, Q. Wang, D. Ma, L. Wang, and Z. Lin, *Adv. Funct. Mater.*, **2008**, 18, 928.
- 19 Printed, Organic & Flexible Electronics: Forecasts, Players & Opportunities 2013-2023
<http://www.idtechex.com/research/reports/printed-organic-and-flexible-electronics-forecasts-players-and-opportunities-2013-2023-000350.asp>
- 20 C. Adachi, M. A. Baldo, and S. R. Forrest, *App. Phys. Lett.*, **2000**, 77, 904.
- 21 Q. Wang and D. Ma, *Chem. Soc. Rev.*, **2010**, 39, 2387.
- 22 G. Yu and J. Wang, in: *Organic Light Emitting Materials and Devices*, Z. Li and H. Meng (Eds.), CRC Press, Boca Raton, FL, **2007**, Chapter 1, pp. 1–43.
- 23 L. Akcelrud, *Prog. Polym. Sci.*, **2003**, 28, 875.
- 24 I. Avilov, P. Minoofar, J. Cornil, and L. De Cola, *J. Am. Chem. Soc.*, **2007**, 129, 8247.
- 25 Q. Pei, G. Yu, C. Zhang, Y. Yang, and A. J. Heeger, *Science*, **1995**, 269, 1066.
- 26 Q. Pie and A. J. Heeger, *Nat. Mater.*, **2008**, 7, 167.
- 27 J. D. Slinker, J. A. Defrancho, M. J. Jaquith, W. R. Silveira, Y.-W. Zhong, J. M. Moran-Mirabal, H. G. Craighead, H. D. Abruna, J. A. Marohn, and G. G. Malliaras, *Nat. Mater.*, **2007**, 6, 894.

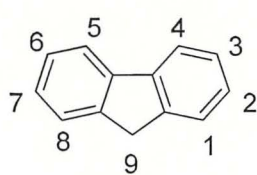
Chapter 2

4,5-Diazafluorene Derivatives as Materials for Optoelectronic Applications

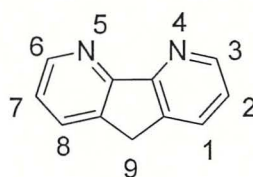
2.1 Introduction

2.1.1 4,5-Diazafluorenes: structural aspects and applications

Fluorene (**2.1**) as its name suggests, is known for its intense fluorescence behaviour and is a common polycyclic aromatic compound. Facile reactions take place at the 2 and 7 position of fluorene (**2.1**), which allows construction of rigid-rod type polymers and co-polymers chain, whereas substitution at the 9-position provides scope to increase the solubility without altering the electronic properties of the backbone.^{1,2,3} The fluorene-based conjugated oligomers are especially known to emit deep blue light with high efficiency both in the solution and in the solid state (film), which is not the common spectral region and therefore is considered to be a good candidate for blue OLED.⁴ 4,5-Diazafluorene (**2.2**) is topologically similar to fluorene, however, presence of the electron deficient nitrogen atoms causes lowering of the LUMO energy level and in addition provides the chelating site to form complexes with metal. Therefore, 4,5-diazafluorene (**2.2**) (DAF) represents an attractive building block for design of novel electron deficient conjugated oligomers, polymers and metal complexes for optoelectronics such as OLED, OPV, OFET and sensors.



2.1



2.2

Unlike fluorene, DAF (**2.2**) is less reactive towards the electrophilic aromatic substitution reaction at 2,7-positions (of its pyridine rings) due to the presence of electron deficient nitrogen atoms, which makes it difficult for using as a building block for synthesising conjugating systems. This is, perhaps, one of the reasons why DAF-based oligomers and polymers are not widely investigated to date (another one is that DAF **2.2** itself is less accessible starting building block compared to cheap commercially available fluorene). As a

part of my Thesis work we tried to address this issue and were able to develop a new efficient method for synthesis of the halogen-substituted DAF derivatives, which will be discussed in the results and discussion section. On the other hand, substitution reactions at the C-9 position is as facile as fluorene (or even more), which offers scope in design and synthesis; similar to those of the existing fluorene moieties.

There has been a tremendous amount of work done on fluorene and its derivatives over the last two decades as materials for optoelectronics and other applications. Indeed, there are over 14,400 hits for the topic "fluorene OR fluoren" while only about 270 hits for the topic "4,5-diazafluorene OR 4,5-diazafluoren" on Web of Science database as of 31/07/2014. In the meantime, according to Web of Science database, there is growing number of citations on the research articles published with the topic "4,5-diazafluorene OR 4,5-diazafluoren" (Fig. 2.1).

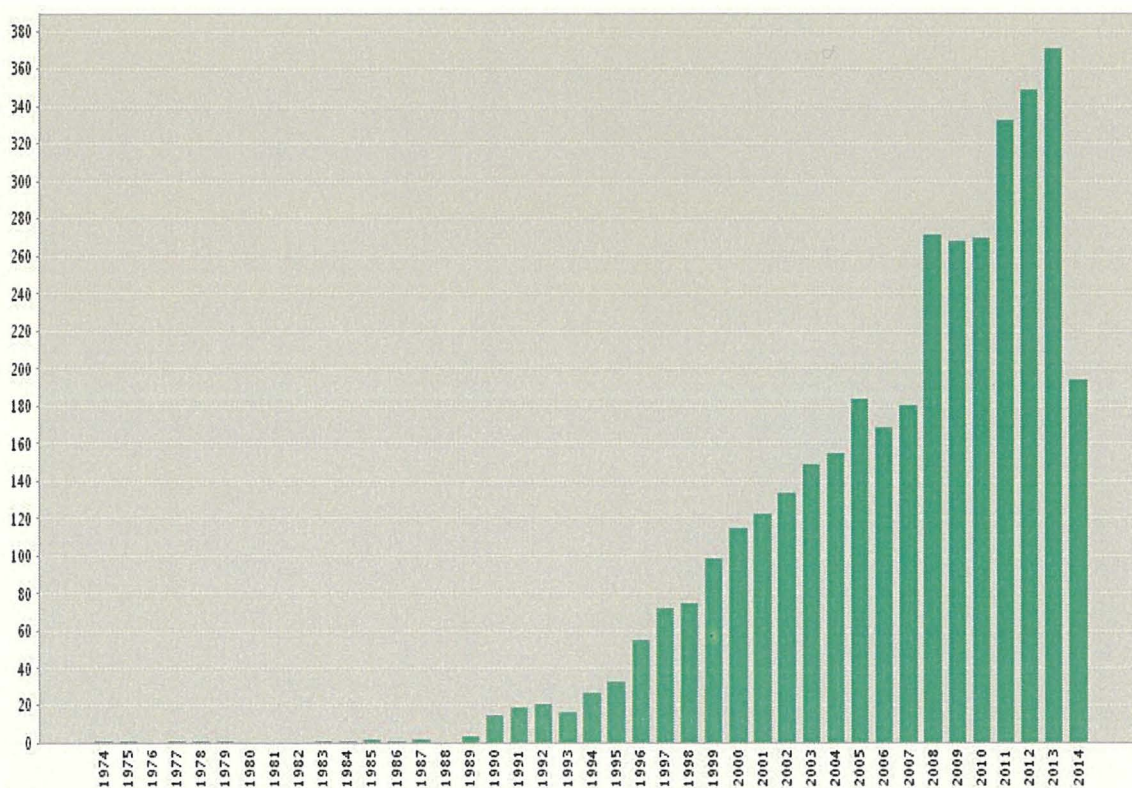
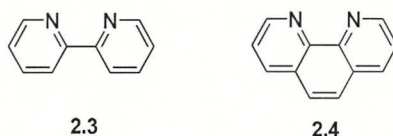


Fig. 2.1 Citations in each year with the topic “4,5-diazafluorene OR 4,5-diazafluoren” on Web of Science™ (Thomson Reuters™) as of 31 July 2014..

Therefore, it can be stated that DAF derivatives in comparison to fluorene derivatives are less studied and represent an emerging new class of material for research. Most of the published literature data on DAF derivatives are toward their transition metal complexes. DAF (2.2) is a

bidentate ligand similar to well studied 2,2'-bipyridine (**2.3**) and 1,10-phenanthroline (**2.4**) ligands. A review article by One and Saito in 2008 describes some of the chemistry and applications of DAFs.⁵ Effect of annelation on aromaticity of 2,2'-bipyridine (**2.3**) was reported by Thummel group in 1985.⁶ They also reported the preparation and properties of variety of 3,3-anealated derivatives of 2,2'-bipyridine including DAF (**2.2**).



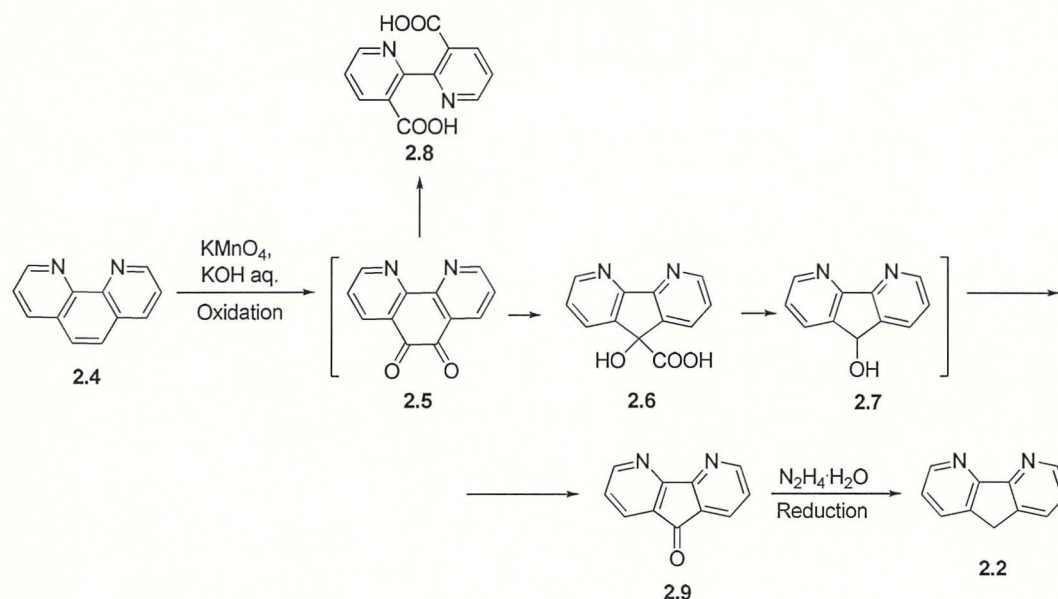
In terms of geometry, the binding site angle between the two nitrogen atoms of DAF is wider compared to 2,2'-bipyridine (**2.3**) and 1,10-phenanthroline (**2.4**) due to the central five membered ring. Also, there are two binding sites available for DAF that is one at C-9 and other at nitrogen atoms. Such subtle differences bring unique properties associated with the metal complexes of DAF derivatives which will be discussed in Section 2.1.3.

Potentially, different positions of DAF (**2.2**) can be functionalised for synthesis of new derivatives, offering wide range of novel materials for research and application in electronics. At the starting time of my PhD study, there were no reports on oligomers and polymers based on DAF (**2.2**) moiety. One of the aims of my PhD work was to elaborate suitable methods of synthesis of conjugated oligomers and polymers based on DAF (**2.2**) and to study their physical properties for potential applications of these materials in organic electronics and photonics (few examples of such materials had been appeared in the literature when our work was in progress). In the following section of this Chapter, synthesis of DAF (**2.2**) and its derivatives along with their properties are discussed from recent articles.

2.1.2 4,5-Diazafluorene: synthesis and properties

Unsubstituted DAF (**2.2**) can be synthesised in good yields from 1,10-phenanthroline (**2.4**) in two steps. The first step involves oxidation of 1,10-phenanthroline with potassium permanganate in basic conditions (aqueous potassium hydroxide) at room temperature to afford 4,5-diazafluoren-9-one (DAFone, **2.9**)^{7,8} and in the second step, reduction of DAFone by Wolff-Kishner reaction with hydrazine hydrate yield DAF (**2.2**)⁹ (Scheme 2.1). The major side product reported during the oxidation step was 2,2'-bipyridyl-3,3'-dicarboxylic acid (**2.8**), which was formed via oxidation of 1,10-phenanthroline-5,6-quinone (**2.5**). The reaction pathway is believed to be through rapid benzil-benzilic acid ring contraction of 1,10-phenanthroline-5,6-quinone (**2.5**→**2.6**). Improvements in yield for the synthesis of DAFone

(**2.9**) was carried out by Plater's group as a one pot synthesis from 1,10-phenanthroline (**2.4**). The modified procedure involved an increased amount of alkali with the addition of dilute solution of KMnO_4 slowly to favour ring contraction which results in an improvement of yield from a previously known procedure of 20% to nearly 60%.¹⁰



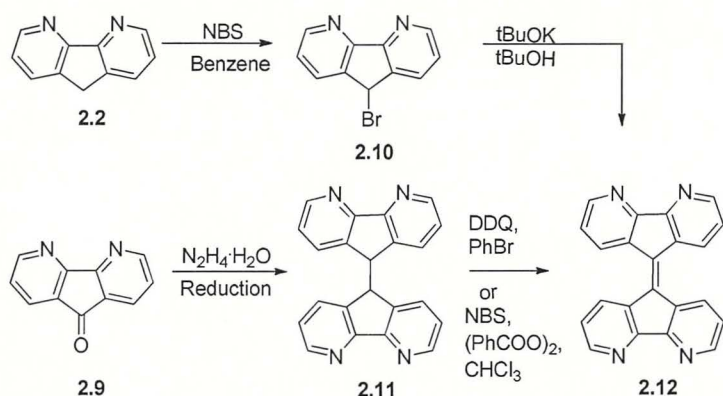
Scheme 2.1 Synthesis of 4,5-diazafluorene (**2.2**).^{7,9}

2.1.2.1 Reactions at C-9 position of 4,5-diazafluorene

Reactions at the C-9 position of DAF (**2.2**) can be performed in similar fashion as that of fluorene chemistry that is well known and studied. The reactions that use DAF (**2.2**) and DAFone (**2.9**) as starting materials to synthesise variety of DAF derivatives at the C-9 position along with their properties are described in this section.

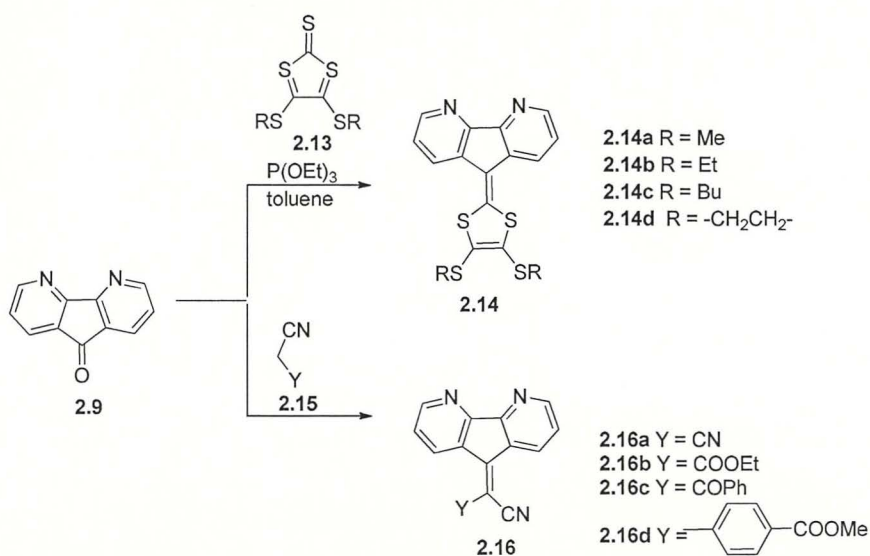
The synthesis and properties of tetradentate bridging DAF-based ligand **2.12** were studied by Connor *et al.*¹¹ This ligand (**2.12**) was used to prepare the dendritic complexes with metal ions to study the intermolecular energy transfer and electron transfer properties. They also reported the 1:1 charge transfer complex of compound **2.12** with 7,7,8,8-tetracyanoquinodimethane (TCNQ) and their molecular structure by X-ray crystallographic study. Tetradentate bridging ligand **2.12** was synthesised in good yield from DAF (**2.2**) as well as from DAFone (**2.9**) as starting materials as depicted in Scheme 2.2. Bromination of **2.2** with *N*-bromosuccinimide afford product **2.10** with ca. 60% yield, which was dehydrobrominated with *t*-BuOK in *t*-BuOH to afford compound **2.12** with the yield of 90%. Another method involves Wolff-Kishner reduction of DAFone **2.9** to afford **2.11** in good yield followed by either

dehydrogenation of **2.11** with 2,3-dichloro-5,6-dicyano-1,4-benzoquinone (**DDQ**) in bromobenzene to afford **2.12** in 85% yield, or the reaction of **2.11** with NBS in the presence of a catalytic amount of dibenzoyl peroxide in chloroform to produce product **2.12** in 86% yield.



Scheme 2.2 Synthesis of a 4,5-diazafluorene-based tetradentate ligand **2.12**.¹¹

Due to the presence of electron deficient nitrogen atoms, DAF-based coordination ligands are in general used as electron acceptor ligands. However, the ease of substitution at the 9-position of DAFone (**2.9**) made it possible to tune the electronic property. For example, the molecules **2.14**¹² and **2.16**¹³ (Scheme 2.3) act as π conjugated donor and π conjugated acceptor ligands. Here, the DAF units were used for metal complexation while the substituent at C-9 position act as electron donating and electron withdrawing moieties in **2.14** and **2.16** respectively, reported by Sako *et al.*^{12,13}



Scheme 2.3 Synthesis of a DAF-based conjugated donor (**2.14**) and acceptor ligands (**2.16**).^{12,13}

The conjugated acceptor ligand **2.16** was synthesised by Knoevenagel condensation of DAFone (**2.9**) and active methylene compounds **2.15** in presence of a base in two different ways. First method employed condensation with piperidine or ammonium acetate-piperidine as bases within 5–40 minutes. Second method was based on thermal reaction using ammonium acetate as base in refluxing benzene-acetic acid for 12–18 hours. The first method was found to give better yields (10 to 14%) and required less reaction time. According to the authors, the conjugated acceptor **2.16a** is a promising electrochromic material.¹³ They have demonstrated an existence of three different stable coloured redox states (neutral **2.16a**, radical cation **2.16a^{•+}**, and dication **2.16a²⁺**) as confirmed by spectroelectrochemical visible absorption measurements (Fig. 2.2a). The cyclic voltammety measurements for molecule **2.16a** showed that the two single electron transfer reduction processes were completely reversible and can be cycled between the two redox states in solution for at least few hours (Fig. 2.2b).¹³

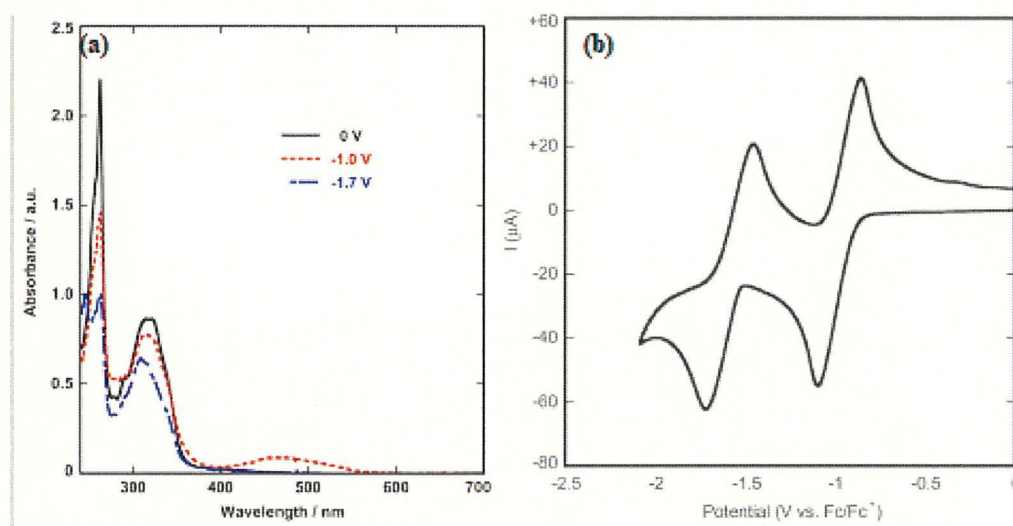
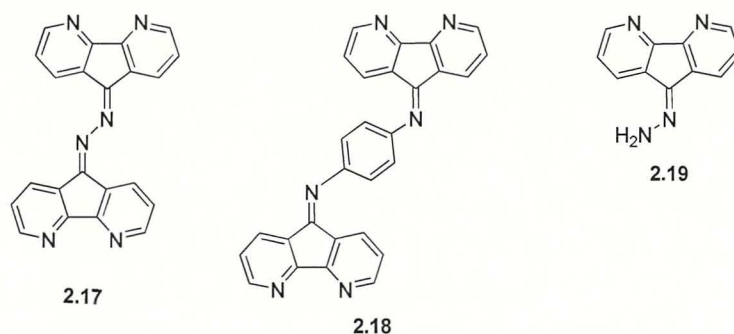
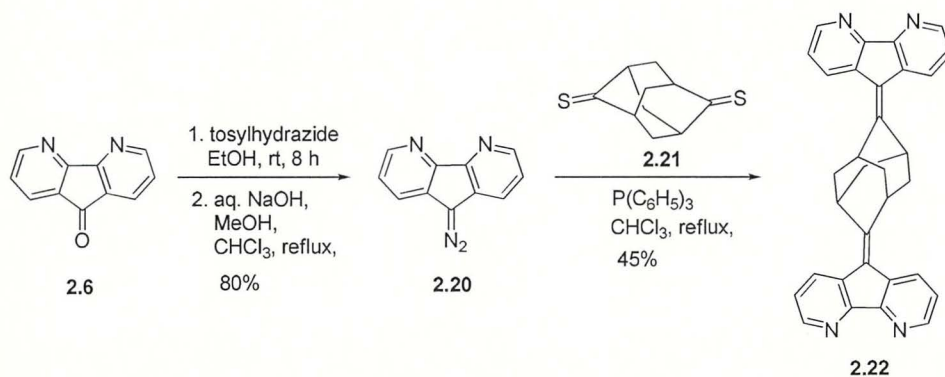


Fig. 2.2 Spectroelectrochemical experiments (a) and cyclic voltammogram (b) of 9-dicyanomethylene-4,5-diazafluorene (**2.16a**) in dichloromethane. Black line: 0 V (**2.16a**), red line: -1 V (**2.16a^{•+}**), blue line: -1.7 V (**2.16a²⁺**).¹³

The condensation reactions of DAFone (**2.9**) with aromatic amines and hydrazines were studied by Rilema *et al.*¹⁴ A series of compounds such as **2.17**, **2.18** and **2.19** were synthesised and characterised by photophysical methods. Some of these compounds, including DAFone (**2.9**), were used as building blocks for synthesis and studies of ruthenium complexes reported by Rilema *et al.*^{15,16}



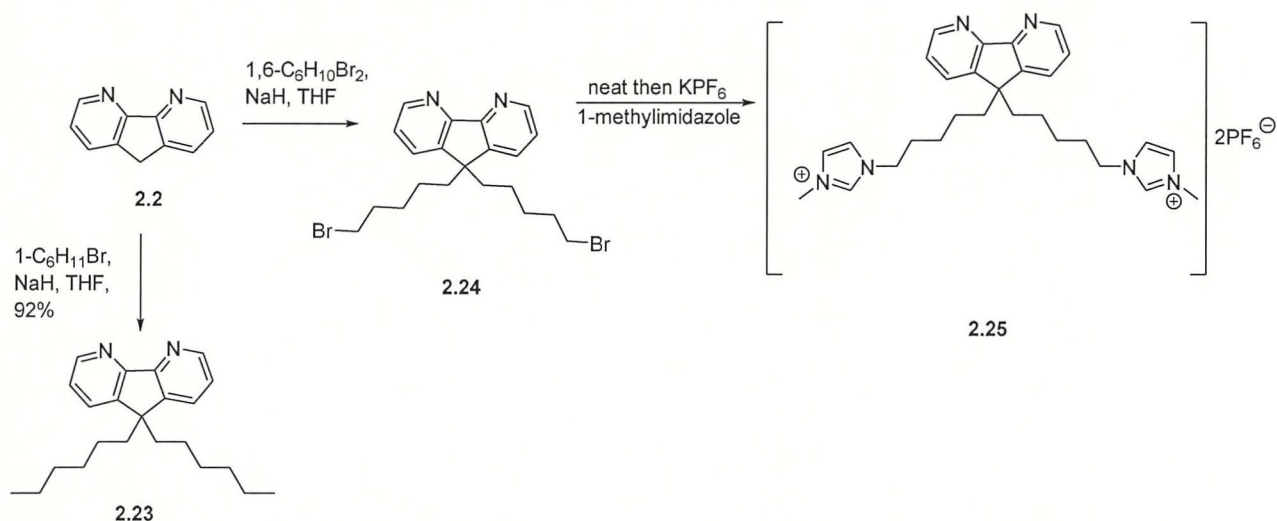
Study of photoinduced energy and electron transfer processes in supramolecular assemblies is an important field of research with many applications including light harvesting, sensors, and charge separation. When the active units for the energy transfer process are metal complexes, the connectors or spacers have to be bridging ligands. Belser *et al.* reported *bis*-chelating bridging ligand **2.22** based on two DAF units connected by adamantane spacer.¹⁷ 9-Diazo-4,5-diazafluorene (**2.20**), synthesised from DAFone (**2.9**), served as a synthon for many such DAF-based bridged ligands for electron and energy transfer studies (Scheme 2.4).¹⁸



Scheme 2.4 Synthesis of a *bis*(bidentate) bridged ligand based on 4,5-diazafluorene, ligand **2.22**.¹⁷

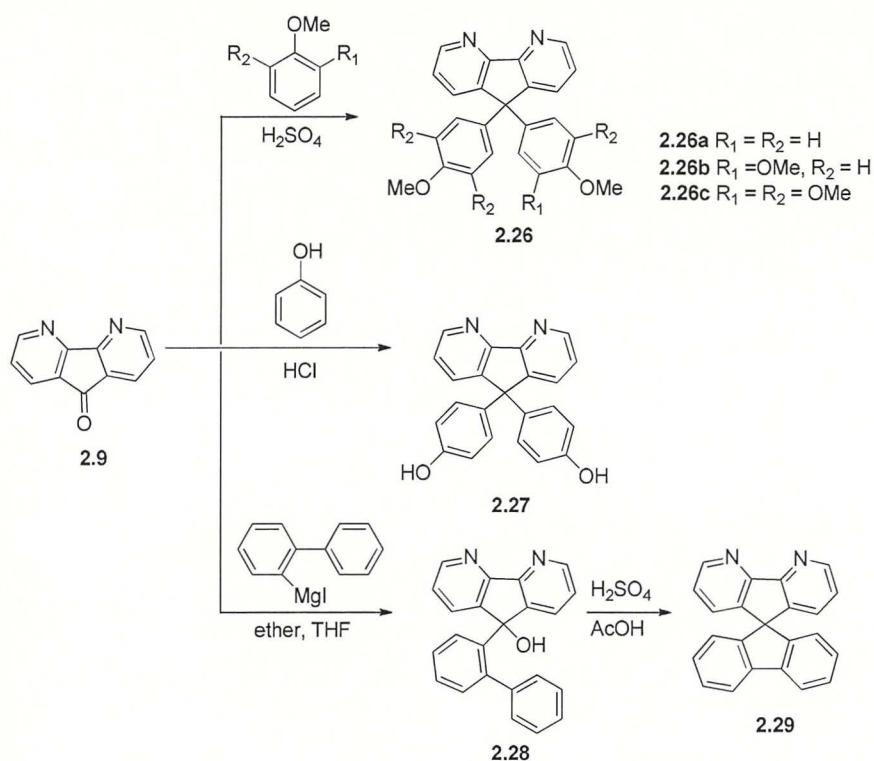
The alkylation of DAF (**2.2**) at the C-9 position can be performed in a way similar to that of known for fluorene (**2.1**) chemistry. In general, 4,5-diazafluorene-9-yl anion is generated by action of strong base and then involved as a nucleophile in nucleophilic substitution reaction with an alkyl halide. Wong *et al.*¹⁹ reported synthesis of C-9 dialkylated compounds **2.23** and **2.24** by alkylation of 4,5-diazafluorene-9-yl anion, generated on deprotonation by NaH with 1-bromohexane and 1,6-dibromohexane, respectively (Scheme 2.5). An alkylation occurs selectively at the C-9 position and not on the pyridine nitrogen atom suggesting much higher reactivity of the carbanion. The dibromo compound **2.24** suffers from self-polymerisation with 43% yield, so could not be purified. Compound **2.25** was prepared *in situ* by treating generated dibromo compound **2.24** with neat 1-methylimidazole, followed by ion-exchange

with potassium hexafluorophosphate to afford ionic compound **2.25**. Compounds **2.23** and **2.25** have been used as ligands to prepare iridium complexes, which were served as emissive materials in light emitting electrochemical cells (LEC) device studies¹⁹ (more details on iridium complexes will be discussed in section 2.1.3.4). Recently, 9,9-dialkyl-4,5-diazafluorene was reported to be useful in the medicinal chemistry field as an antitumor agent.²⁰ The authors emphasised that the chelating properties of the nitrogen atoms played an important role as an antitumor agent. They demonstrated that the hexyl substituted compound **2.23** shows maximum cellular uptake and cytotoxicity in this class of compounds having different alkyl chain lengths at the C-9 position of DAF (**2.2**). These findings indicate the potential usefulness of DAF derivatives in therapeutic applications.



Scheme 2.5 Alkylation of DAF (**2.2**) at the C-9 position and further side-chain functionalisation.¹⁹

Friedel-Crafts reaction of DAFone (**2.9**) with phenols and their alkyl ethers in the presence of an acid is an efficient method of introducing *p*-hydroxyaryl- and *p*-alkoxyaryl substituents at the C-9 position of DAF (**2.26–2.27**) (Scheme 2.6). Saito *et al.*²¹ studied the Friedel-Crafts reactions of DAFone (**2.9** → **2.26**) with anisole and phenol in presence of sulphuric acid and obtained products **2.26a–c** in good yields of 70–90%. Li *et al.*²² reported similar reaction of DAFone (**2.9** → **2.27**) with phenol in presence of hydrochloric acid with somewhat lower yield of 40%. Wong *et al.*²³ reported intramolecular Friedel-Crafts reaction (**2.28** → **2.29**) in presence of catalytic amount of sulphuric acid to synthesise spiro-4,5-diazabifluorene compound **2.29** with yield of 75% (Scheme 2.6). As a part of current thesis work, we report similar Friedel-Crafts reaction of bromo-substituted DAFone with phenol in the presence of sulphuric acid to synthesis 2,7-dibromo substituted compound similar to **2.26a** (with octyl groups instead of methyl) discussed in Chapter 3 in the Result and Discussion Section.

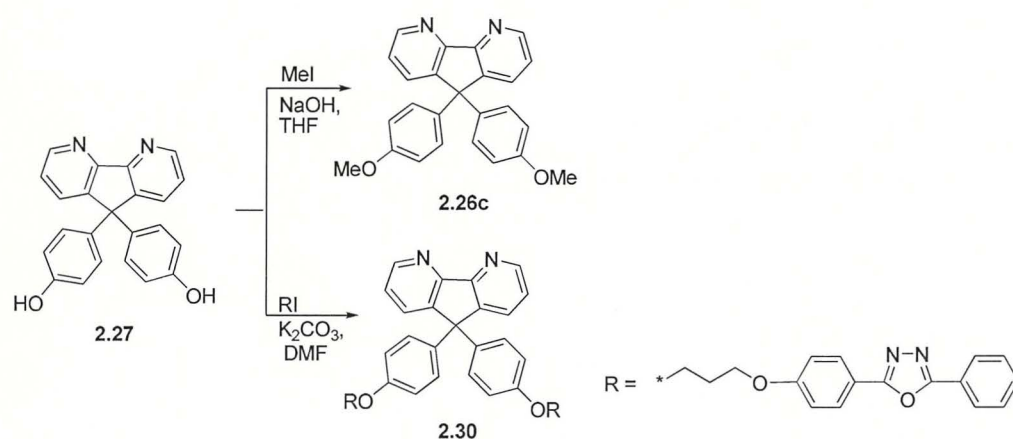


Scheme 2.6 An arylation at the C-9 position of DAF by Grignard and Friedel-Crafts type reactions.^{21,22,23}

9,9'-Diaryl-4,5-diazafluorenes **2.26a-c** were reported as a new type of electron-transporting and hole-blocking materials in electroluminescent devices.²¹ Electron transporting materials are applied to the organic electroluminescent devices for the effective recombination between the electrons and the holes in the emitting layer to afford high efficiency and longer lifetime of OLED.^{24,25} One of the best electron transporting material is 2,9-dimethyl-4,7-diphenyl-1,10-phenanthroline (**BCP**), it is also used as a hole-blocking layer in the electroluminescence devices to achieve high quantum efficiency of the devices. Saito *et al.*²¹ have demonstrated that phosphorescent electroluminescence devices that uses compound **2.26c** showed superior hole-blocking ability compared to **BCP**.



They also reported the molecular structure and molecular packing of compound **2.26c** in the solid state from single crystal X-ray crystallographic analysis.²⁶ The compound **2.26c** showed good electron transporting properties in electroluminescence devices due to its high electron affinity. This property was extended when this compound was used as a ligand for metal complexes. The compound **2.27** was reacted with the alkyl halides to afford **2.26c** and **2.30** (Scheme 2.7), both in good yield of ca. 70%.²¹ The europium complexes of compound **2.26c** and **2.30** were reported to be red-emitters with good electron-transporting properties in OLED.²² A ruthenium complex of compound **2.26c** was also investigated as a dye-sensitising in solar cells by Saito *et al.*²⁷

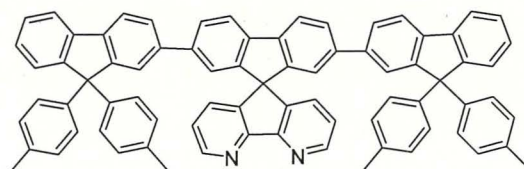


Scheme 2.7 Synthesis of 9,9'-diaryl-4,5-diazafluorene derivatives.²¹

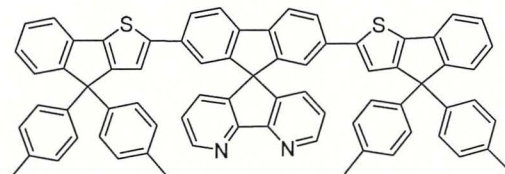
Ter(9,9-diarylfluorene) **2.31** is known as one of the most efficient emitters material for blue OLEDs amongst oligofluorenes, however, due to its low electron affinity causes difficulty in electron injection from common cathode electrodes.²⁸ Wong *et al.* in 2005 demonstrated that incorporation of higher electron affinity DAF moiety into *ter*(9,9-di-*p*-tolylfluorene) to form **2.32** results in more efficient OLED performance. Compound **2.32** showed an enhanced electron injection ability from metal cathode compared to the parent compound **2.31** without altering its characteristic blue emission properties.²³ Similar studies on *ter*fluorene analogue **2.33** reported to have significantly altered physical properties compared to parent *ter*fluorene **2.31**.²⁹



2.31

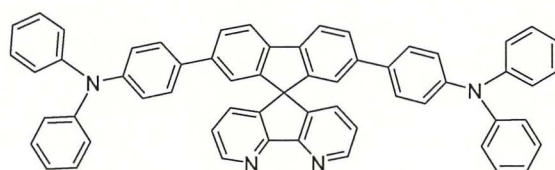


2.32

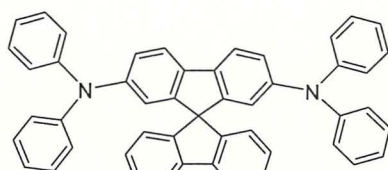


2.33

As mentioned before, DAF has the chelating ability toward transition metal ions and undergoes changes in physical properties upon coordination with metal ions. Therefore, design of donor–acceptor (**D-A**) systems containing DAF units allows new chromophores to be used as metal ion sensors. Design of **D-A** systems which facilitate processes of intramolecular charge transfer (ICT) and photo induced electron transfer (PET) is a common strategy for fluorescence probe sensors.^{30,31,32} Following similar strategy, in year 2006, synthesis and photophysical properties of spirobridge bipolar chromophore donor-acceptor (**D-A**) type molecules such as **2.34**, **2.35** and **2.36**, also reported by Wong's group in a separate publication. Incorporating the DAF unit as an electron acceptor and aryl amino groups as an electron donor moiety, the compounds **2.34**, **2.35** and **2.36** show different photoluminescence behaviour in its complexed and uncomplexed states suggesting a potential for sensing metal ions.³³



2.34



2.35



2.36

They studied the photophysical properties of the various metal ions binding with the compound **2.34**, **2.35** and **2.36**. In particular, the authors has demonstrated that complexation of compound **2.35** with Sr^{2+} ions led to a significant change in the emission wavelength (Fig. 2.3).³³

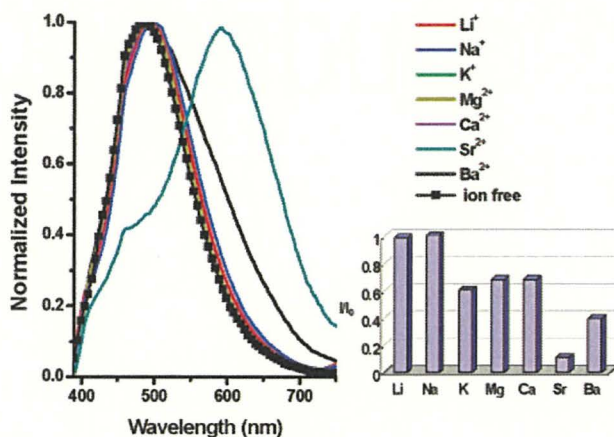


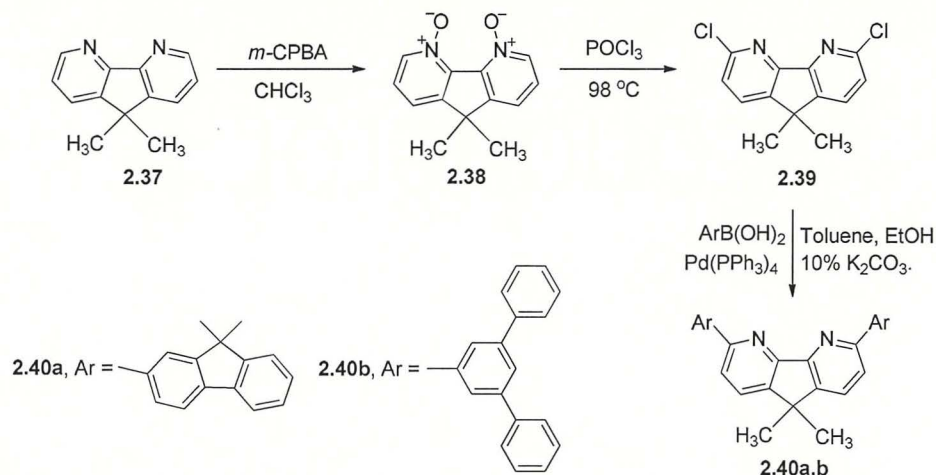
Fig. 2.3 Normalised fluorescence spectra of compound **2.35** (50 μM) in the presence of metal ions (500 μM) upon excitation at 380 nm in THF. Inset: fluorescence responses (I/I_0) of compound **2.35** at emission maxima after adding metal ions; I_0 is referred to the fluorescence intensity of ion-free state.³³

2.1.2.2 Substitution at the 3,6-position of 4,5-diazafluorene

In general, two methods can be best described for the introduction of aryl substituents at the 3,6-position of DAF. First method utilises the intermediate N,N' -dioxide of DAF (Schemes 2.8-2.9)^{36,37} while the other method is based on direct arylation of DAF using aryllithium (Scheme 2.10).³⁴

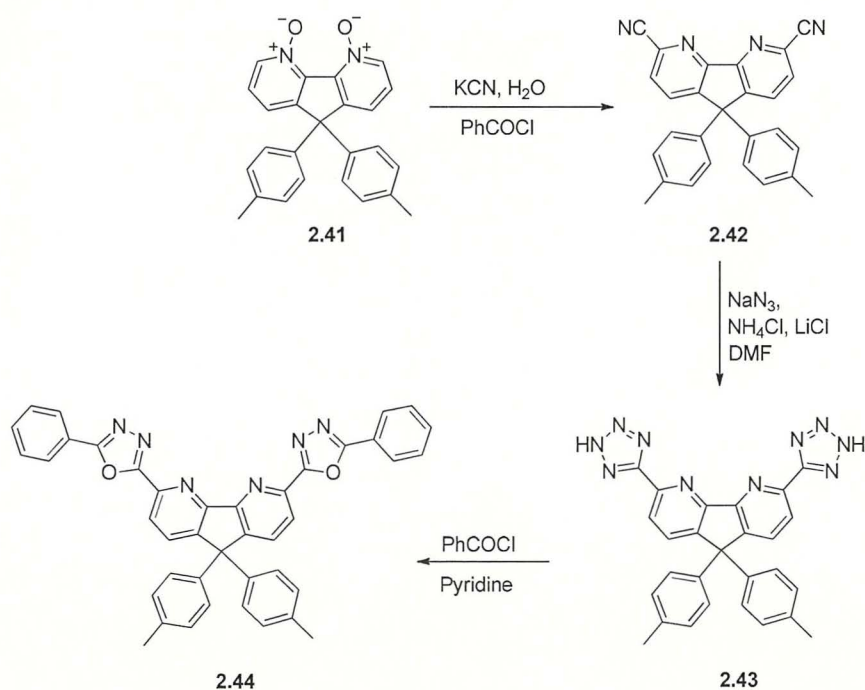
N,N' -dioxide of DAF derivative **2.38** was obtained in good yield by oxidation of compound **2.37** with *meta*-chloroperbenzoic acid (*m*-CPBA) in chloroform (Scheme 2.8).³⁶ As a part of this Thesis work, we also exploited similar approach utilising hydrogen peroxide as the oxidising agent to obtain N,N' -dioxide compound **3.25** with 74% yield (described in Chapter 3, under the Results and Discussion Section). Rozen *et al.* reported synthesis of compound **2.38** from compound **2.37** using $\text{HO}^{\bullet}\text{F}\cdot\text{CH}_3\text{CN}$ as the oxidising agent in DCM with 90% yield.³⁵ Compound **2.38** was treated with trichlorophosphate at 97-98 $^{\circ}\text{C}$, followed by basic work up with NaHCO_3 to afford dichloro-substituted compound **2.39**. Halide substituted product **2.39** was then subjected to Suzuki-type coupling reaction with aryl boronic acid to obtain aryl substituted products **2.40a,b**. In this Thesis work, we prepared similar product

(**3.26**) together with a *mono* chloro-substituted product **3.27** as a side product under similar reaction condition (Chapter 3, under the Results and Discussion Section).



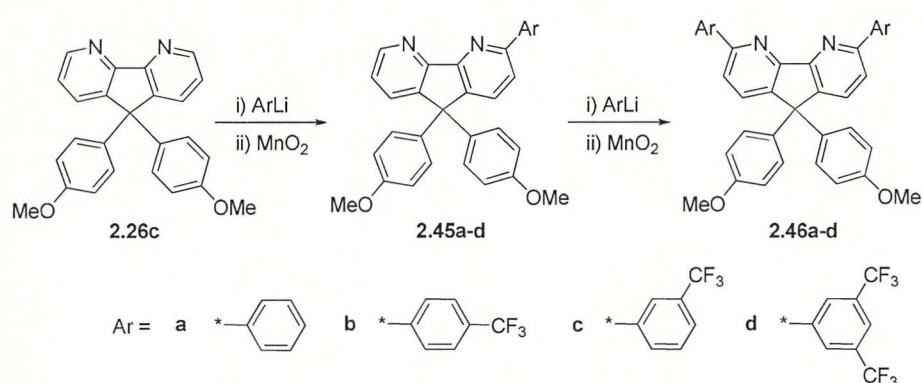
Scheme 2.8 Arylation at 3,6-position of DAF.³⁶

Yen *et al.* reported the oxadiazolyl substituent at the 3,6-position of DAF using *N,N'*-dioxide-4,5-diazafluorene intermediate **2.41** (Scheme 2.9).^{36,37} Compound **2.41** was treated with potassium cyanide in water followed by benzoyl chloride to afford **2.42** with 70% yield. Isolated product **2.42** was then refluxed with sodium azide in presence of ammonium chloride and lithium chloride in dimethylformamide to afford **2.43** with 53% yield. Finally, compound **2.43** was reacted with benzoyl chloride in pyridine to afford desired product **2.44** with 61% yield.



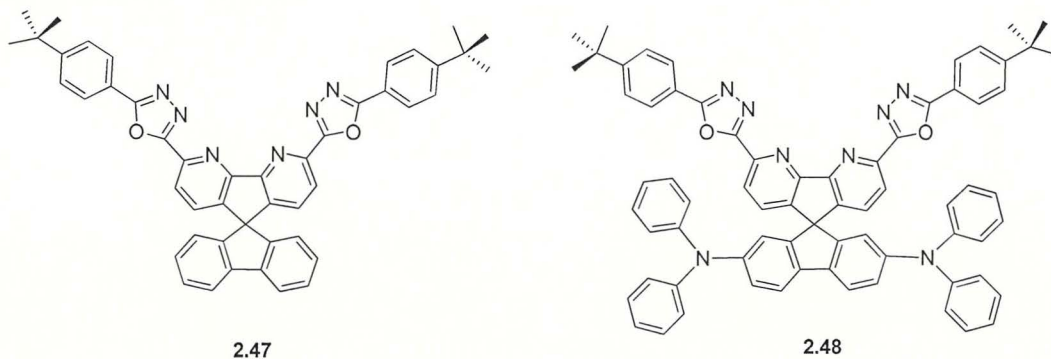
Scheme 2.9 Introduction of aryl oxadiazole group at 3,6-position of DAF.³⁷

A second method, reported by One *et al.*³⁴ involved direct arylation with aryllithium (Scheme 2.10). Compound **2.26c** was reacted with 3.5 equivalent of phenyllithium (PhLi) in toluene to afford compound **2.45** and compound **2.46** with 43% and 3% yields, respectively. Compound **2.45** was further treated with PhLi to afford compound **2.46** with 55% yield. In order to improve the electron transporting properties of compound **2.26c**, π -extended products (**2.45a-d** and **2.46a-d**) were synthesised as an extension of their previous work. The reported electroluminescent device based on compound **2.46d** showed an improved hole blocking properties compared to their previously reported best device performance based on compound **2.26c**. It was demonstrated that this compound possessed a high glass transition temperature of over 100 °C and improved electroluminescence due to increasing electron-transporting ability arising from an extension of the π electron system.³⁴

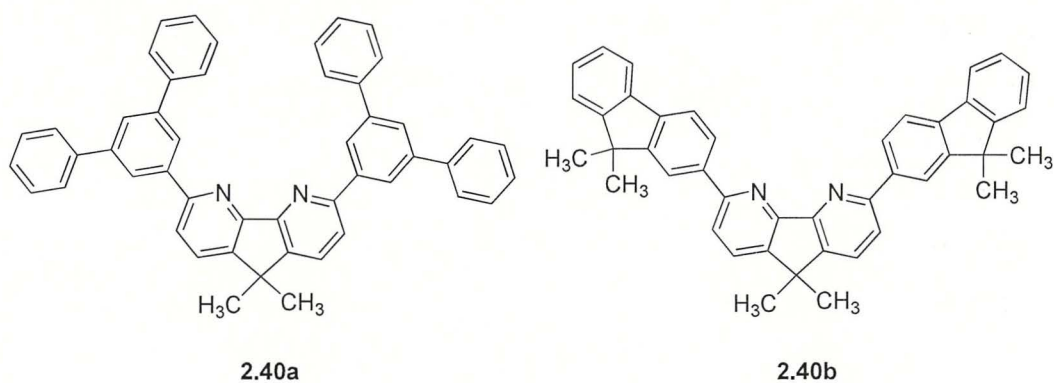


Scheme 2.10 Direct arylation at 3,6-position of DAF.³⁴

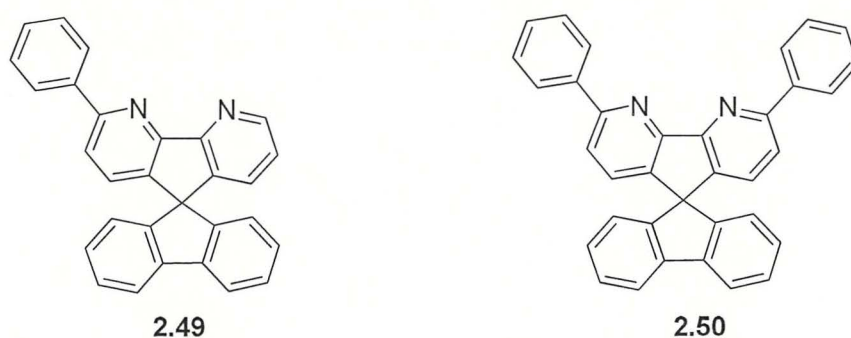
In 2007, researchers at Luminescence Technology Corporation have patented some spiro(fluorene/diazafluorene) derivatives, e.g. compounds (**2.47**, **2.48**), primarily for use as electron-transporting and/or hole-blocking materials or phosphorous hosts in organic electroluminescence devices.³⁶



In 2008, researchers at Canon Kabushiki Kaisha patented alkylated diazafluorene derivatives such as compounds (**40a**, **40b**) claiming them to be useful as a charge transporting materials for electrophotographic photosensitive members, an organic electroluminescence devices, photoelectric transducers, an organic semiconductors and an organic solar cells.³⁷



Huang *et al.* reported synthesis of compounds **2.49** and **2.50**, which were used as ligands for preparing iridium complexes that have been studied as materials for LEC.³⁸ Compounds **2.49** and **2.50** were prepared by direct arylation of spiro-compound **2.26c** with phenyllithium in diethyl ether followed by an oxidation reaction with MnO_2 with 93% and 88% yields, respectively. They have demonstrated that LEC devices based on iridium complexes of π -extended compounds **2.49** and **2.50** showed longer device lifetime and higher stability compared to unsubstituted compound **2.26c** based iridium complex.



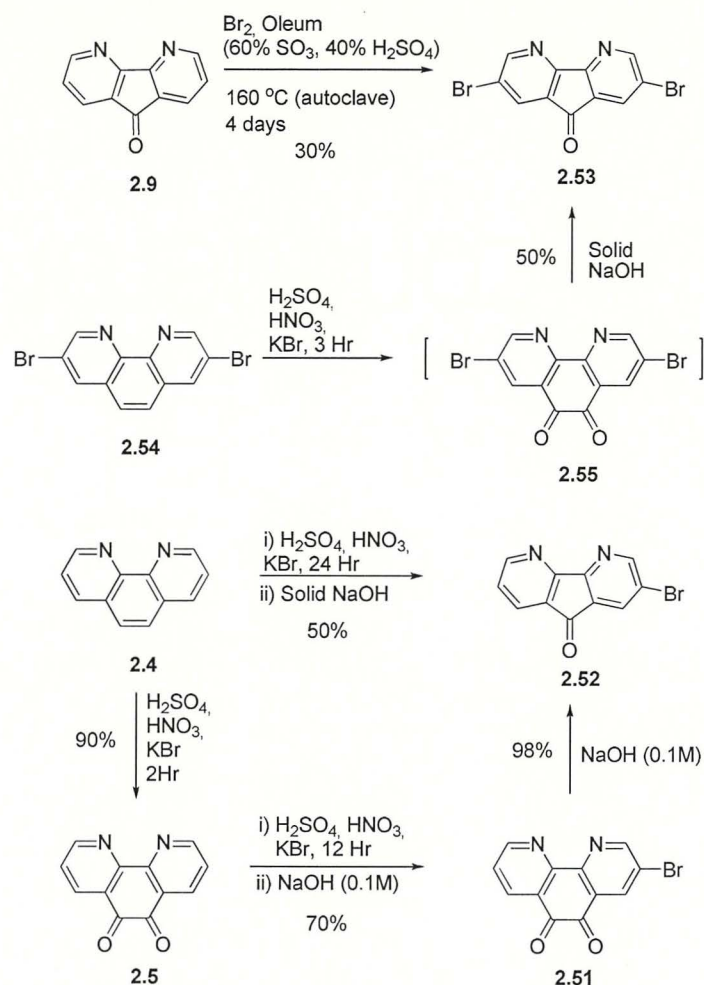
2.1.2.3 Functionalisation at the 2,7-position of 4,5-diazafluorene

It is evident from the examples of the previous Section (2.1.2.2) that functionalisation at the 3,6 positions of DAF (**2.2**) can be successfully exploited for potential applications in organic electronics. However, the 2,7 position of DAF **2.2** have not been functionalised until recently

to make derivatives of DAF due to synthetic difficulties. Earlier the methods of functionalisation at the 2,7-position achieved through direct bromination to DAFone (**2.9**) into dibromoDAFone (**2.9** → **2.53**) was reported by Mlochoski *et al.*⁷⁰ in 1980 (Scheme 2.11). The procedure involved very harsh acidic conditions (60% oleum + bromine), high pressure and temperature, and long reaction time of four days. Moreover, the yield of the reaction was low; and therefore the method is not suitable for large-scale reactions. As part of the current Thesis work, one of the aims was to address this issue and to develop an efficient and milder set of conditions to synthesise 2,7-dibromodafone **2.53** avoiding these harsh conditions (more details are in the Result and Discussion section of this Chapter). Subsequently, several novel derivatives of DAF substituted at the 2,7-position are synthesised and their physical properties have been studied (Chapters 3-5).

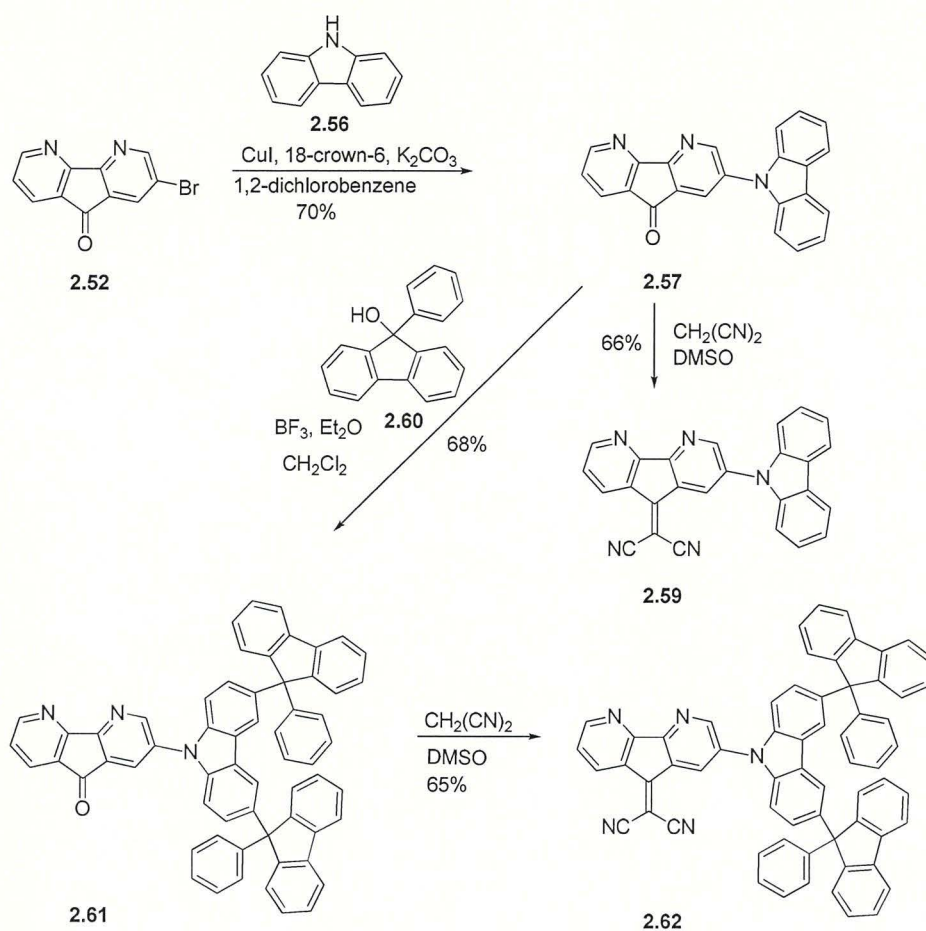
In 2011, Huang *et al.* have reported one pot synthesis of 2-bromo-4,5-diazafluor-9-one (**2.52**) (bromoDAFone) from 1,10-phenanthroline (**2.4**) (Scheme 2.11).³⁹ 1,10-Phenanthroline (**2.4**) was treated with mixture of H₂SO₄/HNO₃/KBr followed by treatment with solid sodium hydroxide to afford compound **2.52** with 50% yield. The reaction proceeded through dione intermediate **2.51**, which underwent rearrangement to form bromoDAFone **2.52**. Later on 2012, Huang's group reported synthesis of dibromoDAFone **2.53** from 3,8-dibromo-1,10-phenanthroline (**2.54**) using similar conditions with 50% yield.⁴⁰ At the same time, our own research using similar reaction scheme (Scheme 2.11) was underway, we attempted to follow the same procedure as reported by Huang *et al.* and found that the reactions (**2.4**→**2.52** and **2.44**→**2.53**) did not give reproducible yields and cannot be scaled up to large amounts (above 500 mg).

In the procedure, that we have developed the dione intermediate **2.55** was isolated first and then in separate reaction treated with a 6.2% NaOH aqueous solution in a large volume of water to afford compound **2.53** with 51% yield. The improved method was found to be suitable for large-scale syntheses (more details are in the Results and Discussion Section of this Chapter).



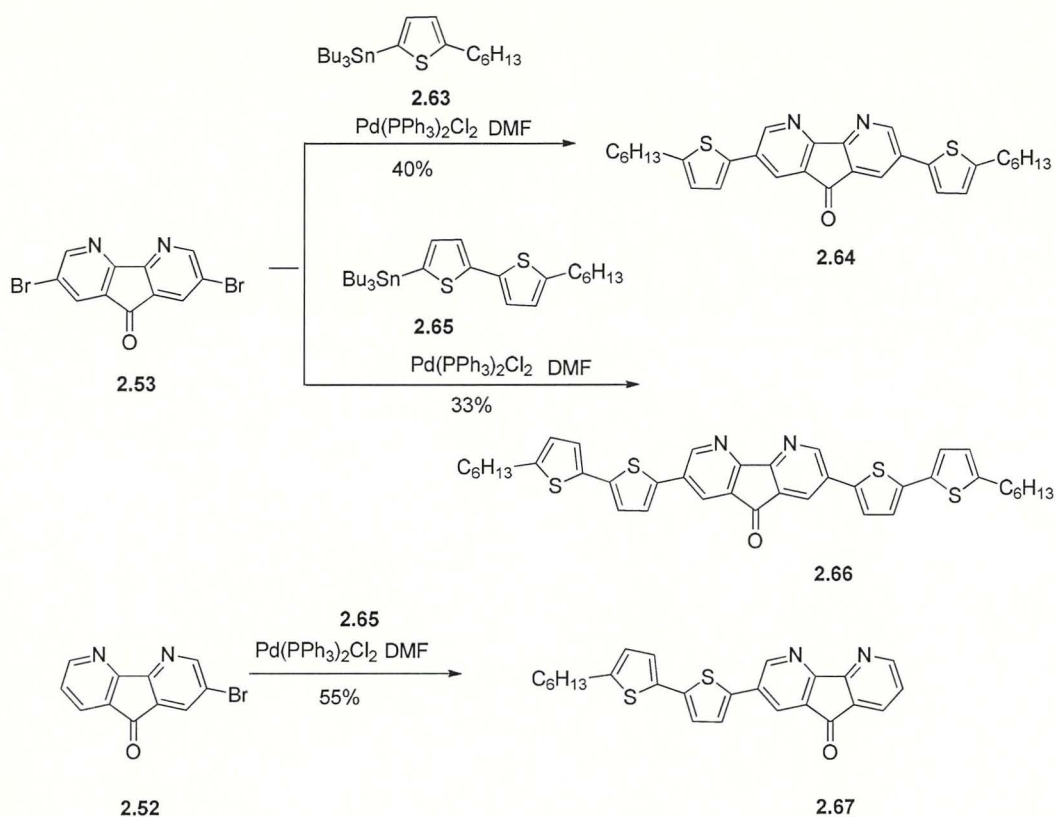
Scheme 2.11 Synthesis of 2-bromoDAFone **2.52** and 2,7-dibromoDAFone **2.53**.^{39,40}

Huang *et al.*³⁸ reported the synthesis of series of donor-acceptor type molecules based on monobromoDAFone **2.52** and dibromoDAFone **2.53** (Schemes 2.12 and 2.13) and studied their photophysical properties. Among the series of donor-acceptor molecules (such as **2.59**, **2.61** and **2.62**), DAF unit acted as acceptor while carbazole or thiophene units as donors. Compound **2.57** was prepared by the Ullmann reaction using CuI, 18-crown ether and K₂CO₃ to afford 70% yield and further Friedel-Crafts reaction of compound **2.57** with **2.60** afforded **2.61** with 68% yield. Treatment of compound **2.57** with malonitrile (**2.58**) yielded donor-acceptor compound **2.59** with 66% yield. The synthesised compounds **2.59**, **2.61** and **2.62** reported to exhibit solvent-dependent fluorescence and low band gap materials, suitable for optoelectronic applications.



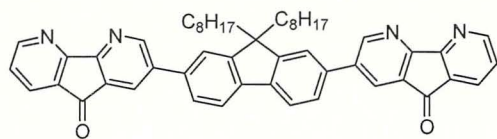
Scheme 2.12 Donor-acceptor type molecules between DAF and carbazole derivatives.³⁸

The D-A type systems such as **2.64**, **2.66** and **2.67** were synthesised by Stille coupling reactions between thiophene derivatives and bromoDAFone **2.52** in DMF catalysed by $\text{Pd}(\text{PPh}_3)_2\text{Cl}_2$. Compounds **2.64**, **2.66** and **2.67** exhibited solvent-dependent fluorescence and are reported to be low energy gap materials and, therefore, can be consider as potential materials for optoelectronic applications.

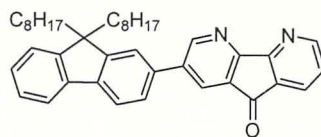


Scheme 2.13 Donor-acceptor type molecules **2.64**, **2.66**, and **2.67** between DAFone and thiophene derivatives.³⁹

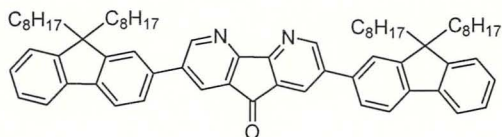
Recently, in 2013, when our work was in progress, Huang *et al.* (also working on DAF derivatives) have reported the synthesis of some co-oligomers and co-polymers of DAF with fluorene units and studied their photophysical properties.⁴¹ The co-oligomers (**2.68–2.70**) were synthesised by Pd catalysed Suzuki couplings reaction in good yields. The copolymer **2.71** containing the DAFone unit was synthesised by Ni-mediated Yamamoto coupling reaction while the copolymers with the different ratio of DAF and fluorene units were synthesised via Pd catalysed Suzuki coupling polymerisation reaction. All the 9,9-dioctyl-substituted DAF-based copolymers (**2.72a–c**) exhibit good solubility in common organic solvents, high quantum efficiency in solution (58–77% in solution) and good thermal stability (decomposition temperature ca. 385 °C), similar to polyfluorenes. These authors have also presented photoluminescent properties of copolymers **2.72** when coordinating with different metal ions and their pH response. The authors highlighted the potential of poly(4,5-diazafluorene) based materials for supramolecular functional materials for thin film devices such as pH and metal ions sensors.⁴¹



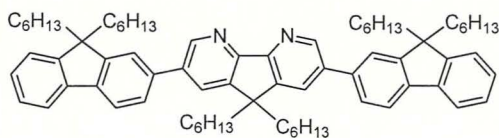
2.68



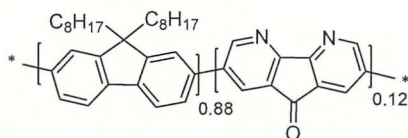
2.73



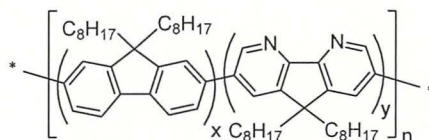
2.69



2.70



2.71



2.72a-c

2.72a, x = 0.95, y = 0.05

2.72b, x = 0.85, y = 0.15

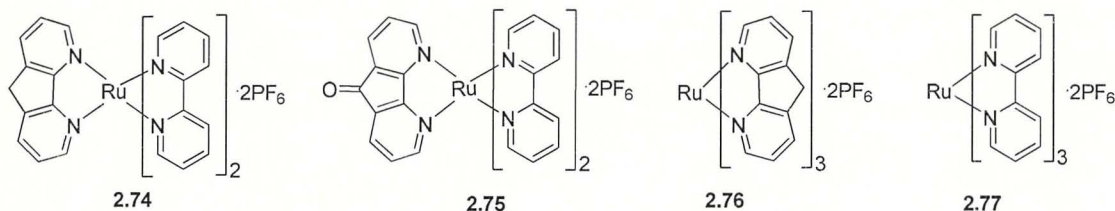
2.72c, x = 0.50, y = 0.50

2.1.3 4,5-Diazafluorenes as ligands for complex formation with transition metals

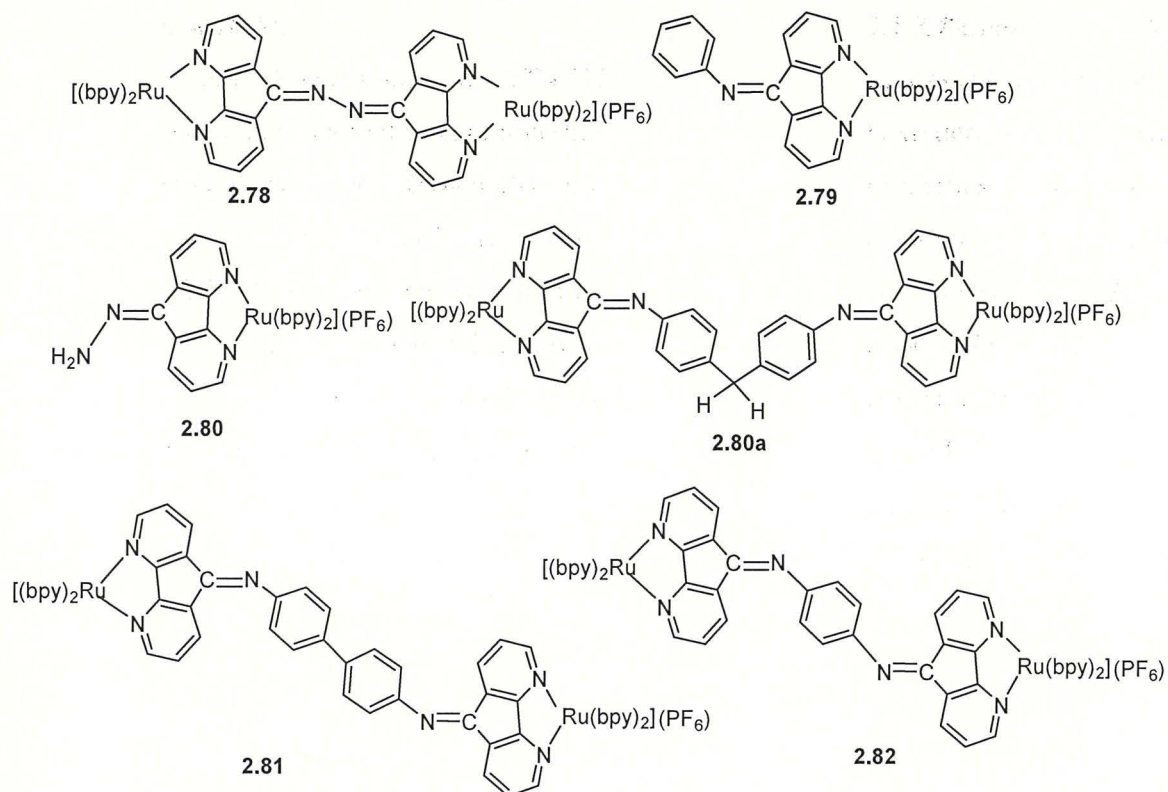
Bidentate nitrogen-contained ligands, as 2,2'-bipyridine (bpy, **2.3**) and 1,10-phenanthroline (phen, **2.4**) are known to form wide range of metal complexes.^{42,43,44} DAF (**2.2**) has similar binding site as bpy (**2.3**) and phen (**2.4**) to serve as ligand to form metal complexes. The methylene bridge in DAF changes the angle of the bipyridine portion of the molecule, which reduces the nitrogen-metal overlap, and therefore DAF (**2.2**) lies lower than bpy (**2.3**) in the spectrochemical series. This fact was supported by the study of emissive properties of Ru and Ni complexes with DAF by Cherry's group in 1984.⁴⁵ The presence of five membered ring results in larger chelate bite for DAFone (**2.9**) in comparison to those with structurally similar bpy (**2.3**) and phen (**2.4**) [N...N distances: 3.00 Å (DAFone), 2.62 Å (bpy), 2.64 Å (phen)]. As a result, chelating of DAFone with metals is known to be highly unsymmetrical, forming one normal and one long bond.⁴⁶ As an example, the single crystal X-ray structure of Co(DAFone)(3,6-di(*t*Bu)semiquinone)₂ reported by Peirpont's group established this fact.⁴⁷ Over the last two decades, a large number of DAF-based metal complexes involving Pd, Co, Cu, Ni, Cd, Mn, Ir, Ru, Re, Ag, Zn, Eu and Pt metal cations have been reported.^{5,46,47,48,49} In the following section, widely investigated metal complexes (Ru, Ir) of DAF for optoelectronic applications, as well as Pd and Rh complexes of DAF as catalysts are discussed.

2.1.3.1 Complexes of 4,5-diazafluorene with Ru

In 1984, Cherry *et al.*⁷ reported synthesis of Ru(II) complexes **2.74**, **2.75**, **2.76** containing DAF derivatives as ligands and investigated their photophysical properties. The photophysical properties of Ru complexes were compared with well known [Ru(bpy)₃]₂PF₆ (**2.77**). The quantum yield of complex **2.74** was reported to be 0.56 at 77 K, which was higher than the complexes **2.75** (0.23), **2.76** (low) and **2.77** (0.33). The emission lifetimes of the complexes **2.74**, **2.75** and **2.77** were measured to be 0.59, 4.3 and 5.2 μs, respectively. While the emission lifetime of the complex **2.76** was too low to be measured. The absorption maximum of **2.74** (574 nm) was found to be slightly red shifted compared to Ru(bpy)₃·2PF₆ (**2.77**) (578 nm). A noted difference in emission intensity of **2.76** is about 50 fold larger than that of **2.74** at 298 K. The complex **2.75** was found to be not emissive at 298 K.



Rillema *et al.*⁵⁰ in 1988 reported the synthesis of series of bimetallic Ru(II) complexes (**2.78**–**2.82**) based on DAF derived ligands (such as **2.17**, **2.18**, **2.19**) and studied their photophysical properties. The absorption maxima (ca. 444 nm, 285 nm, 240 nm) were found to be similar for each of these complexes (**2.78**–**2.82**) in acetonitrile at 298 K. Compared to [Ru(bpy)₃]₂PF₆ complex **2.77**, the MLCT transitions ($d\pi \rightarrow \pi^*$) of these complexes (**2.78**–**2.82**) are blue-shifted (by ca. 10 nm). The oxidation and reduction processes of all these complexes were found to occur at less negative potentials compared to [Ru(bpy)₃]₂PF₆. All of these complexes were found to be non-emissive at room temperature. However, at low temperature (77 K) green-yellow emission with maxima at 566–568 nm were observed, similar to the vibrational component reported for [Ru(bpy)₃]₂PF₆ (578 nm) with a small blue shift of ca. 10 nm. The emission lifetimes of these complexes were reported to be between 4 to 6 μs at 77 K.



A dye-sensitized solar cell (DSSC) using Ru complex **2.83** containing DAF ligand **2.26c** was investigated by One *et al.* in 2007.²⁷ The properties of complex **2.83** was compared with the well-known sensitizer for DSSC, *cis*-bis(thiocyanato-*N*)bis(4,4'-tetrabutylammonium hydrogen dicaroxylato-2,2'-bipyridine- κ^2N)ruthenium(II) dye (red dye **N719**). The conversion efficiency of solar cell made of complex **2.83** was found to be slightly higher (7.3%) compared to complex **N719** (7%). The photocurrent-voltage curves for the respective solar cells are shown in Fig. 2.4.

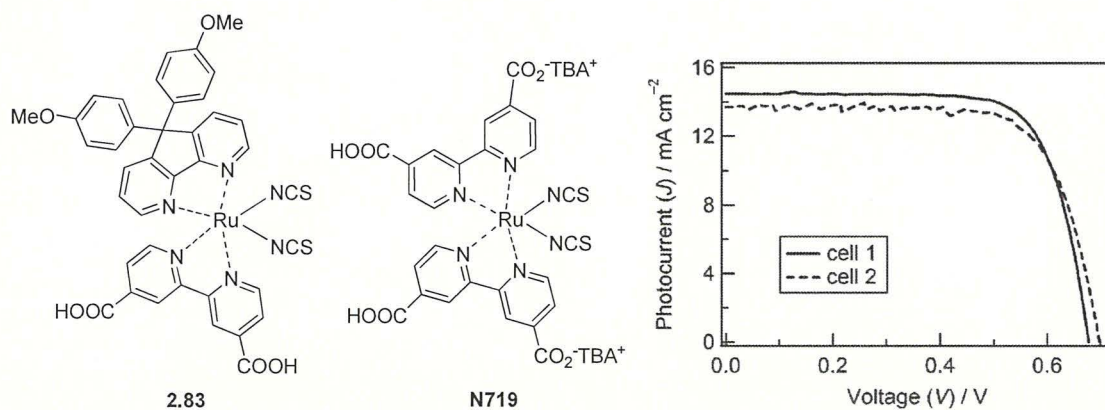
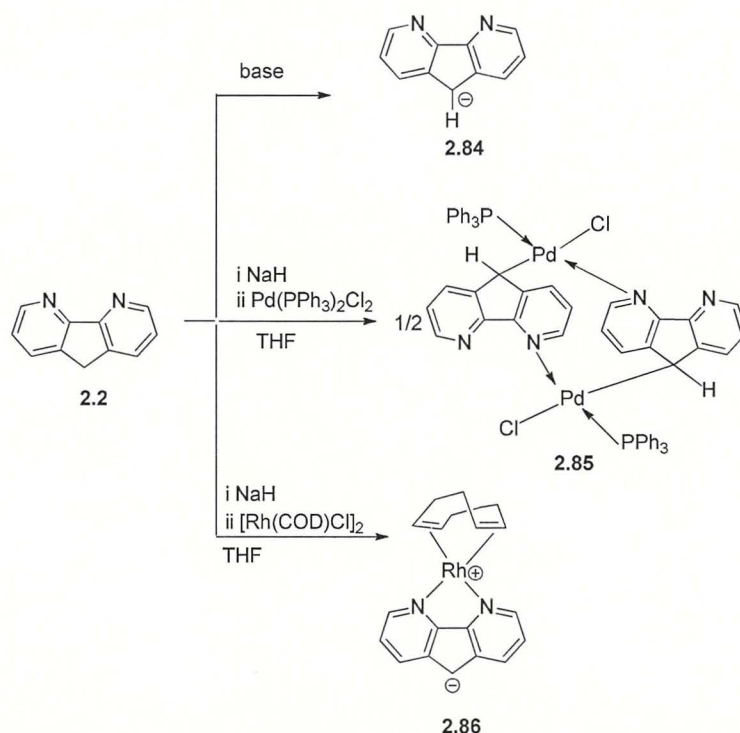


Fig. 2.4 The photocurrent-voltage curves for the DSSC with dye **2.83** (1) and dye **N719** (2).²⁷

The terpedal ligand derived from DAF and their corresponding Ru(II) complexes was recently reported by Cheng's group, displayed somewhat different spectroscopic and electrochromic properties than those of Ru(bpy₃)²⁺ and Ru(phen)₃²⁺ complexes.⁵¹ The same group also reported synthesis a similar derivatives from DAF and their corresponding polynuclear Ru(II) complexes with different linkers and their photophysical properties.^{52,53}

2.1.3.2 Complexes of DAF with Pd

DAF (**2.2**) when subjected to deprotonation at the C-9 position (Scheme 2.13) results in 4,5-diazafluorenyl anion **2.84** which has two types of metal binding sites, namely the two nitrogen atoms and the methylene anion site at the C-9 position. These interesting features of having two binding sites gave rise to the possibility of accommodating two metal centres such as the complex **2.85** with new properties. Song's group has investigated these aspects⁵⁴ in 2008 and the palladium and rhodium chemistries of DAF anion ligand were reported. The structure and the synthesis of the respected metal ions complexes are shown in Scheme 2.14. This research has particularly demonstrated that complex **2.86** shows catalytic activity toward olefin hydrogenation.



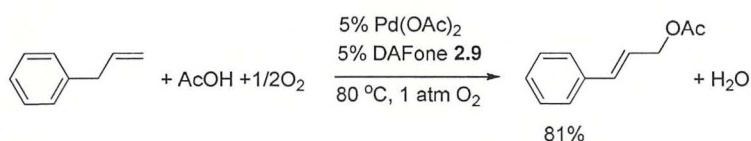
Scheme 2.14 Reactions at different sites of DAF to form metal complexes.⁵⁴

The multiple coordination sites in a given ligand facilitate formation of macrocyclic complexes.^{55,56} As mentioned above, DAF has a multiple coordination sites. This feature has

been utilised in synthesis of ligand 9-(2-(diphenylphosphino)ethyl)-4,5-diazafluorene (DAF_p) for the ligand transfer reaction from the complex [Cu(IPr)DAF_p] (IPr = *N,N'*-bis(2,6-diisopropylphenyl)imidazol-2-ylidene) to Rh(I) and Au(I) metal centres, to form macrocyclic complexes.⁵⁷ DAF adduct with decamethylytterbocene, (C₅Me₅)Yb(DAF) that slowly eliminate H₂ to form (C₅Me₅)Yb(DAF⁻) was recently reported by Andersen groups. They were interested in understanding the mechanism of hydrogen elimination that was studied by spectroscopic and molecular modelling.⁵⁸

2.1.3.3 DAF as ancillary ligand for catalyst

As mentioned previously, the geometry of DAF and the labile binding sites makes its properties different compared to structurally similar bpy and phen ligands. Stahl *et al.* have reported remarkable selectivity and high yields in specific Pd catalysed reactions when DAF ligand was used as ancillary ligand over structurally similar ancillary ligand^{59,60} In general, benzoquinone is used as the oxidant for Pd-catalysed allylic acetoxylation reaction.⁶¹ Replacing benzoquinone with O₂ was considered a major challenge in this area of research.⁶² Stahl *et al.* have demonstrated that using DAFone as ancillary ligand promotes the Pd catalysed allylic acetoxylation reaction at 1 atm of O₂, thus enabling a replacement of benzoquinone with O₂ as an oxidant (Scheme 2.15).⁵⁹ Moreover, DAFone **2.9** was found to be the best ancillary ligand compared to structurally similar nitrogenous ligands in providing good selectivity and high yields. According to the authors, working with the same strategy in search of DAF derivative as potential ligand for other type of Pd catalysed reactions may yield new discoveries in the future. Indeed, Stahl *et al.* went on to discover that DAF (**2.2**) and DAFone (**2.9**) as an ancillary ligand for Pd(II) catalyst enable aerobic oxidative cross-coupling of indoles and benzene, with selectivity at the C2 and C3 positions of indole to afford indole-arylation products.⁶⁰



Scheme 2.15 Allylic acetoxylation reaction mediated by DAFone (**2.9**).⁵⁹

It was reported that DAF derivative undergo a regioselective Bingle-Hirsch reactions, and their crude product purification was found to be easier compared to similar reaction products, which was attributed due to the high polarity of the adduct formed.^{63,64} This led to the

synthesis of new hexakis-fullerene adduct with the two DAF located at trans position in high yields (Fig. 2.5).⁶⁵

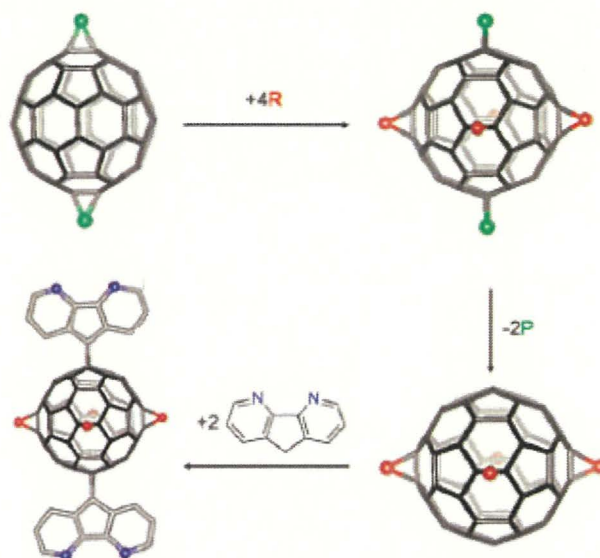
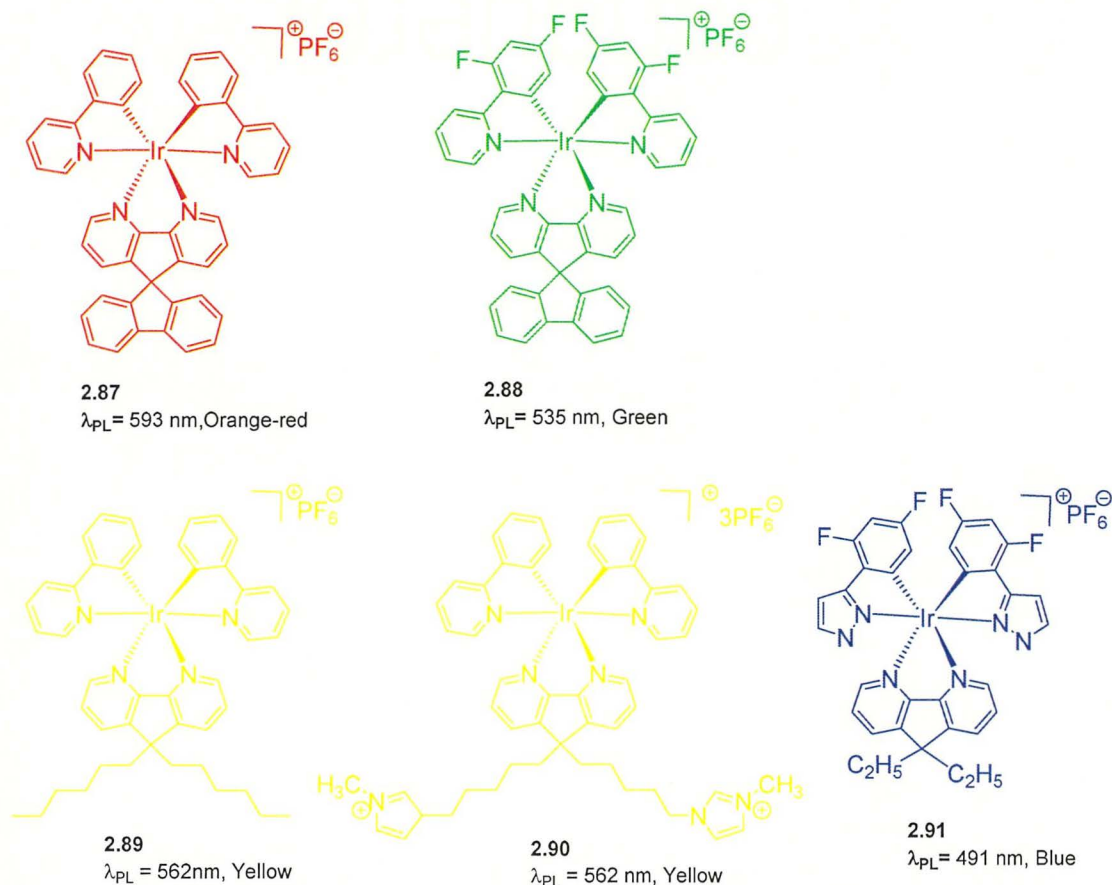


Fig. 2.5 Synthesis of fullerene adduct with DAF.⁶⁵ Green balls are protecting group (anthracene), red balls are the malonate groups.

2.1.3.4 Complexes of Iridium with 4,5-diazafluorene

Iridium complexes (**2.87–2.91**) based on the DAF ligand have been investigated by Wong's group as emissive materials for potential applications in light emitting electrochemical cells (LEC).^{19,38,66,67} The cationic transition-metal complexes containing ligands with good steric hindrance are ideal candidate for application in electrochemical cells. In this regards, DAF based ligands have the potential to be useful for LEC. Complexes **2.87** and **2.88** displayed efficient orange-red and green emission with high quantum yield in solution as well as in neat film. LEC devices using complexes **2.87** and **2.88** have been reported to have highest efficiencies at that time, emphasising the role of sterically hindered ligands (such as **2.29**, **2.49** and **2.50**) in improving the device efficiency.^{38,66} LEC device based on complex **2.90** displayed improved turn on time when compared to similar device with complex **2.89**, which demonstrated the role of the ionic group imidazole in increasing concentration of the mobile ions.¹⁹ Development of highly efficient white light emissions from electroluminescence materials are currently a hot area of OLED applications. The white light emission can be achieved by mixing two or three complementary colours from blended or stacked layers of different emitters in OLED structures. The development of efficient blue, green- and red-emitting transition metal complexes are highly desirable and in particular Ir(III) complexes are highly promising in future optoelectronic application.^{67,68} Complex **2.91** exhibits blue

emission with high quantum yield in solution as well as in film and has been used to prepare first white light emitting electrochemical cell.⁶⁷ As a part of this Thesis work, synthesis of Ir complexes with different substituted DAF and their photophysical properties for LEC application has been presented in Chapter 3.



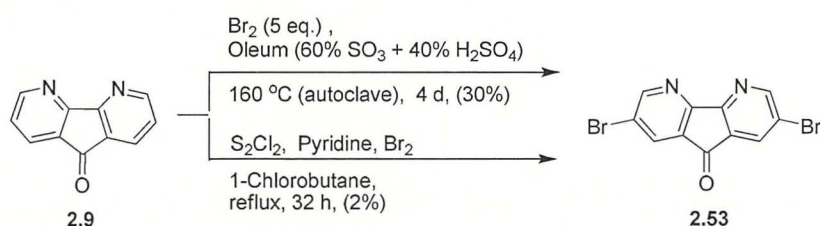
2.2 Results and Discussion

2.2.1 Improved method of the synthesis of 2,7-dibromo-4,5-diazafluorenone (2.53)

DAFone (**2.9**) itself can be easily obtained by oxidation of 1,10-phenanthroline (**2.4**) by using procedures shown in Scheme 2.1.^{7,8} However, its functionalisation at positions 2,7 is not straightforward. 2,7-Dibromo-4,5-diazafluorenone-9-one (**2.53**) is the key building block for targeted synthesis of conjugated oligomers, polymers and metal complexes in our research. Easy access to this key starting compound was therefore very crucial for the progress of the work, which involved not only synthesis of the targeted molecules but also study of their photophysical, electrochemical and other properties. Direct bromination of fluorenone at the 2 and 7-positions are relatively easy and can be carried out even at room temperature in good yield.⁶⁹ However, DAFone (**2.9**) is very difficult to brominate because its pyridine rings are strongly deactivated towards electrophilic aromatic substitution due to the presence of

electron deficient nitrogen atoms, with additional deactivating effect of bridged carbonyl fragment. A method for direct bromination of DAFone (**2.9**) at 2 and 7-positions are described in the literature,⁷⁰ however, it requires very harsh conditions as it uses a mixture of bromine with 60% oleum (60% oleum is not commercially available, so it should be prepared by saturation of commercial 20% oleum with gaseous SO₃ at low temperatures) (Scheme 2.16). Heating of DAFone (**2.9**) in this mixture in an autoclave (or sealed ampoules) at 160 °C for 4 days gives 2,7-dibromo-4,5-diazafluorenone (**2.53**) in low yield of < 30% with substantial amounts of unreacted starting DAFone.⁷⁰ We used this method at the initial stage of our research to make the starting dibromo-DAFone **2.53** monomer. But due to the harsh reaction conditions, difficulties in synthesis, impractical work-up (required neutralisation of large volumes of acids before an extraction of the product), impossibilities to scale up the reaction, as well as safety issues, we were looking for an alternative method of synthesise compound **2.53**.

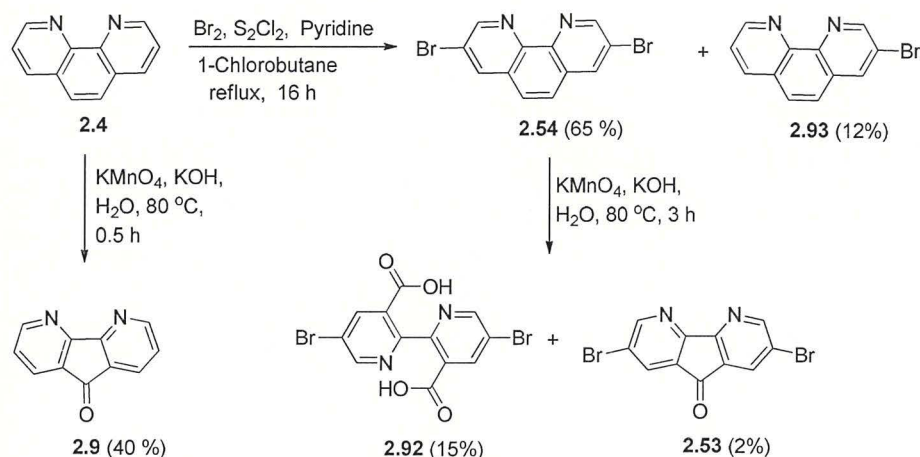
Initially, we tried to perform direct bromination DAFone **2.9** by bromine in presence FeCl₃ as Lewis acid catalyst in different solvents such as dichloromethane or nitrobenzene, and by NBS in sulphuric acid, the method which have been successfully used for bromination of electron-deficient dibenzothiophene-*S,S*-dioxide,⁷¹ but failed to yield any bromination products in all the cases. Bromination of 1,10-phenanthroline (**2.4**) in 1-chlorobenzene with sulphur monochloride and pyridine mixture are known to give 3,8-dibromo-1,10-phenanthroline (**2.54**) in good yield.⁷² We applied this method to the bromination of DAFone (**2.9**) but obtained only very low yield of ca. 2% of dibromo-DAFone **2.53** (Scheme 2.17). These results are understandable because the pyridine rings in DAFone (**2.9**) are strongly deactivated towards electrophilic aromatic substitution (compared to that in phenanthroline **2.4**) by the carbonyl group.



Scheme 2.16 Direct bromination of DAFone **2.9**.

Since direct bromination of DAFone **2.9** in mild conditions failed to give the desired product, we decided to change the synthesis. Oxidation of 1,10-phenanthroline to DAFone **2.9** is a

well-known reaction generally involved action of potassium permanganate with potassium hydroxide in water¹⁰ or action of nitric acid and sulphuric mixture on 1,10-phenanthroline.³⁷ Working on a similar kind of oxidation reaction, our next attempt was to obtain dibromo-DAFone **2.53** from 3,8-dibromo-1,10-phenanthroline (**2.54**). 3,8-Dibromo-1,10-phenanthroline (**2.54**) was synthesised following literature procedure⁷² with some modification on scaled-up synthesis described in experimental section and also noted that 3-bromo-1,10-phenanthroline (**2.93**) was obtained as side product, yield of which varies with concentration of bromine and reaction time.

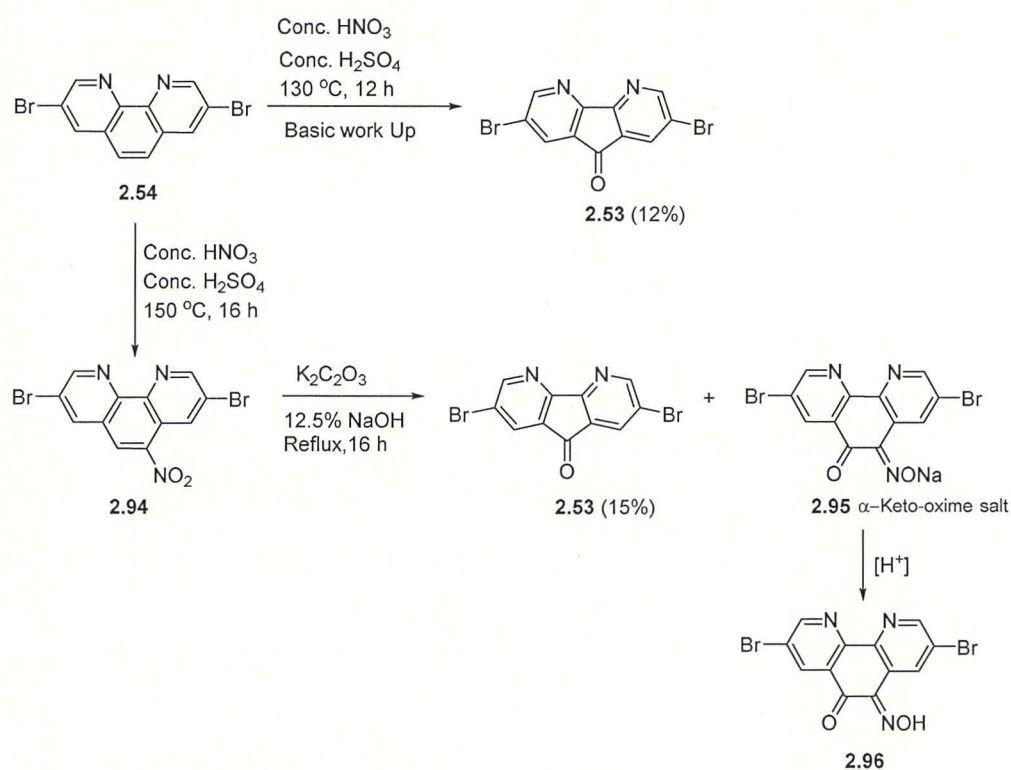


Scheme 2.17 Oxidation of phenanthroline to form **2.9** and **2.53**

When dibromo-phenanthroline **2.54** was subject of oxidation using potassium permanganate and potassium hydroxide in water the major product obtained as 5,5'-dibromo-2,2'-bipyridyl-3,3'-dicarboxylic acid (**2.92**) with only trace amounts of targeted product **2.53**. Oxidation of dibromo-phenanthroline **2.54** with nitric acid and sulphuric acid mixture gave up to 20% of dibromo-DAFone **2.53** in small-scale reaction (below 500 mg scale). However, due to some unknown reasons, when we attempted to scale up the reaction, product yield dropped down drastically and sometimes we even failed to get the product **2.53**. This issue forced us to look for an improved reaction method.

In order to understand the mechanism of the reaction and improve the yield, we tried to isolate the intermediate(s) that is formed during the oxidation process. First assumption was that the reaction might proceed through the nitro intermediate, which can undergo rearrangement smoothly, similarly to the reaction known in the literature for 5-nitrophenanthroline to form DAFone.⁷³ It has been reported that 5-nitro-1,10-phenanthroline under basic conditions undergoes rearrangement through the keto-oxime intermediate with evolution of ammonia to

form DAFone (**2.9**). Working towards a similar strategy, we first isolated 3,8-dibromo-5-nitro-1,10-phenanthroline (**2.94**) and then subjected this to basic reaction conditions to form dibromo-DAFone **2.53**. However, it was found that the reaction, even in a small scale, gives variable yields of **2.53** from batch to batch (up to 15%) and the major product obtained was α -keto-oxime salt **2.95**. Nevertheless, we were able to prepare some amount (ca. 1–2 g) of dibromo-DAFone (**2.53**) through this route. As this method is not suitable for scaling up, we further tried different routes described in next section where the most efficient method to date has been developed. α -keto-oxime salt **2.95** obtained as greenish solid was found to be insoluble in common organic solvents and so we were unable to purify it. For characterisation of α -keto-oxime salt **2.95**, it was first neutralised with diluted H_2SO_4 in water and then extracted with DCM followed by purification by column chromatography to obtain pure α -keto-oxime intermediate **2.96**.



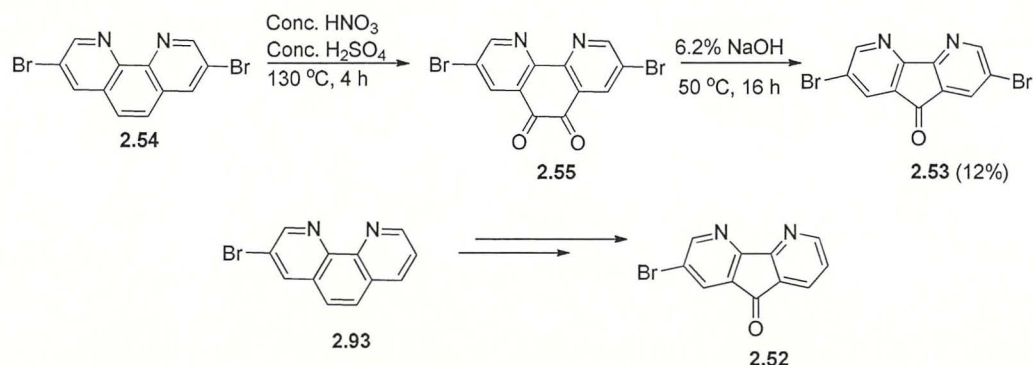
Scheme 2.18 Synthesis of phenanthroline intermediate **2.94** and dibromoDAFone (**2.53**).

2.2.2 Synthesis of 2,7-dibromo 4,5-diazafluoren-9-one (**2.53**) through improved method

To improve the yield further, another route was followed to synthesised compound **2.53** through 3,8-dibromo-1,10-phenanthroline-5,6-quinone (**2.55**). It was found that 3,8-dibromo-1,10-phenanthroline (**2.54**) when treated with conc. nitric acid and sulphuric acid in the presence of potassium bromide heated to $130\text{ }^\circ\text{C}$ for 4 hours, gives exclusively 3,8-dibromo-

1,10-phenanthrolin-5,6-quinone (**2.55**) in good yield (85%). Suspension of 3,8-dibromo-1,10-phenanthrolin-5,6-quinone (**2.55**) in water when treated with diluted NaOH (6.2%) at 55 °C to give the desired product **2.53**, with up to 51% yield. The yield in this reaction was found to be dependent on the concentration of base and the temperature. The best yield was achieved when suspension of 3,8-dibromo-1,10-phenanthrolin-5,6-quinone (**2.55**) in a large volume of water was heated to 55 °C, while adding 6.2% aqueous sodium hydroxide solution slowly. A colour change was observed during the addition of a base. A yellow suspension was observed, which turned to a light green and then black throughout the addition of base. After 16 hours of heating at 55 °C, the mixture turned back to a yellow colour suspension indicating presence of product **2.53**, which can be easily isolated by filtration. This procedure was found to work well in a large scale (up to 25 g scale synthesis have been successfully performed), giving nearly 50% yield of the product without difficulties in separation. Moreover, isolated product **2.53** was found to be pure enough (ca. 90% purity by ¹H-NMR, without purification) to be used in the next reactions and therefore does not require column purification which is difficult due to poor solubility of **2.53** in common organic solvents.

When our work on optimisation of the conditions of this method was in progress, similar approach for synthesis of compound **2.53** from compound **2.54** with conc. HNO₃/conc.H₂SO₄/KBr mixture directly without isolating compound **2.55** was reported by W. Huang *et al.*⁷⁴ In contrast to our approach, the method described by W. Huang *et al.* involved treating the acidic mixture with solid sodium hydroxide, claiming a 50% yield. The same group also reported in their previous publication synthesis of compound **2.52** from 1,10-phenanthroline (**2.4**) as a one-pot reaction.⁷⁵ However, on testing these methods showed that both these methods did not give reproducible results and so are not suitable for scale up.

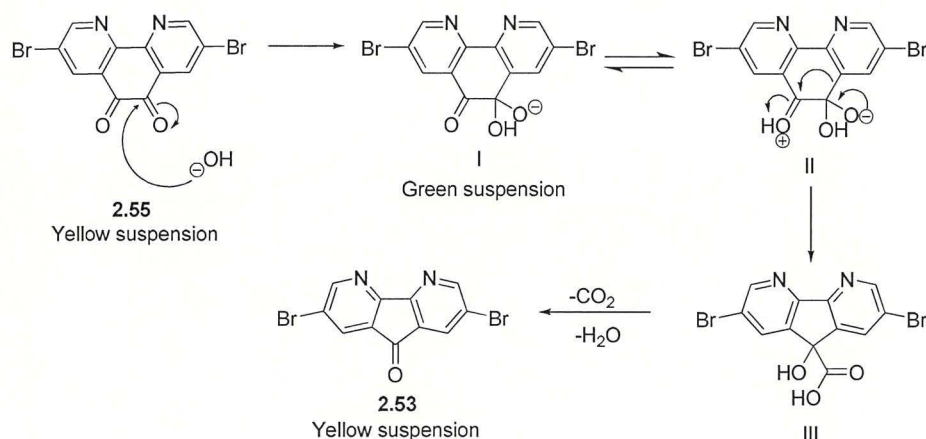


Scheme 2.18 Synthesis of brominated DAFone derivatives with improved yield method.

Our developed method gives reproducible results and works well for scaling up. Moreover, the isolation of the product is easy and does not require column chromatography purifications. This route can also be extended to synthesis of bromo-DAFone **2.52** from 3-bromo-1,10-dibromophenanthroline (**2.93**). These developed procedures can be used to prepare brominated DAFone key building blocks in bulk amounts that opens the door for synthesis of a wide range of novel oligomers, polymers and copolymers based on electron deficient DAF structure as well as propels future research requiring functionalisation at the 2,7 position of DAFone **2.9**.

2.2.3 Proposed mechanism for the synthesis of 2,7-dibromo-4,5-diazafluoren-9-one (**2.53**)

The proposed mechanism for rearrangement of 3,8-dibromo-1,10-phenanthroline-5,6-quinone (**2.55**) to dibromo-DAFone **2.53** under basic condition is depicted on Scheme 2.19. Nucleophilic attack by basic hydroxyl ion at the keto site of 3,8-dibromo-1,10-phenanthroline-5,6-quinone (**2.55**) to form the hydroxyl anion I (greenish suspension as sodium salt). This then undergoes tautomerisation and subsequently undergoes rearrangement from six-member ring (II) to five-member ring (III) structure losing carbon dioxide and water molecule to form dibromoDAFone **2.53** as yellow suspension in water.



Scheme 2.19 Plausible mechanism of ring contraction in dibromophenanthrolinequinone **2.55** to yield dibromoDAFone **2.53**.

2.3 Conclusion

In this Chapter, straightforward synthesis of brominated DAFone, which is a key starting material for this Thesis work, is presented. The key starting material, dibromo-DAFone (**2.53**) was synthesised from commercially available 1,10-phenanthroline in two steps in good yields. The first step involved oxidation with a HNO₃/H₂SO₄/KBr mixture to obtain the intermediate compound **2.55** with 77% yield after column chromatography. In the second step, rearrangement of **2.55** takes place under mild basic conditions to afford **2.53** in good yield. A number of trials have been performed to optimised the conditions of the rearrangement at the second step. The best results have been obtained when a suspension of compound **2.53** in water was treated with NaOH (6.2 %) at 55 °C resulting in upto 51% yields.

The improved method of synthesis is reproducible, can be carried out in mild conditions, and works well in a large-scale reaction. Moreover, the isolated product through the developed method presented does not require column chromatography for purification of product **2.53**, which simplified the procedure, saved the time and decreased cost of the overall synthesis. The developed method allowed the synthesis of the key starting material **2.53** in a multi-gram scale with ca. 51% overall yield making subsequent work on synthesis of DAF-based oligomers, polymers and metal complexes containing possible.

Comprehensive highlights of DAF chemistry and applications in organic electronic are presented and discussed along with the role of DAF as a ligand in metal complexes, particularly with Ru, Ir and Pd metals. Fluorene derivatives have been extensively studied as blue emitting electroluminescent material due to their good photophysical properties. DAF is topologically similar to fluorene moiety but has not been studied in depth; one of the reason, perhaps, is the difficulty of synthesis of halogenated DAF i.e. an accessibility of key building blocks for conjugated oligomers/polymers. The improve method described in this Chapter may serve well for future research work which might require easy excess of halogenated DAFone for developing new material of DAF derivatives.

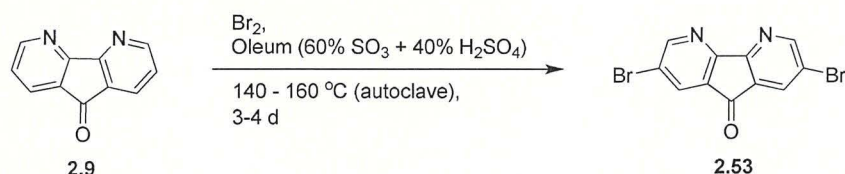
2.4 Experimental

All chemicals and solvents were purchased from Aldrich and Alfa Aesar chemical companies and were used without any further purification. All the solvents in this section of work were used without prior purification. Column chromatography were performed using silica (40–60 μm). Thin layer chromatography were carried out using precoated silica gel (Merck, 20 \times 20 cm, Silica gel 60 F₂₅₄), visualised by UV lamp (254/366 nm).

¹H NMR and ¹³C NMR spectra were recorded on a Bruker Avance 400 MHz, Bruker Avance 500 MHz using deuterated solvents (CDCl₃ or DMSO-*d*₆) as a lock. Chemical shifts are reported in ppm, relative to tetramethylsilane (TMS) peak at 0 ppm. Following abbreviation were used to assign NMR spectra: s= singlet, d= doublet, t= triplet, dd= doublet of doublet, td = doublet of triplet. Mass spectra were recorded on GC-MS 5890 (Hewlett Packard Series II).

Synthesis

2,7-Dibromo-4,5-diazafluorenone (2.53)⁷⁰



60% Oleum was prepared by saturation of commercial 20% oleum with gaseous SO₃ at 20 °C (external cooling as the process is exothermic), the process was controlled by the weight added (final density $d = 1.98 \text{ g mL}^{-1}$). Method of bromination of DAFone is described in ref. [70], we have modified the procedure and two examples are given below

Method A

2,7-Diazafluorenone (2.9)^{7,8} (0.90 g, 4.84 mmol), bromine (5 mL, 194 mmol, 20 eq) and 60% oleum (5 mL) were placed into thick wall ampoule. The ampoule was placed into stain steel bomb to which some amount of methanol was added to compensate the pressure developed in the ampoule during the reaction (*for safety reasons*). The bomb was heated at 140–145 °C for 3 days. After cooling to room temperature, the bomb was opened, the ampoule was cooled down / frozen with liquid nitrogen, carefully opened (*NB: cooling to low temperature is required because of high pressure inside the ampoule due to HBr formed in the reaction*) and left to heat up to room temperature. Excess of bromine, SO₃, and HBr were removed *in vacuo* by water jet pump, the residue was poured onto crashed ice (70 mL) and neutralised with ammonia until pH \sim 8. The solid was filtered off, washed with water till pH = 7 and dried to

afford crude dibromoDAFone **2.53** (1.16 g, 69%) as yellowish powder. According to ^1H NMR analysis, the product contains 18% of unreacted starting DAFone (**2.9**) and ~5% monobromoDAFone (**2.52**) among other by-products. Crude product was recrystallized from acetone (120 mL) to yield pure dibromoDAFone (**2.54**) (0.58 g, 34.5%) as light yellow crystals. According to ^1H NMR, the sample is of 97.5% purity (contains 1.3% DAFone **2.9** and 1.2% bromoDAFone **2.52**) and was further purified by additional recrystallisation.

^1H NMR (400 MHz, CDCl_3): δ (ppm) 8.87 (2H, d, $J = 2.2$ Hz), 8.10 (2H, d, $J = 2.1$ Hz).

^{13}C NMR (100 MHz, CDCl_3): δ (ppm) 186.72, 160.71, 156.35, 134.46, 130.28, 122.58.

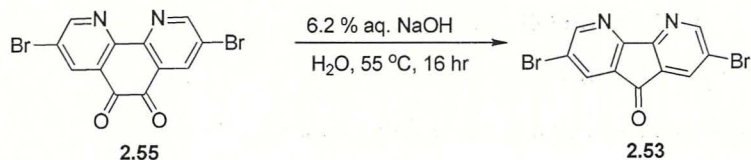
GC-MS (EI⁺) m/z : 337.9 (M^+ , 46%, ^{79}Br , ^{79}Br), 339.9 (M^+ , 100%, ^{79}Br , ^{81}Br), 341.9 (M^+ , 50%, ^{81}Br , ^{81}Br). Calcd. for $\text{C}_{11}\text{H}_4\text{Br}_2\text{N}_2\text{O}$: 337.87.

Method B

2,7-Diazafluorenone (**2.9**) (17.80 g, 0.0977 mol), bromine (50 mL, 1.94 mmol, 20 eq.) and 60% oleum (90 mL) were placed into three thick wall ampoules. The ampoules were placed into stain steel autoclave to which some amount of methanol was added to compensate the pressure developed in the ampoule during the reaction (*for safety reasons*). The autoclave was agitated with heating at 155–160 °C for 4 days. After cooling to room temperature, the autoclave was opened, the ampoules were cooled down / frozen with liquid nitrogen, carefully opened (*NB: cooling to low temperature is required because of high pressure inside the ampoule due to HBr formed in the reaction*) and left to heat up to room temperature. Excess of bromine, SO_3 , and HBr were removed *in vacuo* by water jet pump and the residue was poured onto crashed ice (200 mL). Precipitated salt of dibromo-DAFone was filtered off, transferred into cold water and basified with ammonia. The solid was filtered off, washed with water till pH = 7 and dried to afford dibromoDAFone (**2.53**) (9.70 g, 29%) as yellowish powder. According to ^1H NMR, the purity of the sample is ~ 96–97 %, with DAFone **2.9** as main impurity. The acidic filtrate from separation of dibromoDAFone salt was basified with ammonia, the precipitated was filtered off, washed with water until pH = 7 and dried to afford crude product (4.80 g), which contains a mixture of mono/dibrominated DAFones (**2.53:2.52** ~ 1:2) among other by-products.

Method C

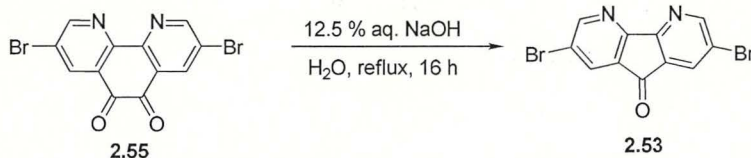
Exp: SG173



A suspension of 3,8-dibromo-1,10-phenanthroline-5,6-dione (**2.55**) (4.10 g, 10.9 mmol) in water (300 mL) was heated at 50 °C. Aqueous NaOH (6.2 % w/v, 24 mL) was added slowly dropwise at 50 °C over a period of 15 minutes, during which colour changes from yellow suspension to light green and then dark black. The mixture was heated at 55 °C for 16 hours, after which the colour changed to yellow. The mixture was allowed to cooled down to room temperature and neutralize with diluted HCl (10%) and then extracted with chloroform (2 × 100 ml). The combined organic layers were washed with water (2 × 50 mL), dried with MgSO₄ and evaporated to afford crude product as yellow solid (2.31 g, 61%). Crude product was purified by column chromatography on silica gel eluting with EA:PE= 2:8 v/v to yield pure product **2.53** as a light yellow solid (1.92 g, 51%), spectroscopically identical with the sample previously described.

Method D

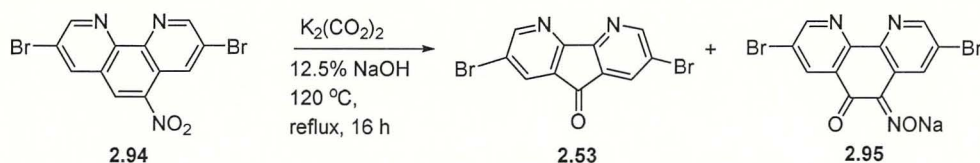
Exp: SG161



Mixture of 3,8-dibromo-1,10-phenanthroline-5,6-dione **2.55** (501 mg, 1.30 mmol), 12.5% w/v aq. NaOH (0.5 mL), and water (3.75 mL) was reflux (100 °C, oil bath) for 16 hour. The mixture turns greenish suspension from yellow suspension. The mixture was allowed to cool down to room temperature, diluted with water (20 mL), and then extracted with dichloromethane (2 × 20 mL). The combined organic layers washed with water (2 × 10 mL), dried with MgSO₄ and evaporated to afford crude product as light brownish solid (182 mg, 39%). Crude product was purified by column chromatography on silica gel eluting with EA:PE = 1:9 v/v to yield pure product **2.53** as a light yellow solid (123 mg, 27%), spectscopically identical with the sample previously described.

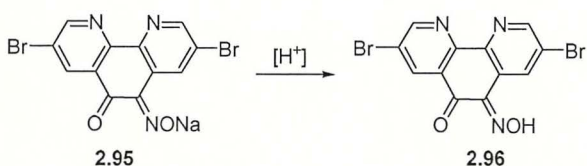
Method E

Exp: SG-097



3,8-Dibromo-5-nitro-1,10-phenanthroline (**2.94**) (100 mg, 0.261 mmol), potassium oxalate (240 mg, 1.30 mmol), NaOH (12.5%, 0.5 mL) and water (1.5 mL) were charged into 50 mL single necked round bottom flask. The mixture was stirred under reflux for 16 hour under nitrogen. After cooling, ethyl acetate (15 mL) was added resulting in greenish precipitate. It was stirred for 15 min and then filtered off. The filtrate containing organic-aqueous solution was separated, organic layer was washed with water (3×10 mL), dried with anhydrous magnesium sulphate and evaporated to afford product **2.53** (35 mg, 40 %), spectroscopically identical to the sample previously described. The filtered off residue was dried in *vacuo* to afford α -keto-oxime salt **2.95** (41 mg) as a greenish solid (note: this product is highly insoluble in common organic solvents, so Na salt was neutralised for characterisation purpose as described below).

3,8-Dibromo-6-(hydroxyimino)-1,10-phenanthrolin-5(6H)-one (**2.96**)

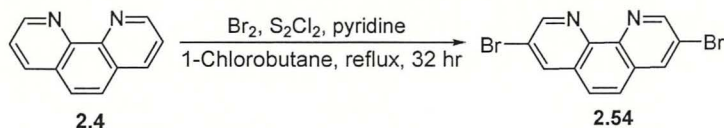


A suspension α -keto-oxime salt **2.95** (25 mg) in water (5 mL) was neutralised with diluted H_2SO_4 (10%) and then extracted with dichloromethane (2×5 mL). The combined organic layers were washed with water (2×5 mL), dried with anhydrous $MgSO_4$, filtered off and evaporated to afford crude product **2.96** as a yellowish solid (9 mg, 38%). Crude product was not purified. Purity by 1H NMR was about 70%.

1H NMR (400 MHz, $CDCl_3$): δ (ppm) 9.50 (1H, d, $J = 2.1$ Hz), 9.33 (1H, d, $J = 2.3$ Hz), 9.10 (1H, d, $J = 2.1$ Hz), 9.06 (1H, d, $J = 2.3$ Hz), 2.17 (1H, s).

3,8-Dibromo-1,10-phenanthroline (**2.54**)⁷²

SG176



Procedure for the synthesis of 3,8-dibromo-1,10-phenanthroline (**2.54**) was adapted from reference 72 with some modification and was successfully used upto 50 g scale reaction is described below:

1,10-Phenanthroline (**2.4**) (50.03 g, 0.252 mol), sulphur monochloride (60.31 g, 0.96 mol), pyridine (21.01 g, 0.27 mol) and 1-chlorobutane (1.2 L) were charged in a three necked 2 L round bottom flask fitted with water condenser (mechanical overhead stirrer was used for stirring). Bromine (133.2g, 0.83 mol) was added carefully dropwise to this mixture at room temperature under stirring for 15 min. The mixture was then stirred under reflux (90 °C internal temperature) for 32 hours and allowed to cool to room temperature, during which yellowish-white solid was precipitated. The yellowish solution was carefully decanted off (*note: odious liquid should be disposed of separately*) and the residue was washed with diethyl ether (2 × 200 mL). Water (500 mL) was added to the remaining whitish solid residue, stirred and basified with 50% aqueous NaOH to pH ~10. The product was then extracted from this basic aqueous mixture with dichloromethane (3 × 500 mL). The combined organic layers were washed with water (2 × 800 mL), followed by washing with brine (2 × 800 mL), dried with anhydrous MgSO_4 , filtered off and evaporated to afford the crude product as brown solid (108.6 g). Crude product was purified by passing through silica gel column (10 × 10 cm) eluting initially with PE (1 L) to remove by-products and then with PE: CHCl_3 = 1:1 v/v (3 L) to afford pure dibromophenanthroline **2.54** as a white solid (61.2 g, 72 %).

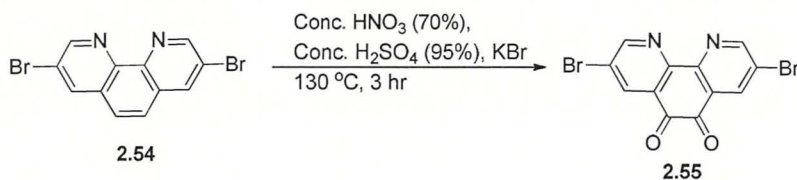
^1H NMR (400 MHz, CDCl_3): δ (ppm) 9.18 (2H, d, J = 2.2 Hz), 8.41 (2H, d, J = 2.2 Hz), 7.75 (2H, s).

^{13}C NMR (100 MHz, CDCl_3): δ (ppm) 151.6, 144.14, 137.54, 129.58, 126.86, 120.21

GC-MS (EI^+) m/z : 336.2 (M^+ , 51%, ^{79}Br , ^{79}Br), 338.1 (M^+ , 100%, ^{79}Br , ^{81}Br), 340 (M^+ , 50%, ^{81}Br , ^{81}Br). Calcd. for $\text{C}_{12}\text{H}_6\text{Br}_2\text{N}_2$: 335.89.

3,8-Dibromo-1,10-phenanthroline-5,6-dione (**2.55**)⁷⁴

Exp: SG166



In an ice cold mixture of conc. nitric acid (12.2 mL; 70%, $d = 1.41 \text{ g mL}^{-1}$, 0.27 mol) and conc. sulphuric acid (24.1 mL; 95%, $d = 1.84 \text{ g mL}^{-1}$, 0.45 mol), was added to 3,8-dibromo-1,10-phenanthroline (**2.54**) (2.01 g, 1.48 mol) and KBr (2.05 g, 0.02 mol). The reaction mixture was stirred with reflux (130 °C, oil bath) for 3 hours, allowed to cooled down to room temperature and poured into ice-cold water (200 mL). 15% Aqueous NaOH was added slowly to the mixture with stirring to adjust pH of the solution to not more than pH ~ 1 to 3, while keeping the temperature of the mixture at 20–25 °C using an ice bath. The light yellow precipitate formed was filtered off, carefully washed with water until neutral and then dried to afford crude product as yellow solid (1.66 g). Filtrate (colourless) was extracted with DCM (2 × 100 mL), dried with anhydrous MgSO_4 , filtered off and solvent was evaporated to afford additional portion of crude product (301 mg) as yellow solid. The combined crude products (1.96 g) were purified by column chromatography on silica gel eluting with PE:EA = 4:1 v/v to yield pure dibromophenanthroline **2.55** as a yellow solid (1.69 g, 77%).

$^1\text{H NMR}$ (400 MHz, CDCl_3): δ (ppm) 9.14 (2H, d, $J = 2.3 \text{ Hz}$), 8.60 (2H, d, $J = 2.3 \text{ Hz}$).

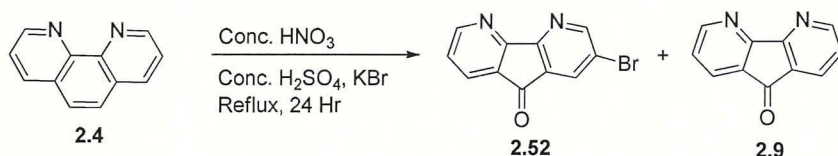
DEPTQ (100 MHz, CDCl_3): δ (ppm) 177.12 (CO), 157.23 (CH), 150.32, 139.82(CH), 128.44, 123.51.

$^{13}\text{C NMR}$ (100 MHz, CDCl_3): δ (ppm) 177.12, 157.59, 150.46, 139.52, 128.44, 123.57.

GC-MS (EI^+) m/z : 337.9 ($[\text{M} - 28 (\text{CO})]^+$, 46%, ^{79}Br , ^{79}Br), 339.9 ($[\text{M} - 28 (\text{CO})]^+$, 100%, ^{79}Br , ^{81}Br), 340 ($[\text{M} - 28 (\text{CO})]^+$, 50%, ^{81}Br , ^{81}Br). Calcd for $\text{C}_{12}\text{H}_4\text{Br}_2\text{N}_2\text{O}$: 365.86.

2-Bromo-4,5-diazafluoren-9-one (**2.52**)³⁸

Exp: SG-019



In a 50 mL two-necked round bottom flask has been charged with 1,10-phenanthroline (**2.4**) (1.12 g, 5.04 mmol), potassium bromide (720 mg, 6.04 mmol), concentrated nitric acid (6 mL; 70%, $d = 1.41 \text{ g mL}^{-1}$, 0.09 mol), and concentrated sulphuric acid (12 mL, 95%, $d = 1.84 \text{ g mL}^{-1}$, 0.21 mol) at room temperature. The reaction mixture was then stirred under reflux (130 °C, oil bath) for 24 hours. The mixture was allowed to cool down to room temperature and poured into water (150 mL). Solid sodium hydroxide has been added to neutralize the acidic solution until $\text{pH} = 7$. The precipitated inorganic salts were filtered off and washed on the filter with chloroform ($3 \times 20 \text{ mL}$). The chloroform layer was separated and the aqueous layer was extracted with chloroform ($2 \times 50 \text{ mL}$). The combined organic layers were washed with water ($2 \times 20 \text{ mL}$), dried over anhydrous MgSO_4 and evaporated to afford crude product (800 mg, 66%) as a dark brown solid. The crude product was purified by column chromatography on silica gel eluting with PE:EA = 2:1 v/v ratio initially and then with 1:1 ratio to isolate two products, pure monobromoDAFone **2.52** as yellow solid (150 mg, 11%) and DAFone (**2.9**) as off-white solid (300 mg, 26%).

Analysis of product **2.52**:

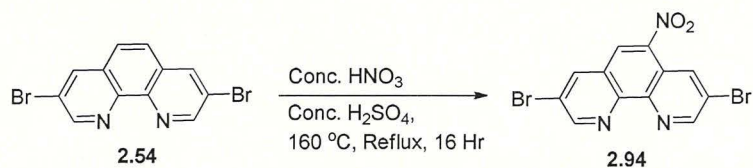
¹H NMR (500 MHz, CDCl_3): δ (ppm) 8.87 (1H, s), 8.82 (1H, d, $J = 5.0 \text{ Hz}$), 8.11 (1H, s), 8.017 (1H, d, $J = 7.6 \text{ Hz}$), 7.40 (1H, dd, $J = 7.5, 2.3 \text{ Hz}$).

¹³C NMR (100 MHz, CDCl_3): δ (ppm) 188.11, 162.73, 161.39, 156.00, 155.54, 134.21, 131.81, 130.46, 129.22, 124.98, 122.32.

GC-MS (EI^+) m/z : 260.0 (M^+ , 100%, ⁷⁹Br), 262.0 (M^+ , 95%, ⁸¹Br). Calcd. for $\text{C}_{11}\text{H}_5\text{BrN}_2\text{O}$: 259.96.

3,8-Dibromo-5-nitro-1,10-phenanthroline (2.94)

Exp: SG 115



500 mL Two necked round bottom flask was charged with 3,8-dibromo-1,10-phenanthroline (**2.54**) (5.01 g, 14.8 mol), concentrated nitric acid (15.1 mL; 70%, $d = 1.41 \text{ g mL}^{-1}$) and concentrated sulphuric acid (30.2 mL; 95%, $d = 1.84 \text{ g mL}^{-1}$). The reaction mixture was stirred under reflux (160 °C, oil bath) for 16 hours. The reaction mixture was allowed to cooled down to room temperature and poured into ice-cold water (100 mL). Saturated sodium hydroxide solution was added to adjust the pH of the solution to ca. 1 to 3. The formed yellow precipitate was filtered off, washed with water and dried in an oven at 100 °C for 1 hour to afford crude compound **2.94** as yellow solid (2.90 g, 51%). The crude product was purified by column chromatography on silica gel eluting with PE:EA = 1:1 v/v ratio to afford pure product **2.94** as a light yellow solid (2.21 g, 39%).

¹H NMR (400 MHz, CDCl₃): δ (ppm) 9.33 (1H, d, $J = 2.2$ Hz), 9.29 (1H, d, $J = 2.0$ Hz), 9.24 (1H, d, $J = 2.2$ Hz), 8.67 (1H, s), 8.58 (1H, d, $J = 2.2$ Hz).

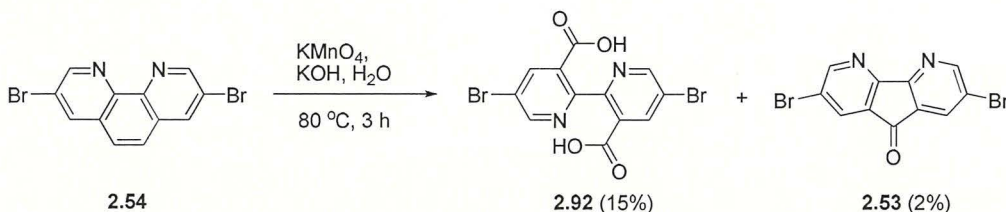
DEBQ (100 MHz, CDCl₃): δ (ppm) 155.05 (CH), 153.95 (CH), 145.61, 144.29, 145.61, 139.28 (CH), 134.56 (CH), 126.43, 125.71 (CH), 122.42, 121.88, 121.62.

¹³C NMR (100 MHz, CDCl₃): δ (ppm) 155.04, 153.04, 145.60, 144.25, 143.89, 139.25, 134.55, 126.43, 125.71, 122.42, 121.92, 121.62.

GC-MS (EI⁺) m/z : 382.9 (M⁺, 100%, ⁷⁹Br, ⁸¹Br), 380.9 (M⁺, 51%, ⁷⁹Br), 384.9 (M⁺, 49%, ⁸¹Br). Calcd. for C₁₂H₅Br₂N₃O₂: 380.87.

5,5'-Dibromo-[2,2'-bipyridine]-3,3'-dicarboxylic acid (2.92)

Exp: TOM 06



3,8-Dibromo-1,10-phenanthroline (**2.54**) (2.01 g, 5.92 mmol) and KOH (0.16 g, 10.8 mmol) were added to water (50 mL) and brought to reflux (110 °C, oil bath). Potassium permanganate (2.96 g, 18.7 mmol) dissolved in water (25 mL) was dropwise added to the refluxing mixture and reflux was continued for 3 hours. The mixture was allowed to cool

down, then filtered off to remove MnO₂ and the solid was washed with water (30 mL). Filtrate (clear aqueous solution) was stirred with dichloromethane (50 mL) for 15 minutes. Organic layer was separated and evaporated to afford crude product **2.53** as yellow solid (41 mg, 2%). The filtrate (aqueous layer) was acidified with diluted HCl and then extracted with chloroform (2 × 50 mL). Combined organic layers were washed with water (2 × 30 mL), dried with MgSO₄ and evaporated to afford pure product **2.92** as white solid (363 mg, 15%).

Analysis for product **2.92**:

¹H NMR (400 MHz, DMSO-*d*₆): δ (ppm) 8.78 (2H, d, *J* = 2.1 Hz), 8.3 (2H, br.s).

DEPTQ (100 MHz, DMSO-*d*₆): δ (ppm) 166.52 (COOH), 155.31, 150.66 (CH), 139.04 (CH), 131.09, 119.41.

¹³C NMR (100 MHz, DMSO-*d*₆): δ (ppm) 166.52, 155.27, 150.65, 139.03, 131.09, 119.41.

References

- 1 J. U. Wallace and S. H. Chen, in: *Polyfluorenes, Advances in Polymer Science – Vol. 212*, U. Scherf and D. Neher (Eds.), Springer-Verlag, **2008**, pp. 145–180.
- 2 D. F. Perepichka, I. F. Perepichka, H. Meng, and F. Wudl, in: *Organic Light Emitting Materials and Devices*, Z. Li and H. Meng (Eds.), CRC Press, Boca Raton, FL, **2007**, Chapter 2, pp. 45–293.
- 3 A. C. Grimsdale, K. L. Chan, R. E. Martin, P. G. Jokisz, and A. B. Holmes, *Chem. Rev.* **2009**, *109*, 897.
- 4 K.-T. Wong, Y.-Y. Chien, R.-T. Chen, C.-F. Wang, Y.-T. Lin, H.-H. Chiang, P.-Y. Hsieh, C.-C. Wu, C. Chou, Y. Su, G.-H. Lee, S.-M. Peng, *J. Am. Chem. Soc.*, **2002**, *124*, 11576.
- 5 K. Ono and K. Saito, *Heterocycles*, **2008**, *75*, 2381.
- 6 R. P. Thummel, F. Lefoulon, and R. Mahadevan, *J. Org. Chem.*, **1985**, *50*, 3824.
- 7 L. J. Henderson, F. R. Fronczek, and W. R. Cherry, *J. Am. Chem. Soc.*, **1984**, *20*, 5876.
- 8 J. P. Mazaleyrat, K. Wright, M. Wakselman, F. Formaggio, M. Crisma, and C. Toniolo, *Eur. J. Org. Chem.*, **2001**, 1821.
- 9 (a) J. Mlochowski and Z. Szulc, *Polish J. Chem.*, **1983**, *57*, 33. (b) P. Piotrowiak, R. Kobectic, R. Timothy, and S. Tapper, *Bull Polish Acad. Sci., Chemistry*, **1994**, *42*, 445. (c) Q. Wang, G. J. Zhou, O. M. Keung, W. Y. Wong, M. C. W. Marcus, G. L. Lu, C. L. Ho, K. H. Lam, X. M. Tao, F. Cheung, C. H. Chui, R. Gambari, R. S. M. Wong, S. W. Tong, K. W. Chan, F. Y. Lau, and G. Y. M. Cheng, *Chem. Med. Chem.*, **2010**, *5*, 559.
- 10 M. J. Plater, S. Kemp, and E. Lattmann, *J. Chem. Soc., Perkin Trans. I*, **2000**, 971.
- 11 M. Riklin, A. von Zelewsky, A. Bashall, M. McPartlin, A. Baysal, J. A. Connor, and J. D. Wallis, *Helv. Chim. Acta.*, **1999**, *63*, 1675.
- 12 (a) K. Sako, M. Kusakabe, and H. Tatemitsu, *Mol. Cryst. Liq. Cryst.*, **1996**, *285*, 101. (b) K. Sako, Y. Misaki, M. Fujiwara, T. Maitani, and H. Tatemitsu, *Chem. Lett.*, **2002**, 592.
- 13 K. Sako, Y. Mugishima, T. Iwanaga, S. Toyota, H. Takemura, M. Watanabe, T. Shinmyozu, M. Shiotsuka, and H. Tatemitsu, *Tetrahedron Lett.*, **2011**, *52*, 5865.

-
- 14 Y. Wang and D.P Rillema, *Tetrahedron*, **1997**, *53*, 12377.
- 15 Y. Wang, W. J. Perez, G.Y. Zheng, D.P. Rillema, and C. L. Huber, *Inorg. Chem.*, **1998**, *37*, 2227.
- 16 Y. Wang and D.P Rillema, *Inorg. Chem. Commun.*, **1998**, *1*, 27.
- 17 S. Bernhard and P. Belser, *Synthesis*, **1996**, 192.
- 18 (a) S. Bernhard and P. Belser, *Synthesis*, **1996**, *26*, 3559. (b) R. N. Warrener, A. B. B. Ferreira, and E. R. T. Tiekink, *Tetrahedron Lett.*, **1996**, *37*, 2161. (c) R. N. Warrener, A. B. B. Ferreira, A. C. Schultz, D. N. Butler, F. R. Keene, and L. S. Kelso, *Angew. Chem. Int. Ed. Engl.*, **1996**, *35*, 2485.
- 19 H.-C. Su, H.-F. Chen, C.-C. Wu, and K.-T. Wong, *Chem. Asian J.*, **2008**, *3*, 1922.
- 20 Q. Wang, M. C.-W. Yuen, G.-L. Lu, C.-L. Ho, G.-J. Zhou, O.-M. Keung, K.-H. Lam, R. Gambari, X.-M. Tao, R. S.-M. Wong, S.-W. Tong, K.-W. Chan, F.-Y. Lau, F. Cheung, G. Y.-M. Cheng, C.-H. Chui, and W.-Y. Wong, *Chem. Med. Chem.*, **2010**, *5*, 559.
- 21 K. Ono, T. Yanase, M. Ohkita, K. Saito, Y. Matsuhita, S. Naka, K. Okada, and H. Onnagawa, *Chem. Lett.*, **2004**, *33*, 276.
- 22 Z. Liu, F. Wen, and W. Li, *Thin Solid Films*, **2005**, *478*, 265.
- 23 K.-T. Wong, R.-T. Chen, F.-C. Fang, C.-C. Wu, and Y.-T. Lin, *Org. Lett.*, **2005**, *7*, 1979.
- 24 C. W. Tang and S. A. Van Slyke, *Appl. Phys. Lett.*, **1987**, *51*, 913.
- 25 C. Adachi, S. Tokito, T. Tsutsui, and S. Saito, *Jpn. J. Appl. Phys.*, **1988**, *27*, L713.
- 26 K. Ono, M. Tomura, and K. Saito, *Acta. Cryst. E*, **2007**, *63*, o4612.
- 27 K. Ono, H. Tanaka, M. Shiozawa, T. Motohiro, S. Kunikane, and K. Saito, *Chem. Lett.*, **2007**, *36*, 892.
- 28 C.-C. Wu, Y.-T. Lin, K.-T. Wong, R.-T. Chen, and Y.-Y. Chin, *Adv. Mater.*, **2004**, *16*, 61.
- 29 K.-T. Wong, T.-Y. Huw, A. Balaiah, T.-C. Chao, F.-C. Fang, C.-T. Lee, and Y.-C. Peng, *Org. Lett.*, **2005**, *7*, 141.
- 30 J. R. Lakowicz, *Principles of Fluorescence Spectroscopy*, Springer, 3rd Ed., **2006**.
- 31 B. Valeur, *Molecular Fluorescence: Principles and Applications*, Wiley-VCH, **2001**.
- 32 Z. Liu, W. He, and Z. Guo, *Chem. Soc. Rev.*, **2013**, *42*, 1568.
- 33 K.-T. Wong, H.-F. Chen, and F.-C. Fang, *Org. Lett.*, **2006**, *8*, 3501.
- 34 K. One, K. Nagano, M. Suto, and K. Saito, *Heterocycles*, **2007**, *71*, 799.
- 35 T. Harel, N. Shefer, Y. Hagooley, and S. Rozen, *Tetrahedron*, **2010**, *66*, 3297.
- 36 F.-W. Yen, C.-Y. Chiu, I.-F. Lin, C.-M. Teng and P.-C. Yen, *U. S. Patent* US7282586-B1, **2007**.
- 37 H. Ohrui, A. Senoo, and T. Kosuge, *U.S. Patent* US200816574-A1, **2008**.
- 38 H.-F. Chen, W.-Y. Huang, S.-W. Chen, T.-C. Wang, S.-W. Lin, S.-H. Chou, C.-T. Liao, H.-C. Su, H.-A. Pan, P.-T. Chou, Y.-H. Liu, and K.-T. Wong, *Inorg. Chem.*, **2012**, *51*, 12114.
- 39 J.-F. Zhao, L. Chen, P.-J. Sun, X.-Y. Hou, X.-H. Zhao, W.-J. Li, L.-H. Xie, Y. Qian, N.-E. Shi, W.-Y. Lai, Q.-L. Fan, and W. Huang, *Tetrahedron*, **2011**, *67*, 1977.
- 40 W.-J. Li, H.-M. Wu, Y.-B. Li, C.-P. Hu, M.-D. Yi, L.-H. Xie, L. Chen, J.-F. Zhao, X.-H. Zhao, N.-E. Shi, Y. Qian, C. Wang, W. Wei, and W. Huang, *Tetrahedron*, **2012**, *68*, 8216.
- 41 W.-J. Li, B. Liu, Y. Qian, L.-H. Xie, J. Wang, S.-B. Li, and W. Huang, *Polym. Chem.*, **2013**, *4*, 1796.
- 42 M. J. Blandamer, J. Burgess, R. John, R. Sherry, R. Haines, and I. Robert, *J. Chem. Soc., Chem. Commun.*, **1980**, 354.
- 43 M. Ocafrain, E. Dolhem, J. Y. Nedelec, and M. Troupel, *J. Organomet. Chem.* **1998**, *571*, 37.

-
- 44 A. M. Pyle, J. P. Rehman R. Meshoyer, C. V. Kumar, N. J. Turro, and J. K. Barton, *J. Am. Chem. Soc.*, **1989**, *111*, 3051.
- 45 L. J. Henderson, Jr., F.R. Fronczek, and W. R. Cherry, *J. Am. Chem. Soc.*, **1984**, *106*, 5876.
- 46 S. Menon and M. V. Rajasekharan, *Inorg. Chem.*, **1997**, *36*, 4983.
- 47 O. S. Jung and C. G. Pierpont, *Inorg. Chem.*, **1994**, *33*, 2227.
- 48 A. Kilic, F. Durap, M. Aydemir, A. Basal, and E. Tas, *J. Organomet. Chem.*, **2008**, *693*, 2835.
- 49 R. G. Xiong, J. Zuo, E. J. Xu, X. Z. Xiao, and X. T. Huang, *Acta Cryst. C*, **1996**, *52*, 521.
- 50 Y. Wang and D. P. Rillema, *Tetrahedron Lett.*, **1988**, *38*, 6627.
- 51 F. Cheng, C. He, H. Yin, N. Tang, and N. Hou, *Z. Anorg. Allg. Chem.*, **2013**, *639*, 1284.
- 52 F. Cheng, J. Chen, F. Wang, N. Tang, and L. Chen, *Trans. Met. Chem.*, **2011**, *36*, 573
- 53 F. Cheng, C. He, H. Yin, and N. Tang, *Trans. Met. Chem.*, **2013**, *38*, 259.
- 54 H. Jiang and D. Song, *Organometallics*, **2008**, *27*, 3587.
- 55 G. F. Swiegers and T. J. Malefetse, *Chem. Rev.*, **2000**, *100*, 3483.
- 56 J. L. Boyer, M. L. Kuhlman, and T. B. Rauchfuss, *Acc. Chem. Res.*, **2007**, *40*, 233.
- 57 R. Tan, F. S. N. Chiu, A. Hadzovic, and D. Song, *Organometallics*, **2012**, *31*, 2184.
- 58 G. Nocton, C. H. Booth, L. Maron, and R. A. Andersen, *Organometallics*, **2013**, *32*, 1150.
- 59 A. N. Campbell, P. B. White, I. Guzei, and S. S. Stahl, *J. Am. Chem. Soc.*, **2010**, *132*, 15116.
- 60 A. N. Campbell, E. B. Meyer, and S. S. Stahl, *Chem. Commun.*, **2011**, *47*, 10257.
- 61 (a) D. R. Stuart and K. Fagnou, *Science*, **2007**, *316*, 1172. (b) D. R. Stuart, E. Villemure, and K. Fagnou, *J. Am. Chem. Soc.*, **2007**, *129*, 12072.
- 62 (a) S. S. Stahl, *Angew. Chem. Int. Ed.*, **2004**, *43*, 3400. (b) K. M. Gligorich and M.S. Sigman, *Chem. Commun.*, **2009**, 3854.
- 63 W. Qian and Y. Rubin, *Angew. Chem. Int. Ed.*, **1999**, *38*, 2356.
- 64 W. Qian and Y. Rubin, *J. Am. Chem. Soc.*, **2000**, *122*, 9564.
- 65 P. Peng, F.-F. Li, F. L. Bowles, V. S. P. K. Neti, A. J. M. Magana, M. M. Olmstead, A. L. Balch, and L. Echegoyen, *Chem. Comm.*, **2013**, *49*, 3209.
- 66 H.-C. Su, F.-C. Fang, T.-Y. Hwu, H.-H. Hsieh, H.-F. Chen, G.-H. Lee, S.-M. Peng, K.-T. Wong, and C.-C. Wu, *Adv. Funct. Mater.*, **2007**, *17*, 1019.
- 67 H.-C. Su, H.-F. Chen, F.-C. Fang, C.-C. Liu, C.-C. Wu, K.-T. Wong, Y.-H. Liu, and S.-M. Peng, *J. Am. Chem. Soc.*, **2008**, *130*, 3413.
- 68 C. Ulbricht, B. Beyer, C. Friebe, A. Winter, and U. S. Schubert, *Adv. Mater.*, **2009**, *21*, 4418.
- 69 (a) J. Gallos and A. Varvoglis, *J. Chem. Res.*, **1982**, *6*, 1649. (b) X. Zhang, J. B. Han, P. F. Li, X. Ji, and Z. Zhang, *Synth. Commun.*, **2009**, *39*, 3804.
- 70 J. Mlochoski and Z. Szulc, *J. Prakt. Chem.*, **1980**, *322*, 971.
- 71 I. I. Perepichka, I. F. Perepichka, M. R. Bryce, and L.-O. Pålsson, *Chem. Commun.*, **2005**, 3397.
- 72 Y. Saitoh, T. Koizumi, K. Osakada, T. Yamamoto, *Can. J. Chem.*, **1997**, *75*, 1336.
- 73 R. D. Gillard, R. P. Houghton, and J. N. Tucker, *J. Chem. Soc., Dalton Trans.*, **1980**, 2102.
- 74 W.-J. Li, H.-M. Wu, Y.-B. Li, C.-P. Hu, M.-D. Yi, L.-H. Xie, L. Chen, J.-F. Zhao, X.-H. Zhao, N.-E. Shi, Y. Qian, C. Wang, W. Wei, and W. Huang, *Tetrahedron*, **2012**, *68*, 8216.
- 75 J.-F. Zhao, L. Chen, P.-J. Sun, X.-Y. Hou, X.-H. Zhao, W.-J. Li, L.-H. Xie, Y. Qian, N.-E. Shi, W.-Y. Lai Q.-L. Fan, and W. Huang, *Tetrahedron*, **2011**, *67*, 1977.

Chapter 3

Cationic Iridium Complexes as Emissive Materials for Light-Emitting Electrochemical Cells

3.1 Introduction

3.1.1 Transition metal complexes for application in light-emitting electrochemical cells

Phosphorescent transition metal complexes are a major focus of research as highly efficient emissive materials for electroluminescent devices such as organic light-emitting diodes (OLED),^{1,2,3} light-emitting electrochemical cells (LEC)^{2,10,12} as well as for other applications such as organic photovoltaics (OPV),^{4,5} chemical sensors^{6,7} and bio-imaging.^{7,8,9} In this regard, the most studied phosphorescent transition metal complexes during the last decade are in this regard based on Cu(I), Cu(II), Cr(III), Re(I), Re(III), Ru(II), Os(II), Ir(III), Pt(II), Pd(II), Au(I) and Au(III) metal cations.^{10,11} In recent years, ionic transition metal complexes (iTMCs) have been extensively investigated as materials for the next generation electronic displays and light-emitting devices. Among them, the cationic iridium complexes have emerged as one of the best candidates for LEC owing to their superior properties such as high quantum yields of emission and facile colour tuning through chemical modification of the ligands.^{10,11,12} Moreover, the phosphorescent nature of iridium complexes (triplet emitters), due to their strong spin-orbit coupling, allows harvesting of emission from both singlet and triplet state excitons resulting up to theoretical limits of 100% internal efficiency (i.e. the number of emitted photons per injected holes/electrons). In other words, the electroluminescent devices made of Ir complexes can reach up to four times the efficiency compared to similar devices composed of purely organic singlet emitters (fluorescent emitter).^{13,14,15} Therefore, design of new complexes, elaboration of methods of their syntheses and finding new ligands for construction of cyclometalated Ir complexes are currently considered to be a hot and promising area of research.

3.1.2 Development of LEC based on ionic transition metals: a brief overview

LEC is emerging as alternatives to OLED because of their simple architecture (Fig. 3.1), easy solution processing, insensitivity toward the work functions of the used electrodes, ability to use air-sensitive electrodes, operate at low voltage, and cost-effectiveness. As mentioned before, the cationic iridium complexes have been increasingly investigated as emissive materials for LEC. They possess several advantages over conventional LEC or polymer LEC because: (a) no additional ion conducting material is needed since the metal complexes are intrinsically ionic; (b) higher electroluminescent efficiency can be achieved due to their phosphorescent nature and (c) good solubility in polar organic solvents or even in aqueous media. Moreover, the emissive layers of LEC contain mobile ions which drift towards the electrode under an applied voltage, inducing doping and consequently Ohmic contacts with the electrodes.^{16,48} These advantages will bring down the cost of visual displays and lighting sources substantially. The operating mechanism of LEC has been discussed in Chapter 1 (Section 1.4).

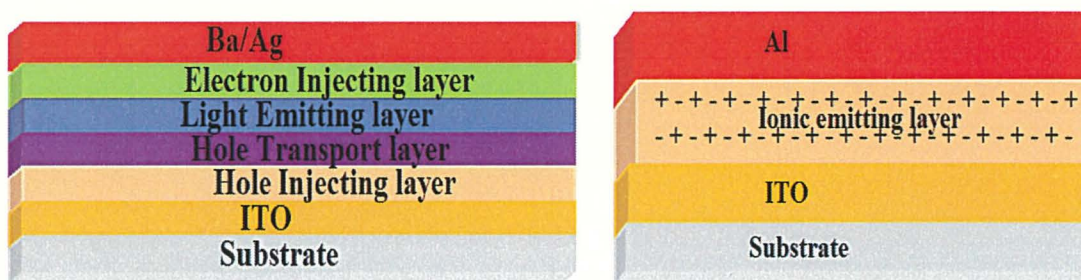


Fig. 3.1 Device structure of OLED and LEC.

Early researches on LEC were focused on Ru(II) and Os(II) complexes and recently ionic Cu(I) and Ir(III) complexes are emerging as ideal materials.^{12,25} The first iTMC based electroluminescent device was reported in 1996 by Rubner *et al.* working at MIT.¹⁷ They demonstrated that a number of thin electroluminescent devices could be fabricated from ruthenium tris-phenanthroline complex **3.1** (the structure is shown in Fig. 3.2) by a simple solution processing. The ruthenium tris-phenanthroline complex **3.1** is an orange-red emitter and the typical light-voltage (L-V) and current-voltage (I-V) curves for a configuration ITO/Ru-complex/Al device are shown in Fig. 3.2. It was also demonstrated that turn-on time of the devices was independent of the film thickness. Further, the device efficiency has been improved up to 0.05% for the ruthenium polyphenanthroline complex by using a self-assembled bilayer of conjugated polymer poly(phenylenevinylene).

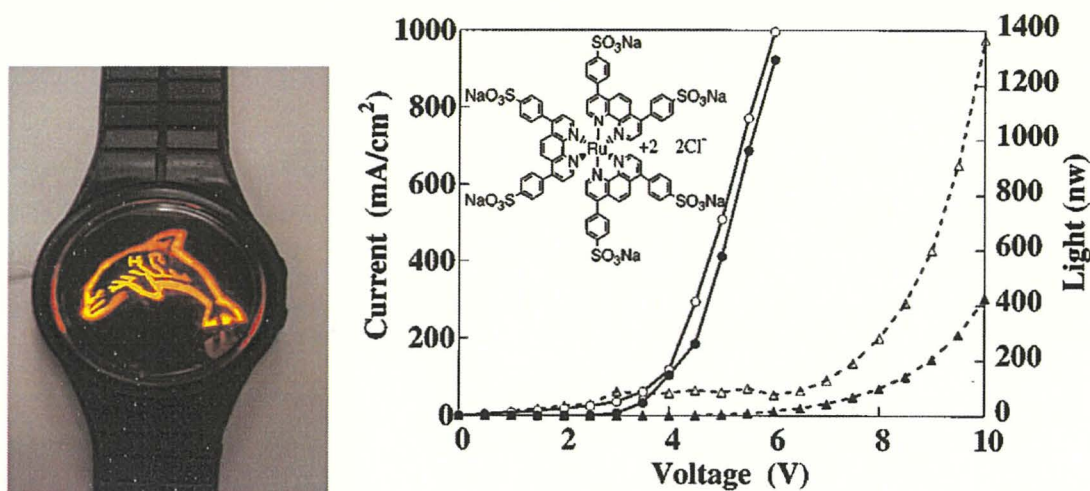


Fig. 3.2 Electroluminescent device based on $[\text{Ru}(\text{bpy})_3]^{2+}$ (left) and light-voltage and current-voltage curves (right) obtained for Ru-polyphenanthroline complex in configuration ITO/Ru-complex/Al device utilising a spin cast film (circles) and a self-assembled film (triangle) of Ru-complex **3.1** (structure is shown as inset).¹⁷

Gong *et al.*¹⁸ reported neutral rhenium (I) (Re^{I}) bipyridine complex for the first time as a light-emitting material. They used the rhenium complex blended in polycarbonate and the ruthenium complex blended in poly(vinyl alcohol) for the fabrication of devices, and the reported device efficiency was about 0.1%. It may be noted that this rhenium complex based device (as it is neutral) represents typical device characteristics of OLED.

The use of different cathode metals such as Al, Ag and Pt resulted in similar device turn-on voltages for ruthenium complex reported by Lyons *et al.*¹⁹ They demonstrated that LEC based on iTMC are independent of electrode work function. Lyons' group also investigated the use of solid electrolyte ($\text{CF}_3\text{SO}_3\text{Li}$) for increasing the device performance of the ruthenium complex. It was demonstrated that device efficiency up to 3% could be achieved using Ru complex.²⁰ Active research followed to increase the performance of Ru complex highlighted in the review article by Malliaras *et al.* in 2003.²¹

Bernhard *et al.* reported electroluminescent devices with efficiencies of ~1% based on osmium complexes that emitted in red-orange region.²² As Ru and Os complexes suffered from the low luminescence efficiency, which limits their practical applications in LEC, further works in search of novel emitters have been shifted to the other transition (and non-transition) metals complexes that can achieve higher device performance. Thus, ionic copper complexes were later studied for LEC, in which case an external quantum efficiency of up to

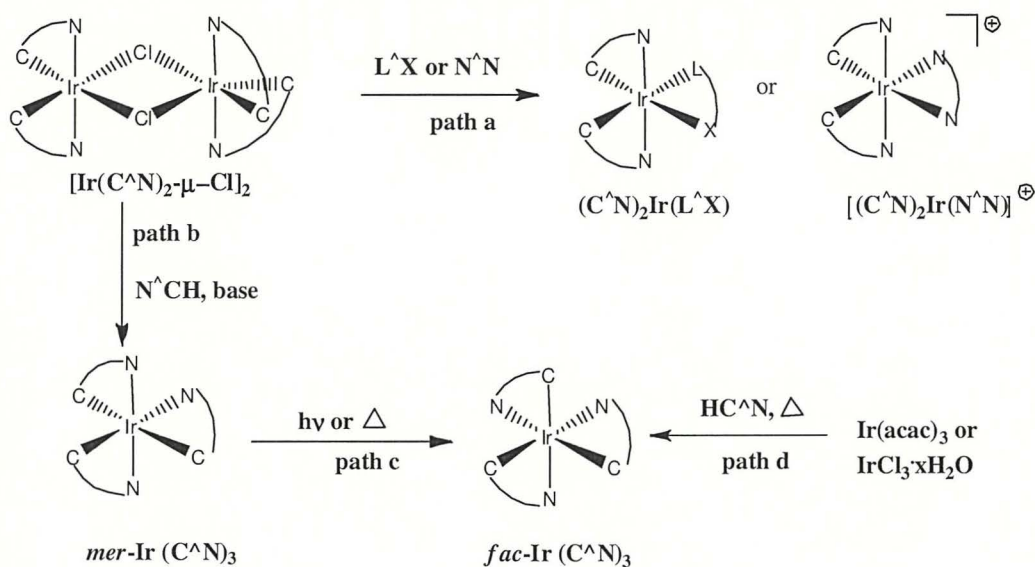
16% was achieved with Al as cathode, but they suffer from the low ligand field stabilisation energies (LFSE) and emit in the long wavelength region of the visible-spectrum, which is not favourable for their practical applications in LEC.²³ The era of Ir complexes as emissive materials began in 2004 when Malliaras' group reported for the first time the use of Ir complexes in LEC.²⁴ According to the authors, Ir complexes have an increased LFSE, which leads to high photo-stability compared to its Ru counterpart. Since then, there have been widespread researches on Ir complexes as the emissive materials for LEC, as is evident from several review articles.^{25,26,27}

3.1.3 General method of the synthesis of iridium(III) complexes and their properties

A wide range of iridium complexes including *mono*-, *bis*- and *tris*-cyclometalated complexes have been synthesised from commercial iridium(III) chloride salt ($\text{IrCl}_3 \times \text{H}_2\text{O}$). Depending on the electron donating ability of the ligand to the central metal, these complexes can be classified in two categories. First, anionic ligand (chloride, cyclometalating ligand) which donate electron density to the metal centre and so the emitting excited states undergoes metal-to-ligand charge transfer (MLCT) and thus oxidation of the metal centre is observed. Second, neutral ligand, which donates less charge density to the metal centre and undergoes emission from the ligand centre, in which case no oxidation of the metal centre is observed. The reduction process for all such complexes are ligand-centred.^{28,29,30,31}

Scheme 3.1 represents the most common strategy for design of various types of Ir(III) complexes. Reaction of an appropriate ligand with $\text{IrCl}_3 \times \text{H}_2\text{O}$ produces a μ -dichloro bridged dimer, $[\text{Ir}(\text{C}^{\wedge}\text{N})_2 \cdot \mu\text{Cl}]_2$, which plays a significant role in the coordination chemistry of such complexes.³² The arc represents the cyclometalating ligand which is abbreviated as $\text{C}^{\wedge}\text{N}$. The chloro-bridged dimer, $[\text{Ir}(\text{C}^{\wedge}\text{N})_2 \cdot \mu\text{Cl}]_2$, can be splitted into a neutral complex or a charged *bis*-cyclometalated complex by reacting with chelating ligand $\text{L}^{\wedge}\text{X}$ (such as β -diketonates, salicylanilide etc.) or $\text{N}^{\wedge}\text{N}$ (such as phen, bpy) with a *trans*- N,N configuration to the $\text{C}^{\wedge}\text{N}$ ligand. *Tris*-cyclometalating complexes can be obtained by the addition of third cyclometalating ligand ($\text{C}^{\wedge}\text{N}$) (Scheme 3.1, path b). By careful selection of the reaction conditions, pure meridional complex can be obtained, including both homoleptic (one type of $\text{C}^{\wedge}\text{N}$ ligand)³³ and heteroleptic *tris*-complexes (different types of $\text{C}^{\wedge}\text{N}$ ligands).^{34,35} A number of meridional complexes *mer*- $\text{Ir}(\text{C}^{\wedge}\text{N})_3$ have been reported to isomerise to facial complexes *fac*- $\text{Ir}(\text{C}^{\wedge}\text{N})_3$ by photolysis or thermal processes (Scheme 3.1, path c). This isomerisation indicates that the meridional complexes are kinetically controlled products whereas the facial complexes are thermodynamically controlled products. To the best of our knowledge, such

isomerisation for cationic iridium complexes $[\text{Ir}(\text{C}^{\wedge}\text{N})(\text{L}^{\wedge}\text{X})]^+$ has not been reported. The thermodynamically controlled facial complexes have been obtained directly for some Ir complexes and are well known for the thermal reaction between ppy and its derivatives ligand with Ir(acac) precursor (acac = acetylacetonate) (path d).^{30,31}



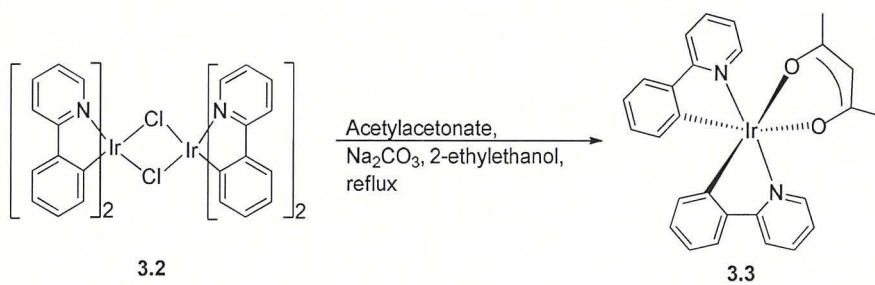
Scheme 3.1 Common synthetic routes to various types of cyclometalated Ir(III) complexes.

Several research groups have demonstrated that the luminescence of iridium complexes originates from the lowest excited state, that is as ligand centred triplet (^3LC) with singlet and triplet metal-to-ligand charge transfer ($^1\text{MLCT}$, $^3\text{MLCT}$) character mixed in through spin-orbit coupling.^{36,37} While both $^1\text{MLCT}$ and $^3\text{MLCT}$ states are mixed with ^3LC states in the emissive state, but it is the $^1\text{MLCT}$ component which provides the predominant change on the physical properties of the Ir complexes.²⁹ Molecular orbital (MO) calculations by density functional theory (DFT) method also predict mixed nature of the excited state for these complexes. DFT calculations provide good predictions of the bond length, angles (often similar to those determined by X-ray crystallography) and photophysical properties such as absorption and emission spectra and HOMO–LUMO energies of Ir complexes. There are instances when time-dependent density functional theory (TD-DFT) calculations provide values that are very close to experimental emission energies. Thus, DFT calculation is an important tool for chemists (not necessarily theoretical scientists) in providing assistance in design of new complexes with desired emission properties of electroluminescent materials. For instance, Yoon *et al.* recently reported the use of DFT calculations for the rational design of deep blue phosphorescent Ir(III) complexes containing (4'-disubstituted-2'-pyridyl)-1,2,4-

tetrazole ancillary ligand, which was then synthesised and characterised for using them to make OLED devices.³⁸

3.1.3.1 Synthesis of neutral iridium(III) complexes

Neutral Ir(III) complexes are mostly used as dopant in OLED. They can be categorised into two groups, namely *bis*-cyclometalated iridium complexes and *tris*-cyclometalated iridium complexes. Synthesis of neutral *bis*-cyclometalated acetoacetate and picolinate complexes, normally involves the chloro-bridged dimer **3.2**, the ligand (e.g. acetylacetonate), weak base (such as Na₂CO₃) and high boiling alcohols (such as 2-ethylethanol) reflux for several hours affording desired products with good yields and purity. For example, synthesis of *bis*-cyclometalated iridium(III) complexes [(ppy)₂Ir(acac)] reported by Thompson *et al.*³⁹ is shown in Scheme 3.2.

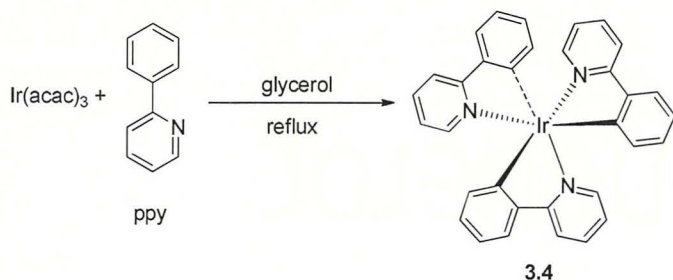


Scheme 3.2 Preparation of a neutral Ir complex, *bis*-cyclometalated iridium complex, [(ppy)₂Ir(acac)] **3.3**.³⁹

Single crystal X-ray crystallography of the complex [(ppy)₂Ir(acac)] showed that iridium has an octahedral configuration, chelated with two ppy and acac in such a fashion that pyridyl groups are in *trans* positions. The quantum yield of emission of the complex **3.3** in solution was reported to be 34% and the luminescence lifetime of 1.6 μs, which is consistent with the emission from a triplet excited state.³⁹ Milder conditions for the synthesis of *bis*-cyclometalated iridium complexes have been developed by various groups, which prevented formation of side products and facilitate an introduction of sensitive functional ligand.^{40,41} For instance, Tsuzuki *et al.*⁴¹ reported a number of *bis*-cyclometalated iridium(III) acetoacetates, which were synthesised by reacting the respective precursor and acetoacetate in a mixture with ethanol and Na₂CO₃ at 50 °C for 2-6 h.

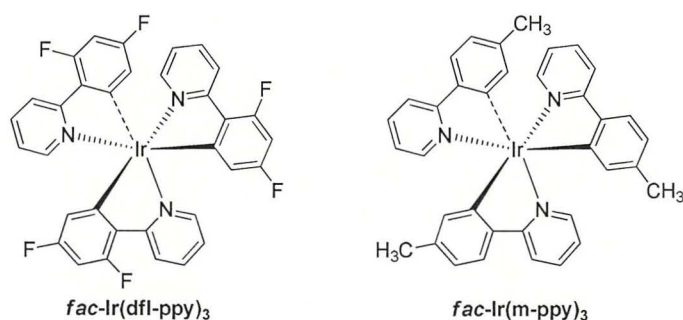
In general, the methods for the synthesis of *tris*-cyclometalated iridium complexes follow the procedure first introduced by Watt *et al.*⁴² where a *tris*-cyclometalated iridium complex, *fac*-

$\text{Ir}(\text{ppy})_3$, was prepared in high yield by refluxing $\text{Ir}(\text{acac})_3$ and phenylpyridine (ppy) in glycerol (Scheme 3.3).



Scheme 3.3 First synthesis of a neutral Ir complex, *tris*-cyclometalated iridium complex, *fac*- $\text{Ir}(\text{ppy})_3$ **3.4**.⁴²

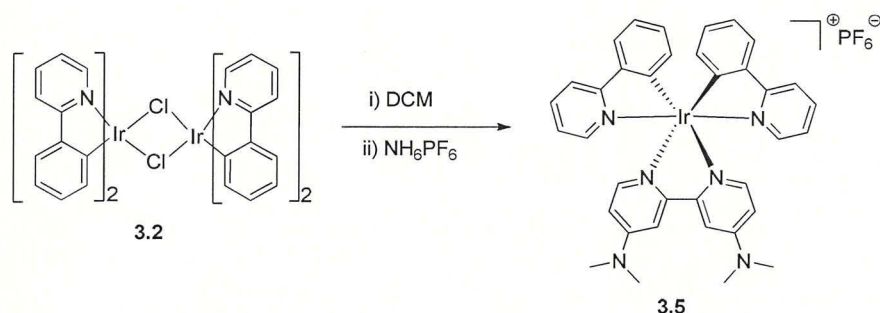
Since then, numerous scientific publications and patents have been published on *tris*-cyclometalated iridium complexes (both homoleptic and heteroleptic) with the variations of ligands in basic structure of $\text{Ir}(\text{ppy})_3$.^{2,3,10,11,12} The variation on 2-phenylpyridine ligand of *tris*-cyclometalated iridium complexes results in interesting change in electronic properties. For example, *fac*- $\text{Ir}(\text{dfl-ppy})_3$, containing electron-withdrawing fluorine atoms at 4,6-position on ppy moiety, emit at 392 nm (at 77K in DCM, lifetime of 27 μs) which is about 100 nm blue shifted compared to *fac*- $\text{Ir}(\text{ppy})_3$ which emit at 492 (at 77K in DCM, lifetime of 3.6 μs) reported by Thompson *et al.*³³



The facial and meridional *tris*-cyclometalated iridium complexes, which are configurational isomers, show notable differences in their physical properties. For example, *mer*- $\text{Ir}(\text{m-ppy})_3$ [m-ppy = 2-(*p*-tolyl)pyridyl] shows the oxidation potential $E_{1/2} = 0.18$ V, whereas for *fac*- $\text{Ir}(\text{tpy})_3$ the oxidation potential $E_{1/2} = 0.30$ V.³³ Their differences on physical properties stems largely from strong *trans*- influence of the phenyl group in the meridional isomer, leading in general easier to oxidation, exhibit broader or red shifted emission, shorter luminescence lifetime and lower quantum yields of emission, compared to the facial isomers.^{33,43}

3.1.3.2 Synthesis of charged iridium(III) complexes

A common method of synthesis for the charged iridium(III) complexes involves the splitting of chloro-bridged dimer complexes (such as **3.2**) under mild conditions, followed by cation exchange, as was introduced by Nave and co-workers.^{43,44} For example, synthesis of $[\text{Ir}(\text{ppy})_2(\text{dma-bpy})]\text{PF}_6$ [dma-bpy = 4,4'-(dimethylamino)-2,2'-bipyridine is shown in Scheme 3.4.⁴⁸



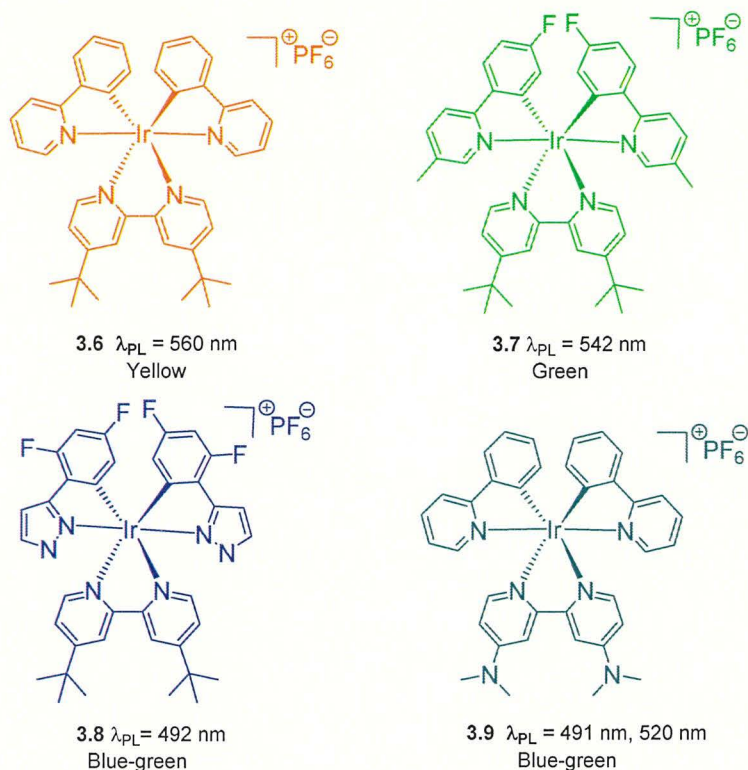
Scheme 3.4 An example of synthesis of the cationic iridium complex, $[\text{Ir}(\text{ppy})_2(\text{dma-bpy})]\text{PF}_6$ **3.5**.⁴⁸

Similar to the neutral iridium complexes, the electronic properties of the charged iridium complexes show a strong dependence on the type of substituent on the cyclometalated ligand and ancillary ligand.^{12,14,29,31} In the following section, the development of cationic iridium complexes for application in LEC is described towards colour tuning, stability as well as possibilities to produce white light emission from these materials.

3.1.3.3 Cationic iridium complexes: Colour tuning

Colour tuning to achieve red, green, and blue emission is an important aspect of material developments to be considered for lighting and/or display applications. The colour tuning of Ir complexes found to be possible by deliberate chemical synthesis. Also, selection of proper ligand proved to be a vital tool to modulate colour tuning, because the π^* -orbital in Ir(III) complexes are localised on the ligand. For example, yellow emission ($\lambda_{\text{PL}} = 560$ nm) was found for $[\text{Ir}(\text{ppy})_2(\text{dtb-bpy})](\text{PF}_6)$ **3.6** (reported for the first time),⁴⁵ while green emission ($\lambda_{\text{PL}} = 542$ nm) was achieved with $[\text{Ir}(\text{fm-ppy})_2(\text{dtb-bpy})](\text{PF}_6)$ **3.7**.⁴⁶ This blue shift of 18 nm was attributed to the strong inductive and mesomeric effect of the fluoro substituent on the phenylpyridine ligand, which was supported by DFT calculation results. To understand the origin of colour tuning in such complexes, Malliaras group carried out DFT calculations modelled for a series of Ir complexes with increasing fluorine content on 2-phenylpyridine

ligand. The DFT calculations clearly indicated that the metal-centred HOMO is highly stabilised by the fluorine atom.⁴⁶



Blue-green emission ($\lambda_{\text{PL}} = 492 \text{ nm}$) was observed for the Ir complexes **3.8** based on the cyclometalated ligand 1-phenylpyrazole reported by Tamaya *et al.*⁴⁷ They demonstrated that emission can be tuned through significant part of the visible spectrum by varying the ligands structure. The Nazeeruddin's group also found a similar trend of colour tuning in the Ir complex **3.9**. The absorption and emission spectra, and CV traces of Ir complex **3.9** reported by Nazeerrudin's group is shown in Fig. 3.3.

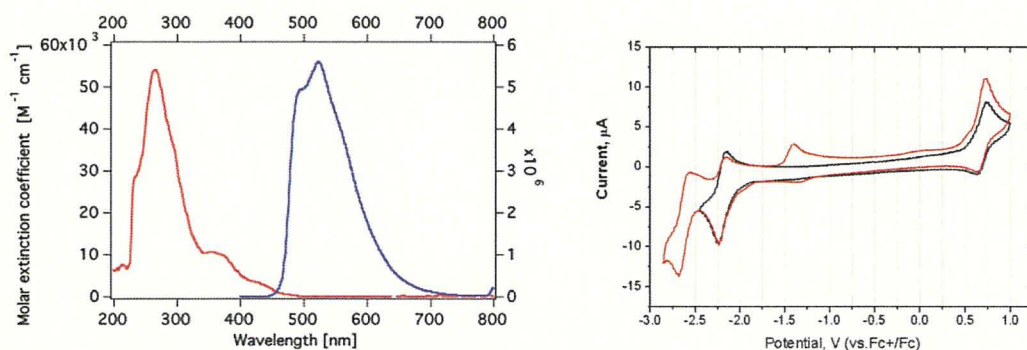


Fig. 3.3 Absorption-emission spectra (left) and cyclic voltammogram (right) spectra of Ir complex **3.9**.⁴⁸

Basing on a photophysical and electrochemical studies of **3.9** they have demonstrated that the destabilization of the ligand-based LUMO orbital results in more than offsets the destabilization of the metal-based HOMO orbitals, both caused by the donor ligand 4,4'-(dimethylamino)-2,2'-bipyridine. This in consequence causes an increase in the gap between the HOMO and LUMO of **3.9** compare to the HOMO–LUMO gap of **3.6** ([Ir (ppy)₂ (dtb-bpy)] PF₆). This effect was also supported by their DFT calculations performed at the B3LYP/LANL2DZ level of theory (Fig. 3.4).

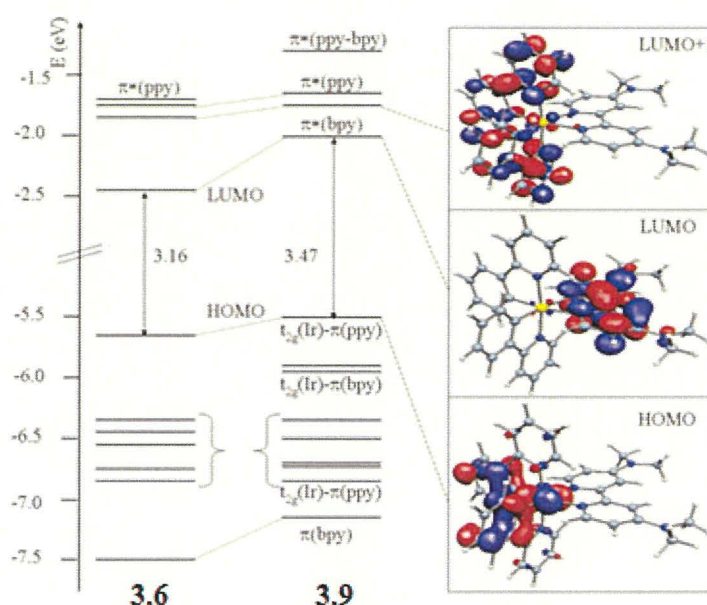


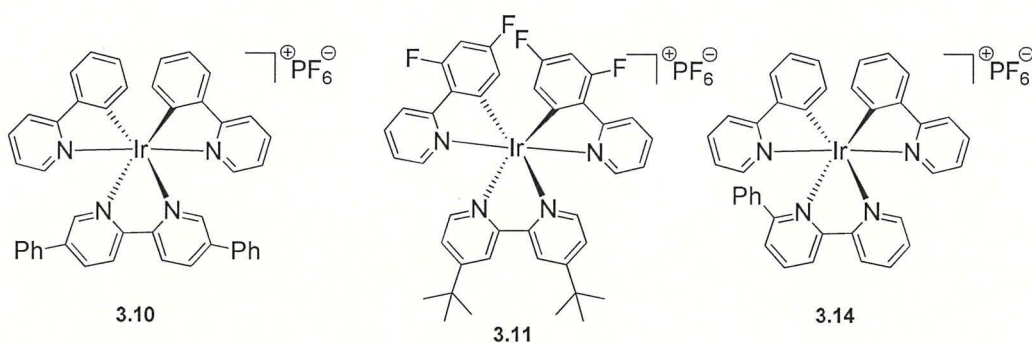
Fig. 3.4 Energy level diagram and character of the frontier MOs of Ir complexes **3.6** and **3.9**. On the right, isodensity of selected MOs is also shown.⁴⁸

3.1.3.4 Cationic iridium complexes: stability and response time

It has been found that during the operation of iTMC-based LEC, severe excited-state self-quenching always occurs, which causes in decreasing the efficiency. This is attributed to the fact that the complexes in the active layers of LEC are closely packed.^{48,49} To control the excited-state-quenching problem and consequently to improve the EL efficiency of LECs, a common approach is to introduce steric hindrance or a bulky side groups in the ancillary ligand of iTMCs. This minimises the non-radiative pathways by forcing an increased intermolecular distance and by inhibiting the non-radiative pathways through rigidification of the complex as a whole. Moreover, bulky groups enhance the hydrophobicity; therefore, hinder the attack of small molecules such as water, which promotes the degradation pathways through the formation of quenchers in the excited states.

Another approach has been to introduce extended π - π stacking interactions, which can stabilise iTMC. Bolink *et al.* followed the strategy of introducing a bulky group, and their Ir complex **3.11**-based device showed an improved efficiency to a great extent. A device based on Ir complex **3.11** showed the highest efficiency at that time.⁵⁰ The same group has also demonstrated that the position of the bulky substituents in the ancillary ligand plays an important role in increasing the device stability and they have reported a highly stable iTMC device based on the Ir complex **3.14**, which contains a bulky group phenyl at the 6 position of bpy.^{52a}

A number of research groups to increase the EL efficiency of iTMCs-based LECs has successfully implemented the approach of utilising bulky ligand, as a result the external efficiency up to 10%⁵¹ and the lifetime of over 1000 h have been reported.⁵² Recently, Slinker's group have demonstrated a similar approach while focusing on the stability of the single layer device based on ITO/**3.10**/Au and compared its performance with the LEC fabricated under the same condition using **3.6** as the emissive layer.⁵³



They have demonstrated an outstanding stability of the emissive material **3.10** of over 15-fold compared to the similar bulky-group substituted stable emissive material **3.6**. The authors highlighted the important aspect in terms of designing new materials for LECs, emphasising on the position of the bulky substituent of Ir complexes, which can influence on their device stability remarkably. The reported stability test is shown in Fig. 3.5, where the radiant flux *versus* time of maximum radiant flux for the two Ir complexes (**3.6** and **3.10**) based LECs biased at -4V is plotted.

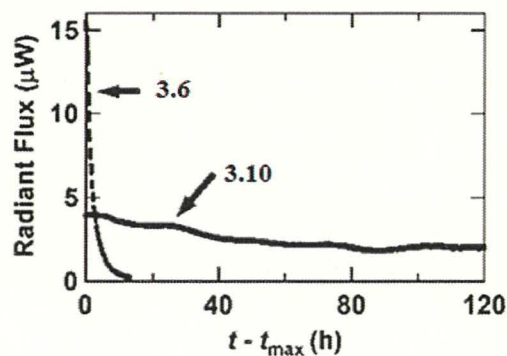
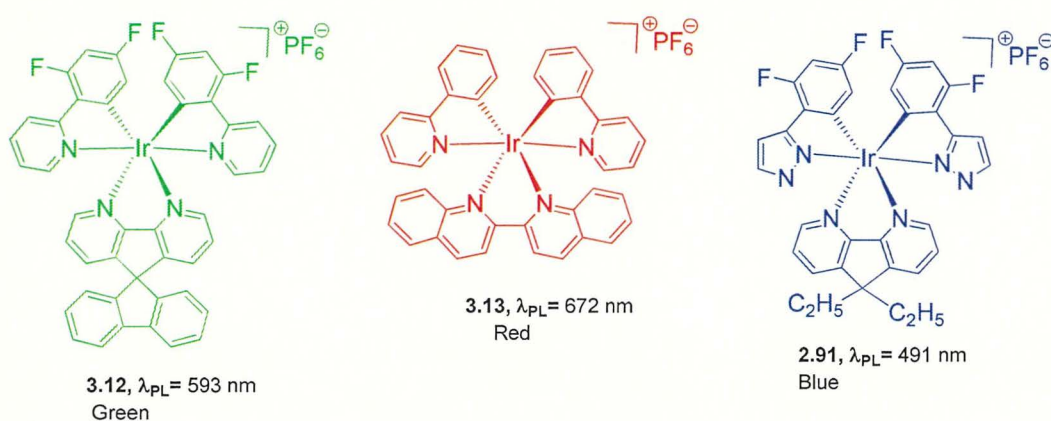


Fig. 3.5 Radiant flux versus time for ITO/3.10/Au and ITO/3.6/Au devices biased at -4V .⁵³

Su *et al.* have reported 4,5-Diazafluorene based Ir complex 3.12⁵⁴ as a green emitting complex. They also demonstrated the effect of increasing steric hindrance of the ancillary ligand (spirodiazfluorene) on enhancing the EL efficiency.



Earlier, Bryce *et al.* reported the Ir complexes based on the fluorenyl group substituted phen ligands, fluorenyl groups at the *meta* positions such as complex 3.15. Fluorenyl groups caused extensions of π -conjugation to the phen ligand. It was demonstrated that the increased ligand conjugation length as in 3.15 led to increased phosphorescence lifetime ($2.57 \mu\text{s}$). A two-layer LEC was formed with the configuration ITO/PEDOT:PSS/Ir complex 3.15/Al, or Ba capped with Al, which attained a maximum brightness efficiency of 9 cdA^{-1} at a large bias of 9 V and the turned-on time of 40 min .⁵⁵ It was observed that the electroluminescence maximum of the complex 3.15 is red-shifted (ca. 40 meV) compared to its photoluminescence maximum (Fig. 3.6).

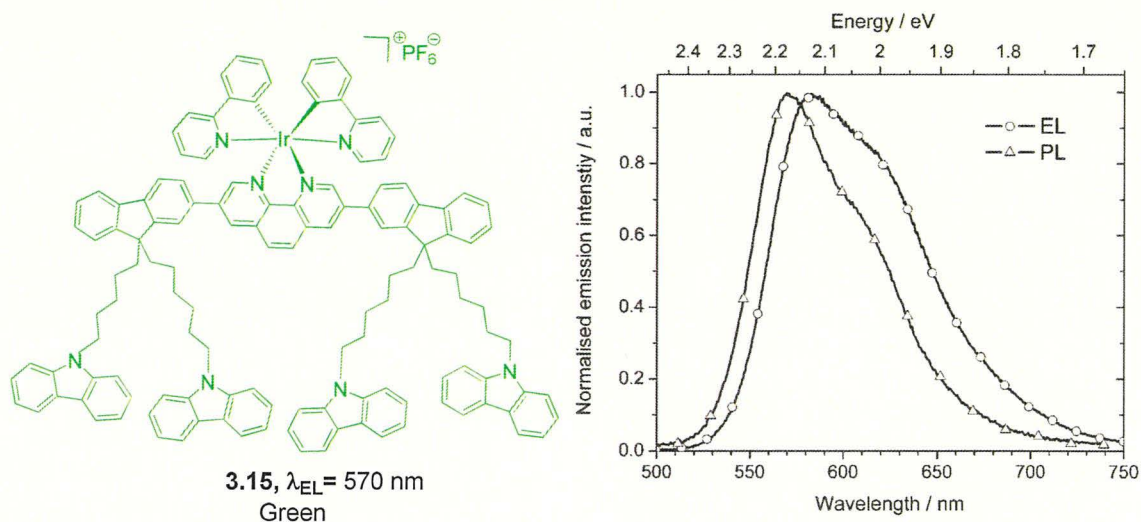
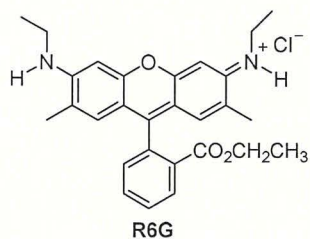


Fig. 3.6 The photoluminescence and electroluminescence spectra of **3.15**.⁵⁵

A useful strategy for tuning the emission colour or to improve the emission efficiency of OLED is to use host-guest approach (also called doping), which involves dispersing the emitting complex (guest) into the matrix of another emitting material (host).^{56,57} Su *et al* recently demonstrated introduction of host-guest approach as a strategy to improve efficiency for LEC.⁵⁸ They reported a highly efficient LEC utilising cationic iridium complex $[\text{Ir}(\text{dfppy})_2(\text{SB})](\text{PF}_6)$ **3.12** as the host and a fluorescent cationic dye R6G as the guest.



The response time is defined as the time required to reach the maximum brightness (or luminescent intensity) at constant bias voltage. The response time for LEC based on iTMC is known to be varied in a wide range, from a few minutes to several hours. For practical applications, response time should be as short as possible. Modification of the iTMC (using short counter ion such as BF_4^-) and its surrounding environment (by adding ionic liquid) to improve conductivity has been a useful strategy to shorten the response time. However, a higher applied voltage is usually required for LEC to shorten the response time and as a result, the electroluminescent material starts to degrade faster, and hence the stability becomes lower. Therefore, a balance has to be found out, which would compensate the trade-off between the response time and the stability.

3.1.3.5 Cationic iridium complexes: White light LECs

The white OLEDs based on polymers and small molecules have been extensively studied for their applications in flat panel and solid state lighting sources. Strategy for the white light emission is achieved either by mixing red, green and blue emitting materials or by mixing two complementary colour emitters, such as blue-green and red emitter materials.⁵⁹ This strategy has been widely used in polymer-based OLED to achieve white light emission.⁶⁰ First polymer-based white LEC was reported in 1997.⁶¹ However, it took a long time to achieve a white LEC based on the iTMC, reported for the first time by Su and co-workers in 2008,⁶² largely due to the limited availability of the iTMC with good colour purity^{21,22} and because of difficulties to stabilise the mixed colour complexes in device.⁵⁸ LECs based on iTMCs have an advantage over polymers based LECs because of the higher EL efficiencies promoted by the phosphorescent nature of iTMCs.^{63,64}

Su's group has achieved the white light by doping a small amount of the red-emitting complex **3.13** into the blue-green-emitting complex **2.91**.⁶² The reported configuration of the LEC was ITO/emissive layer (100 nm)/Ag (150 nm), where the emissive layer contains host **2.91** (80.5 wt%), guest **3.13** (0.4 wt%), and an additional electrolyte BMIMPF₆ (19.1 wt%). It was also reported that the presence of ionic liquid BMIMPF₆ induced longer excited-state lifetimes for both the host and the guest, and the PLQYs are slightly raised, which according to the authors indicates the role of BMIMPF₆ in suppressing the intermolecular interactions.^{51a}

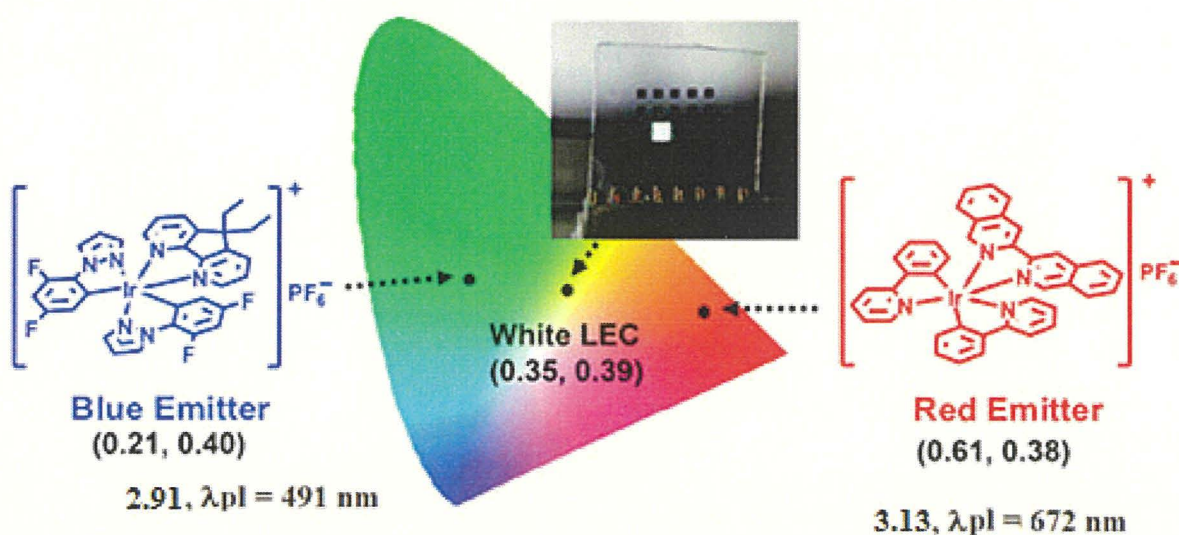


Fig. 3.7 Single doped mixing of two Ir based iTMC **2.91** and **3.13** to achieve white light emission.⁶²

They also demonstrated that with an increase amount of the guest (blue emitter **2.91**) concentrations from 0.2 % to 0.4% the PL intensity of the host emission (red emitter **3.13**) increases, thus effectively enhances the host-to-guest energy transfer, which is accompanied by the shorter lifetimes of the host emission (Fig 3.8, left).⁶² However, the relative intensity of the red emission with respect to the blue emission is larger in EL when compared to PL. In addition, the relative intensity of the host emission increases as the bias decreases (Fig 3.8, right). According to the authors' explanation, lower biases favour charge carrier injection and trapping on the smaller HOMO–LUMO energy gap of guest **2.91**, resulting in a direct carrier recombination/exciton formation on the guest (rather than host-guest energy transfer) so the larger fractions of guest emission are observed.

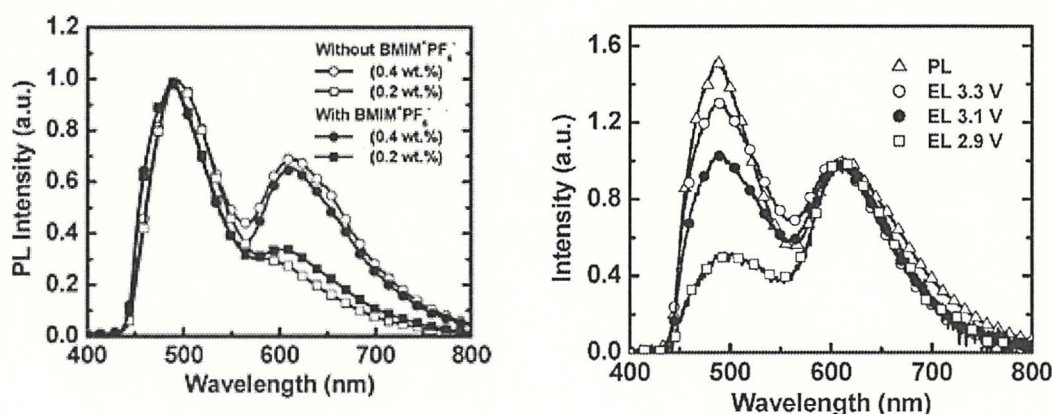
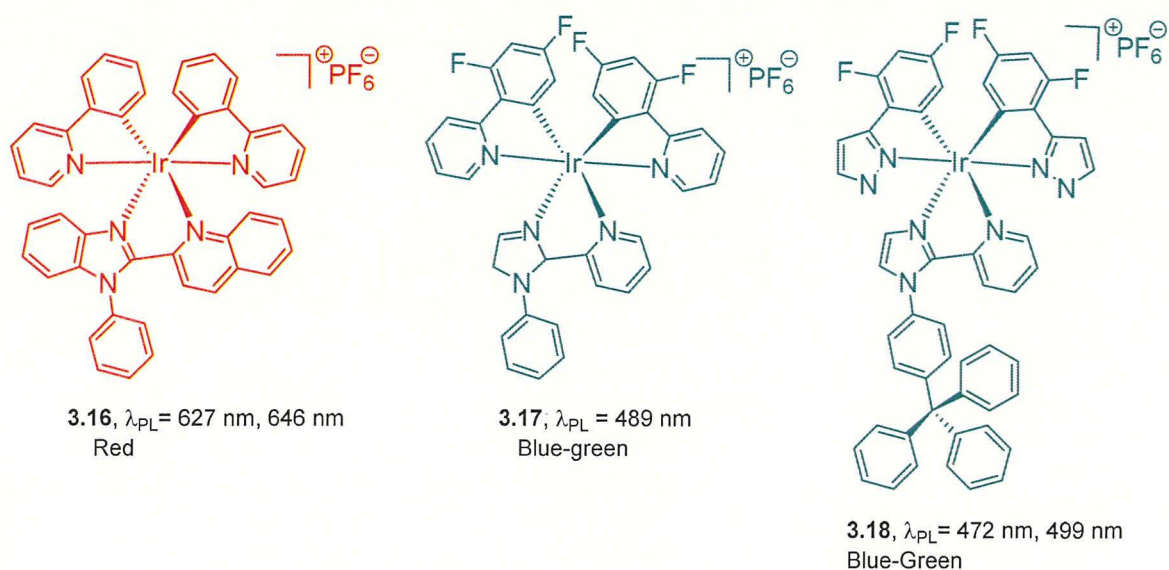


Fig. 3.8 PL spectra of host-guest (**3.13–2.91**) films containing different guest concentrations of **13** (0.4 and 0.2 wt%) without and with BMIMPF₆ (left). The bias-dependent EL spectra of the white LECs made of host-guest (**3.13–2.91**) compared with their PL spectra (right).⁶²

Following the similar single-doped strategy to achieve white LEC, He *et al.* in 2009 reported a white LEC with improved power efficiency.⁶⁵ They used imidazole-type ancillary ligand based iTMC, and a white LEC was realised by doping the red emitting complex **3.16** into the blue-green complex **3.17** matrix.



The doping concentration of complex **3.16** was selected so that the energy-transfer from complex **3.17** (guest) to complex **3.16** (host) was incomplete and the blue-green light and red light were thus mixed to form white light emission (Fig. 3.9). The device structure of this white-light LEC was ITO/PEDOT:PSS/[complex **3.16** : complex **3.17**: BMIMPF₆ (molar ratio 1:0.02:0.35)](100 nm) /Al (120 nm).

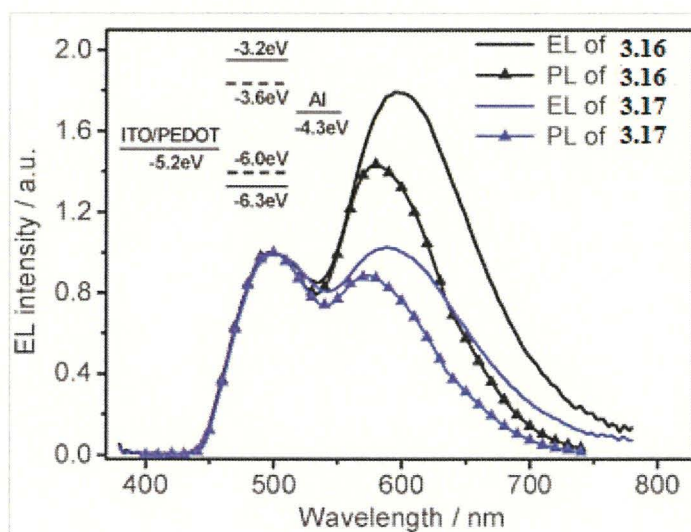


Fig. 3.9 EL spectra of white LECs based on **3.16**–**3.17** (biased at 4.0 V) and corresponding PL spectra of the light-emitting layers. The inset shows the energy levels diagram of the white LECs (the dashed lines represent the energy levels of complex **3.18**).⁶⁵

They have demonstrated that, compared with the blue-green LECs based on the complex **3.17**, the white LECs based on the mixed complexes **3.16–3.17** showed a shortened response time, an increased efficiency as well as increased brightness under similar bias of 4.0 V. According to the authors, the charge-trapping mechanism played an important role in the operation of the white LECs, the electrons and holes can be directly injected into the low energy gap between LUMO and HOMO of complex **3.17** and then trapped there. As a result, the injection barriers at the electrode interfaces are largely reduced and excitons formed directly on the molecules of complex **3.17**, which lead to the shortened response time and increased efficiency and brightness of the white LECs. The same group have reported in 2010 a white LECs utilising doping approach. The reported white LEC was based on a bulky group substituted Ir complexes **3.18** mixed with the complex **3.16**.⁶⁶ The effect of bulky group 4-tritylphenyl (TP) was found to suppress the excited-state self-quenching in the solid state and increases the film-forming ability of the complex. However, at 3.2 V the white LEC based on the mixed complexes **3.16–3.18** showed a lower brightness and efficiency, compared to the blue-green LEC based on the single layer complex **3.18**. As per authors' explanation, the charge-trapping of the red-emitting complex **3.16** played against on the performance of the white LEC, suggesting that charge recombination balance significantly influenced the performances of white LECs.

In the year 2011, Su's group⁶⁷ introduced a double-doped system white LEC with an improved device efficiency. The improved efficiency was attributed to an improved balance of the carrier mobility of the double-doped emissive layer. An efficient blue-emitting host (complex **3.8**) was mixed with a double-doped emissive layer comprising of a red-emitting guest (complex **3.13**) and an orange-emitting guest (complex **3.19**) to prepare the emissive layer of the LEC to achieve white light-emission. The photoluminescence spectra of the Ir complexes **3.8**, **3.13** and **3.19** in DCM solution and in films are shown in Fig. 3.10, depicting that the blue emission properties of the complex **3.8** retain in film, whereas the complex **3.13** and **3.19** undergoes a slight red shift in the film compared to the solution.

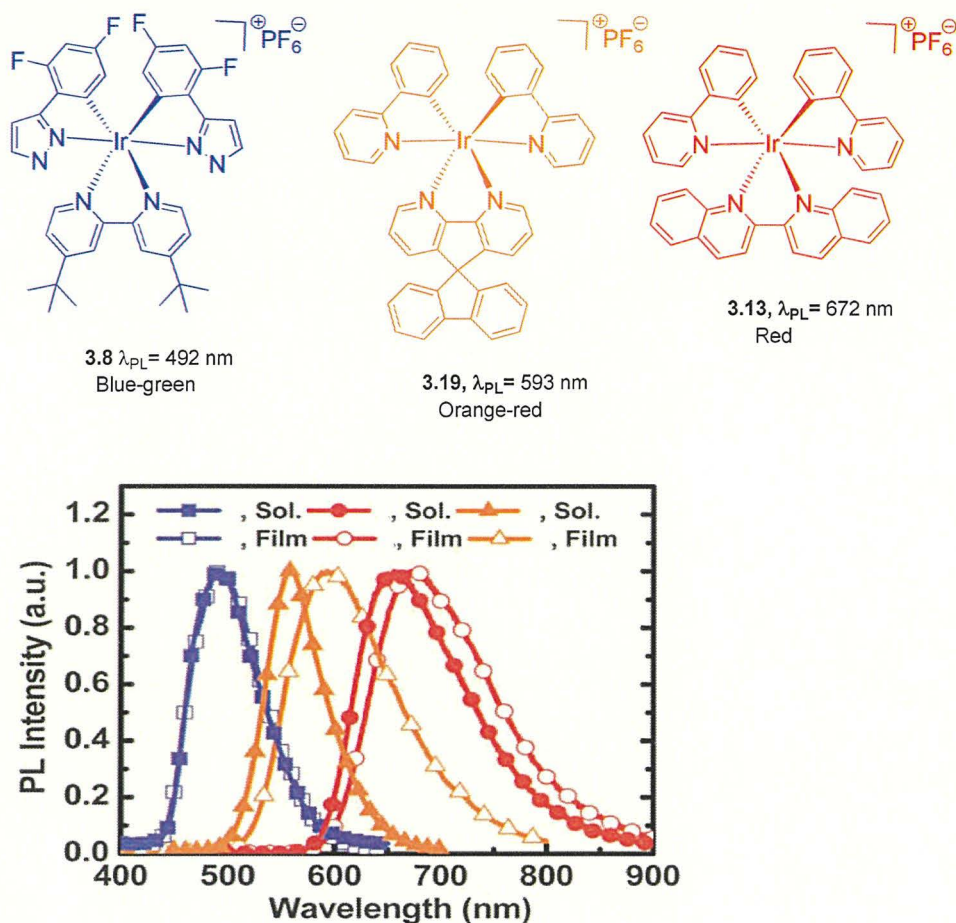


Fig. 3.10 Photoluminescence spectra of Ir complexes **3.8** (blue), **3.19** (orange-red), and **3.13** (red) in dichloromethane and in neat films.⁶⁷

The reported double-doped white LEC showed a peak power efficiency of 15 lmW⁻¹, which is the highest efficiency of white LECs base on iTMC so far. They also demonstrated that the single-doped (**3.13**) and the double-doped (**3.13** and **3.19**) host-guest films exhibits similar PL spectra and comparable PLQYs, while the device efficiencies of the double-doped white LECs are two-fold higher than those of the single-doped white LECs.

Equally, for the evaluation of any other electroluminescent device performance, LEC performance is considered broadly on four categories, namely (1) colour emission, (2) efficiency, (3) stability and (4) response time. The iTMCs based LECs have addressed more or less of these category quite well, which are equivalent to the best known electroluminescent device performance. However, the main drawbacks associated with iTMCs based LECs is the trade-off between the stability and the response time. In other words, when trying to improve the stability of LEC, the response time increases and *vice-*

versa. This trade-off between response time and stability is the central focus for improving performance of LEC and has been highlighted by a number of groups working on LECs.^{24,48,53} Efficient LECs need to have short response time without compromising the stability. Design and synthesis of new materials and understanding the structure-property relationship might resolve the crucial issue that is debarring iTMC based LECs to be applied in practical applications. Future works of research are toward to resolve the issue that seems just a matter of time to come. Most of the cationic iridium complexes based LEC reported so far has been with bpy and phen ligands while only a few DAF based Ir complexes used for LEC are reported so far. As a part of this Thesis work, series of cationic Ir complexes based on DAF ligands have been prepared and their photophysical properties studied in order to understand the structure-property relationship is presented in result and discussion section.

3.2 Results and discussion

3.2.1 Scope and rationale for synthesis of Ir(III) complexes with DAF

Most of the metal complexes with DAF based ligands that are known in literature are discussed in Chapter 2 where the role of iridium complexes with DAF based ligands have been highlighted (Section 2.1.3.4). It can be inferred that DAF containing iridium complexes represent an exciting materials for light-emitting devices. Still, not many literatures are reported for iridium complexes with DAF based ligands to be used for making LECs compared to well-studied bidentate ligand such as bpy and phen. Therefore, this represents an exciting and substantially underdeveloped area of research to synthesis different substituted DAF containing cationic Ir(III) complexes and study their structure-property relationship for using them as emissive materials particularly for LECs. It is apparent from the above discussion of the development of light-emitting electrochemical cell (Sections 3.1.3.3-3.1.3.4) that the substitution of an electron-withdrawing group and/or a bulky group on the ancillary ligands of cationic Ir(III) complexes does have a substantial influence on their device performance such as colour tuning and stability. The major issue has been that the device lifetime of iTMC based LEC at present is low, largely due to their degradation under applied voltage, which prevents them from their pragmatic purpose. In this context, the influence of steric hindrance in improving the device life time of the iTMC based LEC is a matter of much more study and discernment. In our work, we strained to understand this core burning issue by examining the essence of different substituted DAF based iridium complexes to be employed for making LEC, which has the potential to be the next generation lighting source.

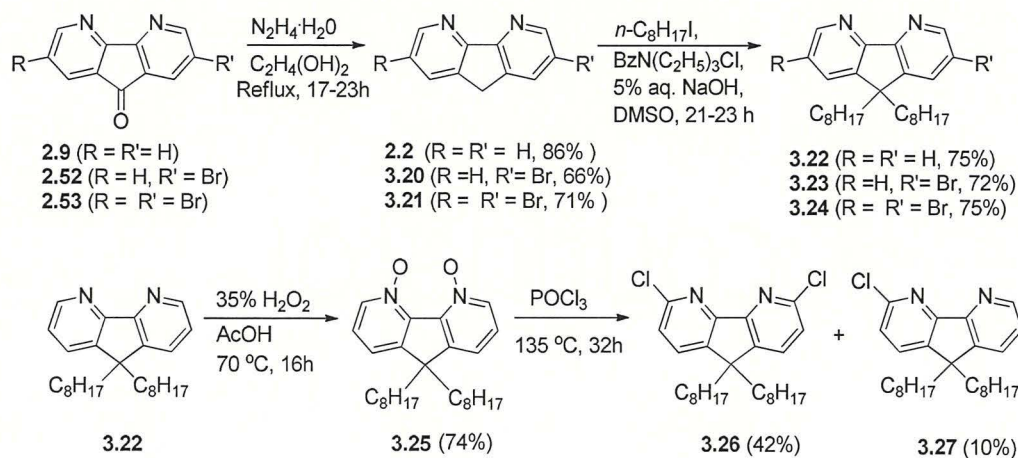
Herein, we present the synthesis of a series of new Ir(III) complexes, [(ppy)₂Ir(DAF)]PF₆ (**3.36-3.48**) and [(dfm-ppy)Ir(DAF)]PF₆ (**3.49**) where ppy = 2-phenylpyridine, dfm-ppy = 2-(2,4-difluorophenyl)-3-methylpyridine, and DAF = substituted 4,5-diazafluorene, and studied their photophysical, electrochemical properties together with DFT calculations. All of the complexes exhibit a strong absorption band (ca. 240–300 nm, Fig. 3.13–3.14) in the UV region in acetonitrile (ACN) assigned to spin-allowed ligand-centred (LC) ¹π–π* transitions and a weak band (ca. 300–450 nm) attributed to MLCT. The photoluminescence spectra of most complexes in ACN are characterised by a broad structureless band, which is assigned to a combination of ³MLCT and ³LC states. They emit green-red light (513–653 nm, Fig. 3.15–3.16) with high quantum yields (8–43%) in ACN. Cyclic voltammetry (CV) measurement of these complexes show reversible or quasi-reversible oxidation peaks and reversible or irreversible reduction peaks with an electrochemical gap, $E_g = E_{1/2}^{oxl} - E_p^{red1}$, of 1.88–3.03 eV (Fig. 3.17–3.19, Table 3.3). DFT and TD-DFT calculations performed at the B3LYP/LANL2DZ level of theory provided deeper knowledge about the electronic properties of the DAF-based Ir complexes. The DFT calculated results of emission properties of complexes are in good agreement with the experimental results of emission energies (deviations of only 2–10 nm, Table 3.6), and HOMO-LUMO gap (linear regression $R^2 > 95$, Fig. 3.26–3.27). The TD-DFT calculations for both the singlet ground state (S₀) and the first triplet state (T₁) have been performed, which concluded that in the singlet ground state (S₀) the HOMO of the complexes is spread between the Ir atom and benzene rings of the 2-phenylpyridine ligand, whereas the LUMO is mainly located on the DAF ligands. One of the Ir complex we have fabricated the device with the configuration ITO/Ir complex **3.45**/Al and was successfully tested as the iTMC based LEC and exhibited a green electroluminescence (576 nm) with a luminescent intensity of 90 cd m⁻².

In the next sections, synthesis of DAF-based ligands, their charged iridium(III) complexes (**3.36-3.49**) and the electronic and steric effects of substituent (R–R₄) in ancillary DAF ligands on electrochemical and spectroscopic properties of their Ir complexes are described in the context of their potential use as emissive materials in LEC devices.

3.2.2 Synthesis of DAF-based ligands

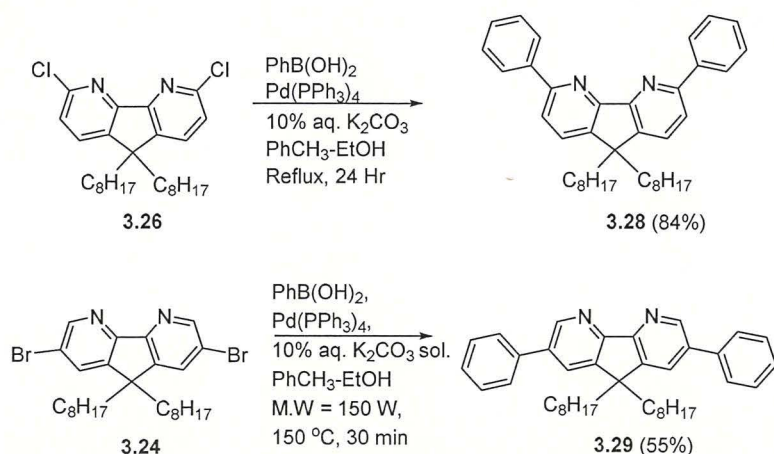
Synthesis of DAF based ancillary ligands (N[^]N) for iridium complexes of the form (C[^]N) Ir (N[^]N) is shown in Schemes 3.5–3.6. 4,5-Diazafluoren-9-one (**2.9**), 2-bromo-4,5-diazafluoren-9-one (**2.52**) and 2,7-dibromo-4,5-diazafluoren-9-one (**2.53**) were synthesised by procedure described in Chapter 2. They were subjected to reduction reactions with hydrazine hydrate in ethylene glycol to afford corresponding 4,5-diazafluorenes **2.2**, **3.20**, and **3.21** in good yields, similar to reactions reported in the literature for fluorene derivatives.⁶⁸ These 4,5-diazafluorenes (**2.2**, **3.20**, **3.21**) were then alkylated at 9 position with *n*-octyl iodide in DMSO using a phase-transfer catalyst to obtain 9,9-dioctyl-4,5-diazafluorene **3.22**, **3.23**, and **3.24** in excellent yields after column purification on silica gel. No alkylation at the pyridine ring was observed in these conditions, suggesting much higher reactivity of the carbanion generated by the action of base on DAF. As mentioned in Chapter 2 (Section 2.1.2.1), alkylation reactions at the C-9 position of DAF are known in literature with the use of different bases such as NaH and *t*-BuOK.⁶⁹ Our reaction condition with NaOH as a base was found to work well and relatively easy to perform; without the need to perform the reaction in anhydrous condition with pre dried solvent and reagents.

The *n*-octyl-DAF **3.22** was used for introduction of chlorine substituents at its 3,6 positions and subsequently chlorinated DAF was used for introduction of phenyl groups (**3.26**→**3.28**). The chlorine atoms were introduced at 3- and 3,6- positions of DAF by a two-step synthesis process. This involve oxidation of pyridine nitrogen atoms to form *N*-oxide-DAF **3.25** using hydrogen peroxide in acetic acid followed by chlorination with phosphorous oxychloride to afford 3,6-dichloroDAF **3.26** as major product in moderate yield (42%) and 3-chloroDAF **3.27** as minor product in low yield (10%), which were separated by column chromatography. Similar reaction with alkyl substituted DAF known in literature has been discussed in Chapter 2 (Section 2.1.2.2).⁷⁰ Here, we also isolated the mono-chlorinated product **3.27** from the crude reaction product. As mentioned before, the effect of electron withdrawing groups on Ir complexes is known to perturb their HOMO–LUMO energies and do tune the colour of the emission. The halogen substituted DAF derivatives (**3.23**, **3.24**, **3.26**, **3.27**) were therefore used as ancillary ligands for iridium complexes (synthesis in next section) in order to see their effect on colour tuning. On the other hand, these halogenated DAF compounds were quite useful for further structural modification and for making oligomers and polymers described in Chapter 4 and 5.



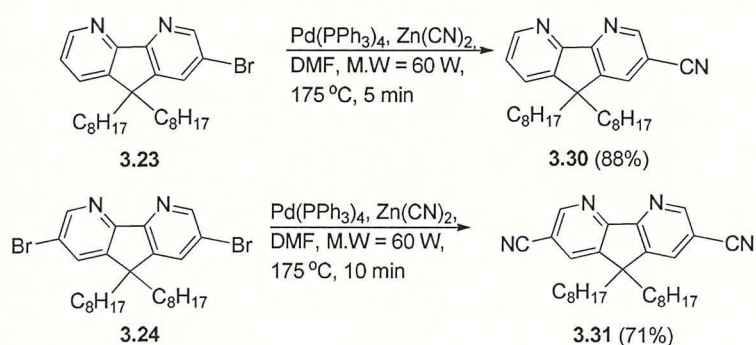
Scheme 3.5 Synthesis of halogenated DAF compounds.

To investigate the effect of steric hindrances and an extended conjugation in DAF ligands on device properties of their iridium complexes, we synthesised DAF derivatives with phenyl groups at the positions 3,6- and 2,7- (**3.28** and **3.29**). For this purpose, synthesised halogenated DAF derivatives **3.24** and **3.26** were reacted separately with phenyl boronic acid in Pd catalysed Suzuki coupling reactions. The 3,6- substitution reaction (**3.26**→**3.28**) was carried out at conventional heating taking 24 hours, while 2,7 substitution reaction (**3.24**→**3.29**) was performed in microwave-assisted conditions taking only 30 min of reaction time. Both conditions gave good yields of target diphenyl-substituted DAF products **3.28** and **3.29** after column chromatography purification (Scheme 3.6). The shorter reaction time of microwave-assisted reaction was attributed to the instantaneous and elevated heating resulting from the microwave coupling directly with the reactive molecules.⁷¹



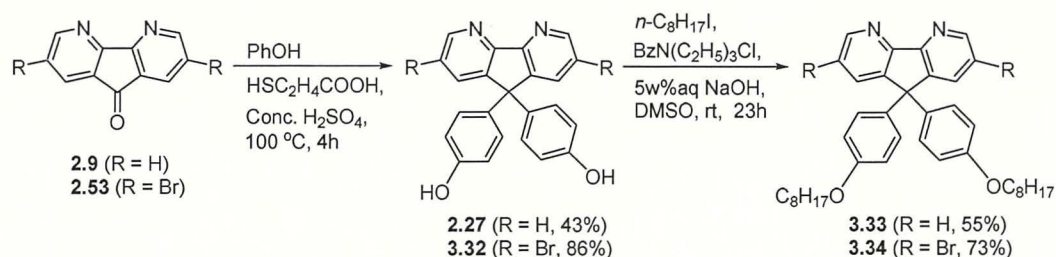
Scheme 3.6 Synthesis of phenyl-substituted DAF derivatives **3.28** and **3.29**.

DFT calculations, performed in parallel to the experimental work of synthesis of novel DAF ligands revealed that an introduction of strong electron-withdrawing cyano group(s) at 2- / 2,7-positions of DAF moiety should result in red-shifted emission spectra of its iridium complexes. Based on these theoretical predictions (see Section 3.2.5 on DFT calculations) we decided to synthesise compounds **3.30** and **3.31**. These syntheses were performed by substitution of halogen atoms in **3.23** and **3.24** with zinc cyanide in presence of catalytic amount of Pd(PPh₃)₄ as catalyst in dimethylformamide under microwave irradiation for just 5–10 minutes, and gave the desired products **3.30** and **3.31** in excellent yields of 88% and 71%, respectively, after column purification on silica gel (Scheme 3.7).



Scheme 3.7 Synthesis of cyano-substituted DAF compounds **3.30** and **3.31**.

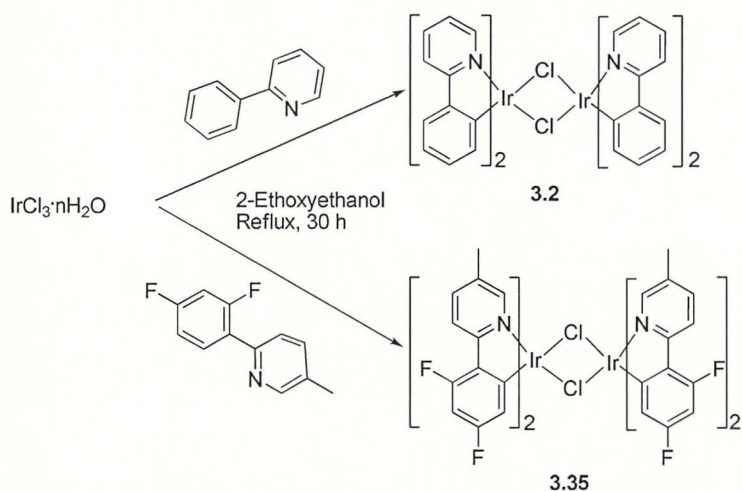
Another functionalisation of DAF moiety to expand the library of DAF ligands for Ir complexes included variation of substituents at the C-9 carbon atom. Previous DAF compounds were 9,9-dioctyl derivatives (to make the complexes soluble, and on the other hand to use some of them as monomers for synthesis of DAF-based oligomers and polymers, – Chapters 4 and 5). In this case we used described method of transformation of fluorenone into 9,9-di(p-hydroxyphenyl)fluorenones), which was successfully exploited previously in synthesis of poly[9,9-di(4-alkoxyphenyl)fluorenes].⁷² Thus, DAFone (**2.9**) or dibromo-DAFone (**2.53**) reacted with phenol at 100 °C in presence of concentrated sulphuric acid and catalytic amount of 3-mercaptopropanoic acid to give 9,9-*bis*(4-hydroxyphenyl)-DAF **2.27** and 2,7-dibromo-9,9-*bis*(4-hydroxyphenyl)-DAF **3.32**, respectively. The literature methods of synthesis of compound **2.27** was discussed in Chapter 2.^{73,74} Compounds **2.27** and **3.32** were then alkylated at hydroxy groups with *n*-iodooctane in DMSO at room temperature in presence of aqueous KOH and phase transfer catalyst (benzyltriethylammonium chloride) to afford *bis*(octyloxyphenyl)-DAF products **3.33** and **3.34** in good yields (65% and 73%, respectively) (Scheme 3.8).



Scheme 3.8 Synthesis of aryl substituted DAF

3.2.3 Synthesis of iridium complexes

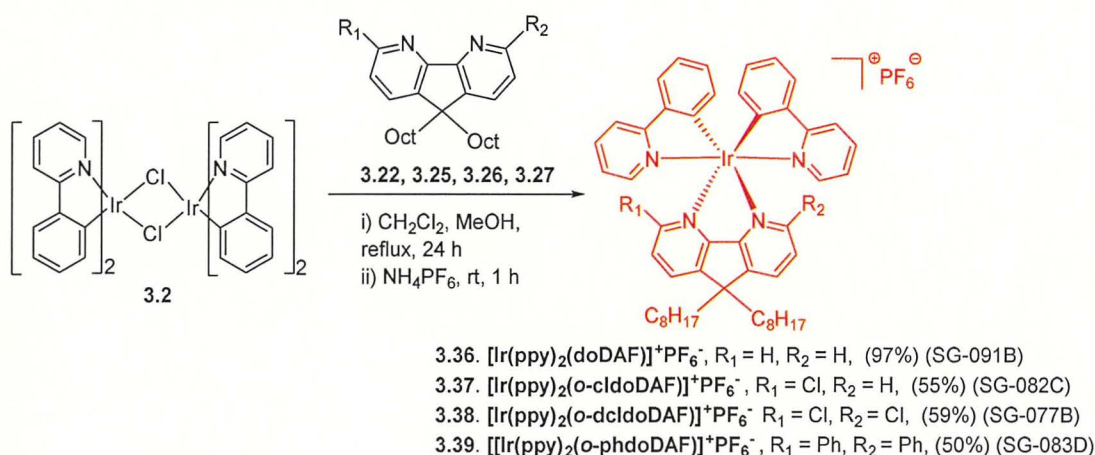
μ -Dichloro-bridged cyclometalated Ir(III) dimers **3.2** and **3.35** of general formula $(\text{C}^{\wedge}\text{N})_2\text{Ir}(\text{i-Cl})_2\text{Ir}(\text{C}^{\wedge}\text{N})_2$, where $\text{C}^{\wedge}\text{N}$ represents a cyclometalating ligand were synthesised according to a literature procedure (Scheme 3.9).⁷⁵ Cyclometalating ligand 2-phenylpyridine is a commercial product, whereas 2-(2,4-difluorophenyl)-5-methylpyridine was prepared by literature procedure.⁷⁶ It was found that the purity of starting ligands is important and freshly distilled 2-phenylpyridine gave more pure dimer (**3.2**) with better yields (70% compared to 42% for commercial unpurified 2-phenylpyridine).



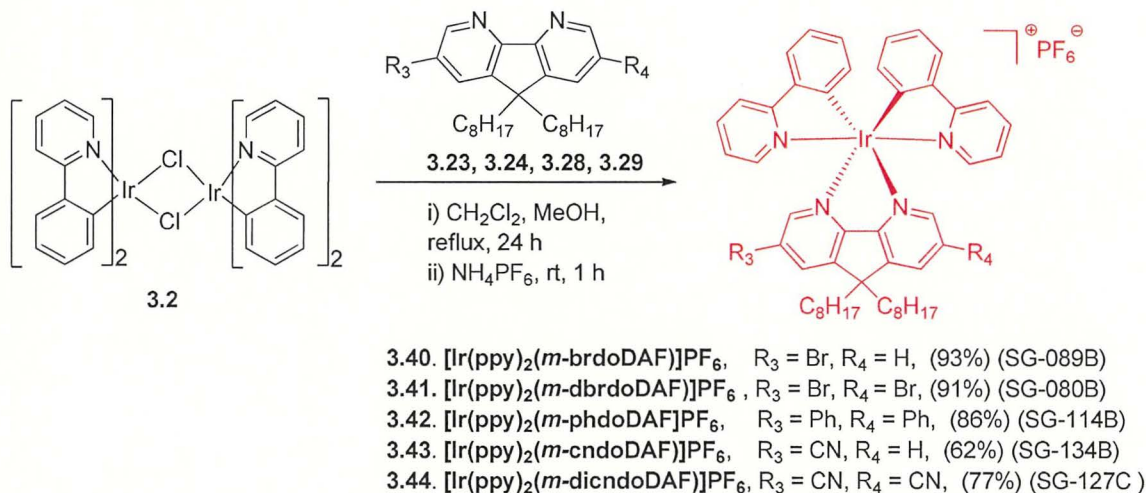
Scheme 3.9 Synthesis of μ -dichloro-bridged cyclometalated Ir(III) dimer **3.2** and **3.35**.

The Ir complexes of general formula $(\text{C}^{\wedge}\text{N})_2\text{Ir}(\text{N}^{\wedge}\text{N})$, where $\text{N}^{\wedge}\text{N}$ represents ancillary ligand and $\text{C}^{\wedge}\text{N}$ represent cyclometalating ligands were synthesised by refluxing the DAF ligands with μ -dichloro-bridged cyclometalated Ir(III) dimers **3.2** and **3.35** for 24 hours in DCM-methanol solution followed by the anion exchange using ammonium hexafluorophosphate (NH_4PF_6) according to literature procedure (more details discussion in Section 3.2.3.2).^{43,44,48} All the complexes prepared were purified by column chromatography on silica gel affording good to excellent yields (50-97%). Schemes 3.10-3.13 depict the syntheses of cationic iridium

complexes **3.36-3.49** containing cyclometalating ligands 2-phenylpyridine/2-(2,4-difluorophenyl)-5-methylpyridine and substituted 4,5-diazafluorenes as ancillary ligands. The Ir complexes with electron withdrawing group (Cl, Br) at *ortho*- and *meta*- position to the N atom of DAF (**3.37**, **3.38**, **3.40**, **3.41**) allowed to investigate the electronic effects on tuning the colour of emission. The phenyl group substituted at *ortho*- and *meta*- to the nitrogen (**3.39**, **3.42**) served as bulky group to see the effect of steric hindrance on their photophysical and electrochemical properties. In addition, phenyl group provides extended conjugation, which could well change the electronic properties.



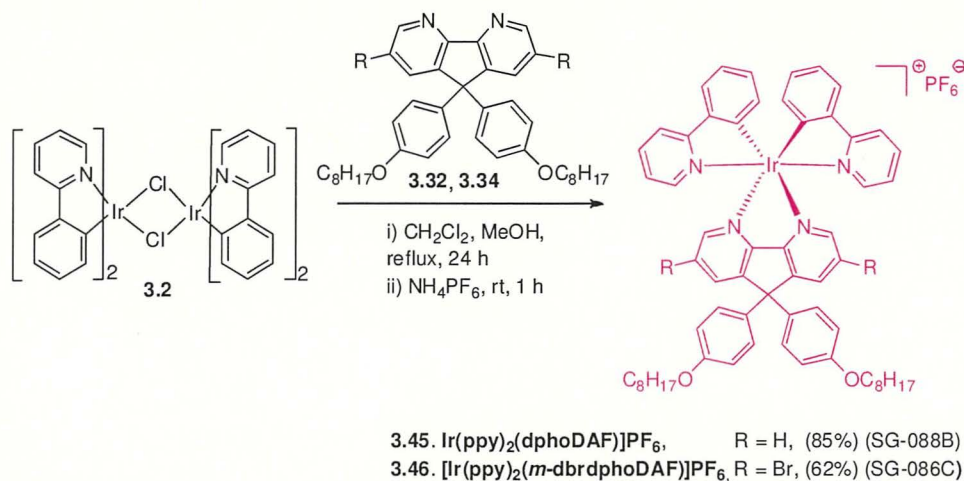
Scheme 3.10 Synthesis of 3,6-disubstituted DAF-based cationic Ir(III) complexes.



Scheme 3.11 Synthesis of 2,7-substituted DAF-based cationic Ir(III) complexes.

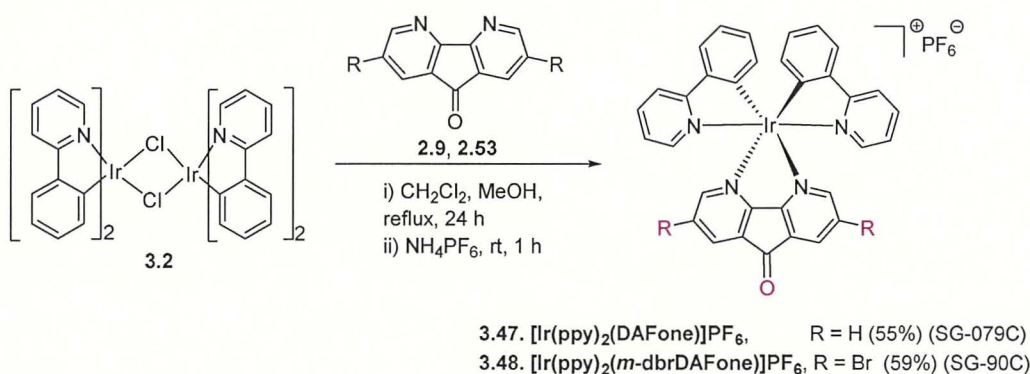
Further variations of the structure of complexes was done by modification of substituents at the C-9 position of DAF ligands, namely by using 9,9-*bis*(4-octyloxyphenyl)-DAF (**3.32** and **3.34**) in synthesis of Ir complexes **3.45**, **3.46**, as shown in Scheme 3.12. This variation at the

C-9 position of DAF was carried out to increase the steric environment in the Ir complexes, which might enhance their photoluminescence quantum yields and stability.



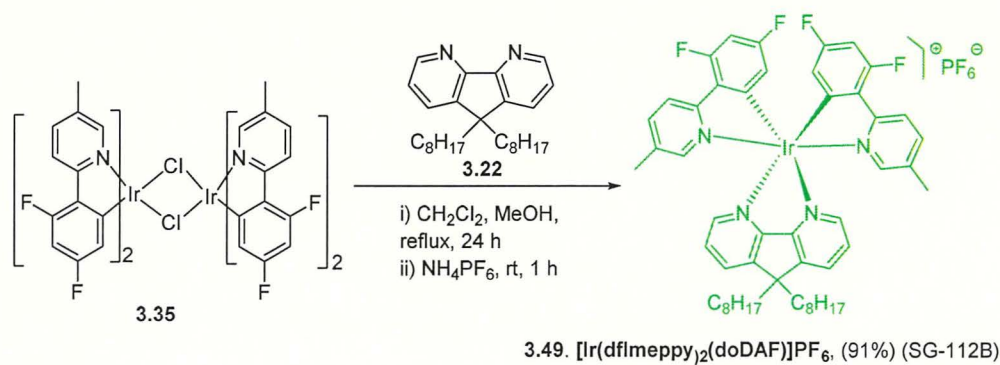
Scheme 3.12 Synthesis of cationic Ir(III) complexes with 9,9-dioctyloxyphenyl-DAF ligands.

Scheme 3.13 depicts the synthesis of cationic Ir complexes (**3.47**, **3.48**) containing DAFone **2.9** and dibromo-DAFone **2.53** as ancillary ligands. While carbonyl group increases the electron withdrawing properties of DAF ligand that might effect on spectral properties of Ir(III) complexes (as predicted by our DFT calculations, Section 3.2.5), compounds **3.47** and **3.48** have been found to be non-emitting materials.



Scheme 3.13 Synthesis of DAFone-based cationic Ir(III) complexes.

As mentioned before, fluoro-substituted 2-phenylpyridine as cyclometalated ligand is known to impart blue shifted emission (Section 3.1.3.3). In this study, we have also synthesised a cationic Ir complex **3.49** (Scheme 3.14) containing the same ancillary ligand DAF as in complex **3.36** but different cyclometalating ligands 2-(2,4-difluorophenyl)-5-methylpyridine aiming to obtain complex with blue shifted emission.



Scheme 3.14 Formation of iridium complex **3.49** containing 2-(2,4-difluorophenyl)-5-methylpyridine (dfm-ppy) as cyclometalating ligand and 9,9-dioctyl-4,5-diazafluorene as ancillary ligand.

All synthesised Ir complexes **3.36-3.49** have been characterised by ¹H NMR, ¹³C NMR, ¹⁹F NMR, ³¹P NMR and MS-ESI. All synthesised complexes have been purified by repeated column chromatography to ensure high purity of the samples prior to photophysical and electrochemical measurements (see next sections). The ratio between DAF and ppy in all these Ir complexes are 1:2 determined from integration of ¹H NMR signals. It has been demonstrated by the sets of signals of ppy and DAF ligands of ¹H NMR spectra of Ir complexes that some of them are non-symmetric (**3.37**, **3.39**, **3.40**, and **3.43**) while the others have C₂-symmetry (**3.36**, **3.38**, **3.41**, **3.42**, **3.44**, **3.45**, **3.46**, **3.47**, **3.48**, and **3.49**). It is worth mentioning here that the two-octyl groups at the C-9 position of DAF ligand itself are orthogonal to the plane of the aromatic ring. As a result, the β-CH₂ at C-9 is under the influence of aromatic ring current and appear down shifted to about 0.7-0.6 ppm. Such shift of β-CH₂ protons are also observed in their Ir complexes. For illustration, ¹H NMR spectra of complex **3.36** and **3.39** are shown in Fig. 3.11 and 3.12. It may also be noted that the resonance signals of the β-CH₂ protons at C-9 slightly changes their shifts with the change of substituents at 2,7- / 3,6- positions of DAF. For instance, this effect can be clear seen in the ¹H NMR spectrum of 3,6-diphenyl substituted DAF Ir complexes **3.39** (Fig. 3.12, β-CH₂ = 0.78-0.61 ppm) as compared to unsubstituted DAF Ir complex **3.36** (Fig. 3.11, β-CH₂ = 1.12-0.90 ppm).

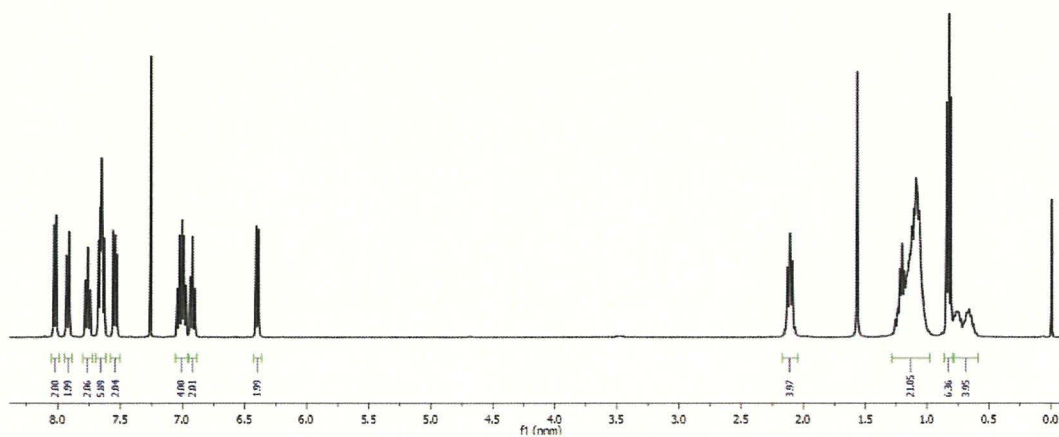


Fig. 3.11 ^1H NMR spectrum of Ir complex **3.36** in CDCl_3 .

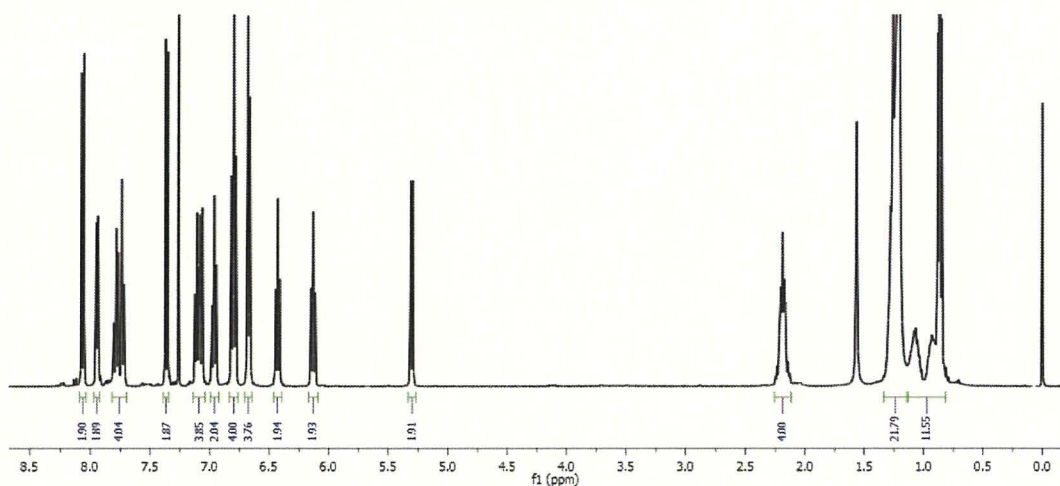


Fig. 3.12 ^1H NMR spectrum of Ir complex **3.39** in CDCl_3 .

Several attempts to grow single crystals for these complexes (**3.36**, **3.37**, **3.38**, **3.39**, and **3.45**) in different solvents and co-solvent systems had been done but none of them provided good quality crystals for single crystal X-ray analysis. The synthesised complexes are well soluble in common organic solvents and are air- and moisture stable materials. Figure 3.13 shows the appearance of the of different synthesised Ir complexes as coloured powder / polycrystalline materials.



Fig. 3.13 Appearances of synthesised iridium complexes with 4,5-diazafluorenes **3.36–3.47** in the solid state.

To illustrate the emissive behaviour of the Ir complexes, consider an appearance of the solutions of about 1 mg of each of the Ir complexes dissolved in 10 mL of dichloromethane (colourless transparent solution). As soon as we irradiated these solution with UV light (360 nm) the emission of colours of the samples can be observed by naked eyes (Fig. 3.14)

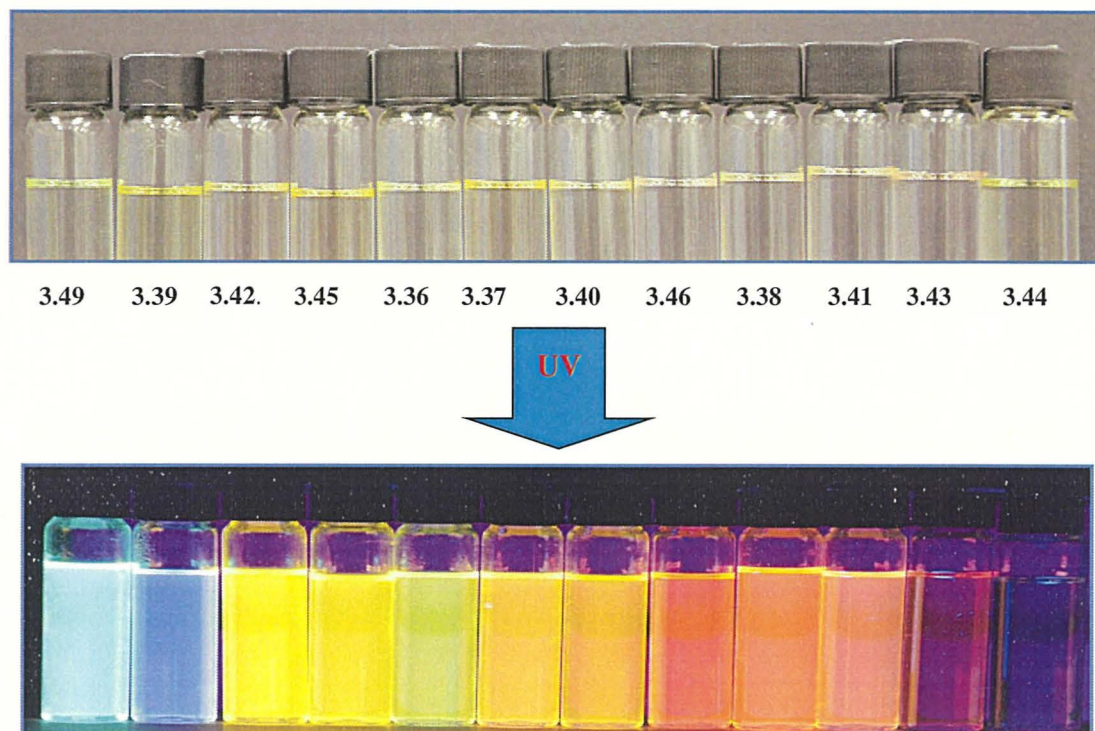


Fig. 3.14 An emission of iridium complexes **3.36–3.49** (except **3.47** and **3.48**) in DCM solution under (a) sunlight (top) and (b) under UV irradiation (360 nm) (bottom).

3.2.4 Photophysical studies of Ir complexes

3.2.4.1 Absorption and emission study of Ir complexes in solution state

The important physical data for Ir complexes (**3.36–3.49**) are listed in Table 3.1. The absorption spectra of Ir complexes were measured in acetonitrile at room temperature. UV-Vis absorption spectra show strong bands between 230 nm to 300 nm can be attributed to spin allowed intraligand ($\pi-\pi^*$) transition.⁷⁷ Absorption spectra of complex **3.37** to **3.48** (Fig. 3.15–3.16) show red shift for substituted DAF compared to unsubstituted DAF (complex **3.36**). Lower energy bands (ca. 300 to 450 nm) can be associated to metal-to-ligand-charge transfer (MLCT).⁷⁸ Absorption spectra of complexes **3.47** and **3.48** show additional longer wavelength

band associated with presence of carbonyl group in the same structure (ca. 400 nm to 500 nm) (Fig. 3.16).

Emission spectra of all the complexes were measured in degassed HPLC grade acetonitrile at room temperature (excited between 400 and 430 nm). They emit green to red light (523–647 nm, Fig. 3.17–3.18) in acetonitrile solution. Complexes **3.47** and **3.48** were found to be non-emissive that was attributed to the forbidden transition of keto group. The broad and structureless characteristic of the emission spectra can be attributed transitions from mixed MLCT / $\pi \rightarrow \pi^*$ states which has been proved for other iridium complexes as determined by high-resolution spectroscopy.²⁹ Photoluminescent quantum yields in acetonitrile were found to be in the range 0.2 to 43 % ([Ru(bpy)₃](PF₆)₂ as internal standard). Quantum yields for the phenyl-DAF complexes was found to be low (4% for **3.39** and 8% for **3.42**) compared to unsubstituted-DAF complex **3.36** (23%). As expected, the quantum yields of the rigid *bis*(octyloxyphenyl)-DAF based Ir complex **3.45** (31%) was found to be higher than the flexible dioctyl-DAF based complex **3.36** (23%). However, due to some unknown reason the quantum yield of similar rigid bromo substituted *bis*(octyloxyphenyl)-DAF Ir complex **3.46** (3.0%) found to be quite low much lower than expected. We have synthesised 2-cyano-DAF and 2,7-dicyano-DAF based Ir complexes (**3.43**, **3.43**) based on our DFT predictions that emission energy should be substantially red-shifted (720.3 nm and 883.9 nm respectively) (Table 3.5). Interestingly, as predicted by DFT calculation, monocyano-DAF based iridium complex **3.43** in acetonitrile was found to emit in deep red region (653 nm, Table 3.1), but with low quantum yield (0.2%) while dicyano-DAF based iridium complex **3.44** was found to be not emissive (PL measured up to 900 nm of spectrum). As expected and supported by our DFT calculation the fluoro substituted ppy based Ir complex **3.49** exhibit about 90 nm blue-shifted emission maximum (513 nm) compared to ppy-based Ir complex **3.36** (583 nm).

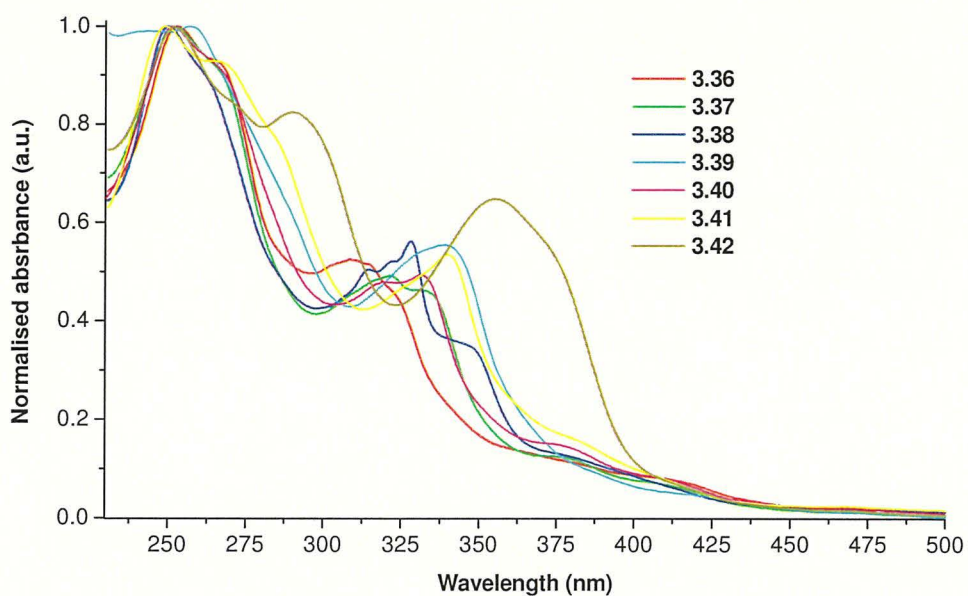


Fig. 3.15 Normalised absorption spectra of cationic Ir(III) complexes **3.36-3.42** in acetonitrile.

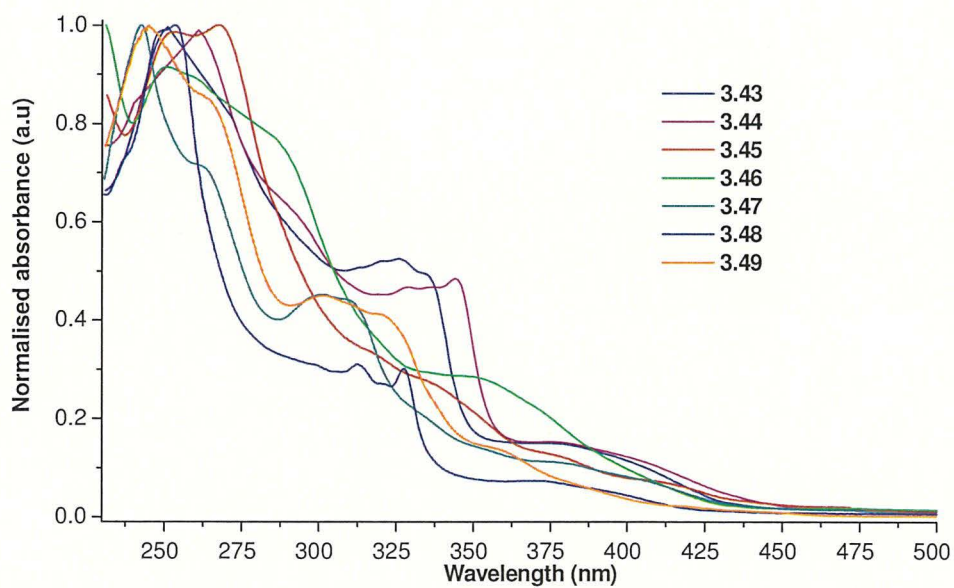


Fig. 3.16 Normalised absorption spectra of cationic Ir(III) complexes **3.43-3.49** in acetonitrile.

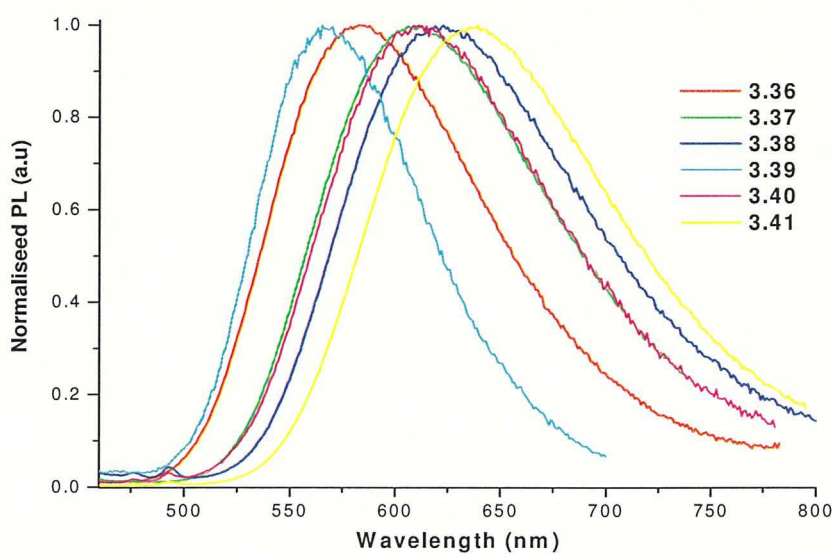


Fig. 3.17 Normalised photoluminescence spectra of complexes **3.36–3.41** in acetonitrile excited between 400 to 430 nm.

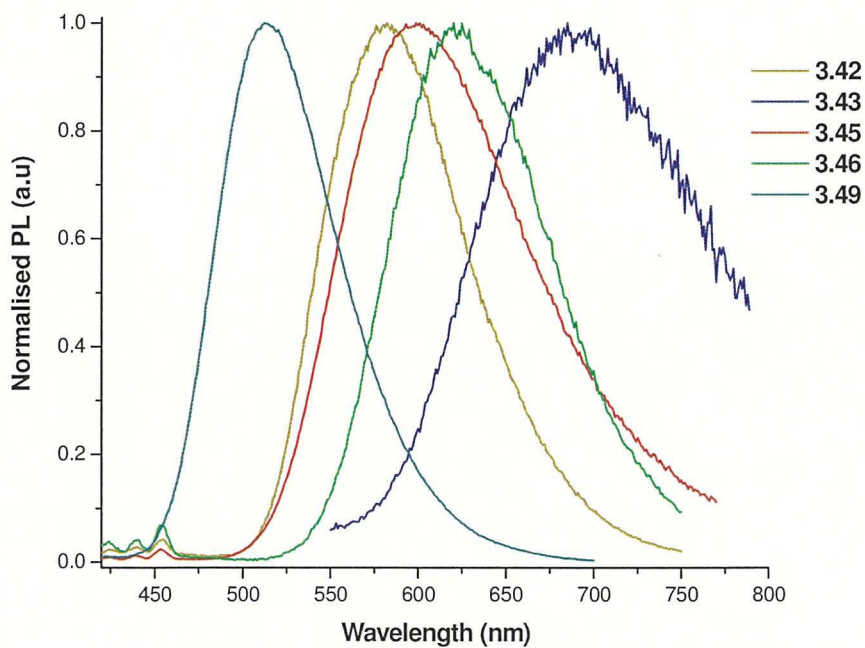
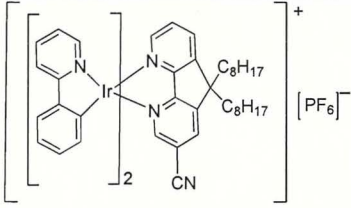
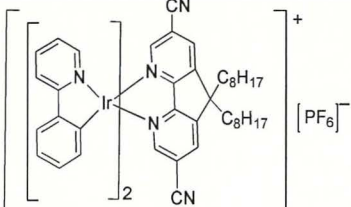
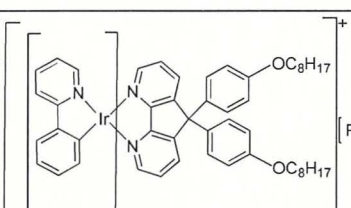
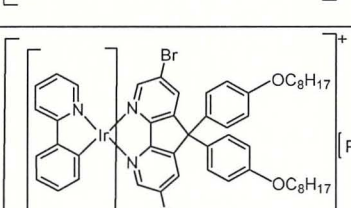
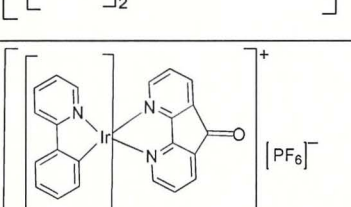
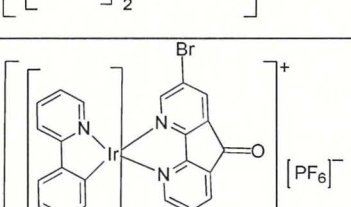
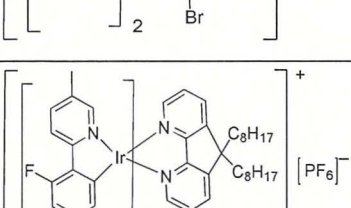


Fig. 3.18 Normalised photoluminescence spectra of complexes **3.42, 3.43, 3.45, 3.46, and 3.49** in acetonitrile, excited between 400 to 430 nm.

Table 3.1 Absorption (λ_{abs}) and photoluminescence data (λ_{PL} , PLQY) for iridium complexes in acetonitrile at room temperature.

Ir complex	Structures of Ir complexes	λ_{abs} (nm) ^a	λ_{PL} (nm) ^b	PLQY, Φ_{PL} (%) ^c
3.36 (SG091B)		253, 269, 313, 386	583	23
3.37 (SG082C)		250, 273, 320, 335, 379, 415, 469	608	27
3.38 (SG077B)		250 267 329 348 381 408	620	20
3.39 (SG083E)		252, 314, 384, 416, 468	567	4.0
3.40 (SG089B)		251, 272, 314, 341, 376, 412	610	28
3.41 (SG080B)		247, 266, 340, 404	636	26
3.42 (SG114B)		251, 290, 354, 420	580	8.0

3.43 (SG134B)		254, 326, 390	687	0.2
3.44 (SG127C)		261, 344, 393	—	—
3.45 (SG088B)		252, 282, 413	597	31
3.46 (SG086E)		248, 266, 288, 361, 419	620	3.0
3.47 (SG079)		241, 265, 297, 315, 383, 413	—	—
3.48 (SG090)		251, 312, 327, 372	—	—
3.49 (SG112)		244, 265, 301, 388	513	43

^aMeasured in ACN at room temperature. ^bMeasured in degassed ACN at room temperature, exited between 400 and 430 nm. ^cIn degassed ACN, using [Ru(bpy)₃](PF₆)₂ as standard ($\Phi_{\text{PL}}^{\text{s}} = 9.5\%$).⁷⁹

3.2.4.2 Electrochemical studies of Ir(III) complexes 3.36–3.49

The redox properties of the complexes **3.36–3.49** (Fig. 3.19–3.21, Table 3.2) were studied by cyclic voltammetry in anhydrous acetonitrile solutions. The oxidation process for the Ir complexes (usually attributed to Ir^{III}/Ir^{IV}) exhibits quasi-reversible or irreversible waves at 100 mV/s (except **3.49**, which shows the reversible oxidation process) and becomes reversible at higher scan rates of 1000 mV/s confirming electrochemical reversibility.

The half-wave oxidation potentials were in the range of 0.88 (**3.45**) to 1.18 V (**3.49**) versus Fc/Fc⁺ redox pair as an internal standard. The highest occupied molecular orbital (HOMO) of [Ir(ppy)₂(N[^]N)]PF₆ complexes are known as the mixture of the orbitals of iridium and the phenyl group of ppy ligand.⁵⁴ The oxidation potentials are linked to the HOMO energies of the complex. Therefore, there is no straightforward correlation between the electron-withdrawing/donating properties of the substituent in the DAF ligands (ancillary ligand) and the oxidation potentials. For example, the introduction of one bromine atom at 2 positions lowers the $E_{1/2}$ by 0.03V, whereas two Br atoms at 2,7 positions increase it by 0.03 V. The modification of the cyclometalating ligands changes the oxidation potential, $E_{1/2}^{ox}$, considerably and no changes is reduction potential. As a result, the redox gap E_g of **3.36** (unsubstituted ppy) is low compared to **3.49** (fluoro substituted ppy) with the differences of their $E_{1/2}^{ox} = 0.25$ V, which is responsible for blue shifted emission of the later. First reduction potentials of the complexes with DAF ligands occurs at -1.6 to -1.8 V, which is lower than for complexes with bipyridine ancillary ligands⁴⁸ and similar to that reported for other Ir^{III} complexes with substituted diazafluorene.^{54,69a}

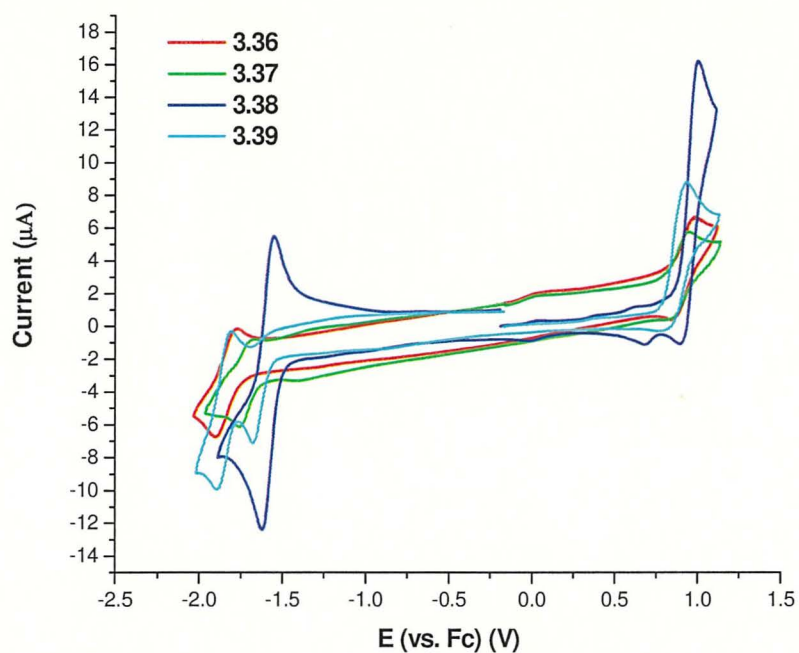


Fig. 3.19 Cyclic voltammogram of complexes **3.36–3.39** in ACN solutions at room temperature containing 0.1 M Bu_4NPF_6 ; scan rate 100 mV/s (**3.36**, **3.37**) and 1000 mV/s (**3.38**, **3.39**).

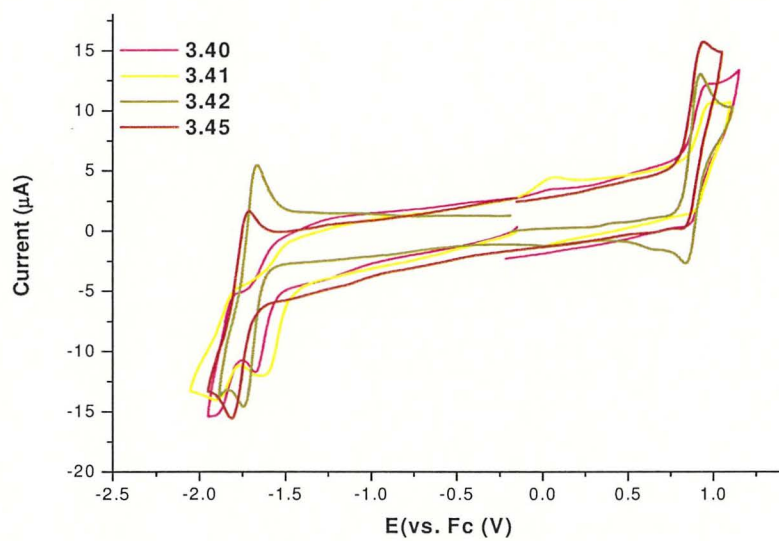


Fig. 3.20 Cyclic voltammogram of complexes (**3.40–3.42**, **3.45**) in ACN solutions at room temperature containing 0.1 M Bu_4NPF_6 ; scan rate 100 mV/s (**3.40**) and 1000 mV/s (**3.41**, **3.42**, **3.45**).

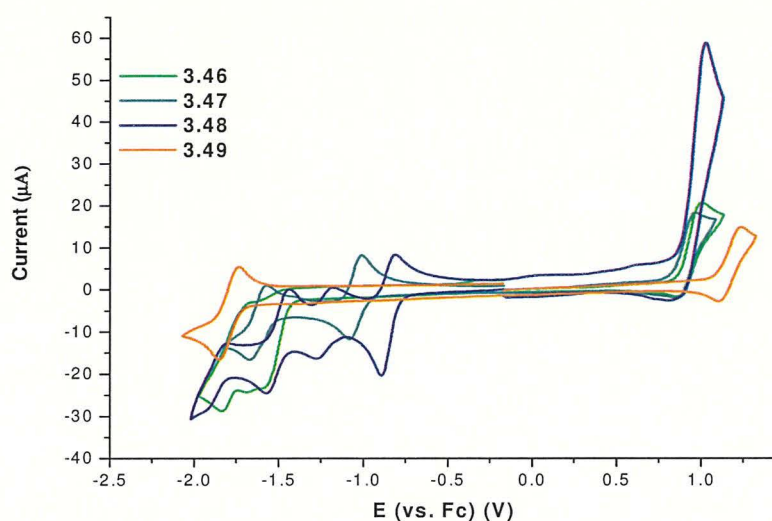


Fig. 3.21 Cyclic voltammogram of complexes **3.46-3.49** in ACN solutions at room temperature containing 0.1 M Bu₄NPF₆; scan rate 100 mV/s (**3.46**, **3.49**) and 1000 mV/s (**3.47**, **3.48**).

Introduction of phenyl substituents (**3.39**, **3.42**, **3.45**, **3.46**) to the DAF ligand shift the reduction peaks to less negative potentials (with respect to unsubstituted DAF in **3.36**), and similarly for substitution by electron-withdrawing halogen atoms. The first reduction peaks of the complexes with 4,5-diazafluorenes substituted at 2 and 7 positions, as well as with 3,6-diphenyl-4,5-diazafluorene (**3.39**, Fig. 3.19) are irreversible (but for **3.45** becomes reversible at 1000 mV/s). Complexes with 4,5-diazafluorenones (**3.47**, **3.48**, Fig. 3.19) are reduced at much less negative potentials (due to the presence of the carbonyl group). Interestingly, the reduction potential of the complex with 4,5-diazafluoren-9-one is ca. 0.4 V less negative than that of the ligand itself (-1.06 V vs. SCE, -1.44 V vs. Fc).⁸⁰ HOMO–LUMO energy gap was found to be lowest for DAFone complex **3.48** (1.88 eV) while highest for fluoro-substituted complex **3.49** (3.03 eV) calculated from cyclic voltammogram (Table 3.2). Overall, the oxidation potentials are independent of the N[^]N ligands and depends strongly on C[^]N ligands. On the other hand, the redox potentials are found to be dependent on the N[^]N ligands.

Table 3.2 Redox potentials of complexes and HOMO-LUMO energies determined by cyclic voltammetry.^a

Ir complex	$E_{1/2}^{ox1}$ (V)	E_p^{red1} (V)	$E_{1/2}^{red1}$ (V)	$E_{1/2}^{red2}$ (V)	$E_{1/2}^{red3}$ (V)	HOMO (eV)	LUMO (eV)	E_g (eV) ^g
3.36	0.92	-1.90	-1.84	-	-	-5.72	-2.90	2.82
3.37	0.92	-1.76	-1.72	-	-	-5.72	-3.04	2.68
3.38	0.96 ^b	-1.62	-1.58	-	-	-5.79	-3.15	2.64
3.39	0.90 ^b	-1.68	^c	-1.85	-	-5.70	-3.12	2.57
3.40	0.90	-1.68	^c	-1.85	-	-5.70	-3.12	2.58
3.41	0.92 ^b	-1.64 ^b	-1.58 ^b	-1.74 ^{bd}	-1.86 ^b	-5.75	-3.20	2.55
3.42	0.88 ^b	-1.75 ^b	-1.71 ^b	-	-	-5.68	-3.06	2.63
3.45	0.88 ^b	-1.81	-1.76 ^b	-	-	-5.68	-2.98	2.70
3.46	0.93	-1.59	^c	-1.59 ^d	-1.76	-5.73	-3.21	2.52
3.47	0.93 ^b	-1.07	-1.04	-1.61		-5.79	-3.91	1.88
3.48	0.99 ^b	-0.89	-0.85	-1.22	-1.50 -1.87 ^e	-5.73	-3.73	2.00
3.49	1.18	-1.85	-1.79	-	-	-5.97	-2.95	3.03

^aMeasured in CH₃CN solutions containing 0.1M Bu₄NPF₆; scan rate 100 mV/s. ^bMeasured at scan rate 1 V/s, ^cIrreversible peak. ^dIrreversible peak potential $E_{1/2}^{red4}/V$. ^fDeduced from equation ($E_{HOMO} = -4.8 - E_{1/2}^{ox1}$; $E_{LUMO} = -4.8 - E_p^{red1}$).⁸¹ ^g $E_g = E_{HOMO} - E_{LUMO}$. (Note: for complex **3.43** and **3.44** CV measurements were not performed).

3.2.5 Computational studies of iridium(III) complexes by DFT method

To provide insight into the electronic structure of the obtained complexes, and to aid in the design of future synthetic targets, DFT and TD-DFT calculations on iridium complexes were carried out. All the computational studies were performed in Gaussian 09⁸² using DFT and TD-DFT method as applied in that software package. For all the Ir complexes geometry was optimised with methyl substituted instead of octyl substituted DAF to save time of calculation, which normally does not affect the outcome of calculated result. The HOMO and LUMO energies were determined using minimised singlet geometries and used them to approximate the triplet geometries. The TD-DFT with hybrid density functional (LANL2DZ) and effective core potentials (ECP) was successfully applied to model the absorption and emission properties of a variety of Ir(III) complexes, most often using B3LYP functional^{83, 84} but also PBE0⁸⁵ and Minnesota⁸⁶ functional were used. It is well known that the inclusion of

solvent effects (by means of a solvation model, for example PCM) is necessary in order to obtain qualitatively correct results.³⁶

The computed vertical excitation energies at the ground state geometries using B3LYP functional, LANL2DZ ECP as a basis set for Ir and 6-31G(d,p) as basis set for other atoms are compiled in Table 3.4. The S_1 and T_1 excited states are almost pure HOMO–LUMO transitions, and, given the localisation of the frontier orbitals, can be classified as MLCT states (except T_1 of **3.39**, which has some intraligand character). The oscillator strengths of S_1 states are vanishingly low; therefore, their energies do not provide a good estimate of the absorption onset. A qualitatively good accordance with experimental absorption spectra observed for the complex **3.36** shown in Fig. 3.22.

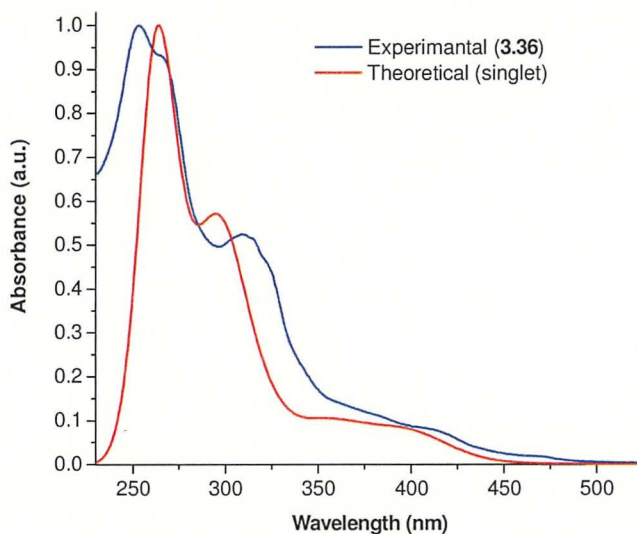


Fig. 3.22 Theoretical UV-Vis spectrum of complex **3.36** (SG091) superimposed with the experimental spectrum in acetonitrile. [Calculated using TD-DFT with B3LYP functional and LANL2DZ basis set with ECP for Ir, 6-31G(d,p) basis set for other atoms, IEF-PCM solvation model in acetonitrile (first 50 singlet transitions, FWHM 300 cm^{-1})]

In all the cases, the HOMO orbital is a mixture of Ir d orbitals and π orbitals of the cyclometalating ligands, whereas LUMO is located exclusively on the DAF ligand. For illustration, the frontier atomic orbital composition of complex **3.39** is shown in Fig. 3.23.

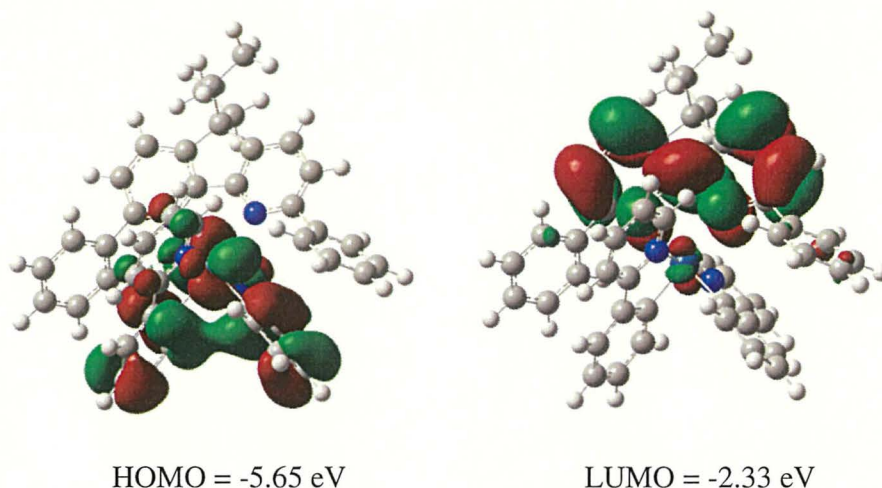


Fig. 3.23 The frontier molecular orbitals of **3.39** (ground state geometry).

[Calculated using B3LYP functional and LANL2DZ basis set with ECP for Ir, and 6-31G(d,p) basis set for other atoms, using IEF-PCM solvation model in acetonitrile]

From the orbital energy level diagram (Fig.3.24) it can be seen that, the presence of the electron withdrawing substituents in cyclometalating ligands (complex **3.49**) stabilised the HOMO more than the LUMO, in contrast, the electron withdrawing substituents in ancillary ligand (complex **3.41**) stabilised the LUMO more than the HOMO, compared to the unsubstituted complex **3.36**. As a result, the HOMO-LUMO gap of complex **3.49** (3.50 eV) is higher while it is lower for the complex **3.41** (3.04 eV), when compared to the complex **3.36** (3.28 eV). These results support the observed experimental blue-shifted emission of complex **3.49** (513 nm) and red-shifted emission of complex **3.41** (636 nm) with respect to the emission maximum of the complex **3.36** (583 nm) in acetonitrile (Table 3.1). In addition, the calculated results support the redox potentials of Ir complexes obtained by CV measurements (Table 3.2). The orbital energy level diagram for the synthesised Ir complexes **3.39-3.49** is shown in Fig. 3.25, which depicts the changes in HOMO-LUMO gap with the change in substitution of ligands.

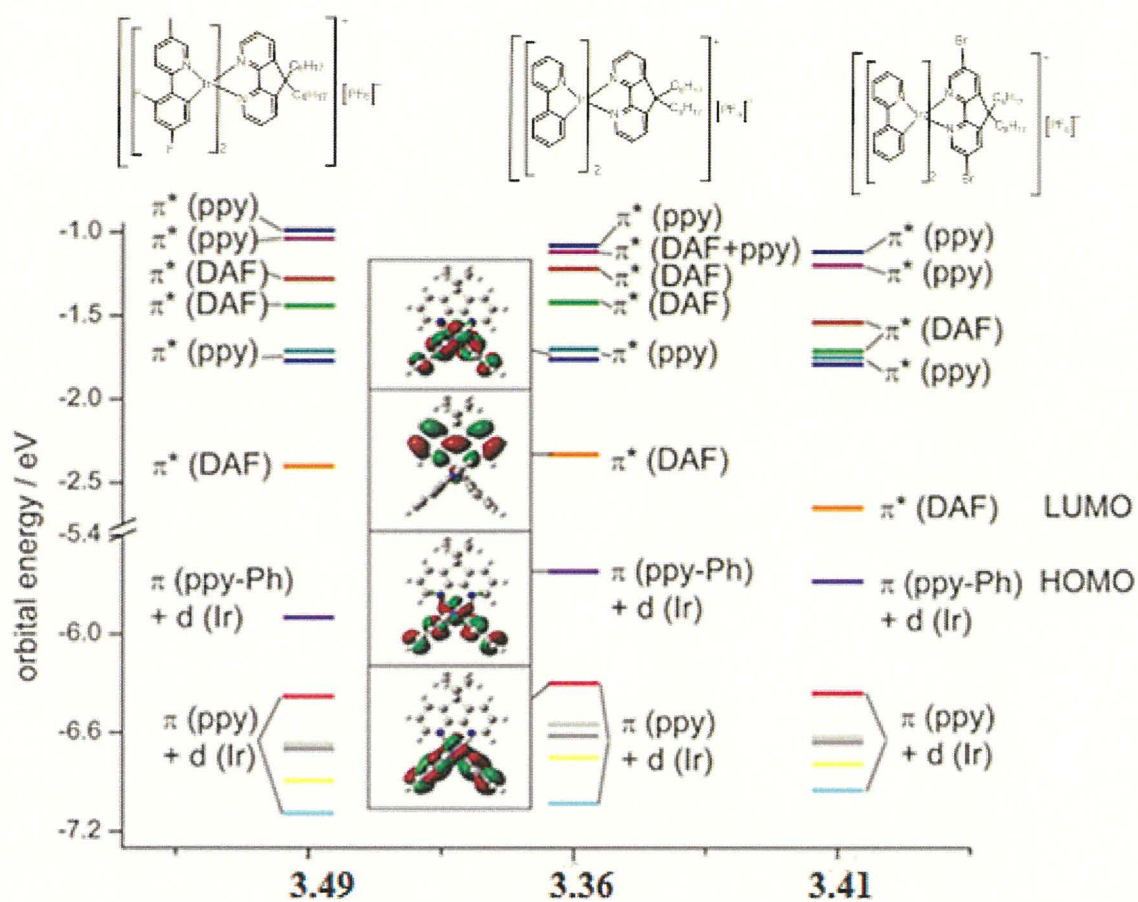


Fig. 3.24 Energy level diagram and character of the frontier MOs of Ir complexes **3.49**, **3.36** and **3.41**. [Calculated using B3LYP and LANL2DZ basis set with ECP for Ir, 6-31G(d,p) basis set for other atoms (with IEF-PCM solvation model), from -7 eV to vacuum level, HOMO orbitals are shown in purple, LUMO in orange On the middle isodensity of selected MOs for Ir complex **3.36** also shown].

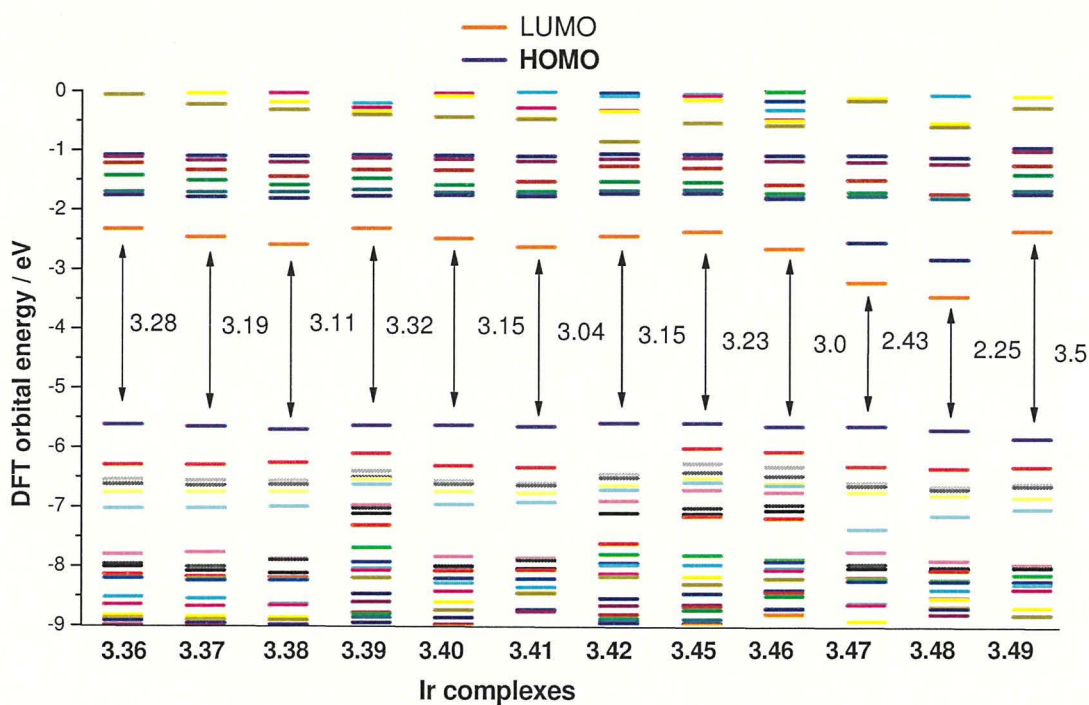
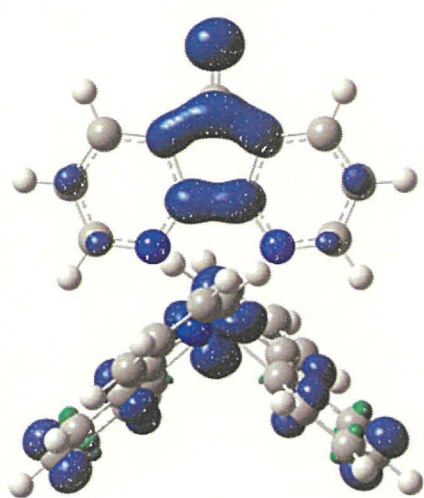


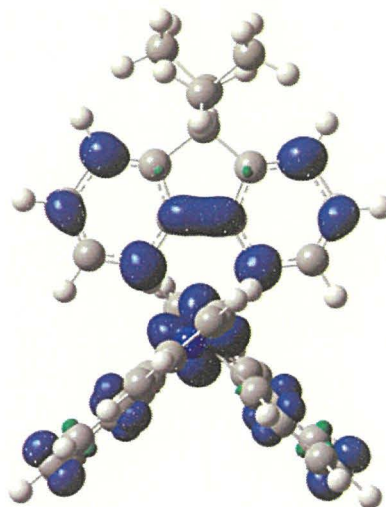
Fig. 3.25 Orbital energies diagram of iridium complexes **3.36–3.49** (except **3.43**, **3.44**). [Calculated by DFT method using B3LYP functional and LANL2DZ basis set with ECP for Ir and 6-31G(d,p) basis set for other atoms (with IEF-PCM solvation model in acetonitrile, from -7 eV to vacuum level, HOMO orbitals are shown in purple, LUMO are in orange.)]

The spin densities of the first triplet state (T_1) of selected complexes have been plotted (Fig. 3.26), to illustrate the localisation of the unpaired electrons. It indicates that the excitation to T_1 implies an electron promotion from the Ir-ppy environment to the ancillary ligands (DAF). In the case of emissive complexes **3.36** and **3.39**, the unpaired spins are located on the iridium d orbital, as well as the π orbitals of the DAF and ppy ligands (note that the phenyl rings of **3.39** do not seem to contribute to delocalization of the unpaired spin). In the T_1 state of **3.47**, the complex with DAFfone, a large proportion of the unpaired spin is located around the C=O group, this excited state can therefore be described as a mixture of ${}^3\text{MLCT}$ (typical for emissive Ir(III) complexes) and fluorenone-like ${}^3\text{IL}$ (which usually decays non-radiative). Additional evidence for the participation of the carbonyl group in the T_1 states of **3.47** and **3.49** is provided by the analysis of changes in geometry between the ground state and T_1 state. In the case of the emissive complexes with DAF derivatives, a decrease (by 0.03–0.09 Å) in Ir-DAF bond lengths were observed, accompanied by a shortening of Ir-C bonds by 0.02–0.03

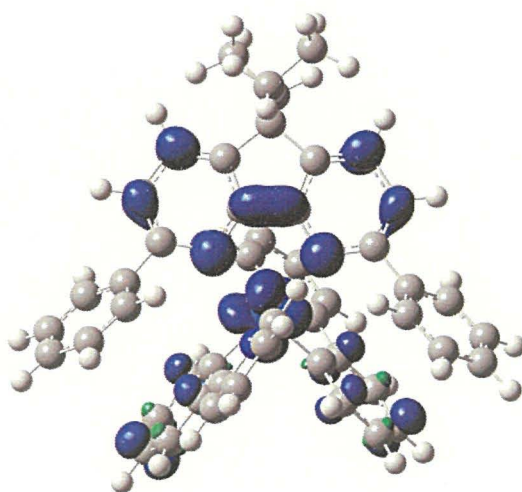
Å. In contrast, the Ir-DAFone bonds in **3.47** and **3.48** are shortened by just 0.014–0.017 Å, the Ir-C bonds undergoes a similar decrease (0.03 Å), while the C=O bonds are elongated by 0.04 Å. The calculated selected bond lengths in ground state and first triplet state of all the Ir complexes are compiled in Table 3.7 and their differences in Table 3.8. The Ir-N (DAF) distances of 3,6 substituted complexes (**3.38**, **3.39**) are comparatively higher than the other complexes suggesting comparatively a distorted structure.



3.47 (SG079)



3.36 (SG091)



3.39 (SG083)

Fig. 3.26 Spin densities in the first triplet excited state of selected complexes.

[Calculated using B3LYP and LANL2DZ basis set with ECP for Ir, and 6-31G (d,p) basis set for other atoms, at T1 geometry, using IEF-PCM solvation model acetonitrile]

Although the DFT frontier orbital energies (especially using a moderately-sized basis set) do not generally represent accurate values of ionization potentials and electron affinities,⁸⁷ the correlation of DFT calculated HOMO and LUMO energies with those of electrochemical redox potentials is very good (Fig. 3.27).

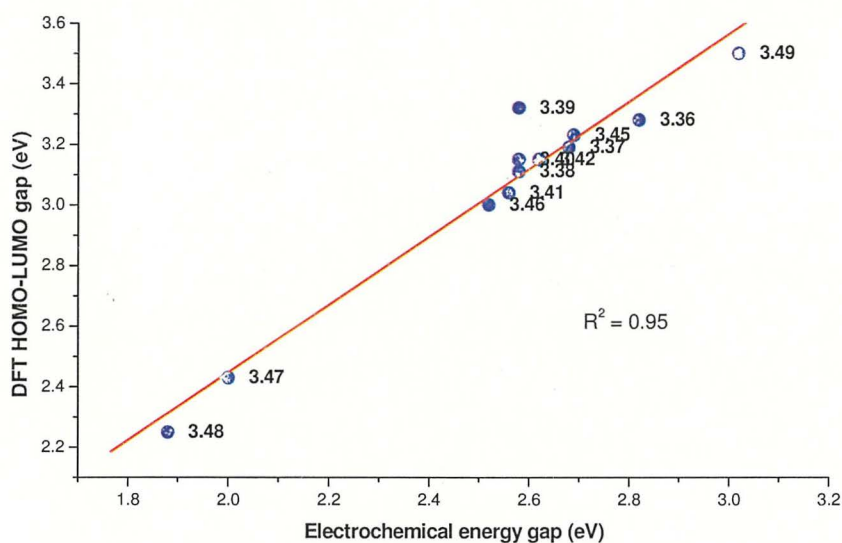


Fig. 3.27 DFT HOMO-LUMO gap (calculated using B3LYP functional, LANL2DZ basis set with ECP for Ir and 6-31G(d,p) basis set for other atoms, IEF-PCM solvation model) *versus* electrochemical energy gap determine by cyclic voltammetry.

The calculated (using B3LYP functional) T_1 and S_1 excited states at the T_1 state geometries have essentially the same character as in the ground state geometries, and the T_1 excitation energies match well the experimental emission maxima (Table 4 5, Fig. 3.28), the average difference being 6.9 nm (0.022 eV), maximum difference (for **3.38**) was 19.3 nm (0.06 eV). These deviations are much smaller than the average error of TD-DFT at B3LYP/TZVP level for singlet excited states of organic molecules (0.07 eV)⁸⁸ and triplet excitations of organic dyes (0.44 eV)⁸⁹ versus best theoretical estimates. Thus, TD-DFT calculations appear to be an excellent tool for prediction of the emitted energy of Ir (III) complexes with DAF. Interestingly, the TD-DFT calculation using B3LYP functional for the cyano-substituted complexes **3.43** and **3.44** predicted emission at far-red region of spectrum 720.3 nm and 883.9 nm. These results derive us to syntheses complexes **3.43** and **3.44** and measure their emission. Experimentally, the complex **3.43** found to weakly emitting at 687 nm, which is highest red-shifted emitting complex among the Ir-complexes **3.36-3.49**. However, the complex **3.44**

found to be not emitting upto 900 nm of spectrum. A better value of emission maximum predicted with MO6 functional instead of B3LYP functional for some of the complexes are listed in Table 3.6.

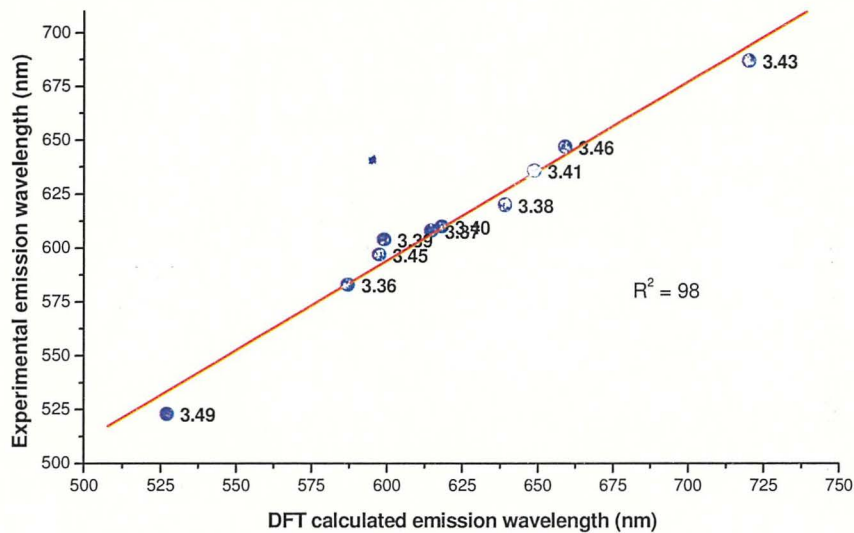


Fig. 3.28 Experimental *versus* theoretical emission wavelengths (with linear fit line), calculated using TD-DFT with B3LYP functional, LANL2DZ basis set with ECP for Ir and 6-31G(d,p) basis set for other atoms.

Table 3.4 Absorption maxima of Ir(III) complexes calculated at ground state geometries for first singlet and triplet excited states, S₁ and T₁.^a

No	S ₁				T ₁			
	λ_{abs} (nm)	f	dominant excitations	Character	λ_{abs} (nm)	dominant excitations	Character	
3.36	473.4	0.0004	HOMO→ LUMO (99%)	¹ MLCT	477.6	HOMO→ LUMO (97%)	³ MLCT	
3.37	489.1	0.0006	HOMO→ LUMO (99%)	¹ MLCT	493.2	HOMO→ LUMO (98%)	³ MLCT	
3.38	502.8	0.0002	HOMO→ LUMO (99%)	¹ MLCT	506.1	HOMO→ LUMO (98%)	³ MLCT	
3.39	466.2	0.001	HOMO→ LUMO (99%)	¹ MLCT	472.6	HOMO→ LUMO (92%), H-5→LUMO (3%)	³ MLCT/ ³ IL	
3.40	498.3	0.0003	HOMO→ LUMO (99%)	¹ MLCT	502.7	HOMO→ LUMO (98%)	³ MLCT	
3.41	521.1	0.0002	HOMO→ LUMO (99%)	¹ MLCT	525.8	HOMO→ LUMO (98%)	³ MLCT	
3.43	569.6	0.0002	HOMO→ LUMO (99%)	¹ MLCT	573.8	HOMO→ LUMO (98%)	³ MLCT	
3.44	668.7	0.0001	HOMO→ LUMO (99%)	¹ MLCT	673.7	HOMO→ LUMO (98%)	³ MLCT	
3.42	499.2	0.0002	HOMO→ LUMO (99%)	¹ MLCT	501.3	HOMO→ LUMO (98%)	³ MLCT	
3.45	484.0	0.0003	HOMO→ LUMO (99%)	¹ MLCT	488.1	HOMO→ LUMO (98%)	³ MLCT	
3.46	527.8	0.0002	HOMO→ LUMO (99%)	¹ MLCT	532.6	HOMO→ LUMO (98%)	³ MLCT	
3.47	657.6	0.0002	HOMO→ LUMO (99%)	¹ MLCT	658.7	HOMO→ LUMO (99%)	³ MLCT	
3.48	724.1	0.0002	HOMO→ LUMO (99%)	¹ MLCT	725.3	HOMO→ LUMO (99%)	³ MLCT	
3.49	436.9	0.0003	HOMO→ LUMO (99%)	¹ MLCT	441.7	HOMO→ LUMO (91%)	³ MLCT	

^aCalculated using TD-DFT with B3LYP functional, LANL2DZ basis and ECP for Ir, 6-31G(d,p) basis for other atoms, for the ground state geometries optimized at the same level, using IEF-PCM solvent model in ACN. (Note: for complexes **3.43**, **3.44** calculations were not performed).

Table 3.5 Emission maxima data calculated at first triplet excited state geometry of studied iridium complexes.^a

No	T ₁ , λ _{PL} / nm	Dominant excitations	Character	λ _{PL} (exp) / nm	Difference
3.36	587.2	HOMO→LUMO (98%)	³ MLCT	583	4.2
3.37	614.8	HOMO→LUMO (99%)	³ MLCT	608	6.8
3.38	639.3	HOMO→LUMO (99%)	³ MLCT	620	19.3
3.39	599.2	HOMO→LUMO (98%)	³ MLCT	604	6.0
3.40	618.3	HOMO→LUMO (99%)	³ MLCT	610	8.3
3.41	649.0	HOMO→LUMO (99%)	³ MLCT	636	13.0
3.42	604.8	HOMO→LUMO (87%)	³ MLCT	600	4.8
3.43	720.3	HOMO→LUMO (99%)	³ MLCT	687	32.3
3.44	883.9	HOMO→LUMO (99%)	³ MLCT	–	–
3.45	597.5	HOMO→LUMO (99%)	³ MLCT	597	0.5
3.46	659.3	HOMO→LUMO (99%)	³ MLCT	647	12.3
3.47	929.4	HOMO→LUMO (99%)	³ MLCT	–	–
3.48	1054.1	HOMO→LUMO (100%)	³ MLCT	–	–
3.49	527.2	HOMO→LUMO (94%)	³ MLCT	523	4.2

^aCalculated using TDDFT with B3LYP functional, LANL2DZ basis and ECP for Ir, 6-31G(d,p) basis for other atoms, at T₁ state geometries optimized (with UKS) at the same level, using IEF-PCM solvent model.

Table 3.6 Emission maximum calculated at first triplet excited state geometry, comparison of B3LYP and M06.^{a,b}

No	B3LYP, T ₁ $\lambda_{\text{PL}}(\text{calc})$ (nm)	M06, T ₁ λ_{PL} (calc, nm)	λ_{PL} (exp, nm)	$\Delta\lambda_{\text{PL}}$ (calc-exp) (nm) (B3LYP)	$\Delta\lambda_{\text{PL}}(\text{calc}-\text{exp}) / \text{nm}$ (M06)
3.36	587.2	576.6	583	+4.2	-4.4
3.37	614.8	600.2	608	+6.8	-7.8
3.38	639.3	614.7	620	+19.3	-5.3
3.39	599.2	596.8	604	-4.8	+7.2
3.40	618.3	606.9	610	+8.3	-3.1
3.41	649.0	638.4	636	+13.0	+2.4
3.42	604.8	–	600	+4.8	–
3.43	720.3	–	687	-32.3	–
3.44	883.9	–	–	–	–
3.45	597.5	586.6	597	+0.5	-10.4
3.46	659.3	–	647	+12.3	–
3.47	929.4	–	–	–	–
3.48	1054.1	–	–	–	–
3.49	527.2	518.4	523	+4.2	-4.6

^a Calculated using TD-DFT with B3LYP or M06 functional, LANL2DZ basis and ECP for Ir, 6-31G(d,p) basis for other atoms, at T₁ state geometries optimized (with UKS) at the same level, using IEF-PCM solvent (acetonitrile) model. ^b PBE0/6-31G(d,p) results: **3.38** (SG077): emission at 589.4 nm (error -36.4 nm); SG091: emission at 548.1 nm (error -38.9 nm). B3LYP/6-311G(2d,p) results:**3.38** (SG077): emission at 644.7 nm (error 24.7 nm);**3.36** (SG091): emission at 596.6 nm (error 13.6 nm).

Table 3.7 Selected bond lengths in ground state and first triplet excited state.^a

No.	Ir–N (DAF)		Ir–N (ppy)		Ir–C (ppy)		C=O	
	S ₀	T ₁	S ₀	T ₁	S ₀	T ₁	S ₀	T ₁
3.36	2.287	2.252	2.082	2.078	2.014	1.991		
3.37	2.257	2.244	2.079	2.077	2.005	1.982		
3.38	2.382	2.329	2.081	2.079	2.010	1.985		
3.39	2.375	2.321	2.082	2.072	2.016	1.990		
3.40	2.296	2.259	2.081	2.079	2.014	1.990		
3.41	2.298	2.263	2.082	2.080	2.013	1.987		
3.42	2.291	2.259	2.081	2.078	2.014	1.991		
3.43	2.254	2.227	2.072	2.081	1.974	1.986		
3.44	2.303	2.277	2.083	2.082	2.013	1.984		
3.45	2.290	2.254	2.080	2.079	2.014	1.989		
3.46	2.301	2.266	2.082	2.080	2.012	1.986		
3.47	2.307	2.290	2.082	2.081	2.012	1.984	1.212	1.256
3.48	2.317	2.303	2.083	2.082	2.011	1.981	1.210	1.253
3.49	2.276	2.237	2.080	2.076	2.011	1.992		

^aCalculated using RB3LYP (S₀ state) or UB3LYP (T₁ state), using LANL2DZ basis set with ECP for Ir, 6-31G(d,p) basis set for other atoms, and IEF-PCM solvation model.

Table 3.8 Selected differences in bond lengths between the T₁ and S₀ geometries.^{a, b}

Ir complex	Ir–N (DAF)	Ir–N (ppy)	Ir–C (ppy)	C=O
	T ₁ –S ₀	T ₁ –S ₀	T ₁ –S ₀	T ₁ –S ₀
3.36	-0.035	-0.004	-0.023	
3.37	-0.012	-0.002	-0.022	
3.38	-0.054	-0.002	-0.025	
3.39	-0.054	-0.010	-0.027	
3.40	-0.037	-0.002	-0.024	
3.41	-0.034	-0.002	-0.026	
3.42	-0.032	-0.003	-0.023	
3.43	-0.032	-0.009	-0.012	
3.44	-0.026	-0.001	-0.029	
3.45	-0.036	-0.002	-0.024	
3.46	-0.035	-0.002	-0.026	
3.47	-0.017	-0.001	-0.029	0.043
3.48	-0.014	-0.001	-0.030	0.043
3.49	-0.039	-0.004	-0.019	

^aCalculated using RB3LYP (S₀ state) or UB3LYP (T₁ state), using LANL2DZ basis set with ECP for Ir, 6-31G(d,p) basis set for other atoms, and IEF-PCM solvation model. ^bDihedral angles between DAF and Ph ring of complex **137** (SG083) are 68.3 (in the ground state S₀) and 58.4 (in the first triplet excited state T₁).

3.2.6 Device test for a LEC based on the iridium(III) complex

Initial test of synthesised Ir complexes for using as electroluminescent material for LEC devices was performed at the School of Electronic Engineering of Bangor University. LEC was prepared by spin coating of solution of iridium complex in acetonitrile on ITO clean surface and then aluminium (100 nm) contact was deposited by thermal evaporation in vacuum. The first successful LEC device was made for the Ir complex **3.45** (emit yellow light in acetonitrile, $\lambda_{PL} = 597$ nm) in a simple device configuration ITO/**3.45**/Al (100 nm), which exhibited green electroluminescence (EL) with a maximum of $\lambda_{EL} = 567$ nm, i.e. the EL maximum is blue-shifted (by 30 nm) with respect to its PL emission maximum. Luminance intensity was measured at three different potentials of 3V, 3.5 V and 4 V respectively (Fig. 3.31). It was found that device with complex **3.45** shows maximum luminance of around 90 cd/m² at 4 V. The response time for the simple device in this configuration ITO/**3.45**/Al (100

nm) was found to be ca. 18 minutes (Fig 3.31). In order to improve the response time, ionic liquid 1-butyl-3-methylimidazolium hexafluorophosphate (BMIM:PF₆) was added into the electroluminescent material **3.45** and a LEC device with the configuration ITO/complex **3.45**:BMIMPF₆ (0.2%)/Al(100 nm) was tested. However, the prepared LEC device with ionic liquid failed to give EL emission. The more detailed studies will be carried out in collaboration with physicist experts in the LEC devices.

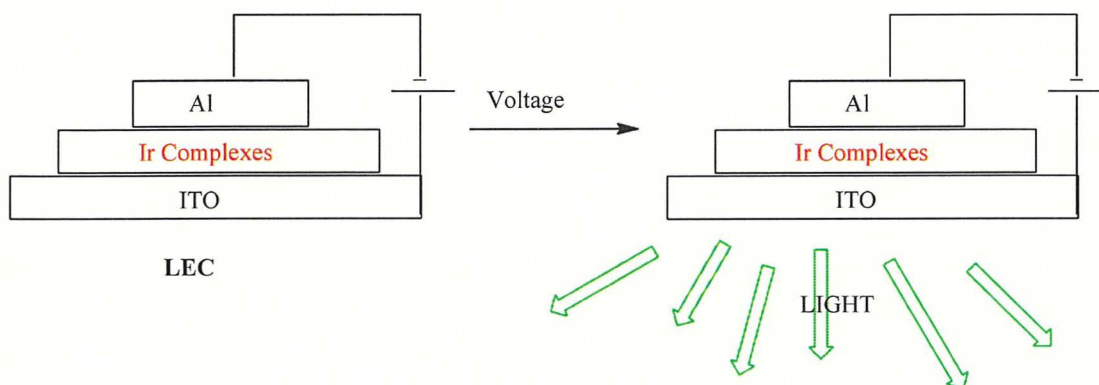


Fig. 3.29 Simplified diagram depicting operation of Light-emitting electrochemical cells.

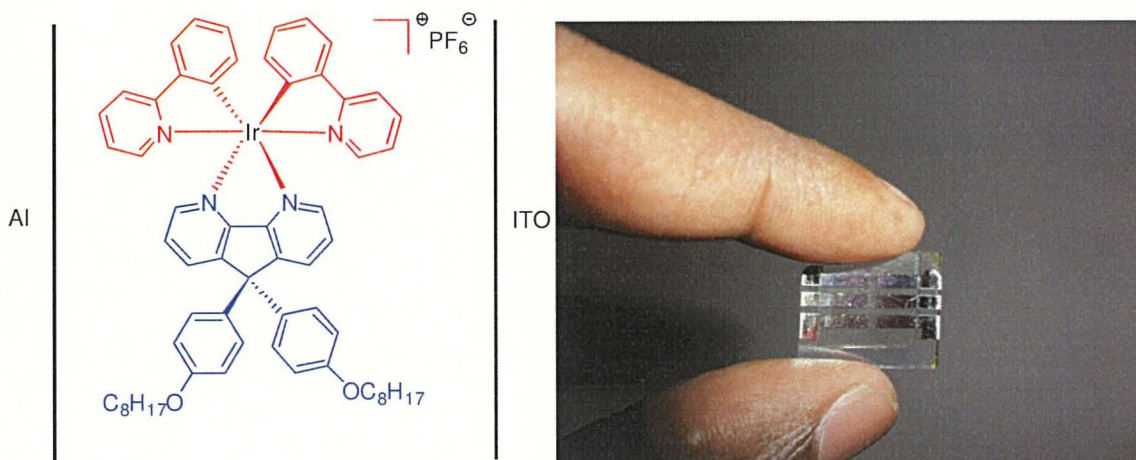


Fig. 3.30 LEC prepared with the configuration ITO/**3.45**/Al.

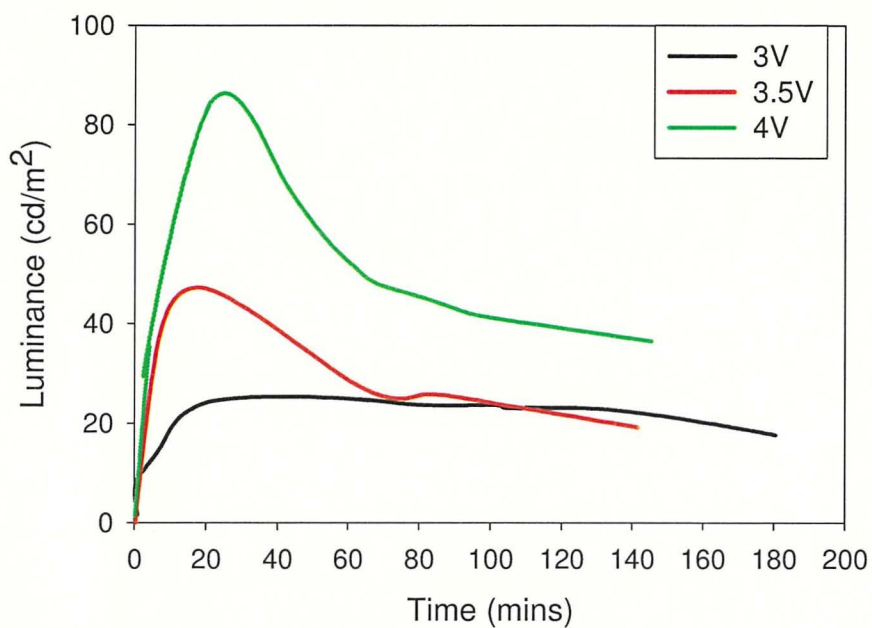


Fig. 3.31 Luminance intensity *versus* time at bias voltage +3, +3.5 and 4 V for LEC base on $\text{Ir}(\text{ppy})_2(\text{dphoDAF})\text{PF}_6$ (3.45) complex.

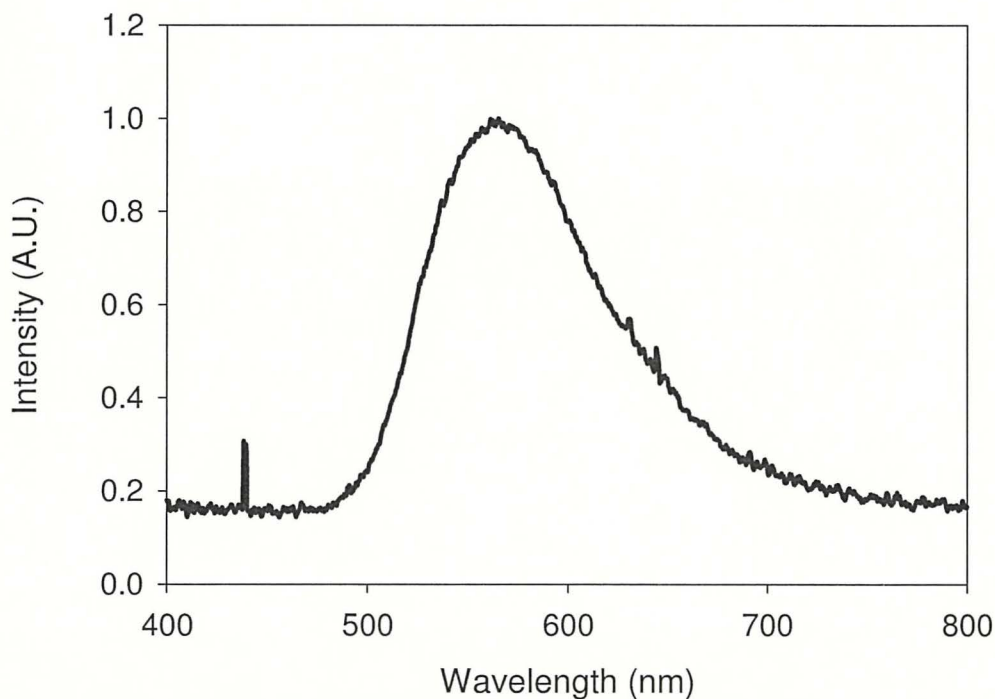


Fig. 3.32 Electroluminescence spectrum for $\text{Ir}(\text{ppy})_2(\text{dphodaf})\text{PF}_6$ (3.45)

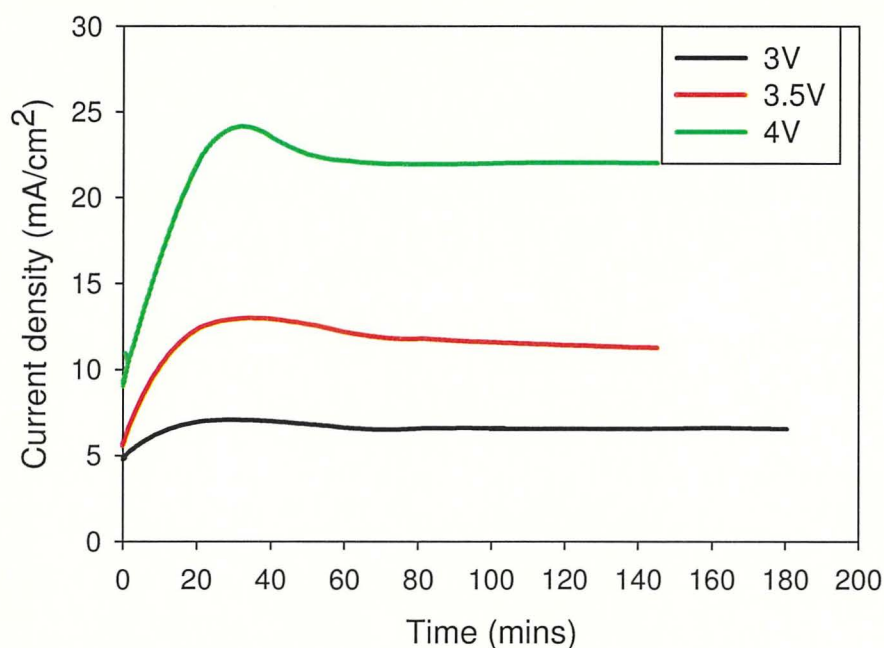


Fig. 3.33 Current density *versus* time at bias voltage of +3, +3.5 and 4 V for $\text{Ir}(\text{ppy})_2(\text{dphodaf})]^+\text{PF}_6^-$ (**3.45**).

3.3 Conclusion

Structural variations on basic structure of 4,5-diazafluorene have been performed to prepare different substituted DAF based ligands, which were used for synthesising Ir(III) complexes. Structural variation at 2,3,6,7 and 9 positions of DAF was achieved by introducing halogens, alkyl, and aryl groups. DAFone derivatives (**2.9**, **2.52**, **2.53**), they have been reduced with hydrazine hydrate and then have been subjected to alkylation at 9-position using *n*-iodooctane to obtain 9,9-dioctyl substituted DAF ligands (**3.22**, **3.23**, **3.24**) in good yields (> 75%). Octyl substituted DAF ligand **3.22** was oxidised with hydrogen peroxide and then treated with phosphorous oxychloride to introduce chlorine groups at the 3,6-position (**3.26**, **3.27**). Chloro-substituted DAF ligand **3.26** was reacted with phenyl boronic acid in the presence of a Pd catalyst to introduce phenyl groups at 3,6-positions. Similarly, phenyl groups was introduced by substitutions at the 2,7-positions to afford ligand **3.29** using bromo-substituted DAF ligand **3.24**. Cyano groups were also introduced in 2,7-positions using bromo-substituted DAF ligand (**3.23**, **3.24**) with zinc cyanide and Pd catalyst in microwave-assisted reaction to obtain cyano substituted DAF ligands **3.30** and **3.31** respectively in good yields (> 70%). Aryl groups were introduced at 9 position of DAF in two steps respectively. First, DAFones **2.9**/ or **2.53** were treated with phenol in concentrated sulphuric acid with catalytic amount of mercaptopropionic acid to afford hydroxyphenyls substituted DAF **2.27** and **3.32**. Then, these

derivatives were alkylated with *n*-iodooctane to afford 4-*n*-octylphenyl substituted DAF ligands **3.33** and **3.34** respectively. Series of novel iridium complexes of general formula [(ppy)₂Ir(DAF)]PF₆ (14 compounds in total) based on various substituted 4,5-diazafluorenes as ancillary ligands **3.36-3.44** have been successfully synthesised. Cationic Ir complexes **3.36-3.44** were prepared by refluxing DAF ligands with μ -dichloro-bridged cyclometalated Ir(III) dimers (**3.2** or **3.35**) in dichloromethane and methanol solution followed by anion exchange with NH₄PF₆. All the synthesised ligands and iridium complexes have been purified by flash column chromatography on silica gel and fully characterised by ¹H NMR, ¹³C NMR, ¹⁹F, ³¹P and MS (ESI) techniques.

The photophysical properties of Ir complexes **3.36-3.44** have been studied by absorption and emission spectroscopy and their electrochemical properties have been studied by cyclic voltammetry. The particular emphasis on to the studied was to understand the effect of structural variations in the DAF ligand (ancillary ligand) on the photophysical and electrochemical properties of their Ir(III) complex. For instance, the effect of phenyl substituted at 2,7-positions of DAF Ir(III) complex (**3.42**) was to provided extended conjugation, while similar substitutions at 3,7- positions **3.39** caused both steric effect and extended conjugation. Compared to unsubstituted DAF Ir complex (**3.36**), phenyl substituted DAF Ir complex **3.39** and **3.41** showed blue-shifted emission (ca. 15 nm and 3 nm, respectively) and about two-three fold lower photoluminescence quantum yields in acetonitrile. Similarly, by introducing an electron withdrawing groups (Cl, Br, and CN) resulted in perturbation of electronic energy levels of Ir complexes and influenced on the photophysical properties, i.e. colour tuning of their emissions. Bathochromic shift (~60 nm) observed assigned to electronic effect of the halides on the ancillary ligand while hypsochromic shift (~50 nm) was assigned to electronic effect of the halides on the cyclometalating ligand. The absorption spectra of all Ir complexes in acetonitrile showed a strong band between 230 nm to 300 nm which were assigned to intraligand (π - π^*) transition, and weaker band between 300 to 450 nm assign to metal-to-ligand charge transfer transitions. The Ir complexes showed emission from green light, $\lambda_{PL} = 513$ nm (**3.49**) to red light, $\lambda_{PL} = 620$ nm (**3.46**) of visible spectrum in acetonitrile and thus provided a range of different colour emitting materials for use as electroluminescent active layers in LECs. The photoluminescence spectra of Ir complexes in acetonitrile are characterised by structureless broad band assigned to combination of ³MLCT and ³LLCT (³ π - π^*). Cyano-substituted Ir complex **3.43** (CN is at 2 position of DAF) was found to have extremely low PLQY of only 0.2 % and emit at extreme red region ($\lambda_{PL} = 687$ nm) while dicyano substituted DAF Ir

complex at 2,7-position **3.44** was found to be not emissive material (PL measurement performed up to 900 nm). DAFone Ir complexes (**3.47** and **3.48**) having keto-group at C-9 were found to be non-emitting materials as well. The photoluminescence quantum yields for the rest of Ir complexes in solution were in the range 4–31%.

The redox properties of Ir complexes have been investigated by cyclic voltammetry (CV) in acetonitrile under inert atmosphere. For all the complexes **3.36–3.49** the half wave potential for oxidation processes were assigned to metal centred Ir^{III}/Ir^{IV} couple showing reversible or quasi-reversible oxidation waves [$E_{1/2, \text{ox}1} = +0.88\text{V}$ (**3.45**) to $+1.18\text{V}$ (**3.49**), versus Fc/Fc⁺ in CH₃CN]. The reduction processes of Ir complexes in acetonitrile were characterised predominantly by quasi-reversible or irreversible waves [$E_{\text{p}, \text{red}1} = -1.07\text{V}$ (**3.47**) to -1.90V (**3.36**)]. The HOMO–LUMO energy gap determined from the oxidation and the reduction potential of Ir complexes are in the range of 3.03–1.88 eV.

To understand more deeply, the electronic structure of the synthesised Ir complexes **3.36–3.49**, the DFT and TD-DFT calculation studies were carried out. Both DFT and TD-DFT calculations were performed at B3LYP/LANL2DZ level of theory provides triplet energies that match well with the experimental energies for most of the synthesised Ir complexes (deviations are ~ 2–10 nm). Excellent correlation were observed between computational HOMO/LUMO energies and experimental estimations from CV measurements. TD-DFT calculation determined that the singlet ground state (S₀) implies that, the HOMO orbitals in the complexes spread between the Ir atom and the phenylpyridine ligand, whereas the LUMO is dominantly located on DAF ligand. The presented method using TDDFT with B3LYP functional and LANL2DZ basis set with ECP for Ir, 6-31G (d, p) basis set for other atoms may be used to design and predicting properties of unknown complex. A LEC device using Ir complex **3.45** with the configuration ITO/**3.45**/Al was tested. The tested LEC device showed electroluminescence at 567 nm, which is about 30 nm blue-shifted from the photoluminescence in acetonitrile. The response time was about 18 minutes with 90 cd/m² luminescence intensity at bias voltage 4V. The LEC study for the other emitting complexes will be carried out in the near future in collaboration with the physicist.

3.4 Experimental

Chemicals

Chemicals purchased were used without further purification except 2-phenylpyridine which was redistilled before use. All the reaction involving $\text{IrCl}_3 \cdot \text{H}_2\text{O}$ or any other Ir(III) species were carried out in an inert atmosphere. Cyclometalated Ir(III) dichloro-bridged dimer of the general formula $(\text{C}^{\wedge}\text{N})_2\text{Ir}(\text{i-Cl})_2\text{Ir}(\text{C}^{\wedge}\text{N})_2$ (where $\text{C}^{\wedge}\text{N}$ represents a cyclometalating ligand) were synthesized by a literature procedure.⁷⁵ All the solvents such as THF, toluene and dioxane were dried with appropriate drying agents, and then redistilled before use. The catalyst tetrakis(triphenylphosphine)palladium(0) was synthesised according to the literature procedure.⁹⁰

Instrumentation

NMR details given in Chapter 2. Electron spray ionisation (ESI^+) mass spectra of synthesised Ir complexes were recorded on microTOF LC Bruker Daltonics mass spectrometer. Electron impact (EI^+) mass spectra were recorded on Thermo Scientific Trace1300 with positive mode ionisation.

UV-Vis electron absorption and emission spectra were measured in 10 mm path length quartz cells at room temperature, in HPLC grade solvents using Shimadzu UV-3600 spectrophotometer and Horiba Yvon Fluoromax-4 spectrofluorometer, respectively. Photoluminescence quantum yields (PLQY) were determined in acetonitrile using $[\text{Ru}(\text{bpy})_3](\text{PF}_6)_2$ as reference standard; each solution was freshly prepared and carefully degassed prior to measurement.

Cyclic voltammetry experiments were carried out using Metrohm Autolab PGSTAT302N potentiostat-galvanostat, in acetonitrile solutions containing 0.1 M Bu_4NPF_6 as supporting electrolyte, under argon or nitrogen atmosphere. Platinum disc ($d = 2$ mm) and platinum wire ($d = 0.2$ mm) served as the working and counter electrodes, respectively. The reference electrode (Ag/Ag^+) was used as silver wire immersed in mixture of 0.01M AgNO_3 + 0.1 M Bu_4NPF_6 in acetonitrile, separated from the solution by a Vycor frit. After CV measurements of each iridium complexes, a calibration scan was run with small amount of ferrocene in electrolyte.

Fabrication and Characterization of LEC Devices

LEC device was fabricated by spin-coating at 1 krpm for 60 sec the complex **3.45** dissolved in acetonitrile (20 mg/mL) on indium tin oxide (ITO, anode) coated glass substrates to form a 100 nm thick film, solvent removed *in vacuo* without annealing, followed by thermal evaporation of a 100 nm Al top contact (cathode), the device was encapsulated in the glove box. The electrical and emission characteristics of LEC were measured under constant bias voltages of +3V, +3.5V and + 4V. The device was driven by a source-measurement unit (SMU) and the emission intensity was measured using a Si photodiode calibrated with Photo Research PR650. EL spectra of the devices were measured by a calibrated Ocean Optic spectrometer with a CCD array detector

Determination of Photoluminescence Quantum Yields

All samples were prepared in HPLC grade acetonitrile. Samples were carefully degassed prior to measurement. A solution of [Ru(bpy)₃](PF₆)₂ in degassed acetonitrile was used as reference standard for calculating quantum yields. A stock solution of ca. 0.1 absorbance was prepared and then diluted to prepare four solutions of absorbance close to 0.05, 0.04, 0.03 and 0.01. The linearity between absorption and emission for each sample was verified and the Pearson regression factor (R²) for the linear fit of each sample set of data was registered repeated until at least at 0.9. The photoluminescence quantum yields of the samples (Φ_x) were calculated by equation:⁹¹

$$\Phi_x = \Phi_s \times (I_x/I_s) \times (F_s/F_x) \times (n_x/n_s)^2$$

Where the I_s and I_x are the integrated emission intensities of the standard and the sample solution under identical conditions. Φ_s is the quantum yields of the standard {for [Ru(bpy)₃](PF₆)₂, Φ_s = 9.5%⁷⁹}, n_x and n_s denote refractive indexes of solvents used in measurements of studied compounds and standard, respectively. F_x and F_s indicates fraction of light absorbed for sample and reference standard.

The gradient for each sample is proportional to that sample's fluorescence quantum yields.⁹² Conversion into absolute quantum yield is achieved through the equation given below:

$$\Phi_x = \Phi_s \times (\text{Grad}_x/\text{Grad}_s) \times (n_x/n_s)^2$$

Where *Grad* is the gradient from the plot of integrated fluorescence intensity vs. absorbance. The experimental uncertainty in the PL quantum yield is in order of 10%. For example, a plot of integrated area intensity of emission of each solution of a sample (**141**) versus absorbance of same set of solution is shown in Fig. 3.34.

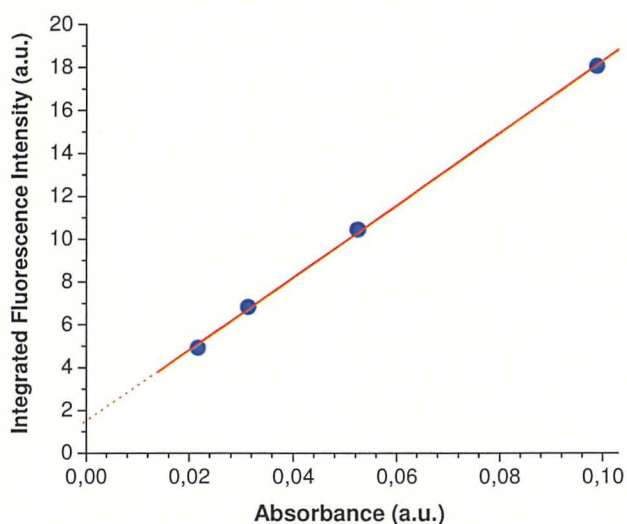
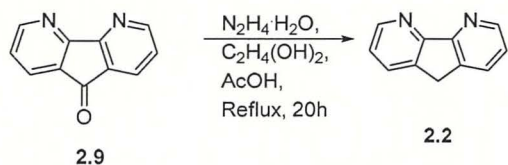


Fig. 3.34 Linear plot of integrated intensity of PL spectra versus intensity of absorbance spectra for sample **3.45** (SG088b), used for calculating photoluminescent quantum yield ($R^2 = 0.99$, PLQY $\phi_x = 31\%$).

Synthesis of DAF based ligands

4,5-Diazafluorene (2.2)

Exp: SG-013



A suspension of 4,5-diazafluoren-9-one (**2.9**) (5.11 g, 0.028 mmol) in hydrazine hydrate (116 mL), ethylene glycol (130 mL) and acetic acid (2.5 mL) was heated at reflux ($T = 140\text{-}150\text{ }^\circ\text{C}$, oil bath) for 20 hours. The reaction mixture was cooled down to room temperature and water (200 mL) was added. The product was extracted with chloroform (200 mL), washed with water ($3 \times 100\text{ mL}$), dried over anhydrous MgSO_4 , evaporated to afford the crude product **2.2** as a white solid. The crude product was recrystallised with petroleum ether (15 mL) to yield product **2.2** (4.10 g, 86%) as an off-white solid.

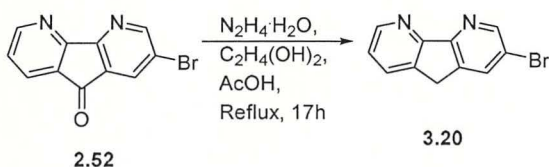
$^1\text{H NMR}$ (500 MHz, CDCl_3): δ (ppm) 8.74 (2H, d, $J = 4.7\text{ Hz}$), 7.88 (2H, d, $J = 7.6\text{ Hz}$), 7.30 (2H, dd, $J = 7.6, 4.8\text{ Hz}$), 3.88 (2H, s).

$^{13}\text{C NMR}$ (126 MHz, CDCl_3): δ (ppm) 158.57, 149.47, 136.82, 132.65, 122.70, 31.91.

MS (GCTOF, EI^+) m/z : 168.07 ($[\text{M}]^+$, 100%). Calcd. for $\text{C}_{11}\text{H}_8\text{N}_2$: 168.06.

3-Bromo-4,5-diazafluorene (3.20)

Exp: SG-026



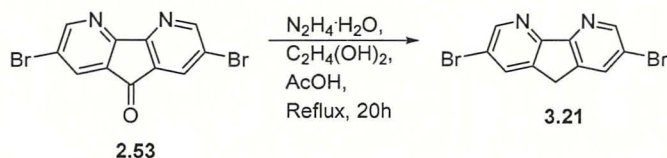
A suspension of 2-bromo-4,5-diazafluoren-9-one **2.52** (1.31 g, 5.06 mmol) in a solution of hydrazine hydrate (15 mL), ethylene glycol (24 mL) and acetic acid (0.75 mL) were reflux (oil bath, $T = 135\text{-}140\text{ }^\circ\text{C}$) for 17 hours. The reaction mixture was allowed to cool down to room temperature. The precipitate was filtered, washed with water ($3 \times 15\text{ mL}$) and dried *in vacuo* to yield pure product **3.20** (800 mg, 66%) as an off-white solid.

$^1\text{H NMR}$ (500 MHz, CDCl_3): δ (ppm) 8.80 (1H, d, $J = 1.9\text{ Hz}$), 8.75 (1H, d, $J = 4.8\text{ Hz}$), 8.02 (1H, d, $J = 1.0$), 7.89 (1H, d, $J = 8.3\text{ Hz}$), 7.32 (1H, dd, $J = 7.6, 4.8\text{ Hz}$), 3.80 (2H, s).

$^{13}\text{C NMR}$ (126 MHz, CDCl_3): δ (ppm) 157.67, 157.24, 150.90, 149.54, 138.93, 137.32, 135.71, 133.17, 123.00, 120.29, 31.73.

2,7-Dibromo-4,5-diazafluorene (3.21)

Exp: SG-001



A suspension of 2,7-dibromo-4,5-diazafluoren-9-one (**2.53**) (500 mg, 1.46 mmol) in a mixture of hydrazine hydrate (6 mL, 192 mmol), ethylene glycol (8 mL) and acetic acid (0.25 mL) was heated under reflux (oil bath, T = 135–140 °C) for 20 hours, during which complete dissolution was observed. The reaction mixture was allowed to cooled down to room temperature and the solid was collected by filtration, washed with water (20 mL) and dried *in vacuo* to afford pure product **3.21** (345 mg, 71%) as light brown solid.

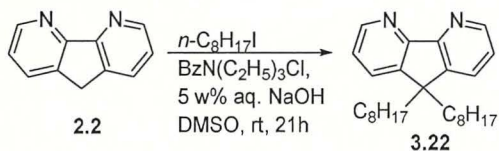
¹H NMR (400 MHz, CDCl₃): δ (ppm) 8.78 (2H, d, J = 1.1 Hz), 8.02 (2H, J = 1.2 Hz), 3.86 (2H, s).

¹³C NMR (126 MHz, CDCl₃): δ (ppm) 156.43, 150.92, 138.71, 135.72, 120.31, 31.73.

MS (ESI⁺) m/z: 346.87 ([M+Na]⁺, 49%, ⁷⁹Br, ⁷⁹Br), 348.87 ([M+Na]⁺, 100%, ⁷⁹Br, ⁸¹Br), 350.87 ([M+Na]⁺, 49%, ⁸¹Br, ⁸¹Br). Calcd. for C₁₁H₆Br₂N₂: 323.89.

9,9-Dioctyl-4,5-diazafluorene (3.22)

Exp: SG-014



Mixture of 4,5-diazafluorene (**2.2**) (3.10 g, 0.018 mol), benzyltriethylammonium chloride (10 mg, 0.02 mmol) in 50 mL of dimethyl sulfoxide was stirred for 10 minutes and then 50% aqueous NaOH (12 mL) was added resulting in a deep orange coloration of a solution. In this mixture, *n*-iodooctane (11.04 g, 0.046 mol) was added drop wise over a period of 10 minutes and then the mixture was stirred at room temperature for 21 hours. After completion of reaction time, 5% aqueous NaCl (100 mL) was added and then extracted with dichloromethane (2 × 50 mL). The combined organic layer was washed with water (3 × 100 mL), dried over anhydrous MgSO₄, filtered off and evaporated to afford crude product (6.21 g, 88%) as brown semi solid. The crude product was purified by column chromatography on silica gel eluting with PE:EA = 1:1 v/v to yield pure compound **3.22** (3.10 g, 44.2%) as light

brown solid together with somewhat less pure product **3.22** (2.1 g, 30.4%) as brown solid. The combined yield of dioctyl-DAF **3.22** was 74.6%.

¹H NMR (400 MHz, CDCl₃): δ (ppm) 8.69 (2H, dd, *J* = 4.8, 1.4 Hz), 7.70 (2H, dd, *J* = 7.7, 1.4 Hz), 7.28 (2H, dd, *J* = 7.7, 4.9 Hz), 2.03–1.94 (4H, m), 1.77–1.62 (2H, m), 1.30–0.94 (22H, m), 0.82 (6H, t, *J* = 7.1 Hz), 0.70–0.59 (4H, m).

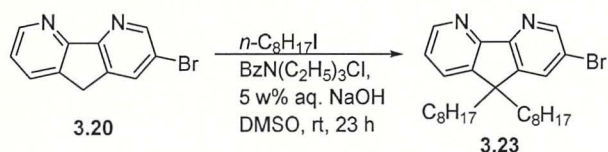
¹³C NMR (101 MHz, CDCl₃): δ (ppm) 158.49, 149.46, 144.98, 130.63, 122.93, 51.33, 39.20, 31.72, 29.87, 29.14, 29.09, 24.00, 22.56, 14.05.

DEPTQ NMR (101 MHz, CDCl₃): δ (ppm) 158.58, 149.53 (CH), 144.91, 130.56 (CH), 122.90 (CH), 51.33 (C-9), 39.22, 31.73, 29.89, 29.15, 29.10, 24.01, 22.56, 14.05 (CH₃).

MS (EI⁺) *m/z*: 392.31 ([M]⁺, 100%). Calcd for C₂₇H₄₀N₂: 392.32

2-Bromo-9,9-dioctyl-4,5-diazafluorene (**3.23**)

Exp: SG-040



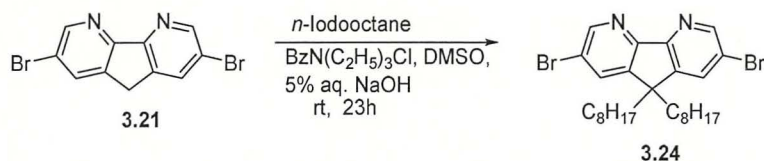
In a 50 mL single necked round bottom flask charged with 2-bromo-4,5-diazafluorene (**3.20**) (800 mg, 3.23 mmol), benzyltriethylammonium chloride (5 mg, 0.01 mmol), and dimethyl sulfoxide (15 mL) was stirred for 10 min at room temperature and then 50 w% aqueous solution of NaOH (4 mL) was added, resulting in a deep blue colouration of mixture. Into this mixture, *n*-iodooctane (1.94 g, 8.09 mmol) was added drop wise within 10 minutes and then stirred for 23 hours at room temperature. After completion of reaction time, 5 wt% aqueous NaCl (100 mL) was added and then extracted with dichloromethane (2 × 100 mL). The combined organic layers were washed with water (3 × 50 mL), dried over anhydrous MgSO₄, and the solvent was evaporated to afford the crude product (1.21 g, 78%) as a brown oil. The crude product was purified by flash chromatography on silica gel column (10 cm × 4 cm) eluting with PE: EA mixture with gradual increase in amount of EA from 10% to 30% to yield pure product **3.23** (1.12 g, 72%) as a brown solid.

¹H NMR (500 MHz, CDCl₃): δ (ppm) 8.74 (1H, d, *J* = 2.0 Hz), 8.69 (1H, dd, *J* = 4.8, 1.3 Hz), 7.83 (1H, d, *J* = 2.0 Hz), 7.70 (1H, dd, *J* = 7.6, 1.3 Hz), 7.31 (1H, dd, *J* = 7.6, 4.8 Hz), 2.02–1.90 (4H, m), 1.25–1.04 (20H, m), 0.81 (6H, t, *J* = 7.2 Hz), 0.69–0.60 (4H, m).

^{13}C NMR (126 MHz, CDCl_3): δ (ppm) 157.40, 157.01, 150.62, 149.67, 146.82, 144.95, 133.43, 130.86, 123.32, 120.48, 51.59, 39.08, 31.71, 29.81, 29.10, 29.08, 24.01, 22.56, 14.04.
MS (GC-TOF, EI⁺) m/z : 470.22 ($[\text{M}]^+$, 100%, ^{79}Br), 472.22 ($[\text{M}]^+$, 80%, ^{81}Br). Calcd for $\text{C}_{27}\text{H}_{39}\text{BrN}_2$: 470.22.

3,7-Dibromo-9,9-dioctyl-4,5-diazafluorene (3.24)

Exp: SG-011



A single necked round bottom flask charged with 2,7-dibromo-4,5-diazafluorene (**3.21**) (500 mg, 1.53 mmol), benzyltriethylammonium chloride (3 mg, 0.01 mmol), in dimethyl sulfoxide (9 mL) was stirred for 10 min then 50 w% aqueous solution of NaOH (2 mL) was added resulting in a deep blue colouration of the mixture. Into this blue mixture, *n*-iodooctane (923 mg, 3.84 mmol) was added drop wise and was stirred for 23 hours at room temperature. The resulting mixture was diluted with 5% aqueous NaCl solution (50 mL) and then extracted with dichloromethane (2×50 mL). The combined organic layers were washed with water (2×20 mL), dried over anhydrous MgSO_4 and evaporated to yield a crude product (780 mg) as dark brown oil. The crude product was purified by column chromatography on silica gel eluting with PE:EA = 2:8 v/v to afford pure product **3.24** (630 mg, 75%) as light brown solid.
 ^1H NMR (400 MHz, CDCl_3) δ 8.75 (2H, d, $J = 2.0$ Hz), 7.83 (2H, d, $J = 2.0$ Hz), 2.02–1.88 (4H, m), 1.30–0.99 (20H, m), 0.83 (6H, t, $J = 7.1$ Hz), 0.69–0.61 (4H, m).

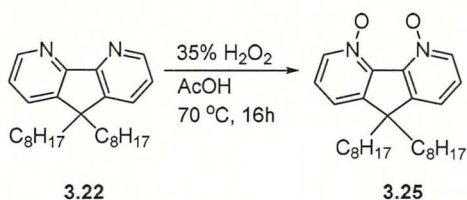
^{13}C NMR (101 MHz, CDCl_3): δ (ppm) 156.05, 150.94, 146.60, 133.51, 120.80, 51.71, 38.99, 31.70, 29.76, 29.10, 29.08, 24.01, 22.57, 14.05.

DEPTQ NMR (101 MHz, CDCl_3) δ 156.10, 150.99 (CH), 146.64, 133.55 (CH), 120.84, 51.75(C-9), 39.04, 31.75, 29.80, 29.14, 29.13, 24.05, 22.62, 14.10 (CH_3).

MS (ESI⁺) m/z : 549.14 ($[\text{M}+\text{H}]^+$, 50%, ^{79}Br , ^{79}Br), 551.14 ($[\text{M}+\text{H}]^+$, 100%, ^{79}Br , ^{81}Br), 553.14 ($[\text{M}+\text{H}]^+$, 51%, ^{81}Br , ^{81}Br). Calcd. for $\text{C}_{27}\text{H}_{38}\text{Br}_2\text{N}_2$: 548.14.

9,9-Dioctyl-4,5-diazafluorene-*N,N*-dioxide (3.25)

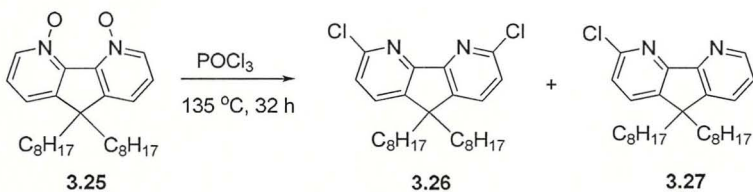
Exp: SG-067



Under nitrogen, in a two-neck flask charged with 9,9-dioctyl-4,5-diazafluorene (**3.22**) (500 mg, 1.25 mmol), 35 % v/v aqueous solution of hydrogen peroxide (145 mg, 7.64 mmol) and acetic acid (3 mL) was stirred at 70 °C for 16 hours. After cooling, the mixture was concentrated into a small volume under reduced pressure on rotavapour and then dilute with water (50 mL), extracted with dichloromethane (2 × 50 mL). The combined organic layers were washed with water (2 × 10 ml), dried over anhydrous MgSO₄, filtered off and the solvent was evaporated under reduced pressure on rotavapor to afford crude product **3.25** (450 mg, 83%) as brown oil. The crude compound **3.25** was used in the next step without further purification.

3,6-Dichloro-9,9-dioctyl-4,5-diazafluorene (3.26) and 3-chloro-9,9-dioctyl-4,5-diazafluorene (3.27)

Exp: SG-068



Under nitrogen, in a two-necked flask charge with 9,9-dioctyl-4,5-diazafluorene-*N,N*-dioxide (**3.25**) (1.50 g, 3.54 mmol) and phosphoryl trichloride (POCl₃) (10 mL, 0.106 mol) were heated at 135 °C (oil bath) for 32 hours. The mixture was cooled down to room temperature and concentrated at reduced pressure to remove excess POCl₃. The residue was basified with 4 M NaOH aqueous solution and then extracted with dichloromethane (3 × 50 mL). The combined organic layers were washed with water (3 × 30 mL), dried over anhydrous MgSO₄ and the solvent was evaporated to afford the crude product (2.01 g) as brown oil, which was purified by column chromatography on silica gel eluting with PE:EA mixture with gradual increase of the EA amount from 5% to 10% to yield product **3.26** (550 mg, 34%) as a white solid, somewhat pure product **3.26** (100 mg, 6%) as a white solid and pure by-product **3.27** (150 mg, 10%) as a light brown oil.

Analytical data for dichloro-DAF **3.26**:

¹H NMR (500 MHz, CDCl₃): δ (ppm) 7.66 (2H, d, *J* = 8.0 Hz), 7.35 (2, d, *J* = 8.0 Hz), 2.02 – 1.90 (4H, m), 1.30–0.96 (20H, m), 0.82 (6H, t, *J* = 7.2 Hz), 0.71–0.57 (4H, m).

¹³C NMR (126 MHz, CDCl₃): δ (ppm) 157.73, 152.15, 144.29, 133.21, 124.10, 51.27, 38.92, 31.83, 29.92, 29.24, 29.20, 24.15, 22.68, 14.16.

MS (EI⁺) *m/z*: 460.24 ([M]⁺, 100%, ³⁵Cl, ³⁷Cl), 459.23 ([M]⁺, 50%, ³⁵Cl, ³⁵Cl), 461.23 ([M]⁺ 51%, ³⁷Cl, ³⁷Cl). Calcd. for C₂₇H₃₈Cl₂N₂: 460.24.

Analytical data for monochloro-DAF **3.27**:

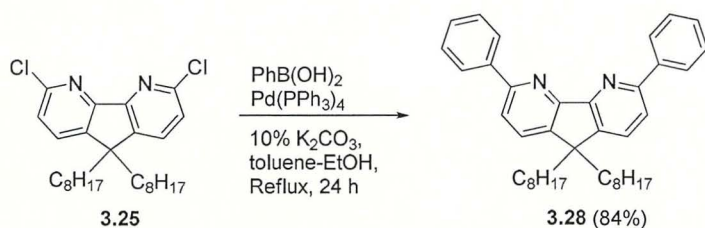
¹H NMR (500 MHz, CDCl₃): δ (ppm) 8.66 (1H, d, *J* = 4.5 Hz), 7.70 (1H, d, *J* = 7.6 Hz), 7.61 (1H, d, *J* = 8.0 Hz), 7.30–7.26 (2H, m), 1.93 (4H, m), 1.14–0.98 (20H, m), 0.75 (6H, m), 0.56 (4H, m).

¹³C NMR (500 MHz, CDCl₃): δ (ppm) 158.72, 157.58, 156.90, 151.86, 149.38, 145.61, 144.16, 143.69, 133.97, 133.05, 130.99, 123.93, 123.45, 51.13, 38.76, 31.55, 29.98, 29.80, 29.68, 29.06, 25.90, 24.01, 23.85, 22.53.

MS (EI⁺) *m/z*: 426.26 ([M]⁺, 100%, ³⁵Cl), 427.26 ([M]⁺, 30%, ³⁷Cl). Calcd. for C₂₇H₃₉ClN₂: 426.28.

9,9-Dioctyl-3,6-diphenyl-4,5-diazafluorene (3.28)

Exp: SG-041



Under argon, three-necked Schlenk flask (50 mL) charge with 3,6-dichloro-9,9-dioctyl-4,5-diazafluorene (**3.26**) (101 mg, 0.216 mmol), phenylboronic acid (66 mg, 0.541 mmol) and Pd(PPh₃)₄ (12 mg, 5 mol%) were three times evacuating and back filled with argon and then degassed toluene (3 mL), ethanol (1 mL) and 10% aqueous K₂CO₃ solution (1 mL) was added via septum. The resulting mixture was degassed with argon for 15 minutes and then reflux (oil bath, T = 110 °C) for 24 hours under argon atmosphere. After cooling, water (20 mL) was added and extracted with ethyl acetate (2 × 20 mL). The combined organic layers were washed with water (3 × 20 mL), dried over anhydrous MgSO₄ and the solvent was evaporated to afford the crude product (110 mg, 93%) as brown oil, which was purified by column chromatography on silica gel eluting with PE:EA= 9:1 v/v ratio to yield pure product **3.28** (103 mg, 84%) as an off-yellow solid.

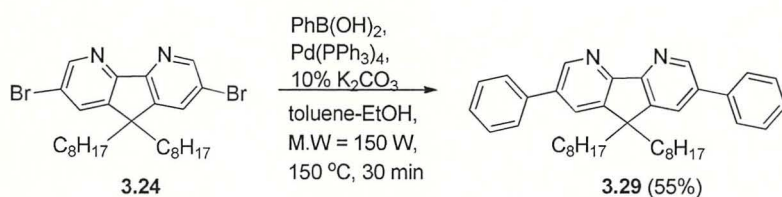
$^1\text{H NMR}$ (500 MHz, CDCl_3): δ (ppm) 8.25 (4H, d, $J = 7.6$ Hz), 7.83 (4H, q, $J = 8.0$ Hz), 7.52 (4H, t, $J = 7.6$ Hz), 7.44 (2H, t, $J = 7.3$ Hz), 2.12–1.96 (4H, m), 1.41–0.95 (20H, m), 0.81 (6H, t, $J = 7.1$ Hz), 0.75–0.60 (4H, m).

$^{13}\text{C NMR}$ (101 MHz, CDCl_3): δ (ppm) 158.48, 157.37, 144.25, 139.20, 131.38, 128.96, 128.63 ($\times 2\text{C}$), 127.38 ($\times 2\text{C}$), 120.21, 50.91, 39.38, 31.74, 29.96, 29.19, 29.13, 24.14, 22.57, 14.06.

$\text{MS (EI}^+)$ m/z : 544.37 (M^+ , 100%). Calcd. for $\text{C}_{39}\text{H}_{48}\text{N}_2$: 544.38.

9,9-Dioctyl-2,7-diphenyl-4,5-diazafluorene (3.29)

Exp: 110



A dried heavy-walled pyrex tube (25 mL) charged with 9,9-dioctyl-2,7-dibromo-4,5-diazafluorene (**3.24**) (100 mg, 0.182 mmol), phenyl boronic acid (56 mg, 0.456 mmol) and $\text{Pd(PPh}_3)_4$ (11 mg, 5 mol%) was three times evacuating and back filled with argon and then degassed 10% K_2CO_3 (1 mL), toluene (8 mL) and ethanol (1 mL) were added via septum. The mixture was degassed with argon for 15 minutes and then irradiate with microwaves (150 watt) in a microwave reactor at 150 °C for 30 minutes. After cooling, the mixture was partition between ethyl acetate (20 mL) and water (20 mL). The organic layer was separated, washed with water (3×10 mL), dried with anhydrous MgSO_4 and evaporated to afford the crude product (150 mg) as blackish semi solid. The crude product was purified by column chromatography eluting with PE:EA in the ratio 4:1 to afford the product **3.29** (55 mg, 55.5 %) as a brown oil and an impure mixture (60 mg) as blackish oil.

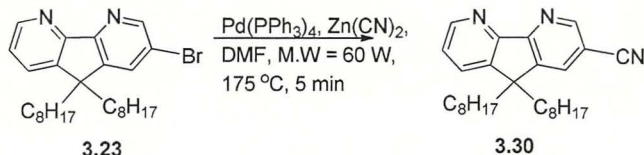
$^1\text{H NMR}$ (500 MHz, CDCl_3): δ (ppm) 8.95 (2H, d, $J = 2.06$ Hz), 7.88 (2H, d, $J = 2.36$ Hz), 7.69 (4H, dd, $J = 8.2, 1.5$ Hz), 7.52 (4H, t, $J = 7.50$ Hz), 7.43 (2H, t, $J = 7.5$ Hz), 2.09 (4H, m), 1.28–1.03 (20H, m), 0.83–0.74 (10H, m).

$^{13}\text{C NMR}$ (101 MHz, CDCl_3): δ (ppm) 157.42, 148.71, 145.61, 138.43, 136.20, 129.24, 128.98 ($\times 2\text{C}$), 128.26, 127.51 ($\times 2\text{C}$), 51.59, 39.42, 31.83, 30.01, 29.23 ($\times 2\text{C}$), 24.24, 22.68, 14.15.

$\text{MS (EI}^+)$ m/z : 544.36 (M^+ , 100%). Calcd. for $\text{C}_{39}\text{H}_{48}\text{N}_2$: 544.38.

2-Cyano-9,9-dioctyl-4,5-diazafluorene (3.30)

Ex.SG132



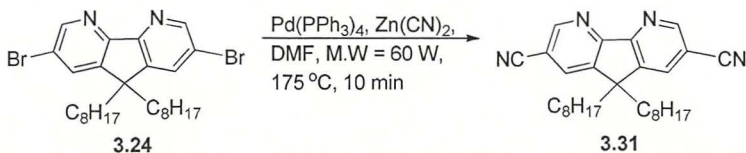
A dried heavy-walled 10 mL Pyrex tube was charged with 2-bromo-9,9-dioctyl-4,5-diazafluorene **3.23** (201 mg, 0.424 mmol), Zn(CN)₂ (49 mg, 0.424 mmol) and Pd(PPh₃)₄ (20 mg, 4 mol%) in DMF (2 mL). The mixture was degassed with nitrogen for 15 min before exposed to microwave irradiation (60 W) in a microwave reactor at 175 °C for 5 minutes. The mixture (brown colour) allowed to cool down to room temperature, then diluted with ethyl acetate (25 mL) and brine (10 mL). The organic phase was separated followed by washing with water (2 × 10 mL), dried with anhydrous MgSO₄ and then evaporated to afford a crude product as brown oil (292 mg). The crude product was purified by column chromatography using silica gel eluting with PE:EA in the ratio 9:1 to afford the product **3.30** (152 mg, 88%) as a brown oil.

¹H NMR (400 MHz, CDCl₃): δ (ppm) 8.9 (1H, d, *J* = 1.8 Hz), 8.77 (1H, dd, *J* = 4.8, 1.3 Hz) 7.95 (1H, d, *J* = 1.8 Hz), 7.78 (1H, dd, *J* = 4.8, 1.3 Hz), 7.41 (1H, m), 2.04–1.95 (4H, m), 1.25–1.06 (20H, m), 0.82 (6H, t, *J* = 6.7 Hz), 0.66–0.60 (4H, m).

¹³C NMR (100 MHz, CDCl₃): δ (ppm) 161.90, 156.49, 152.69, 150.45, 146.40, 144.83, 133.46, 131.06, 124.52, 108.30, 51.88, 38.89, 31.66, 29.74, 29.08, 29.04, 24.07, 22.52, 14.02.

2,7-Dicyano-9,9-dioctyl-4,5-diazafluorene (3.31)

Ex.SG126



In a dried 10 mL Pyrex tube was charged with 2,7-dibromo-9,9-dioctyl-4,5-diazafluorene (**3.24**) (100 mg, 0.0912 mmol), Zn(CN)₂ (42 mg, 0.364 mmol) and Pd(PPh₃)₄ (12 mg, 6 mol

(%) in DMF (2 mL). The mixture was degassed with nitrogen for 15 minutes before exposed to microwave irradiation (60 W) in microwave reactor at 175 °C for 10 minutes. The mixture (brown colour) was allowed to cool down to room temperature before diluting with ethyl acetate (20 mL). The organic phase was separated, washed with water (3 × 10 mL), dried with anhydrous MgSO₄ and evaporated to afford a crude product as brown oil (140 mg). The crude product was purified by column chromatography using silica gel eluting with PE:EA in the ratio 9:1 to afford pure product **3.31** (58 mg, 71%).

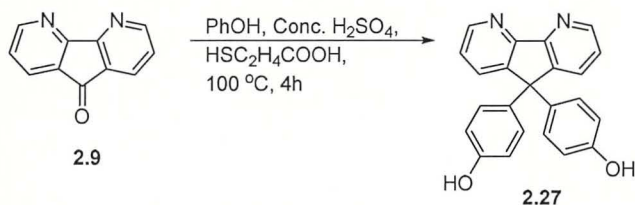
¹H NMR (400 MHz, CDCl₃) δ (ppm) 9.04 (2H, d, *J* = 1.1 Hz), 8.03 (2H, d, *J* = 1.1 Hz), 2.07–2.03 (4H, m), 1.25–1.08 (20H, m), 0.84 (6H, t, *J* = 6.9 Hz), 0.66–0.60 (4H, m)

DEPTQ (100 MHz, CDCl₃): δ (ppm) 159.39, 153.20 (CH), 146.00, 134.15(CH), 116.65, 109.78, 52.51(C-9), 38.79, 31.76, 29.66, 29.06, 29.04, 24.21, 22.52, 13.79 (CH₃).

MS (ESI⁺) *m/z*: 465.39 ([M+Na]⁺). Calcd. for C₂₉H₃₈N₄: 442.31.

9,9-Bis(4-hydroxyphenyl)-4,5-diazafluorene(**2.27**)^{73,74}

Exp: SG-069



Under nitrogen, a two-necked flask was charged with 2,7-dibromo-4,5-diazafluoren-9-one (**2.9**) (1.01 g, 5.493 mmol) and phenol (3.00 g, 31.9 mmol) were heated to 100 °C (oil bath). 3-Mercaptopropionic acid (50 μL, 0.573 mmol) has been added to the stirring melt, then conc. H₂SO₄ (2.0 mL, 37.55 mmol, 95%, 1.84 g/mL) slowly added drop wise via syringe for over 30 min under vigorous stirring. The reaction mixture was stirred at 100 °C for 4 hours. Heating has been stopped and methanol (6 mL) has been added. The mixture was neutralized with 8 M NaOH solution and the precipitate was filtered off, washed with water (2 × 5 mL) dried under vacuum to afford a crude product (1.54 g) as whitish solid. The crude product was purified by recrystallisation with DCM (20 mL) to afford compound **2.27** (0.876 g, 43.2%) as an off-white solid.

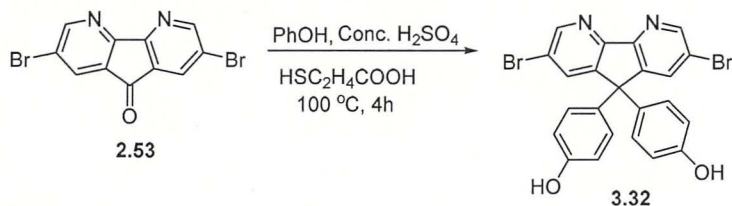
¹H NMR (500 MHz, DMSO-*d*₆): δ (ppm) 9.41 (2H, s, 2OH), 8.67 (2H, dd, *J* = 1.4 Hz, *J* = 4.8 Hz), 7.92 (2H, dd, *J* = 7.8, 1.5 Hz), 7.42–7.40 (2H, m), 6.91 (4H, dd, *J* = 8.5, 2.1 Hz), 6.65 (4H, dd, *J* = 8.5, 1.7 Hz).

^{13}C NMR (100 MHz, DMSO- d_6): δ (ppm) 156.48, 156.35, 146.59, 134.15, 133.81, 128.58, 123.82, 115.27, 59.56.

MS (GC-TOF, EI $^+$) m/z : 352.12 (M^+ , 100%). Calcd. for $\text{C}_{23}\text{H}_{16}\text{N}_2\text{O}_2$: 352.12.

2,7-Dibromo-9,9-bis(4-hydroxyphenyl)-4,5-diazafluorene (3.32)

Exp: SG-071



Under nitrogen, a two necked flask was charged with 2,7-dibromo-4,5-diazafluoren-9-one (**2.53**) (1.01 g, 2.96 mmol) and phenol (1.67 g, 17.71 mmol) and heated to $100\text{ }^\circ\text{C}$ (oil bath). In this stirring melt, 3-mercaptopropionic acid ($50\text{ }\mu\text{L}$, 0.573 mmol) was added and then conc. H_2SO_4 ($892\text{ }\mu\text{L}$, 32.7 mmol) was slowly added drop wise via syringe over a period of 30 min. The mixture was then stirred at $100\text{ }^\circ\text{C}$ for 4 hours. After heating has been stopped, methanol (6 mL) was added. The mixture was neutralised with 8 M NaOH aqueous solution resulting in precipitation. The precipitate was filtered off, washed with water ($2 \times 5\text{ mL}$) and dried *in vacuo* to afford a crude product (1.8 g) as a white solid. The crude product was purified by recrystallisation with DCM (20 mL) to afford compound **3.32** (1.31 g, 86%) as an off-white solid.

^1H NMR (500 MHz, DMSO- d_6): δ (ppm) 9.54–9.44 (2H, broad, 2OH), 8.81 (2H, d, $J = 2.1$ Hz), 8.12 (2H, d, $J = 2.1$ Hz), 6.97–7.94 (4H, m), 6.68–6.65 (4H, m).

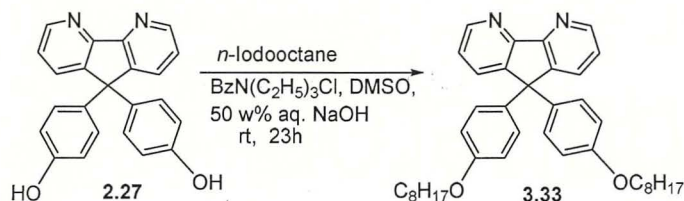
^{13}C NMR (100 MHz, DMSO- d_6): δ (ppm) 156.77, 154.30, 148.37, 136.35, 132.59, 128.73, 120.70, 120.30, 115.47, 59.69.

MS (ESI $^+$) m/z : 508.97 [$M + \text{H}$] $^+$ (49%, ^{79}Br , ^{79}Br), 510.97 [$M + \text{H}$] $^+$ (100%, ^{79}Br , ^{81}Br), 512.96 [$M + \text{H}$] $^+$ (51%, ^{81}Br , ^{81}Br).

MS (GC-TOF, EI $^+$) m/z : 507.95 (M^+ , 49%, ^{79}Br , ^{79}Br), 509.93 (M^+ , 100%, ^{79}Br , ^{81}Br), 511.94 (M^+ , 51%, ^{81}Br , ^{81}Br). Calcd. for $\text{C}_{23}\text{H}_{14}\text{Br}_2\text{N}_2\text{O}_2$: 509.94.

9,9-Bis(4-octyloxyphenyl)-4,5-diazafluorene (3.33)

Exp: SG-087



In a single necked round bottom flask charged 9,9-*bis*(4-hydroxyphenyl)-4,5-diazafluorene (**2.27**) (200 mg, 0.567 mmol), benzyltriethylammonium chloride (3 mg, 0.011 mmol), in dimethyl sulfoxide (5 mL) and the mixture was stirred for 10 min. 50 %w/v NaOH aqueous solution (1 mL) was added and the mixture was stirred for 15 minutes. Then *n*-iodooctane (286 mg, 1.19 mmol) was added drop wise and the mixture was stirred for 23 hours at room temperature. 5 %w/v NaCl aqueous solution (10 mL) and dichloromethane (25 mL) were added to the reaction mixture, stirred for 15 minutes and the organic layer was separated, washed with water (3 × 10 mL), dried over anhydrous magnesium sulphate and evaporated to yield a crude product (380 mg) as dark brown oil. The crude product was purified by column chromatography on silica gel eluting with DCM:MeOH = 99:1 v/v to yield compound **3.33** (180 mg, 55%) as a light brown solid.

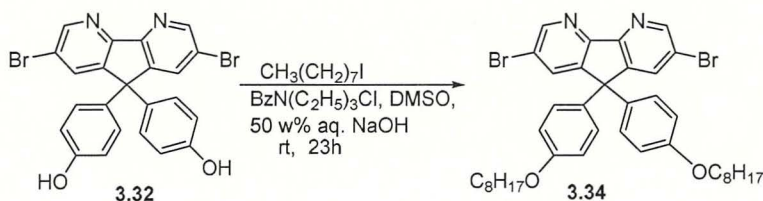
¹H NMR (500 MHz, CDCl₃): δ (ppm) 8.72 (2H, dd, *J* = 5.10, 1.48 Hz), 7.76 (2H, d, *J* = 1.23 Hz,), 7.29 – 7.27 (2H, m), 7.09 – 7.06 (4H, m), 6.78 – 6.76 (4H, m), 3.90 (4H, t, *J* = 6.24 Hz), 1.78 – 1.72 (4H, m), 1.45 – 1.40 (4H, bm), 1.33 – 1.28 (16H, bm), 0.89 (6H, t, *J* = 6.9 Hz).

¹³C NMR (101 MHz, CDCl₃): δ (ppm) 158.39 (C), 157.42 (C), 150.00, 146.33(C), 135.48(C), 133.57, 128.86, 123.44, 114.37, 67.98 (OCH₂), 60.29 (C-9), 31.80, 29.33, 29.24, 29.23, 26.04, 22.65, 14.10 (CH₃).

MS (GC-TOF, EI⁺) *m/z*: 576.41 (M⁺, 100 %). Calcd. for C₃₉H₄₈N₂O₂: 576.37.

2,7-Dibromo-9,9-bis(4-octyloxyphenyl)-4,5-diazafluorene (3.34)

Exp: SG-072



In a single necked round bottom flask was charged with 2,7-dibromo-9,9-bis(4-hydroxyphenyl)-4,5-diazafluorene (**3.32**) (1.01 g, 1.99 mmol) and benzyltriethylammonium chloride (3 mg, 0.011 mmol) in dimethyl sulfoxide (5 mL), and the mixture was stirred for 10 min. 50 wt% NaOH aqueous solution (1 mL) was added and the mixture was stirred for 15 minutes. Then *n*-iodooctane (789 μL , 4.374 mmol) was added drop wise and the mixture was stirred for 23 hours at room temperature. 5 w% NaCl aqueous solution (20 mL) and dichloromethane (80 mL) were added to the reaction mixture, stirred for 15 minutes and then the organic layer was separated, washed with water (2×20 mL), dried over anhydrous magnesium sulphate and evaporated to yield a crude product (2.0 g) as dark brown oil. The crude product was purified by column chromatography on silica gel eluting with PE:DCM = 4:1, v/v to yield compound **3.34** (1.03g, 73%) as a light brown solid.

$^1\text{H NMR}$ (500 MHz, CDCl_3): δ (ppm) 8.75 (2H, d, $J = 2.0$ Hz), 7.82 (2H, d, $J = 2.0$ Hz), 7.02 (4H, dd, $J = 6.7, 2.1$ Hz), (4H, dd, $J = 6.8, 2.1$ Hz), 3.90 (4H, t, $J = 6.42$ Hz), 1.77–1.72 (4H, m), 1.45–1.39 (4H, m), 1.34–1.13 (16H, m), 0.87 (6H, t, $J = 6.25$ Hz).

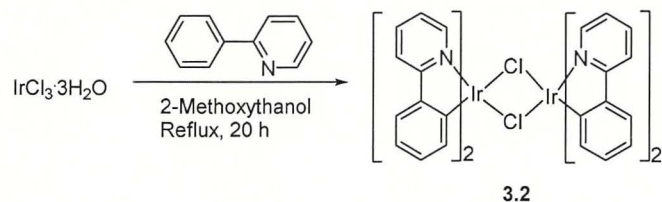
$^{13}\text{C NMR}$ (126 MHz, CDCl_3): δ (ppm) 158.94, 155.09, 151.60, 148.11, 136.46, 134.13, 128.92, 121.17, 114.92, 68.22, 60.44, 31.96, 29.48, 29.38, 26.20, 22.81, 14.26.

MS (GC-TOF, EI^+) m/z : 732.20 (35%, ^{79}Br , ^{79}Br), 734.21 (100%, ^{79}Br , ^{81}Br), 736.19 (35%, ^{81}Br , ^{81}Br). Calcd. for $\text{C}_{39}\text{H}_{46}\text{Br}_2\text{N}_2\text{O}_2$: 734.19 (M^+ , 100.0%), 732.19 (51.4%), 736.19 (48.6%).

3.4.2 Synthesis of μ -dichloro-bridged cyclometalated Ir (III) dimer

Bis-(μ)-chlorotetrakis(2-phenylpyridinato- C^2,N)diiridium(III) (**3.2**)⁷⁵

Exp: SG-055



Under argon, iridium(III) chloride hydrate (131 mg, 0.371 mmol), 2-phenylpyridine (240 μ L, 1.67 mmol), 2-methoxyethanol (8.0 mL) and water (2.5 mL) were charged in a 50 mL round bottom flask. The mixture was reflux (130 $^{\circ}$ C, oil bath) for 20 hours (light green colour suspension turns yellow after 30–40 minutes of heating). After cooling to room temperature, the yellow precipitate was filtered out on a glass frit. The precipitate was washed with 95% ethanol (10 mL) followed by acetone (10 mL) and then dissolved in DCM (15 mL) and filtered. Toluene (1.5 mL) and hexane (1.5 mL) were added to the filtrate, which was then reduced in volume by evaporation at reducing pressure to 5 mL, and cooled to afford yellow crystals which was collected by filtration, washed with hexane (5 mL) and dried *in vacuo* to afford product **3.2** as a yellow solid (84 mg, 42.2%).

Note: ^1H NMR showed some unknown impurity.

Dimer, *bis*-(μ)-chlorotetrakis(2-phenylpyridinato- C^2,N)diiridium(III), was re-synthesised with redistilled 2-phenylpyridine and fresh 2-ethoxy ethanol instead of 2-methoxy ethanol with the following modified procedure.

Exp: SG-62

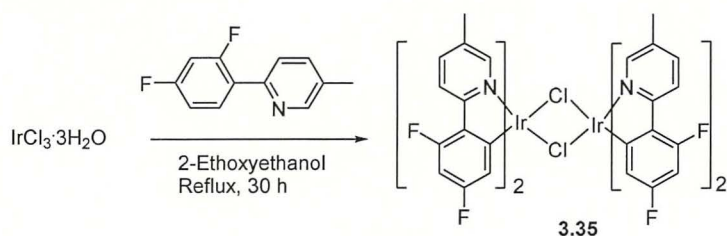
Under argon, iridium(III) chloride hydrate (1.12 g, 3.18 mmol), 2-phenylpyridine (2.24 g, 14.3 mmol), 2-ethoxyethanol (80 mL) and water (25 mL) were charged in 250 mL round bottom flask. The mixture was stirred under reflux (140 $^{\circ}$ C, oil bath) for 30 hours (light green colour suspension turns yellow after 30–40 minutes of heating). After cooling to room temperature, the yellow precipitate was filtered out. The precipitate was washed with 95% ethanol (100 mL) followed by acetone (100 mL) and then dried *in vacuo* to afford the product **3.2** as a yellow solid (1.12 g, 70.5%).

^1H NMR (500 MHz, CDCl_3): δ (ppm) 9.24 (4H, d, $J = 7.3$ Hz), 7.86 (4H, d, $J = 7.9$ Hz), 7.73 (4H, t, $J = 8.1$ Hz), 7.48 (4H, d, $J = 7.7$ Hz) 6.78–6.72 (8H, m), 6.55 (4H, t, $J = 7.1$ Hz), 5.92 (4H, d, $J = 8.6$ Hz).

Bis-(μ)-chlorotetrakis{2-(2,4-difluorophenyl)-5-methylpyridinato- C^2,N }diiridium(III)

(**3.35**)^{32,39,93}

Exp: SG-111



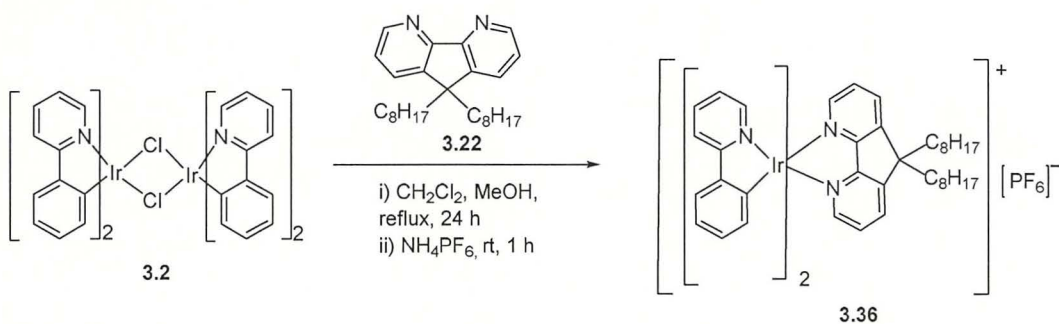
Under argon, IrCl_3 hydrate (500 mg, 1.42 mmol), 2-(2,4-difluorophenyl)-5-methylpyridine (640 mg, 3.12 mmol), 2-ethoxyethanol (15 mL) and water (5 mL) were charged in 100 mL round bottom flask. The mixture was reflux (140 °C, oil bath) for 30 hours (light green colour suspension turns yellow after 30–40 minutes of heating). After cooling to room temperature, the yellow precipitate was filtered out. The precipitate was washed with water (30 mL) followed by diethyl ether (15 mL) then dried *in vacuo* to afford the product **3.35** (730 mg, 80.6%) as a yellow solid.

$^1\text{H NMR}$ (400 MHz, CDCl_3): δ (ppm) 8.92 (4H, d, $J = 5.8$ Hz), 8.10 (4H, s), 6.60 (4H, d, $J = 6.2$ Hz), 6.34–6.28 (4H, m), 5.32 (4H, dd, $J = 8.0, 2.2$ Hz), 2.67 (12H, s).

3.4.3 Synthesis of Iridium Complexes

$\text{Ir}(\text{ppy})_2(\text{doDAF})\text{PF}_6$ (**3.36**)

Exp: SG-091



Under argon, *bis*-(μ)-chlorotetrakis(2-phenylpyridinato- C^2,N)diiridium(III) (**3.2**) (50 mg, 0.046 mmol) and 9,9-dioctyl-4,5-diazafluorene (**3.22**) (37 mg, 0.093 mmol) and a solution of methanol (10 mL) and dichloromethane (10 mL) were charged into a 50 mL round bottom flask. The mixture was reflux (70 °C, oil bath) for 24 hours under dark, during heating complete dissolution was observed. After cooling to room temperature, NH_4PF_6 (400 mg, 2.45 mmol) was added and stirred for 1 hour at room temperature. The solvent was removed

by evaporation and the residue was purified by column chromatography on silica gel eluting with DCM:MeOH = 100:1 to afford the complex **3.36** (92 mg, 97.0 %) as a yellow solid.

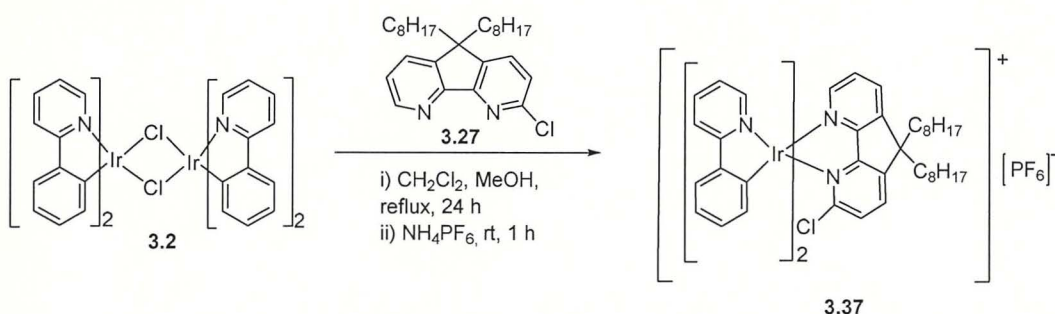
¹H NMR (400 MHz, CDCl₃): δ (ppm) 8.02 (2H, dd, *J* = 7.7, 0.8 Hz), 7.92 (2H, d, *J* = 8.1 Hz), 7.76 (2H, td, *J* = 8.0, 1.4 Hz), 7.68–7.63 (6H, m), 7.56–7.53 (2H, m), 7.04–6.97 (4H, m), 6.92 (2H, td, *J* = 7.5, 1.2 Hz), 6.40 (2H, dd, *J* = 7.6, 0.6 Hz), 2.15–2.07 (4H, m), 1.25–1.07 (20H, m), 0.83 (6H, t, *J* = 6.9 Hz), 0.78–0.61 (4H, m).

¹³C NMR (100 MHz, CDCl₃): δ (ppm) 167.95, 160.83, 148.89, 147.74, 145.17, 144.79, 143.85, 138.31, 134.48, 132.02, 130.56, 127.62, 124.52, 123.16, 122.88, 119.57, 59.61, 37.38, 31.70, 29.56, 29.26, 29.05, 24.57, 22.57, 14.04.

MS (ESI⁺) *m/z*: 893.47 ([*M*–PF₆]⁺, 100%). Calcd. for C₄₉H₅₆IrN₄: 893.41.

[Ir(ppy)₂(*o*-cldoDAF)]PF₆ (**3.37**)

Exp: SG-082



Under argon, *bis*-(μ)-chlorotetrakis(2-phenylpyridinato-C²,N)diiridium(III) (**3.2**) (50 mg, 0.046 mmol) and 3-chloro-9,9-dioctyl-4,5-diazafluorene (**3.27**) (43 mg, 0.093 mmol) and a solution of methanol (10 mL) and dichloromethane (10 mL) were charged into a 50 mL round bottom flask. The mixture was reflux (70 °C, oil bath) for 24 hours under dark, during heating complete dissolution was observed. After cooling to room temperature, NH₄PF₆ (400 mg, 2.451 mmol) was added and stirred for 1 hour at room temperature. The solvent was removed by evaporation and the residue was purified by column chromatography on silica gel eluting with DCM to afford the complex **3.37** (55 mg, 55%) as a yellow solid.

¹H NMR (400 MHz, CDCl₃): δ (ppm) 8.05–8.01 (2H, m), 7.95–7.92 (3H, m), 7.81–7.75 (2H, m), 7.63 (2H, td, *J* = 7.3, 1.2 Hz), 7.56–7.47 (4H, m), 7.09 (1H, td, *J* = 6.6, 1.4 Hz), 7.01 (1H, td, *J* = 7.1, 1.1 Hz), 6.98–6.92 (2H, m), 6.87 (1H, td, *J* = 7.5, 1.2 Hz), 6.83 (1H, td, *J* = 7.5, 1.3 Hz), 6.30 (1H, dd, *J* = 7.6, 0.9 Hz), 6.22 (1H, dd, *J* = 8.0, 0.9 Hz) 2.14–2.06 (4H, m), 1.23–1.07 (20H, m), 0.85–0.81 (6H, m), 0.77–0.67 (4H, m).

¹³C NMR (100 MHz, CDCl₃): δ (ppm) 168.82, 167.10, 161.02, 160.39, 153.63, 150.04, 148.37, 147.59, 147.08, 146.04, 143.98, 143.84, 143.41, 140.58, 138.50, 138.35, 136.79,

134.42, 132.52, 131.29, 130.70, 130.11, 128.24, 127.97, 124.53, 124.30, 123.57, 123.19, 122.87, 122.63, 119.71, 119.54, 58.18, (37.33, 37.21), (31.71, 31.70), (29.55, 29.54), (29.32, 29.23), (29.09, 29.07), (24.59, 24.56), 22.57, 14.08.

DEPTQ NMR (100 MHz, CDCl₃): δ (ppm) 168.83, 167.10, 161.05, 160.38, 153.63, 150.15 (CH), 148.46 (CH), 147.56 (CH), 147.09, 143.96, 143.90, 143.39, 140.61, 139.79, 138.43 (CH), 138.27 (CH), 136.74 (CH), 134.45 (CH), 132.52 (CH), 131.31 (CH), 130.72 (CH), 130.14 (CH), 128.18 (CH), 127.95 (CH), 124.50 (CH), 124.28 (CH), 123.59 (CH), 123.19 (CH), 122.87 (CH), 122.65 (CH), 119.63 (CH), 119.48 (CH), 58.47, (37.29, 37.17), (31.73, 31.71), (29.56, 29.55), (29.35, 29.26), (29.10, 29.08), 24.62, 22.59, 14.08.

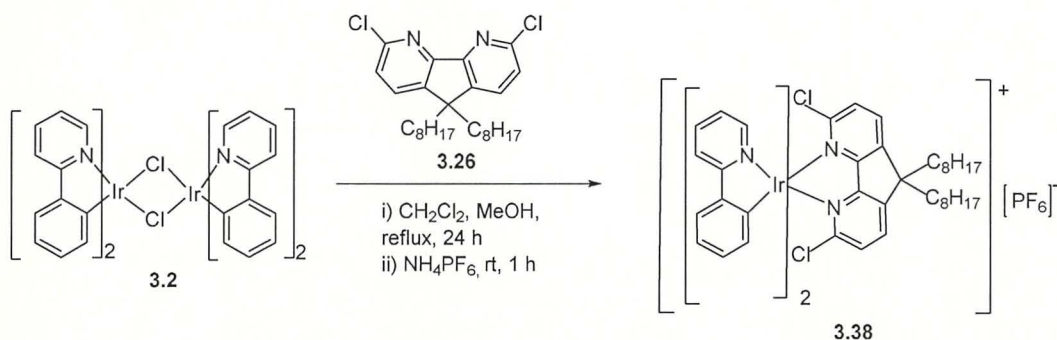
³¹P NMR (162 MHz, CDCl₃): δ (ppm) -144.4 (sept, ¹J_{PF} = 713 Hz, PF₆).

¹⁹F NMR (377 MHz, CDCl₃): δ (ppm) -73.2 (d, ¹J_{PF} = 713 Hz, PF₆).

MS (ESI⁺) *m/z*: 927.41 ([M-PF₆]⁺, 100%, ³⁵Cl), 929.4059 ([M-PF₆]⁺, 30%, ³⁷Cl). Calcd. for C₄₉H₅₅ClIrN₄: 927.37.

[Ir(ppy)₂(*o*-dclidoDAF)]PF₆ (**3.38**)

Exp: SG-077



Under argon, *bis*-(μ)-chlorotetrakis(2-phenylpyridinato-C²,N)diiridium(III) (**3.2**) (51 mg, 0.047 mmol) and 3,6-dichloro-9,9-dioctyl-4,5-diazafluorene (**3.26**) (44 mg, 0.095 mmol) and a solution of methanol (10 mL) and dichloromethane (10 mL) were charged into a 50 mL round bottom flask. The mixture was reflux (70 °C, oil bath) for 24 hours under dark, during heating complete dissolution was observed. After cooling to room temperature, NH₄PF₆ (400 mg, 2.45 mmol) was added and stirred for 1 hour at room temperature. The solvent was removed by evaporation and the residue was purified by column chromatography on silica gel eluting with DCM to afford the complex **3.38** (62 mg, 62.3%) as a yellow solid.

¹H NMR (400 MHz, CDCl₃): δ (ppm) 8.05 (2H, d, *J* = 8.16 Hz), 7.93 (2H, d, *J* = 8.2 Hz), 7.82–7.79 (4H, m), 7.57 (2H, d, *J* = 7.3 Hz), 7.50 (2H, d, *J* = 8.1 Hz), 7.06 (2H, t, *J* = 6.5 Hz), 6.93 (2H, t, *J* = 7.3 Hz), 6.77 (2H, t, *J* = 7.4 Hz), 6.11 (2H, d, *J* = 7.7 Hz), 2.11 (4H, t, 8.1 Hz), 1.25–1.05 (20H, m), 0.83 (6H, t, *J* = 6.8), 0.72–0.66 (4H, m).

^{13}C NMR (100 MHz, CDCl_3): δ (ppm) 167.95, 160.60, 153.54, 149.46, 144.80, 143.47, 143.03, 138.47, 136.58, 131.84, 130.09, 129.01, 124.25, 123.18, 122.874, 119.629, 57.03, 37.196, 31.72, 29.54, 29.29, 29.12, 24.57, 22.59, 14.08.

DEPTQ NMR (100 MHz, CDCl_3): δ (ppm) 167.93, 160.58, 153.54, 149.39 (CH), 144.76, 143.49, 143.02, 138.52 (CH), 136.60 (CH), 131.83 (CH), 130.05 (CH), 129.04 (CH), 124.26 (CH), 123.18 (CH), 122.85 (CH), 119.66 (CH), 57.02, 37.21, 31.70, 29.53, 29.27, 29.11, 24.53, 22.58, 14.08 (CH_3).

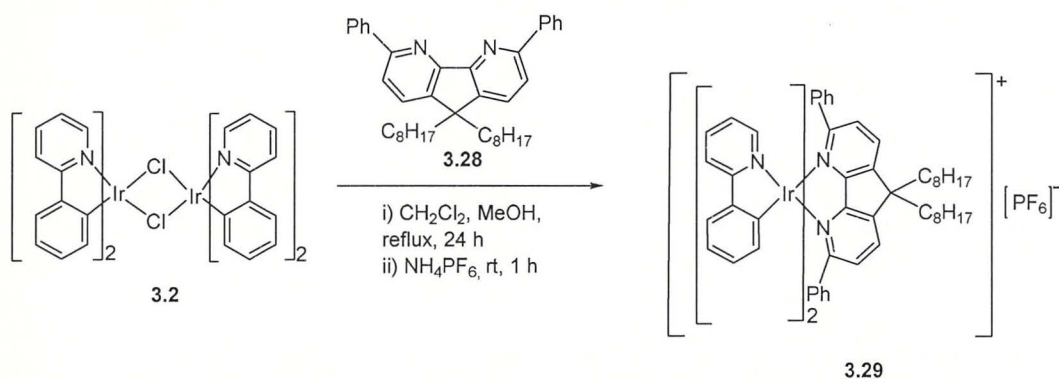
^{31}P NMR (162 MHz, CDCl_3): δ (ppm) -144.4 (sept, $^1J_{\text{PF}} = 713$ Hz, PF_6).

^{19}F NMR (377 MHz, CDCl_3): δ (ppm) -73.3 (d, $^1J_{\text{PF}} = 713$ Hz, PF_6).

MS (ESI $^+$) m/z : 961.35 ($[\text{M}-\text{PF}_6]^+$, 100%, ^{35}Cl , ^{37}Cl), 963.35 ($[\text{M}-\text{PF}_6]^+$, 60%, ^{35}Cl , ^{37}Cl), 965.35 ($[\text{M}-\text{PF}_6]^+$, 15%, ^{37}Cl , ^{37}Cl). Calcd. for $\text{C}_{49}\text{H}_{54}\text{Cl}_2\text{IrN}_4$: 961.34.

$[\text{Ir}(\text{ppy})_2(o\text{-dphdoDAF})]\text{PF}_6$ (**3.39**)

Exp: SG-083



Under argon, bis-(μ)-chlorotetrakis(2-phenylpyridinato- C^2 ,N)diiridium(III) (**3.2**) (51 mg, 0.046 mmol) and 3,6-diphenyl-9,9-dioctyl-4,5-diazafluorene (**3.28**) (50 mg, 0.093 mmol) and a solution of methanol (10 mL) and dichloromethane (10 mL) were charged into a 50 mL round bottom flask. The mixture was reflux (70 °C, oil bath) for 24 hours under dark, during heating complete dissolution was observed. After cooling to room temperature, NH_4PF_6 (400 mg, 2.45 mmol) was added and stirred for 1 hour at room temperature. The solvent was removed by evaporation and the residue was purified by column chromatography on silica gel eluting with $\text{DCM}:\text{MeOH} = 100:1$ to afford the product as a brown solid (100 mg). The product was further purified by column chromatography on silica gel eluting with EA:PE, starting with 1:9 ratio and gradually increasing polarity to 1:1 ratio, to afford the complex **3.39** (55 mg, 50.9%) as a yellow solid.

^1H NMR (400 MHz, CDCl_3): δ (ppm) 8.06 (2H, d, $J = 7.9$ Hz), 7.94 (2H, d, $J = 5.5$ Hz), 7.80–7.72 (4H, m), 7.36 (2H, d, $J = 7.9$ Hz), 7.10–7.06 (4H, m), 6.96 (2H, t, $J = 7.4$ Hz),

$J = 6.5$ 6.80 (4H, t, $J = 7.9$ Hz), 6.67 (4H, d, $J = 7.4$ Hz), 6.43 (2H, s, $J = 7.1$ Hz), 6.13 (2H, t, $J = 6.5$ Hz), 5.30 (2H, d, $J = 7.2$ Hz), 2.25–2.12 (4H, m), 1.25–1.21 (20H, m), 1.12–0.90 (4H, m), 0.86 (6H, t, $J = 6.8$ Hz).

$^{13}\text{C NMR}$ (100 MHz, CDCl_3): δ (ppm) 168.31, 163.23, 161.32, 149.61, 144.77, 142.71, 142.39, 138.09, 136.80, 133.96, 131.39, 129.89, 129.08, 128.68, 127.85 ($\times 2\text{C}$), 127.60 ($\times 2\text{C}$), 123.64, 122.45, 121.56, 119.19, 56.46, 37.66, 31.78, 29.79, 29.34, 29.26, 24.91, 22.65, 14.11.

DEPTQ NMR (100 MHz, CDCl_3): δ (ppm) 168.11, 163.12, 161.22, 149.52 (CH), 144.67, 142.62, 142.28, 137.97 (CH), 136.70, 133.86 (CH), 131.28 (CH), 129.79 (CH), 128.57 (CH), 127.74 ($\times 2\text{CH}$), 127.50 ($\times 2\text{CH}$), 123.52 (CH), 122.34 (CH), 121.45 (CH), 119.08 (CH), 56.36, 37.55, 31.68, 29.69, 29.24, 29.16, 24.81, 22.54, 14.01.

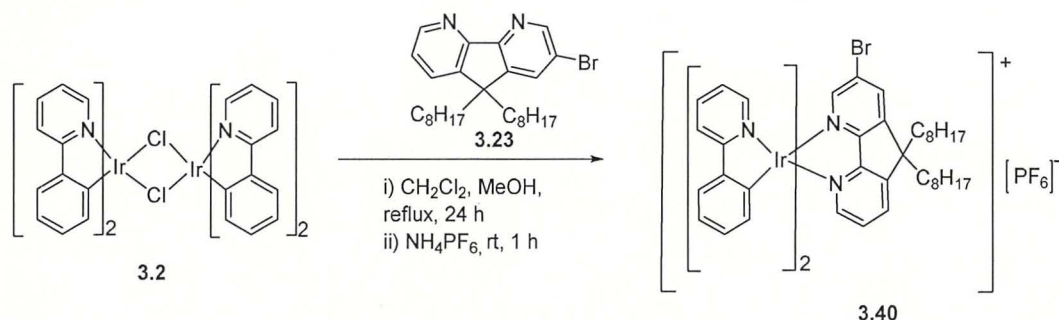
$^{31}\text{P NMR}$ (162 MHz, CDCl_3): δ (ppm) -144.4 (sept, $^1J_{\text{PF}} = 713$ Hz, PF_6).

$^{19}\text{F NMR}$ (377 MHz, CDCl_3): δ (ppm) -73.2 (d, $^1J_{\text{PF}} = 713$ Hz, PF_6).

$\text{MS (ESI}^+)$ m/z : 1045.52 ($[\text{M}-\text{PF}_6]^+$, 100%), 1046.53 ($[\text{M}-\text{PF}_6]^+$, 42%), 1043.52 ($[\text{M}-\text{PF}_6]^+$, 38%), 1044.52 ($[\text{M}-\text{PF}_6]^+$, 20%), 1047.53 ($[\text{M}-\text{PF}_6]^+$, 10%), 1048.53 ($[\text{M}-\text{PF}_6]^+$, 2%). Calcd. for $\text{C}_{61}\text{H}_{64}\text{IrN}_4$: 1045.48.

$[\text{Ir}(\text{ppy})_2(m\text{-brdoDAF})]\text{PF}_6$ (**3.40**)

Exp: SG-089



Under argon, *bis*-(μ)-chlorotetrakis(2-phenylpyridinato- C^2,N)diiridium(III) (**3.2**) (50 mg, 0.046 mmol) and 2-bromo-9,9-dioctyl-4,5-diazafluorene (**3.23**) (44 mg, 0.093 mmol) and a solution of methanol (10 mL) and dichloromethane (10 mL) were charged into a 50 mL round bottom flask. The mixture was reflux (70 °C, oil bath) for 24 hours under dark, during heating complete dissolution was observed. After cooling to room temperature, NH_4PF_6 (400 mg, 2.45 mmol) was added and stirred for 1 hour at room temperature. The solvent was removed by evaporation and the residue was purified by column chromatography on silica gel eluting with $\text{DCM}:\text{MeOH}$ in the ratio 100:1 to afford the complex **3.40** (98 mg, 93.1%) as a light orange solid.

¹H NMR (400 MHz, CDCl₃): δ (ppm) 8.09 (1H, d, *J* = 1.2 Hz), 8.05 (1H, dd, *J* = 7.7, 0.8 Hz), 7.95–7.92 (2H, m), 7.81, 7.77 (2H, m), 7.68–7.58 (7H, m), 7.05–6.98 (4H, m), 6.91 (2H, dq, *J* = 7.8, 1.2 Hz), 6.38 (1H, dd, *J* = 7.7, 0.8 Hz), 6.33 (1H, dd, *J* = 7.7, 0.8 Hz), 2.17–2.03 (4H, m), 1.34–0.99 (20H, m), 0.82 (6H, t, *J* = 7.7 Hz), 0.78–0.68 (4H, m).

¹³C NMR (100 MHz, CDCl₃): δ (ppm) 167.77, 167.74, 159.79, 159.47, 149.11, 148.86, 148.72, 148.12, 146.39, 145.38, 144.22, 143.92, 143.63, 143.50, 138.56, 138.53, 137.26, 134.90, 132.05, 131.85, 130.67, 130.60, 128.39, 124.61, 124.57, 123.53, 123.43, 123.28, 123.11, 123.09, 119.72, 119.69, 59.90, (37.20, 37.17), 29.52, (29.26, 29.24), 29.07, (24.69, 24.63), 22.59, 14.08.

DEPTQ NMR (100 MHz, CDCl₃): δ (ppm) 167.71, 167.70, 159.75, 159.49, 149.06 (CH), 148.84 (CH), 148.73 (CH), 148.11 (CH), 146.36, 145.36, 144.20, 143.92, 143.66, 143.49, 138.61 (CH), 138.58 (CH), 137.26 (CH), 134.87 (CH), 132.04 (CH), 131.83 (CH), 130.63 (CH), 130.59 (CH), 128.36 (CH), 124.62 (CH), 124.57 (CH), 123.51 (CH), 123.47, 123.31 (CH), 123.10 (CH), 123.07 (CH), 119.74 (× 2CH), 59.89, (37.20, 37.16), 31.69, 29.50, (29.24, 29.22), 29.07, (24.67, 24.61), 22.58, 14.08.

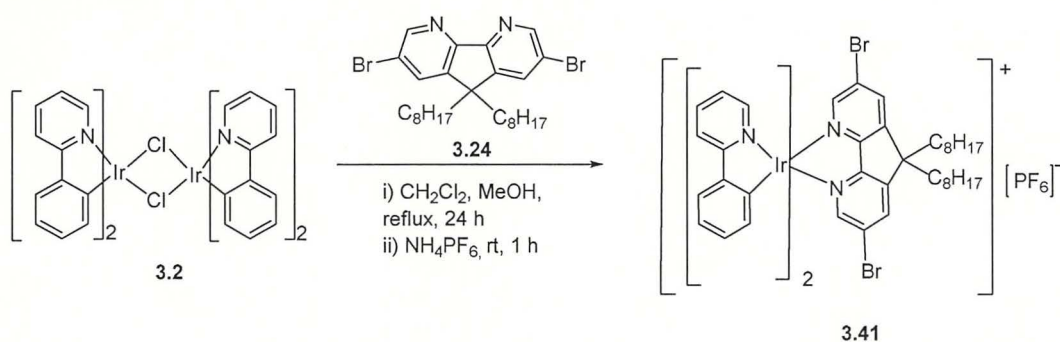
³¹P NMR (162 MHz, CDCl₃): δ (ppm) -144.4 (sept, ¹*J*_{PF} = 713 Hz, PF₆).

¹⁹F NMR (377 MHz, CDCl₃): δ (ppm) -73.2 (d, ¹*J*_{PF} = 713 Hz, PF₆).

MS (ESI⁺) *m/z*: 971.36 ([M–PF₆]⁺, 100%), 973.35 ([M–PF₆]⁺, 60%, ⁸¹Br), 972.3561 ([M–PF₆]⁺, 40%, ⁷⁹Br). Calcd. for C₄₉H₅₅BrIrN₄: 971.32.

[Ir(ppy)₂(*m*-dbrdoDAF)]PF₆ (**3.41**)

Exp: SG-080



Under argon, *bis*-(μ)-chlorotetrakis(2-phenylpyridinato-C²,N)diiridium(III) (**3.2**) (51 mg, 0.046 mmol) and 9,9-dioctyl-2,7-dibromo-4,5-diazafluorene (**3.24**) (51 mg, 0.093 mmol) and a solution of methanol (10 mL) and dichloromethane (10 mL) were charged into a 50 mL round bottom flask. The mixture was reflux (70 °C, oil bath) for 16 hours under dark, during heating complete dissolution was observed. After cooling to room temperature, NH₄PF₆ (400 mg, 2.45 mmol) was added and stirred for 1 hour at room temperature. The solvent was

removed by evaporation and the residue was purified by column chromatography on silica gel eluting with DCM:MeOH in the ratio 100:1 to afford the complex **3.41** (102 mg, 91%) as a crystalline orange solid.

¹H NMR (400 MHz, CDCl₃): δ (ppm) 8.12 (2H, d, *J* = 1.4 Hz), 7.93 (2H, d, *J* = 8.0 Hz), 7.80 (2H, td, *J* = 1.4 Hz, *J* = 8.1 Hz), 7.71 (2H, d, *J* = 5.7 Hz), 7.67–7.66 (4H, m), 7.12 (2H, td, *J* = 1.3 Hz, *J* = 8.1 Hz), 7.04 (2H, d, *J* = 1.0 Hz, *J* = 7.3 Hz), 6.92 (2H, td, *J* = 1.2 Hz, *J* = 7.5 Hz), 6.31 (2H, d, *J* = 7.5 Hz), 2.09 (4H, t, *J* = 8.3 Hz), 1.25–1.13 (20H, m), 0.89–0.77 (10H, m).

¹³C NMR (100 MHz, CDCl₃): δ (ppm) 167.51, 158.45, 149.32, 149.08, 146.61, 143.73, 143.02, 138.68, 137.68, 131.91, 130.69, 124.60, 124.17, 123.27, 123.27, 119.71, 60.06, 36.80, 31.72, 29.50, 29.29, 29.12, 24.82, 22.60, 14.09.

DEPTQ NMR (100 MHz, CDCl₃): δ (ppm) 167.50, 158.46, 149.42 (CH), 149.06 (CH), 146.63, 143.73, 143.07, 138.60 (CH), 137.70 (CH), 131.92 (CH), 130.70 (CH), 124.57 (CH), 124.14, 123.72 (CH), 123.25 (CH), 119.64 (CH), 60.03, 36.76, 31.73, 29.52, 29.31, 29.12, 24.85, 22.61, 14.09.

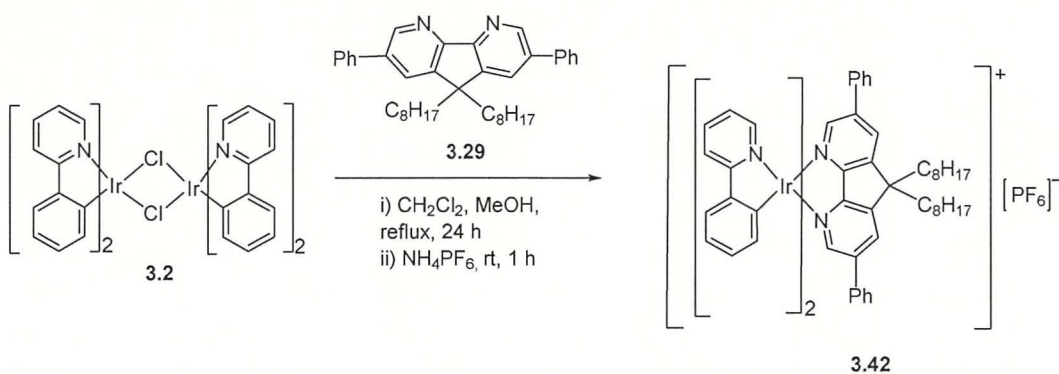
³¹P NMR (162 MHz, CDCl₃): δ (ppm) -144.5 (sept., ¹*J*_{PF} = 713 Hz, PF₆).

¹⁹F NMR (377 MHz, CDCl₃): δ (ppm) -73.2 (d, ¹*J*_{PF} = 713 Hz, PF₆).

MS (ESI⁺) *m/z*: 1051.25 ([M–PF₆]⁺, 100%, ⁷⁹Br, ⁸¹Br), 1049.26 ([M–PF₆]⁺, 68%, ⁷⁹Br, ⁷⁹Br), 1052.25 ([M–PF₆]⁺, 28%, ⁸¹Br, ⁸¹Br). Calcd. for C₄₉H₅₄Br₂IrN₄: 1051.23.

Ir(ppy)₂(*m*-dphdoDAF)]PF₆ (**3.42**)

Exp: SG-114



Under argon, *bis*-(μ)-chlorotetrakis(2-phenylpyridinato-C²,N)diiridium(III) (**3.2**) (52 mg, 0.046 mmol) and 2,7-diphenyl-9,9-dioctyl-4,5-diazafluorene (**3.29**) (50 mg, 0.093 mmol) and a solution of methanol (10 mL) and dichloromethane (10 mL) were charged into a 50 mL round bottom flask. The mixture was reflux (70 °C, oil bath) for 24 hours under dark, during heating complete dissolution was observed. After cooling to room temperature, NH₄PF₆ (400

mg, 2.45 mmol) was added and stirred for 1 hour at room temperature. The solvent was removed by evaporation and the residue was purified by column chromatography on silica gel eluting with EA:PE in the ratio 1:9 gradually increasing the polarity to 1:1 to afford the complex **3.42** (95 mg, 86.3%) as an orange solid.

$^1\text{H NMR}$ (400 MHz, CDCl_3): δ (ppm) 8.14 (2H, d, $J = 1.1$ Hz), 7.94 (2H, dd, $J = 8.8, 1.7$ Hz), 7.80–7.77 (6H, m), 7.68 (2H, dd, $J = 7.6, 1.2$ Hz), 7.49–7.42 (10H, m), 7.09–7.02 (4H, m), 6.94 (2H, dd, $J = 7.5, 1.2$ Hz), 6.41 (2H, dd, $J = 7.6, 1.1$ Hz), 2.21 (4H, t, $J = 8.2$ Hz), 1.27–1.12 (20H, m), 0.94–0.85 (4H, m), 0.81 (6H, t, $J = 6.7$ Hz).

$^{13}\text{C NMR}$ (100 MHz, CDCl_3): δ (ppm) 167.86, 159.36, 149.21, 146.20, 145.75, 144.44, 143.87, 141.30, 138.43, 135.99, 132.62, 132.01, 130.62, 129.52, 129.62 ($\times 2$), 127.62 ($\times 2$), 124.52, 123.41, 122.98, 119.57, 59.76, 37.20, 31.72, 29.58, 29.32, 29.11, 24.89, 22.60, 14.06.

DEPTQ NMR (100 MHz, CDCl_3): δ (ppm) 167.35, 159.36, 149.21 (CH), 146.20 (CH), 145.74, 144.45, 143.87, 141.29, 138.42 (CH), 135.99, 132.62 (CH), 132.01 (CH), 130.61 (CH), 129.52 (CH), 129.45 (CH) ($\times 2$), 127.62 (CH) ($\times 2$), 124.52 (CH), 123.41(CH), 122.97 (CH), 119.56 (CH), 59.75, 37.19, 31.72, 29.58, 29.32, 29.11, 24.89, 22.60, 14.06 (CH_3).

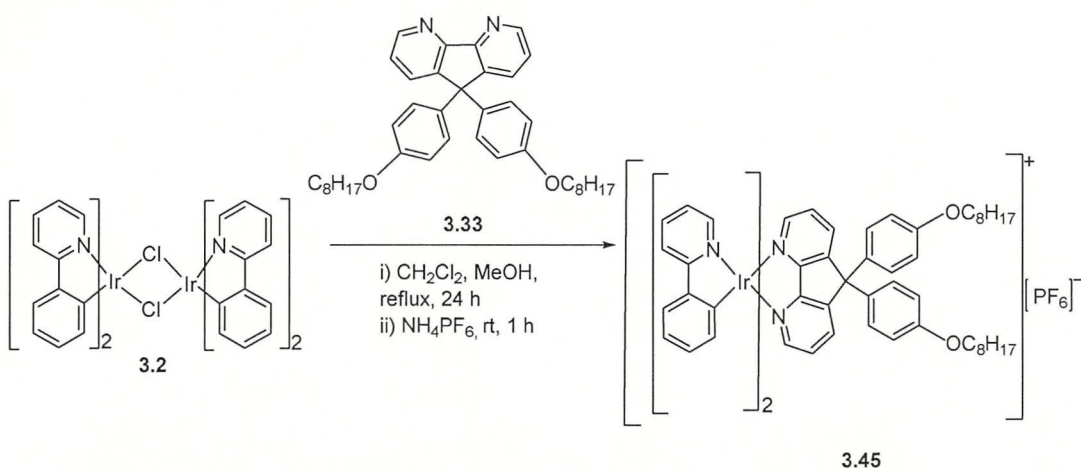
$^{31}\text{P NMR}$ (162 MHz, CDCl_3): δ (ppm) -144.4 (sept, $^1J_{\text{PF}} = 713$ Hz, PF_6).

$^{19}\text{F NMR}$ (377 MHz, CDCl_3): δ (ppm) -73.2 (d, $^1J_{\text{PF}} = 714$ Hz, PF_6).

$\text{MS (ESI}^+)$ m/z : 1045.49 ($[\text{M-PF}_6]^+$, 100%), 1046.46 ($[\text{M-PF}_6]^+$, 55%), 1043.50 ($[\text{M-PF}_6]^+$, 38%), 1044.48 ($[\text{M-PF}_6]^+$, 25%), 1047.39 ($[\text{M-PF}_6]^+$, 2%). Calcd. for $\text{C}_{61}\text{H}_{64}\text{IrN}_4$: 1045.48.

[Ir(ppy)₂(dphoDAF)]PF₆ (3.45)

Exp: SG-088



Under argon, *bis*-(μ)-chlorotetrakis(2-phenylpyridinato- C^2,N)diiridium(III) (**3.2**) (51 mg, 0.046 mmol) and 9,9-*bis*(4-octyloxyphenyl)-4,5-diazafluorene (**3.33**) (53 mg, 0.093 mmol) and a solution of methanol (10 mL) and dichloromethane (10 mL) were charged into a 50 mL

round bottom flask. The mixture was reflux (70 °C, oil bath) for 24 hours, during heating complete dissolution was observed. After cooling to room temperature, NH₄PF₆ (400 mg, 2.45 mmol) was added and stirred for 1 hour at room temperature. The solvent was removed by evaporation and the residue was purified by column chromatography on silica gel eluting with DCM:MeOH in the ratio 100:1 to afford the complex **3.45** (95 mg, 85.2%) as a light yellow solid.

¹H NMR (400 MHz, CDCl₃): δ (ppm) 7.98 (2H, d, *J* = 7.8 Hz), 7.90 (2H, d, *J* = 8.1 Hz), 7.81–7.71 (4H, m), 7.68–7.64 (4H, m), 7.50 (2H, dd, *J* = 7.9, 5.3 Hz), 7.11 (2H, t, *J* = 6.6 Hz), 7.08–6.98 (6H, m), 6.91 (2H, td, *J* = 7.5, 1.3 Hz), 6.82 (4H, d, *J* = 7.8 Hz), 6.39 (2H, dd, *J* = 7.6, 0.9 Hz), 3.90 (4H, t, *J* = 6.6 Hz), 1.72 (4H, p, *J* = 6.6 Hz), 1.43–1.38 (4H, m), 1.32–1.26 (16H, m), 0.87 (6H, t, *J* = 6.9 Hz).

DEPTQ NMR (100 MHz, CDCl₃): δ (ppm) 167.74, 160.07, 159.25, 149.13 (CH), 148.22 (CH), 145.95, 144.55, 143.87, 138.43 (CH), 136.29 (CH), 132.13, 131.10 (CH), 130.56 (CH), 128.31 (CH), 128.09 (× 2) (CH), 124.45 (CH), 123.62 (CH), 122.89 (CH), 119.48 (CH), 115.14 (× 2) (CH), 68.13, 67.26, 31.80, 29.33, 29.21, 29.20, 26.02, 22.65, 14.10.

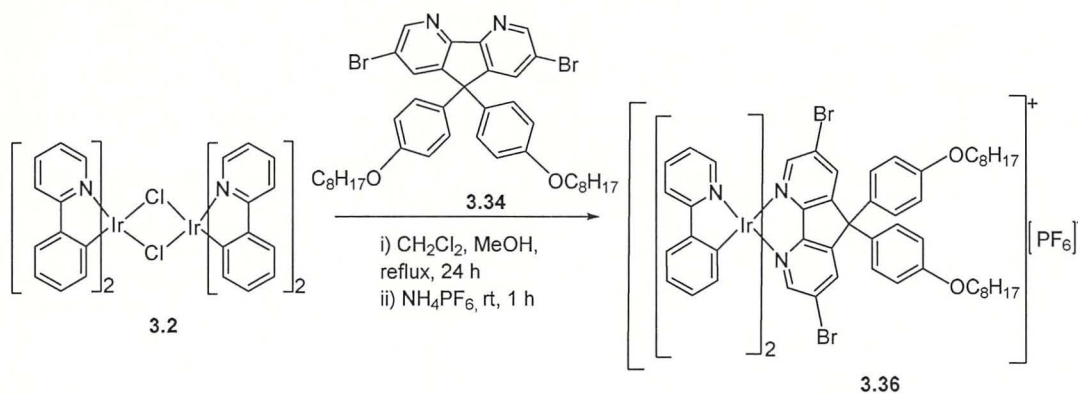
³¹P NMR (162 MHz, CDCl₃): δ (ppm) -144.4 (sept, ¹*J*_{PF} = 713 Hz, PF₆).

¹⁹F NMR (377 MHz, CDCl₃): δ (ppm) -73.2 (d, ¹*J*_{PF} = 713 Hz, PF₆).

MS (ESI⁺) *m/z*: 1077.50 ([M-PF₆]⁺, 100%). Calcd. for C₆₁H₆₄IrN₄O₂: 1077.47.

[Ir(ppy)₂(*m*-dbrdphoDAF)]PF₆ (**3.46**)

Exp: SG-086



Under argon, *bis*-(μ)-chlorotetrakis(2-phenylpyridinato-C²,N)diiridium(III) (**3.2**) (51 mg, 0.046 mmol) and 9,9-*bis*(4-octyloxyphenyl)-2,7-dibromo-4,5-diazafluorene (**3.34**) (68 mg, 0.093 mmol) and a solution of methanol (10 mL) and dichloromethane (10 mL) were charged into a 50 mL round bottom flask. The mixture was stirred under reflux (70 °C, oil bath) for 24 hours in the dark (complete dissolution was observed during heating). After cooling to room temperature, NH₄PF₆ (400 mg, 2.45 mmol) was added and the mixture was stirred for 1 hour

at room temperature. The solvent was removed by evaporation and the residue was purified by column chromatography on silica gel eluting with DCM:MeOH = 100:1 to afford the complex **3.46** (80 mg, 62.3%) as an orange solid.

¹H NMR (400 MHz, CDCl₃): δ (ppm) 8.03 (2H, d, *J* = 1.5 Hz), 7.92 (2H, td, *J* = 1.2 Hz, *J* = 8.0 Hz), 7.83–7.79 (4H, m), 7.69 (2H, d, *J* = 1.5 Hz), 7.65 (2H, dd, *J* = 8.0, 1.0 Hz), 7.24–7.23 (2H, m), 7.07–7.02 (6H, m), 6.93 (2H, td, *J* = 7.4, 1.3 Hz), 6.86 (4H, td, *J* = 8.8, 2.0 Hz), 6.32 (2H, dd, *J* = 7.6, 1.0 Hz), 3.92 (4H, t, *J* = 6.5 Hz), 1.77–1.70 (4H, m), 1.41–1.38 (4H, m), 1.30–1.25 (16H, m), 0.88 (6H, t, *J* = 6.8 Hz).

¹³C NMR (100 MHz, CDCl₃): δ (ppm) 167.16, 159.59, 157.74, 149.67, 149.49, 147.10, 143.72, 142.78, 139.19, 138.74, 131.89, 130.99, 130.74, 128.35 (× 2), 124.68, 124.54, 124.10, 123.29, 119.60, 115.44 (× 2), 68.71, 67.60, 31.83, 29.32, 29.22, 29.18, 26.01, 22.65, 14.10.

DEPTQ NMR (100 MHz, CDCl₃): δ (ppm) 167.36, 159.59, 157.74, 149.67 (CH), 149.50 (CH), 147.10, 143.72, 142.79, 139.20 (CH), 138.74 (CH), 131.90 (CH), 131.00, 130.70 (CH), 128.35 (× 2CH), 124.68, 124.54 (CH), 124.10 (CH), 123.29 (CH), 119.60 (CH), 115.44 (× 2CH) 68.22 (× 2), 31.81, 29.33, 29.22, 29.18, 26.02, 22.66, 14.10.

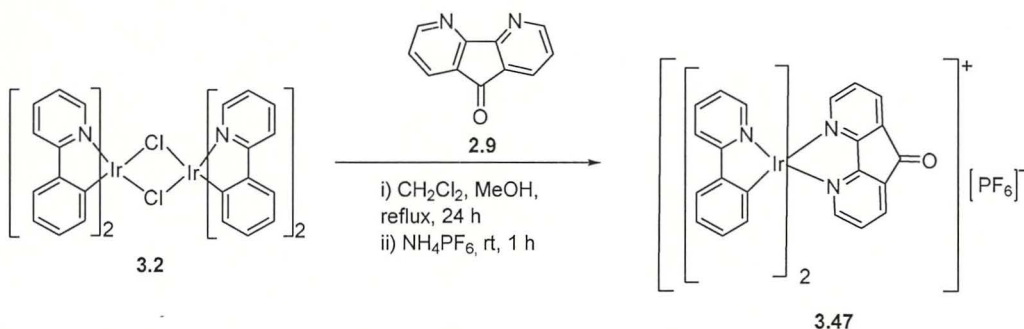
³¹P NMR (162 MHz, CDCl₃): δ (ppm) -144.4 (sept, ¹*J*_{PF} = 713 Hz, PF₆).

¹⁹F NMR (377 MHz, CDCl₃): δ (ppm) -73.2 (d, ¹*J*_{PF} = 713 Hz, PF₆).

MS (ESI⁺) *m/z*: 1235.32 [M-PF₆]⁺, 100%, ⁷⁹Br, ⁸¹Br), 1233.32 [M-PF₆]⁺, 63%, ⁷⁹Br, ⁷⁹Br), 1236.32 [M-PF₆]⁺, 45%, ⁸¹Br, ⁸¹Br). Calcd. for C₆₁H₆₂Br₂IrN₄O₂: 1235.29.

Ir(ppy)₂(DAFone)]PF₆ (**3.47**)

Exp: SG-079



Under argon, *bis*-(μ)-chlorotetrakis(2-phenylpyridinato-C²,N)diiridium(III) (**3.2**) (52 mg, 0.046 mmol) and 4,5-diazafluoren-9-one (**2.9**) (17 mg, 0.093 mmol) and a solution of methanol (10 mL) and dichloromethane (10 mL) were charged into a 50 mL round bottom flask. The mixture was reflux (70 °C, oil bath) for 24 hours under dark, during heating complete dissolution was observed. After cooling to room temperature, NH₄PF₆ (400 mg, 2.451 mmol) was added and stirred for 1 hour at room temperature. The solvent was removed

by evaporation and the residue was purified by column chromatography on silica gel eluting with DCM:MeOH = 100:1 to afford the product as reddish solid (50 mg). The product was further purified by column chromatography on silica gel eluting with PE:Acetone gradually increasing polarity from 9:1 to 1:1 to afford the complex **3.47** (35 mg, 55.2%) as a red solid.

$^1\text{H NMR}$ (400 MHz, acetone- D_6): δ (ppm) 8.26 (2H, dd, $J = 7.6, 1.0$ Hz), 8.11 (2H, d, $J = 8.1$ Hz), 8.00 (2H, d, $J = 5.7$ Hz), 7.88–7.83 (4H, m), 7.76–7.70 (4H, m), 7.05 (2H, dd, $J = 5.9, 1.2$ Hz), 6.92 (2H, td, $J = 9.7, 1.0$ Hz), 6.80 (2H, td, $J = 7.5, 1.2$ Hz), 6.28 (2H, d, $J = 7.6$ Hz).

$^{13}\text{C NMR}$ (100 MHz, acetone- D_6): δ (ppm) 186.42, 167.39, 166.50, 154.99, 152.48, 150.51, 144.41, 143.77, 138.96, 134.41, 131.77, 131.03, 130.15, 124.69, 123.80, 122.94, 119.70.

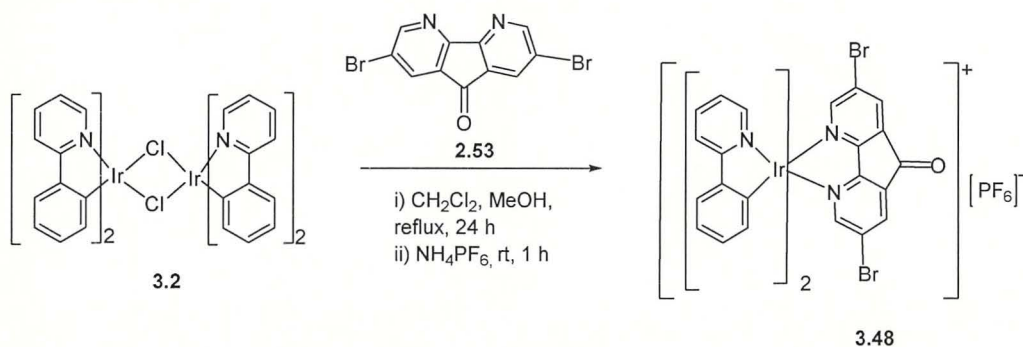
$^{31}\text{P NMR}$ (162 MHz, acetone- D_6): δ (ppm) -144.3 (sept, $^1J_{\text{PF}} = 708$ Hz, PF_6).

$^{19}\text{F NMR}$ (377 MHz, acetone- D_6): δ (ppm) -72.6 (d, $^1J_{\text{PF}} = 708$ Hz, PF_6).

$\text{MS (ESI}^+)$ m/z : 683.16 ($[\text{M}-\text{PF}_6]^+$, 100%). Calcd. for $\text{C}_{33}\text{H}_{22}\text{IrN}_4\text{O}$: 683.14

$\text{Ir}(\text{ppy})_2(m\text{-dbrDAFone})\text{PF}_6$ (3.48)

Exp: SG-090



Under argon, *bis*-(μ)-chlorotetrakis(2-phenylpyridinato- C^2, N)diiridium(III) (**3.2**) (50 mg, 0.046 mmol) and 2,7-dibromo-4,5-diazafluoren-9-one (**2.53**) (32 mg, 0.093 mmol) and a solution of methanol (10 mL) and dichloromethane (10 mL) were charged into a 50 mL round bottom flask. The mixture was reflux (70 °C, oil bath) for 24 hours, during heating complete dissolution was observed. After cooling to room temperature, NH_4PF_6 (400 mg, 2.45 mmol) was added and stirred for 1 hour at room temperature. The solvent was removed by evaporation and the residue was purified by column chromatography on silica gel eluting with DCM:MeOH in the ratio 100:1 to afford the product as dark red solid (67 mg). The product was further purified by column chromatography on silica gel eluting with PE:Acetone in the ratio 9:1 gradually increasing the concentration of acetone to 1:1 to afford the complex **3.48** (31 mg, 33.5%) as a dark red solid.

$^1\text{H NMR}$ (400 MHz, CDCl_3): δ (ppm) 8.24 (2H, d, $J = 1.5$ Hz), 7.92–7.90 (4H, m), 7.79 (2H, td, $J = 7.8, 1.4$ Hz), 7.73 (2H, d, $J = 1.6$ Hz), 7.65 (2H, d, $J = 7.6$ Hz), 7.22 (2H, td, $J = 6.3,$

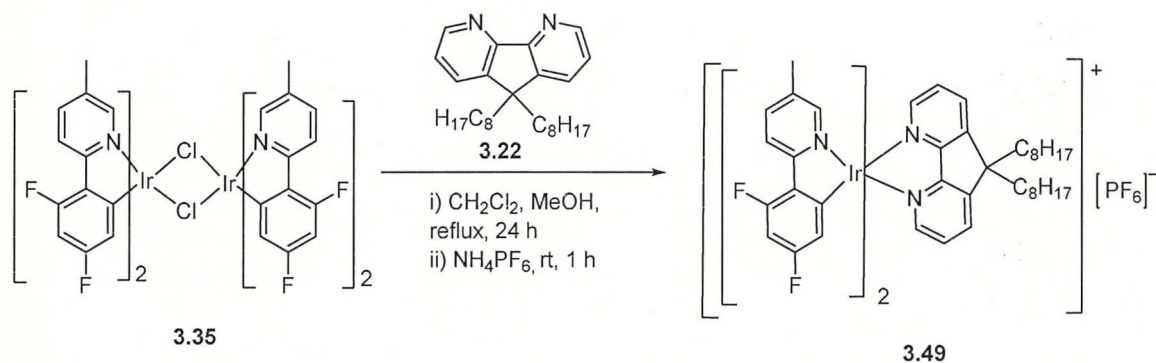
1.4 Hz), 7.03 (2H, td, $J = 7.4, 1.2$ Hz), 6.91 (2H, td, $J = 7.5, 1.4$ Hz), 6.28 (2H, dd, $J = 7.6, 0.9$ Hz).

^{13}C NMR (100 MHz, CDCl_3): δ (ppm) 183.02, 167.06, 163.53, 153.04, 144.09, 141.85, 138.90, 138.44, 132.04, 131.81, 130.77, 126.22, 124.71, 123.66, 119.71.

MS (ESI⁺) m/z : 841.01 ($[\text{M}-\text{PF}_6]^+$, 100%, ^{79}Br , ^{81}Br), 839.01 ($[\text{M}-\text{PF}_6]^+$, 64%, ^{81}Br , ^{81}Br), 843.11 ($[\text{M}-\text{PF}_6]^+$, 25%, ^{79}Br , ^{79}Br). Calcd. for $\text{C}_{33}\text{H}_{20}\text{Br}_2\text{IrN}_4\text{O}$: 840.96.

[Ir(dfmeppy)₂(doDAF)]PF₆ (3.49)

Exp: SG-112



Under argon, *bis*-(μ)-chlorotetrakis{2-(2,4-difluorophenyl)-5-methylpyridinato-C²,N}diiridium(III) (**3.35**) (80 mg, 0.0628 mmol) and 9,9-dioctyl-4,5-diazafluorene (**3.22**) (49 mg, 0.125 mmol) and a solution of methanol (10 mL) and dichloromethane (10 mL) were charged into a 50 mL round bottom flask. The mixture was reflux (70 °C, oil bath) for 24 hours under dark, during heating complete dissolution was observed. After cooling to room temperature, NH₄PF₆ (400 mg, 2.451 mmol) was added and stirred for 1 hour at room temperature. The solvent was removed by evaporation and the residue was purified by column chromatography on silica gel eluting with DCM:MeOH in the ratio 100:1 to afford the complex **3.49** (130 mg, 91.0 %) as a light green solid.

^1H NMR (400 MHz, CDCl_3): δ (ppm) 8.11–8.06 (4H, m), 7.70 (2H, dd, $J = 5.2, 1.0$ Hz), 7.63–7.60 (2H, m), 7.43 (2H, d, $J = 6.0$ Hz), 6.85 (2H, d, $J = 6.0$ Hz), 6.58–6.52 (2H, m), 5.80 (2H, dd, $J = 8.4, 2.0$ Hz), 2.52 (6H, s), 2.12 (4H, p, $J = 8.2$ Hz), 1.25–1.02 (20H, m), 0.83 (6H, t, $J = 7.1$ Hz), 0.77–0.62 (4H, m).

^{13}C NMR (100 MHz, CDCl_3): δ (ppm) (164.54, 164.50, 164.41, 164.35, 163.77, 163.70), (162.22, 162.09, 161.98, 161.98, 161.85), 160.66, (159.74, 159.63), 151.39, 148.45, 148.38, 148.25, 147.49, 145.47, 135.08, 127.99, 124.57, 124.34, (114.54, 114.52, 114.37, 114.34), (99.51, 99.33, 99.19) 59.93, 37.26, 31.77, 29.59, 29.39, 29.08, 24.69, 22.57, 21.56, 14.07.

DEPTQ NMR (100 MHz, CDCl₃): δ (ppm) (164.53, 164.43, 153.76, 163.70), (162.22, 161.97, 161.84), 160.67, 159.63, 151.38, 148.44, 148.37, 148.27(CH), 147.27 (CH), 145.50, 135.07(CH), 127.96 (CH), 124.59 (CH), 124.34 (CH), (114.52, 114.34) (CH), (99.60, 99.34, 99.07) (CH). 59.93, 37.23, 31.77, 29.59, 29.40, 29.08, 24.70, 22.58, 21.57 (CH₃), 14.07 (CH₃).

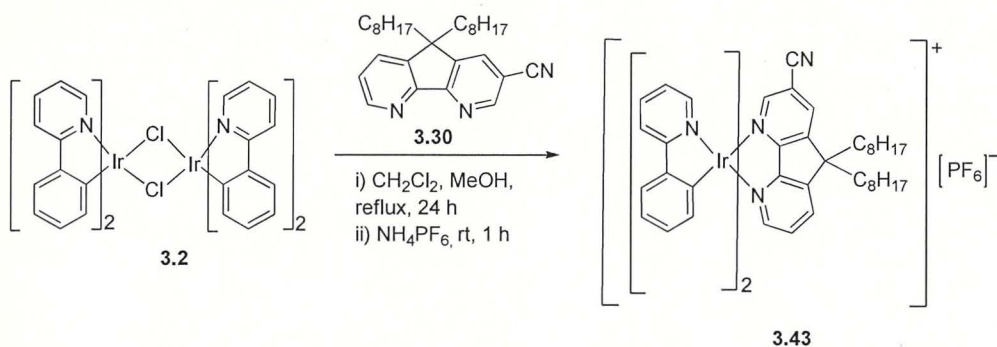
³¹P NMR (162 MHz, CDCl₃): δ (ppm) -144.4 (sept, ¹J_{PF} = 713 Hz, PF₆).

¹⁹F NMR (377 MHz, CDCl₃): δ (ppm) -73.2 (d, ¹J_{PF} = 714 Hz, PF₆), -106.1 (s, ArF), -109.0 (s, ArF).

MS (ESI⁺) *m/z* : 993.27 ([M-PF₆]⁺, 100%). Calcd. for C₅₀H₅₆F₂IrN₄: 993.41.

Ir(ppy)₂(*m*-endoDAF)]PF₆ (**3.43**)

Exp: SG-134



Under argon, *bis*-(μ)-chlorotetrakis(2-phenylpyridinato-C²,N)diiridium(III) (**3.2**) (51 mg, 0.046 mmol) and 2-dicyano-9,9-dioctyl-4,5-diazafluorene **3.30** (39 mg, 0.093 mmol) and a solution of methanol (10 mL) and dichloromethane (10 mL) were charged into a 50 mL round bottom flask. The mixture was reflux (70 °C, oil bath) for 24 hours under dark, during heating complete dissolution was observed. After cooling to room temperature, NH₄PF₆ (400 mg, 2.45 mmol) was added and stirred for 1 hour at room temperature. The solvent was removed by evaporation and the residue was purified by column chromatography on silica gel eluting with DCM:MeOH = 100:1 to afford the complex **3.43** (80 mg, 62%) as a red solid.

¹H NMR (400 MHz, CDCl₃): δ (ppm) 8.15–8.12 (2H, m), 7.94–7.92 (2H, td, *J* = 8.2, 1.9 Hz), 7.88 (1H, d, *J* = 1.2 Hz), 7.80–7.73 (4H, m), 7.70–7.63 (4H, m), 7.10–7.03 (4H, m), 6.98–6.91 (2H, m), 6.39–6.33 (2H, dd, *J* = 7.7, 0.6 Hz), 2.17–2.06 (4H, m), 1.24–1.06 (18H, m), 0.92–0.87 (2H, m), 0.86 (6H, t, *J* = 6.7 Hz), 0.72–0.65 (4H, m).

¹³C NMR (100 MHz, CDCl₃): δ (ppm) 167.68, 167.48, 164.11, 158.49, 150.76, 149.49, 149.24, 148.88, 147.33, 145.13, 143.79, 143.73, 143.63, 143.02, 138.59, 138.50, 137.22, 135.17, 132.10, 131.85, 130.83, 130.69, 129.54, 124.67, 124.51, 123.65, 123.63, 123.20,

119.64, 119.58, 115.33, 112.45, 60.01, (36.84, 36.73), 31.71, 29.54, 29.29, 29.09, (24.91, 24.78), 22.59, 14.08.

DEPTQ NMR (100 MHz, CDCl₃): δ (ppm) 167.68, 167.48, 164.11, 158.49, 150.77 (CH), 149.50 (CH), 148.88 (CH), 147.33, 145.13, 143.79, 143.73, 143.63, 143.02, 138.59 (CH), 138.50 (CH), 137.22 (CH), 135.17 (CH), 132.10 (CH), 131.85 (CH), 130.83 (CH), 130.69 (CH), 129.54 (CH), 124.67 (CH), 124.52 (CH), 123.66 (CH), 123.64 (CH), 123.39, 123.20 (CH), 119.64 (CH), 119.58 (CH), 115.33, 112.45, 60.01, (36.83, 36.73), 31.72, 29.55, 29.29, 29.09, (24.91, 24.78), 22.59, 14.08.

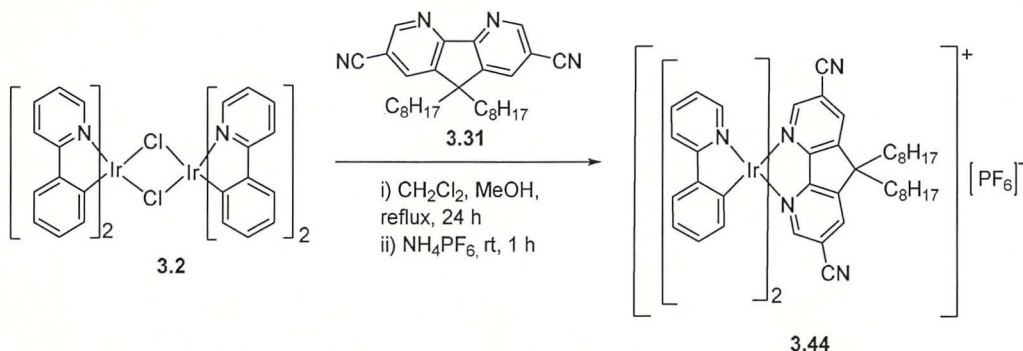
³¹P NMR (162 MHz, CDCl₃): δ (ppm) -144.6 (sept, ¹J_{PF} = 713 Hz, PF₆).

¹⁹F NMR (377 MHz, CDCl₃): δ (ppm) -73.2 (d, ¹J_{PF} = 714 Hz, PF₆), -106.1 (s, ArF), -109.0 (s, ArF).

MS (ESI⁺) *m/z*: 918.41 ([M-PF₆]⁺, 100%). Calcd. for C₅₀H₅₅IrN₅: 918.41.

Ir(ppy)₂(*m*-dcndoDAF)]PF₆ (3.44)

Ex. SG 127



Under argon, *bis*-(μ)-chlorotetrakis(2-phenylpyridinato-C²,N)diiridium(III) **3.2** (52 mg, 0.046 mmol) and 2,7-dicyano-9,9-dioctyl-4,5-diazafluorene (**3.31**) (42 mg, 0.093 mmol) and a solution of methanol (10 mL) and dichloromethane (10 mL) were charged into a 50 mL round bottom flask. The mixture was reflux (70 °C, oil bath) for 24 hours under dark, during heating complete dissolution was observed. After cooling to room temperature, NH₄PF₆ (400 mg, 2.45 mmol) was added and stirred for 1 hour at room temperature. The solvent was removed by evaporation and the residue was purified by column chromatography on silica gel eluting with DCM:MeOH = 100:1 to afford the product (100 mg, 97%) as a brown solid. The product was further purified by column chromatography on silica gel eluting with PE:EA = 8:2 to afford the complex **3.44** (80 mg, 77%) as a brown solid.

¹H NMR (400 MHz, CDCl₃): δ (ppm) 8.25 (2H, s), 7.93 (4H, d, *J* = 8.1 Hz), 7.82–7.76 (2H, m), 7.73 (2H, d, *J* = 5.6 Hz), 7.68 (2H, d, *J* = 7.4 Hz), 7.14 (2H, t, *J* = 6.5 Hz), 7.08 (2H, t, *J*

= 7.5 Hz), 6.95 (2H, td, $J = 7.6, 0.9$ Hz), 6.32 (2H, d, $J = 7.5$ Hz), 2.12 (4H, t, $J = 8.4$ Hz), 1.38–1.07 (20H, m), 1.03–0.90 (4H, m), 0.85 (6H, t, $J = 7.0$ Hz).

¹³C NMR (100 MHz, CDCl₃): δ (ppm) 167.39, 161.99, 151.64, 150.12, 147.10, 143.82, 142.23, 138.99, 138.33, 132.12, 131.12, 124.89, 124.29, 123.91, 119.86, 115.20, 114.32, 60.51, 36.32, (32.14, 31.94), (29.91, 29.75), 29.52, 29.34, 25.36, (22.91, 22.81), 14.30.

DEPTQ (101 MHz, CDCl₃): δ (ppm) 167.18, 161.78, 151.43 (CH), 149.94 (CH), 146.89, 143.61, 142.03, 138.78 (CH), 138.11 (CH), 131.92(CH), 130.92 (CH), 124.69 (CH), 124.08, (CH) 123.70 (CH), 119.64 (CH), 114.99, 114.12, 60.21, 36.12, 31.73, 29.55, 29.32, 29.13, 25.12, 22.60, 14.09.

References

- 1 R. C. Evans, P. Douglas, and C. J. Winscom, *Coord. Chem. Rev.*, **2006**, *250*, 2093.
- 2 P. T. Chou and Y. Chi, *Chem. Eur. J.*, **2007**, *13*, 380.
- 3 E. Holder, B. M. W. Langeveld, and U. S. Schubert, *Adv. Mater.*, **2005**, *17*, 1109.
- 4 P. Peumans, A. Yakimov, and S. R. Forrest, *J. Appl. Phys.*, **2003**, *93*, 3693.
- 5 A. Hagfeldt, G. Boschloo, L. C. Sun, L. Kloo, and H. Pettersson, *Chem. Rev.*, **2010**, *110*, 6595.
- 6 V. W. W. Yam and K. K. W. Lo, *Chem. Soc. Rev.*, **1999**, *28*, 323.
- 7 Z. Liu, W. He, and Z. Guo, *Chem. Soc. Rev.*, **2013**, *42*, 1568.
- 8 V. Fernandez-Moreira, F. L. Thorp-Greenwood, and M. P. Coogan, *Chem. Commun.*, **2010**, *46*, 186.
- 9 Q. Zhao, C. H. Huang, and F. Y. Li, *Chem. Soc. Rev.*, **2011**, *40*, 2508.
- 10 B. Happ, A. Winter, M. D. Hager, and U. S. Schubert, *Chem. Soc. Rev.*, **2012**, *41*, 2222.
- 11 H. Xiang, J. Cheng, X. Ma, X. Zhou, and J. J. Chruma, *Chem. Soc. Rev.*, **2013**, *42*, 6128.
- 12 C. Ulbricht, B. Beyer, C. Friebe, A. Winter, and U. S. Schubert, *Adv. Mater.*, **2009**, *21*, 4418.
- 13 Y. Kawamura, K. Goushi, J. Brooks, J. J. Brown, H. Sasabe, and C. Adachi, *Appl. Phys. Lett.*, **2005**, *86*, 071104.
- 14 Y. Yersin, *Top. Curr. Chem.*, **2004**, *241*, 1.
- 15 I. Avilov, P. Minoofar, J. Cornil, and L. De Cola *J. Am. Chem. Soc.*, **2007**, *129*, 82478
- 16 Q. Pei and A. J. Heeger, *Nature*, **2007**, *7*, 167.
- 17 J. K. Lee, D. S. Yoo, E. S. Handy, and M. F. Rubner, *Appl. Phys. Lett.*, **1996**, *69*, 1686.
- 18 X. Gong, P. K. Ng, and W. K. Chan, *Adv. Mater.*, **1998**, *10*, 1337.
- 19 C. H. Lyons, E. D. Abbas, J. K. Lee, and M. F. Rubner, *J. Am. Chem. Soc.*, **1998**, *120*, 12100.
- 20 K. A. Rogers, P. Kumar, R. Citak, and K. H. Sandhage, *J. Am. Ceram. Soc.*, **1999**, *82*, 757.
- 21 J. Slinker, D. Bernards, P. L. Houston, H. D. Abrun, S. Bernhard, and G. G. Malliaras, *Chem. Commun.*, **2003**, 2392.
- 22 S. Bernhard, X. Gao, G. G. Malliaras, and H. D. Abruña, *Adv. Mater.*, **2002**, *14*, 433.
- 23 Q. S. Zhang, Q. G. Zhou, Y. X. Cheng, L. X. Wang, D. G. Ma, X. B. Jing, and F. S. Wang, *Adv. Funct. Mater.*, **2006**, *16*, 1203.
- 24 J. D. Slinker, A. A. Gorodetsky, M. S. Lowry, J. Wang, S. Parker, R. Rohl, S. Bernhard, and G. G. Malliaras, *J. Am. Chem. Soc.*, **2004**, *126*, 2763.

-
- 25 T. Hu, L. He, L. Duan, and Y. Quie, *J. Mater. Chem.*, **2012**, *22*, 4206.
- 26 J. D. Slinker, J. Rivnay, J. S. Moskowitz, J. B. Parker, S. Bernhard, H. D. Abruna, and G. G. Malliaras, *J. Mater. Chem.*, **2007**, *17*, 2976.
- 27 M. Felici, P. Contreras-Carballada, J. M. M. Smits, R. J. M. Nolte, R. M. Williams, L. De Cola, and M. C. Feiters, *Molecules*, **2010**, *15*, 2039.
- 28 I. M. Dixon, J-P Collin, J-P Sauvage, L Flamigni, S. Encinas, and F. Barigelletti, *Chem. Soc. Rev.*, **2000**, *29*, 385.
- 29 H. Yersin (Ed.), *Highly Efficient OLEDs with Phosphorescent Materials*, Wiley-VCH, **2008**.
- 30 H. Yersin, *Top. Curr. Chem.*, **2004**, *241*, 1.
- 31 L. Flamigni, A. Barbieri, C. Sabatini, B. Venture, and F. Barigelletti, *Top. Curr. Chem.*, **2007**, *281*, 143.
- 32 S. Lamansky, P. Djurovich, D. Murphy, F. Abdel-Razzaq, R. Kwong, I. Tsyba, M. Bortz, B. Mui, R. Bau, and M. E. Thompson, *Inorg. Chem.*, **2001**, *40*, 1704.
- 33 A.B. Tamayo, B. D. Alleyne, P. I. Djurovich, S. Lamansky, I. Tsyba, N. N. Ho, and M. E. Thompson, *J. Am. Chem. Soc.*, **2003**, *125*, 7377.
- 34 M. C. DeRosa, P. J. Mosher, G. P. A. Yap, K. S. Focsaneanu, R. J. Crutchley, and C. E. B. Evans, *Inorg. Chem.*, **2003**, *42*, 4864.
- 35 S. Q. Huo, J. C. Deaton, M. Rajeswaran, and W. C. Lenhart, *Inorg. Chem.*, **2006**, *45*, 3155.
- 36 V. R. Nikitenko and J. M. Lupton, *J. Appl. Phys.*, **2003**, *93*, 5973.
- 37 H. Yersin and W. Humbs, *Inorg. Chem.*, **1999**, *38*, 5820.
- 38 H. J. Park, J. N. Kim, H. Yoo, K. Wee, S. O. Kang, D. W. Cho, H. J. Park, J. N. Kim, H.-J. Yoo, K.-R. Wee, S. O. Kang, D. W. Cho, and U. C. Yoon, *J. Org. Chem.*, **2013**, *78*, 8054.
- 39 S. Lamansky, P. Djurovich, D. Murphy, F. Abdel-Razzaq, H.-E. Lee, C. Adachi, P. E. Burrows, S. R. Forrest, and M. E. Thompson, *J. Am. Chem. Soc.*, **2001**, *123*, 4304.
- 40 M. C. DeRosa, D. J. Hodgson, G. D. Enright, B. Dawson, C. E. B. Evans, and R. J. Crutchley, *J. Am. Chem. Soc.*, **2004**, *126*, 7619.
- 41 H. Zhen, J. Luo, W. Yang, Q. Chen, L. Ying, Z. Jianhua, H. Wu, and Y. Cao, *J. Mater. Chem.*, **2007**, *17*, 2824.
- 42 K. Dedeian, P. I. Djurovic, F. O. Garces, G. Carlson, and R. J. Watts, *Inorg. Chem.*, **1991**, *30*, 1685.
- 43 F. Nave and A. Crispini, *Eur. J. Inorg. Chem.*, **2000**, 1039.
- 44 F. Nave, A. Crispini, S. Campagna, and S. Serroni, *Inorg. Chem.*, **1999**, *38*, 2250.
- 45 J. D. Slinker, A. A. Gorodetsky, M. S. Lowry, J. Wang, S. Parker, R. Rohl, S. Bernhard, and G. G. Malliaras, *J. Am. Chem. Soc.*, **2004**, *126*, 2763.
- 46 J. D. Slinker, C. Y. Koh, G. G. Malliaras, M. S. Lowry, and S. Bernhard, *Appl. Phys. Lett.*, **2005**, *86*, 173506.
- 47 A. B. Tamayo, S. Garon, T. Sajoto, P. I. Djurovich, I. M. Tsyba, R. Bau, and M. E. Thompson, *Inorg. Chem.*, **2005**, *44*, 8723.
- 48 L. He, L. Duan, J. Qiao, R. J. Wang, P. Wei, L. D. Wang, and Y. Qiu, *Adv. Funct. Mater.*, **2008**, *18*, 2123.
- 49 H. J. Bolink, L. Cappelli, S. Cheylan, E. Coronado, R. D. Costa, N. Lardies, M. K. Nazeeruddin, and E. Orti, *J. Mater. Chem.*, **2007**, *17*, 5032.
- 50 H. J. Bolink, E. Coronado, R. D. Costa, N. Lardies, and E. Orti, *Inorg. Chem.*, **2008**, *47*, 9149.

-
- 51 (a) H.-C. Su, C.-C. Wu, F.-C. Fang, and K.-T. Wong, *Appl. Phys. Lett.*, **2006**, *89*, 261118; (b) H.-C. Su, F.-C. Fang, T.-Y. Hwu, H.-H. Hsieh, H.-F. Chen, G.-H. Lee, S.-M. Peng, K.-T. Wong, and C.-C. Wu, *Adv. Funct. Mater.*, **2007**, *17*, 1019; (c) Q. Zhang, Q. Zhou, Y. Cheng, L. Wang, D. Ma, X. Jing, and F. Wang, *Adv. Funct. Mater.*, **2006**, *16*, 1203.
- 52 (a) H. J. Bolink, E. Coronado, R. D. Costa, E. Ortí, M. Sessolo, S. Graber, K. Doyle, M. Neuberger, C. E. Housecroft, and E. C. Constable, *Adv. Mater.*, **2008**, *20*, 3910. (b) R. D. Costa, E. Ort, H. J. Bolink, S. Graber, C. E. Housecroft, and E. C. Constable, *Adv. Funct. Mater.*, **2010**, *20*, 1511.
- 53 L. Sun, A. Galan, S. Ladouceur, J. D. Slinker, and E. Zysman-Colman, *J. Mater. Chem.*, **2011**, *21*, 18083.
- 54 H. C. Su, F. C. Fang, T. Y. Hwu, H. H. Hsieh, H. F. Chen, G. H. Lee, S. M. Peng, K. T. Wong, and C. C. Wu, *Adv. Funct. Mater.*, **2007**, *17*, 1019.
- 55 X. Zeng, M. Tavasli, I. F. Perepichka, A. S. Batsanov, M. R. Bryce, C.-J. Chiang, C. Rothe, and A. P. Monkman, *Chem. Eur. J.*, **2008**, *14*, 933.
- 56 H.-C. Su, C.-C. Wu, F.-C. Fang, and K.-T. Wong, *Appl. Phys. Lett.*, **2006**, *89*, 261118.
- 57 F.-C. Chen, Y. Yang, and Q. Pei, *Appl. Phys. Lett.*, **2002**, *81*, 4278.
- 58 H. C. Su, Y. H. Lin, C. H. Chang, H. W. Lin, C. C. Wu, F. C. Fang, H. F. Chen, and K. T. Wong, *J. Mater. Chem.*, **2010**, *20*, 5521.
- 59 V. W. W. Yam (Ed.), *WOLEDs and Organic Photovoltaics*, Springer-Verlag, **2010**.
- 60 G. M. Farinola and R. Ragni, *Chem. Soc. Rev.*, **2011**, *40*, 3467.
- 61 Y. Yang and Q. B. Pei, *J. Appl. Phys.*, **1997**, *81*, 3294.
- 62 H. C. Su, H. F. Chen, F. C. Fang, C. C. Liu, C. C. Wu, K. T. Wong, Y. H. Liu, and S. M. Peng, *J. Am. Chem. Soc.*, **2008**, *130*, 3413.
- 63 L. He, J. Qiao, L. Duan, G. F. Dong, D. Q. Zhang, L. D. Wang, and Y. Qiu, *Adv. Funct. Mater.*, **2009**, *19*, 2950.
- 64 L. He, L. Duan, J. Qiao, G. F. Dong, L. D. Wang, and Y. Qiu, *Chem. Mater.*, **2010**, *22*, 3535.
- 65 L. He, J. Qiao, L. Duan, G. F. Dong, D. Q. Zhang, L. D. Wang, and Y. Qiu, *Adv. Funct. Mater.*, **2009**, *19*, 2950.
- 66 L. He, L. Duan, J. Qiao, G. Dong, L. Wang, and Y. Qiu, *Chem. Mater.*, **2010**, *22*, 3535.
- 67 H.-C. Su, H.-F. Chen, Y.-C. Shen, C.-T. Liao and K.-T. Wong, *J. Mater. Chem.*, **2011**, *21*, 9653.
- 68 (a) J. Mlochowski and Z. Szulc, *Polish J. Chem.*, **1983**, *57*, 33; (b) P. Piotrowiak, R. Kobectic, R. Timothy, and S. Tapper *Bull. Polish Acad. Sci., Chemistry*, **1994**, *42*, 445.
- 69 (a) H.-C. Su, H.-F. Chen, C.-C. Wu, and K.-T. Wong, *Chem. Asian J.*, **2008**, *3*, 1922; (b) Q. Wang, M. C.-W. Yuen, G.-L. Lu, C.-L. Ho, G.-J. Zhou, O.-M. Keung, K.-H. Lam, R. Gambari, X.-M. Tao, R. S.-M. Wong, S.-W. Tong, K.-W. Chan, F.-Y. Lau, F. Cheung, G. Y.-M. Cheng, C.-H. Chui, and W.-Y. Wong, *Chem. Med. Chem.*, **2010**, *5*, 559.
- 70 (a) F.-W. Yen, C.-Y. Chiu, I.-F. Lin, C.-M. Teng, and P.-C. Yen, *US Patent US7282586-B1*, **2007**; (b) H. Ohrui, A. Senoo, and T. Kosuge, *US Patent US200816574-A1*, **2008**.
- 71 B. L. Hayes, *Microwaves Synthesis; Chemistry at the Speed of Light*, CEM publishing, **2002**.
- 72 J. H. Ahn, C. Wang, I. F. Perepichka, M. R. Bryce, M. C. Petty, *J. Mater. Chem.*, **2007**, *17*, 2996.
- 73 K. Ono, T. Yanase, M. Ohkita, K. Saito, Y. Matsuhita, S. Naka, K. Okada, and H. Onnagawa, *Chem. Lett.*, **2004**, *33*, 276.
- 74 Z. Liu, F. Wen, and W. Li, *Thin Solid Films*, **2005**, *478*, 265.

-
- 75 (a) S. Sprouse, K. A. King, P. J. Spellane, and R. J. Watts, *J. Am. Chem. Soc.*, **1984**, *106*, 6647; (b) O. Lohse, P. Thevenin, and E. Waldvogel, *Synlett*, **1999**, *1*, 45.
- 76 J. I. Goldsmith, W. R. Hudson, M. S. Lowry, T. H. Anderson, and S. Bernhard, *J. Am. Chem. Soc.*, **2005**, *127*, 7502.
- 77 S.-J. Liu, Q. Zhao, R.-F. Chen, Y. Deng, Q.-L. Fan, F.-Y. Li, L.-H. Wang, C.-H. Huang, and W. Huang, *Chem. Eur. J.*, **2006**, *12*, 4351.
- 78 (a) K. A. King and R. J. Watts, *J. Am. Chem. Soc.*, **1987**, *109*, 1589; (b) F. O. Graces, K. A. King, and R. J. Watts, *Inorg. Chem.*, **1988**, *27*, 3464.
- 79 K. Suzuki, A. Kobayashi, S. Kaneko, K. Takehira, T. Yoshihara, H. Ishida, Y. Shiina, S. Oishic, and S. Tobita, *Phys. Chem. Chem. Phys.*, **2009**, *11*, 9850.
- 80 Y. Wang, W. Perez, G.Y. Zheng, and D. P. Rillema, *Inorg. Chem.*, **1998**, *37*, 2051.
- 81 J. Pommerehne, H. Vestweber, W. Guss, R. F. Mahrt, H. Bässler, M. Porsch, and J. Daub, *Adv. Mater.*, **1995**, *7*, 551.
- 82 M. J. Frisch, G. W. Trucks, H. B. Schlegel, G. E. Scuseria, M. A. Robb, J. R. Cheeseman, G. Scalmani, V. Barone, B. Mennucci, G. A. Petersson, H. Nakatsuji, M. Caricato, X. Li, H. P. Hratchian, A. F. Izmaylov, J. Bloino, G. Zheng, J. L. Sonnenberg, M. Hada, M. Ehara, K. Toyota, R. Fukuda, J. Hasegawa, M. Ishida, T. Nakajima, Y. Honda, O. Kitao, H. Nakai, T. Vreven, J. A. Montgomery, Jr., J. E. Peralta, F. Ogliaro, M. Bearpark, J. J. Heyd, E. Brothers, K. N. Kudin, V. N. Staroverov, R. Kobayashi, J. Normand, K. Raghavachari, A. Rendell, J. C. Burant, S. S. Iyengar, J. Tomasi, M. Cossi, N. Rega, J. M. Millam, M. Klene, J. E. Knox, J. B. Cross, V. Bakken, C. Adamo, J. Jaramillo, R. Gomperts, R. E. Stratmann, O. Yazyev, A. J. Austin, R. Cammi, C. Pomelli, J. W. Ochterski, R. L. Martin, K. Morokuma, V. G. Zakrzewski, G. A. Voth, P. Salvador, J. J. Dannenberg, S. Dapprich, A. D. Daniels, O. Farkas, J. B. Foresman, J. V. Ortiz, J. Cioslowski, and D. J. Fox, Gaussian, Inc., Wallingford CT, **2009**, Gaussian 09, Revision A.02.
- 83 S. Fantacci and F. D. Angelis, *Coord. Chem. Rev.*, **2011**, *255*, 2704.
- 84 K. Świderek and P. Paneth, *J. Phys. Org. Chem.*, **2009**, *22*, 845.
- 85 T. Liu, B. -H. Xia, Q.-C. Zheng, X. Zhou, Q.-J. Pan, and H.-X. Zhang, *J. Comput. Chem.*, **2010**, *31*, 628.
- 86 E. Baranoff, B. F. E. Curchod, F. Monti, F. Steimer, G. Accorsi, I. Tavernelli, U. Rothlisberger, R. Scopelliti, M. Grätzel, and M. K. Nazeeruddin, *Inorg. Chem.*, **2012**, *51*, 799.
- 87 U. Salzner and R. Baer, *J. Chem. Phys.*, **2009**, *131*, 231101.
- 88 D. Jacquemin, E. A. Perpète, I. Ciofini, C. Adamo, R. Valero, Y. Zhao, and D. G. Truhlar, *J. Chem. Theory Comput.*, **2010**, *6*, 2071.
- 89 D. Jacquemin, E. A. Perpète, I. Ciofini, and C. Adamo, *J. Chem. Theory Comput.*, **2010**, *6*, 1532.
- 90 P. Fitton and J. E. McKeon, *J. Chem. Soc. Chem. Commun.*, **1968**, *4*.
- 91 H. Ishida, S. Tobita, Y. Hasegawa, R. Kotaoh, and K. Nozaki, *Coord. Chem. Rev.*, **2010**, *254*, 2449.
- 92 (a) A. T. R. Williams, S. A. Winfield, and J. N. Miller, *Analyst*, **1983**, *108*, 1067; (b) Jobin Yvon Horiba Manual for Measurement: calculation of fluorescence quantum yields from acquired data.
- 93 (a) F. J. Coughlin, M. S. Westrol, K. D. Oyler, N. Byrne, C. Kraml, E. Zysman-Colman, and M. S. Lowry. S. Bernhard, *Inorg. Chem.*, **2008**, *47*, 2039; (b) M. S. Lowry, W. R. Hudson, Jr. R. A. Pascal, and S. Bernhard, *J. Am. Chem. Soc.*, **2004**, *126*, 14129.

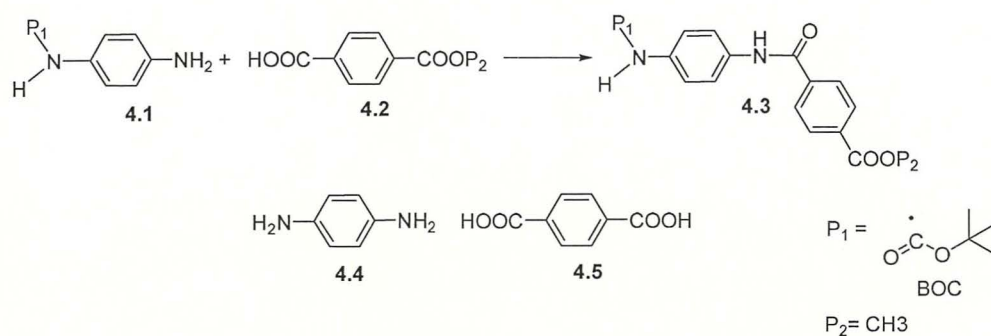
Chapter 4

4,5-Diazafluorene-Based Oligomers

4.1 Introduction

Conjugated material could be polymers and/or well-defined systems such as dendrimers and oligomers. The conjugated oligomers, which are small molecules, can serve as model compound for understanding the properties of conjugated polymers and are found to be attractive candidates for particular applications such as the organic field effect transistor (OFET),¹ organic light emitting diode (OLED),² and organic photovoltaic (OPV)³ devices.^{4,5} One of the important aspect of monodisperse π -conjugated oligomers, unlike polymer system, is to provide a direct correlation between structure and properties. However, synthesis of oligomers is more tedious and requires multiple steps. Nevertheless, they can be purified by the common method of column chromatography and sublimation, which are not possible with polymers.⁶ Another important aspect of oligomers is the ease of structural modification by synthesis compared to polymer counterpart.⁷

In general, oligomer synthesis follows a step-wise chain length increase strategy with well-defined end groups. For example, consider a coupling reaction between the protected amine **4.1** and acid **4.2** to produce amide-linked product **4.3** as a monomer unit; the protecting groups P_1 (amine protecting group, e.g. *tert*-butyloxycarbonyl) and P_2 (acid protecting group, e.g. Methyl ester) can be separately cleaved and the next coupling reaction can be initiated at either end to increase the chain length. Oligomers can also be prepared by random approach; for instance, a direct coupling between diamine **4.4** and diacid **4.5** with varying the stoichiometry of the reaction to favour the oligomers formation.

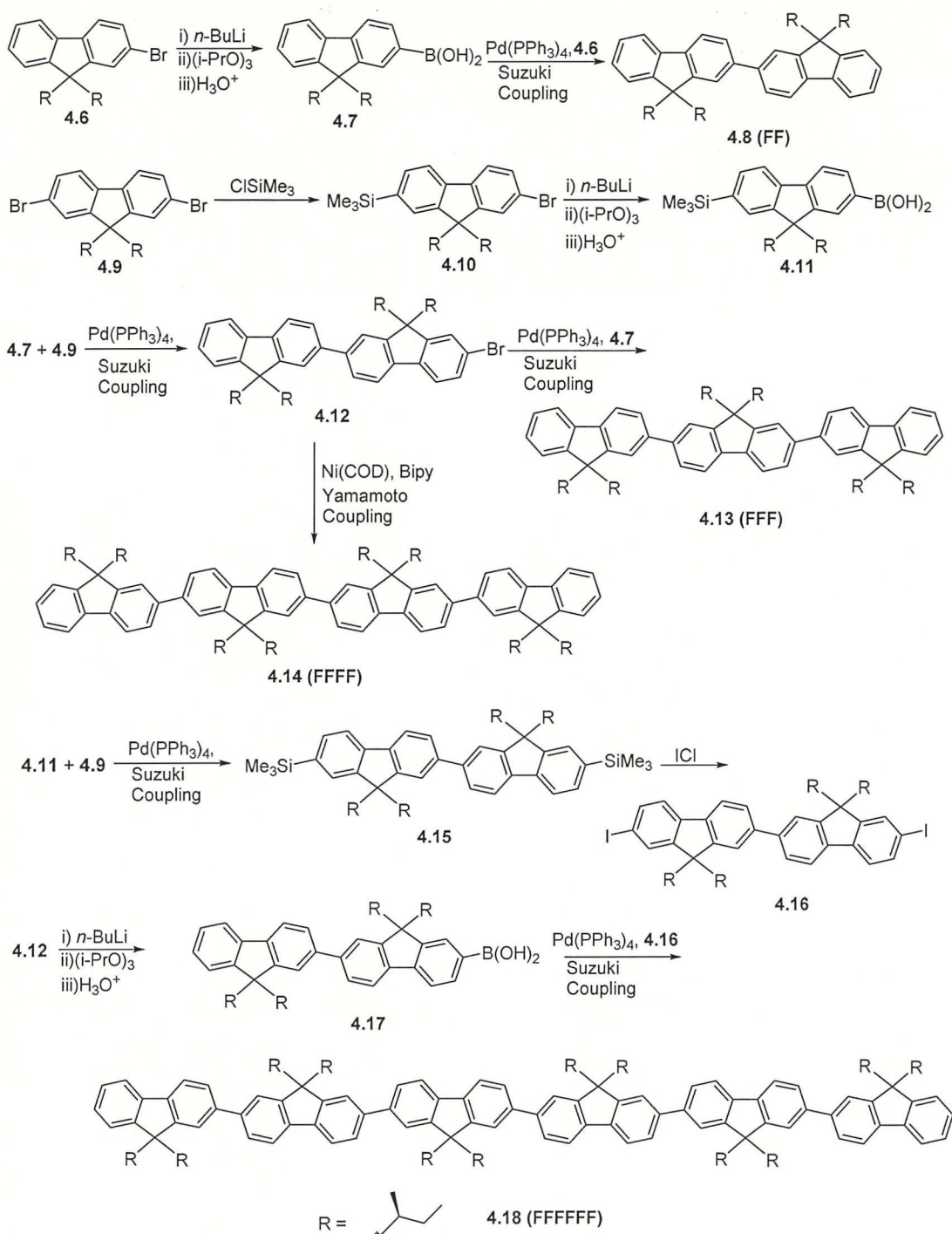


Conjugated oligomers systems are increasingly attracting the attention of materials science researcher for electronic application. The simplest conjugated oligomers in terms of structure are the oligoenes, consisting of alternating π - π bond extending over the whole molecule. Aromatic conjugated oligomers consisting of monomer units such as benzene, pyrrole, thiophene and combination of aromatic and aliphatic unit such as stilbene. An important feature of oligomers research is to establish relationship between chain length and physical properties, which are extrapolated to understand the behaviour of polymer. Oligomers can be polydisperse, but monodisperse oligomers are assumed to provide a more precise structure-property relationship.³⁹ The primary requirement for measurement of physical parameters such as the mobility of charge carriers in photoconductivity and PLQY of excitons in photoluminescence is that the sample should be in a highly pure state; otherwise, the impurities in the sample may lead to incorrect results or misleading interpretation. Oligomers in this regards have an advantage over polymers because they can be purified by zone melting or vacuum sublimation and chromatography techniques. Furthermore, oligomers plays an important role for understanding the structure of polymer, the mechanism of formation of polymer, and also for optimising or developing reaction condition required for polymer synthesis. It may be stated that, the significance of oligomers is not to be overestimated from polymers. Both oligomers and polymers have their own merit as materials for potential applications. In this chapter, synthesis of 4,5-diazafluorene based oligomers and their physical properties together with DFT calculation studies is presented. A brief discussion of fluorene oligomers, which is structurally similar to 4,5-diazafluorene oligomers is also presented.

4.1.1 Oligofluorenes: Synthesis and Properties

Fluorene based oligomers and polymers are studied extensively during the last two decades for their highly efficient, blue-emission, good thermal and electrochemical stability, high charge mobility and easily tuneable properties through chemical modifications and co-polymerisation for device application.^{8,9} Monodisperse oligofluorenes can be synthesised with high purity and demonstrated good performance with high stability as blue emitter in OLEDs.^{10,11,12} Oligofluorenes are constructed from the fluorene monomer usually via Pd(0) catalysed Suzuki coupling between aryl boronic acids/esters and aryl halides, nickel-promoted Yamamoto coupling between aryl halides, and ferric chloride-catalysed Scholl reaction between aryl halides. Chen *et al.* in 2002 have reported the synthesis of the first series of chiral monodisperse oligofluorenes.¹³ A common issue associated with the synthesis of long chain length oligomers is following: as the chain length grows with the longer oligomers synthesis, purification becomes more and more difficult due to the presence of similar

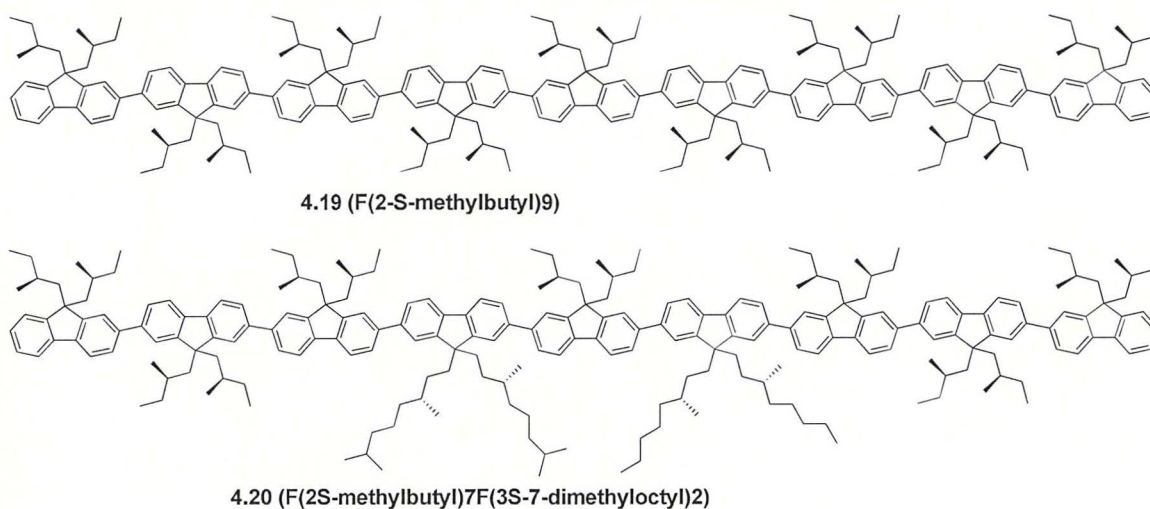
properties different chain length impurities, which are difficult to separate by conventional column chromatography. However, oligofluorenes with up to 16 fluorene units have been successfully synthesised by Chen's group following convergent/divergent approach using Suzuki and Yamamoto coupling reactions.¹³ As an example of fluorene oligomer synthesis, construction of dimer **4.8** (FF), trimer **4.13** (FFF), tetramer **4.14** (FFFF), and hexamer **4.18** (FFFFFF) of fluorene with 2-S-ethylbutyl group at 9-position is depicted in Scheme 4.1. In the reported procedure, halogen substituted fluorene derivative **4.6** was subjected to basic butyl lithium reaction at low temperature followed by treatment with isopropyl boronates and then by hydrolysis in acidic medium giving boronic acid substituted fluorene **4.7** in good yields (80%). Boronic acid **4.7** and halogen substituted fluorene **4.6** were coupled (C-C bond formation) in presence of Palladium (0) catalyst, Pd(PPh₃)₄, to yield the shortest oligomer **4.8** dimer (FF) with excellent yields (92%). Silyl group protection and deprotection for halogen-substituted fluorene were employed to prepare the higher monodisperse oligomers such as **4.18** hexamer (FFFFFF).



Scheme 4.1 Synthesis of monodisperse oligofluorenes.¹³

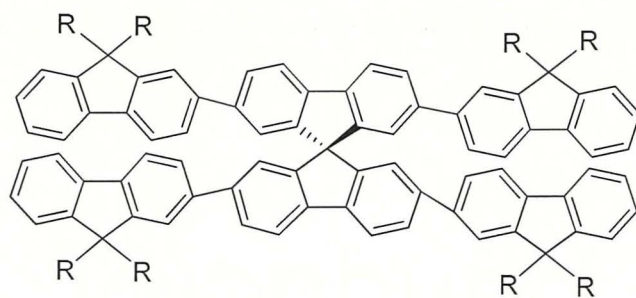
It was demonstrated that the chain length of oligofluorenes plays an important role in solid morphology. For instance, phase transition temperature found to increase with increase in chain length. Furthermore, dimer through tetramer are amorphous and the higher chain length oligomers forms cholesteric mesomorphism with varying degree of crystallisation. Chen *et al.* also demonstrated that replacement of bulky substituent at 9-position of fluorene oligomers changes the morphology of the thin film. Thus, replacement of two sets of 2-S-methylbutyl

group in nonamer **4.19** with the bulkier 3S-7-dimethyloctyl group to form nonamer **4.20** results in cholesteric mesomorphism without crystallisation on heating as well as on cooling. According to the authors, this finding can be explained from the simulation studies, which reveal that insertion of bulkier 3S-7-dimethyloctyl group avoids the formation of braided chiral assemblies, which in turn, allowed the molecules to organise into cholesteric stack.¹³

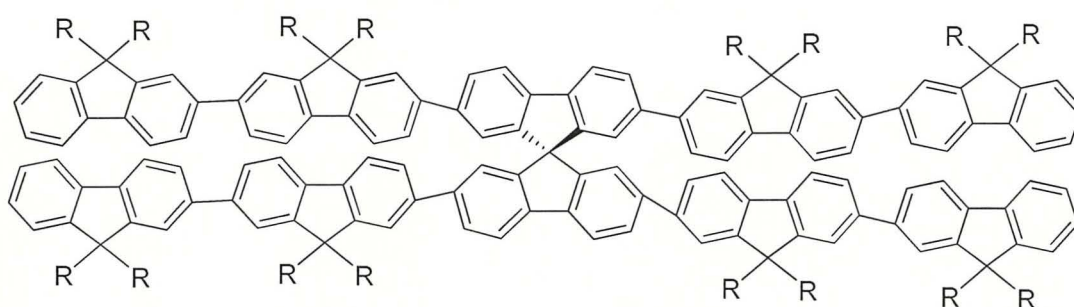


Ease of substitution at C-9 position of fluorene allows controlling the solubility and molecular packing behaviour of conjugated oligofluorenes. In terms of morphological properties, fluorene based conjugated oligomers show high thermal stability (decomposition temperature determined by thermal gravimetric analysis is over 400 °C) and high solubility (in case of terfluorene, the solubility is 800 g L⁻¹ in toluene).¹⁴ Fluorene-based oligomers are either intrinsically highly crystalline or glass-forming materials (spiro-configured pentafluorene showed glass transition temperature T_g of 330 °C with no crystallisation or melting temperature up to 550 °C).¹⁵ Crystalline conjugated oligomers are desired materials for special application such as OFET. Some of fluorene based oligomers [e.g. **4.35 (FTTF)**] forms highly polycrystalline films upon vacuum deposition onto substrate and have been successfully employed as active component in OFET.^{16,31}

A series of spiro-linked oligofluorenes (such as spiro-linked terfluorene **4.21** and pentafluorene **4.22**) have been reported to exhibit blue emission with high photoluminescence quantum efficiency of upto 50% in neat films.^{17,18} They have been synthesised in good yields following similar Suzuki and Yamamoto coupling reactions described above for oligofluorenes.



Spirolinked terfluorene **4.21a** R = C₈H₁₇,
4.21b R = C₃H₇



Spirolinked pentafluorene **4.22a** R = C₈H₁₇,
4.22b R = C₃H₇

Phase transition temperatures of some of the spiro-linked oligofluorenes determined by differential scanning calorimetry (DSC) are shown in Fig 4.1. The spiro-linked terfluorenes **4.21a** and **4.21b**, underwent glass transition (T_g) at 60 and 179 °C, respectively, and upon heating beyond T_g they were crystallised at T_k of 84 and 243 °C (T_k is crystallisation temperature), respectively. On further heating, these crystalline materials showed melting points, T_m , at 194 and 348 °C, respectively. In contrast to these oligomers, spiro-linked pentafluorenes, **4.22a** and **4.22b**, are morphologically stable and no T_k and T_m were detected beyond T_g , which was observed at 56 and 202 °C, respectively. It was noted that shorter alkyl substituted spiro-linked oligofluorenes have elevated T_g .

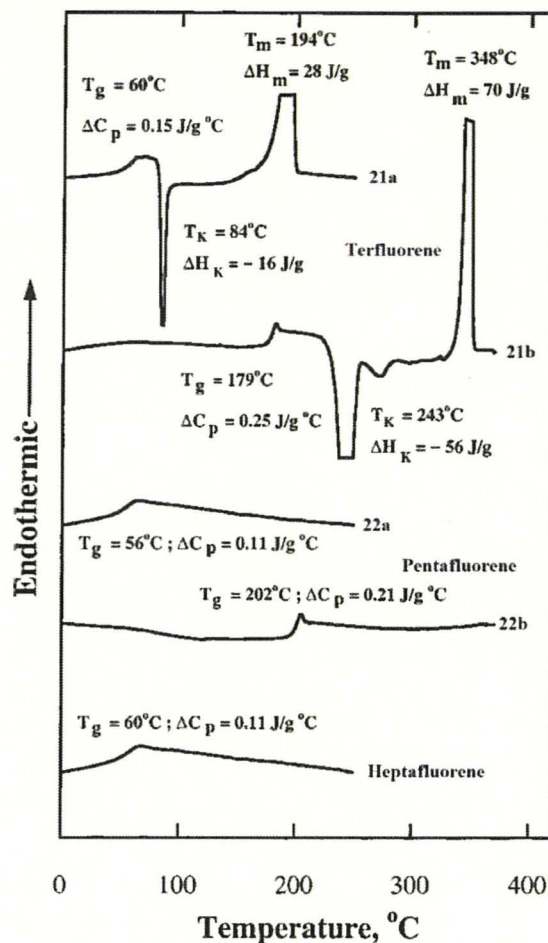


Fig. 4.1 Differential scanning calorimetric (DSC) curves of spiro-linked terfluorenes (4.21a,b), pentafluorenes (4.22a,b) and heptafluorene; heating scan rates are 20 °C/min.¹⁸

The morphology of spin-coated films, in general, indicates the feasibility for device application. Crystallisation tends to hinder charge transport and causes poor contact, therefore, glass film with elevated T_g and amorphous nature are the desired characteristics for practical device applications. The spin-coated films of all the spiro-linked oligofluorenes exhibited amorphous character, which was determined by electron diffraction method. Furthermore, pristine films of the spiro-oligofluorenes exhibited almost identical spectroscopy to that of dilute solutions, and upon prolonged heating of the neat films almost did not changes the emissive properties or the quantum yields.¹⁸ Working extensively on oligofluorenes, Chen's group in reported a series of homologous, glass forming, nematic oligofluorenes synthesised by similar convergent/divergent approach.¹⁰ They reported T_g close to 150 °C and a T_c beyond 375 °C for their novel oligofluorenes. To determine the spectral stabilities of synthesised oligofluorenes, the ono-domain glassy nematic films of oligofluorenes obtained by spin-coating technique were thermally annealed at 10 to 20 °C

above their respective T_g for 15–30 min. As an example, the absorption and emission spectra of pristine film of nonafluorene **4.23** and the effect of heating on their UV and PL spectra are shown in Fig. 4.2. Prolonged heating the film of nonafluorene above the glass transition temperature (at 125 °C up to 96 hours) did not result in crystallisation or any observable changes in the emission colour. Thus the heating did not affect the emission spectral stability. However, a loss in emission intensity was observed, which was attributed to the diminished absorption of photoexcitation and some nonradiative decay paths.

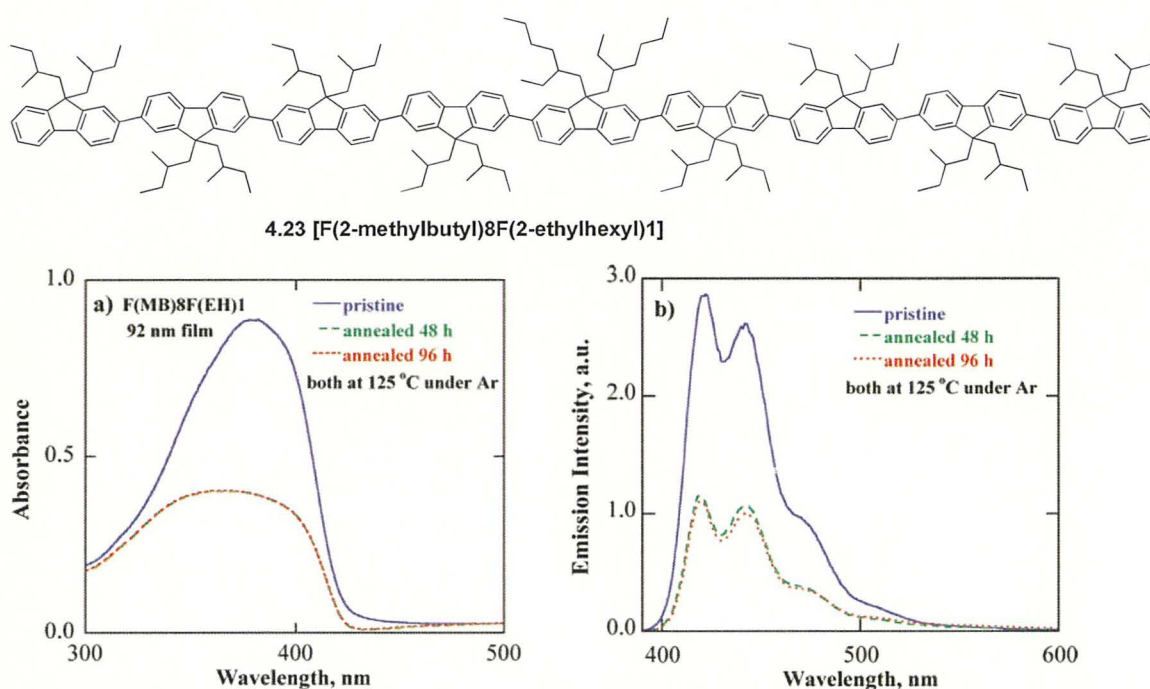
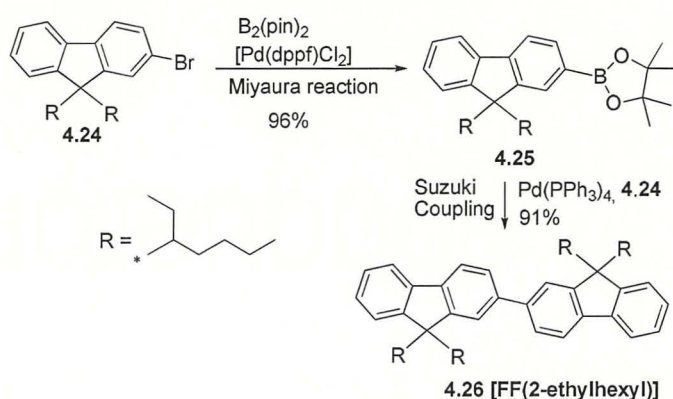


Fig. 4.2 Effect of prolonged heating on UV and PL spectra of pristine film of nonamer **4.23**. (The samples was heated at 125 °C, which is 10 °C above glass transition temperature T_g).¹⁰

Earlier, Andraud *et al.* reported synthesis of monodisperse fluorene oligomers ($n = 1$ to 6) with hexyl substituent at 9-position with a stepwise increase in chain length using Suzuki and Yamamoto couplings. They demonstrated that optical properties of oligofluorenes showed dependence on the chain length.¹⁹ Weeger *et al.* reported similar oligofluorenes up to heptamer with an improved method of syntheses. They used Pd-catalysed transformation of bromine-substituted fluorene to boronic esters of fluorene (known as Miyaura reaction) under a mild condition for the first time, thereby, avoiding the conventional use of strongly basic organo lithium reagent to synthesis fluorene boronic acids.²³ For instance, the reported synthesis of dimer **4.26** [FF(2-ethylhexyl)] utilizing Miyaura reaction (**4.24** → **4.25**) followed by Suzuki coupling (**4.25** → **4.26**) is shown in Scheme 4.2.



Scheme 4.2 Synthesis of fluorene dimer **4.26** [FF(2-ethylhexyl)] using Miyaura and Suzuki couplings.²³

Furthermore, they found that, the pure oligofluorenes as solid films do not show the undesired green-band emission (also known as 'keto defect'), which is a common characteristic of the polyfluorenes (more detailed discussion on keto defect is presented in Chapter 5). This may be attributed to the lower energy of HOMO of oligofluorenes (upto 6-8 units) compared to polyfluorenes. The oligofluorenes from tetramer to heptamer exhibit a liquid-crystalline phase with a well-defined isotropisation temperature, which allowed extrapolation to an expected isotropization temperature of the polymer of around 475 °C. In addition, the oligomers showed an increase in the glass transition temperature with the increase in chain length; this allowed extrapolation to a hypothetical glass transition temperature of polymer at around 64 °C.²³

Fluorene oligomers represent an unique and emerging class of compound for application in optoelectronic devices. In addition, their photophysical and electronic properties provide important information for understanding the behaviour of polyfluorene analogues.²⁰ Successful synthesis and isolation of oligofluorenes of different lengths has enabled the determination of effective conjugation length by various research groups to be between 11 and 14 repeating units for polyfluorenes.^{21,22,23} Estimation of conjugation length from linear dependence of $1/\lambda_{\text{max}}$ vs. $1/n$ (n is the monomer unit) for oligomers was reported by Weeger *et al.*²³ as 14 repeating unit for poly[9,9-di-(2-ethylhexyl)fluorenyl-2,7-diyl] and by Miller *et al.* for Poly(9,9-dihexylfluorenes) as 11.8 (Fig.4.3).²¹

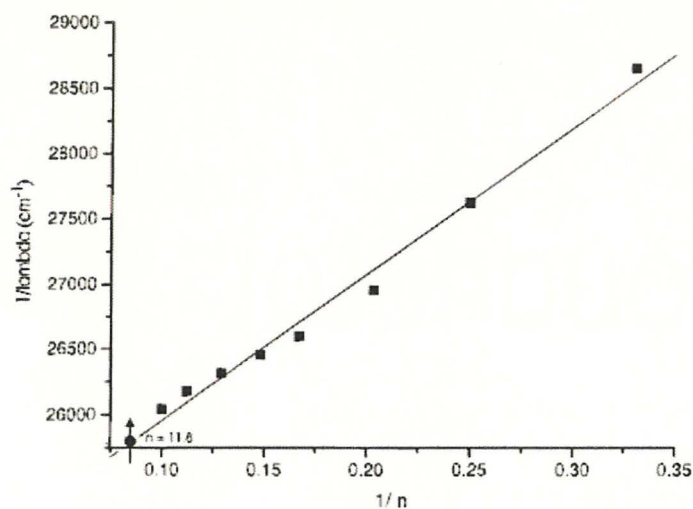
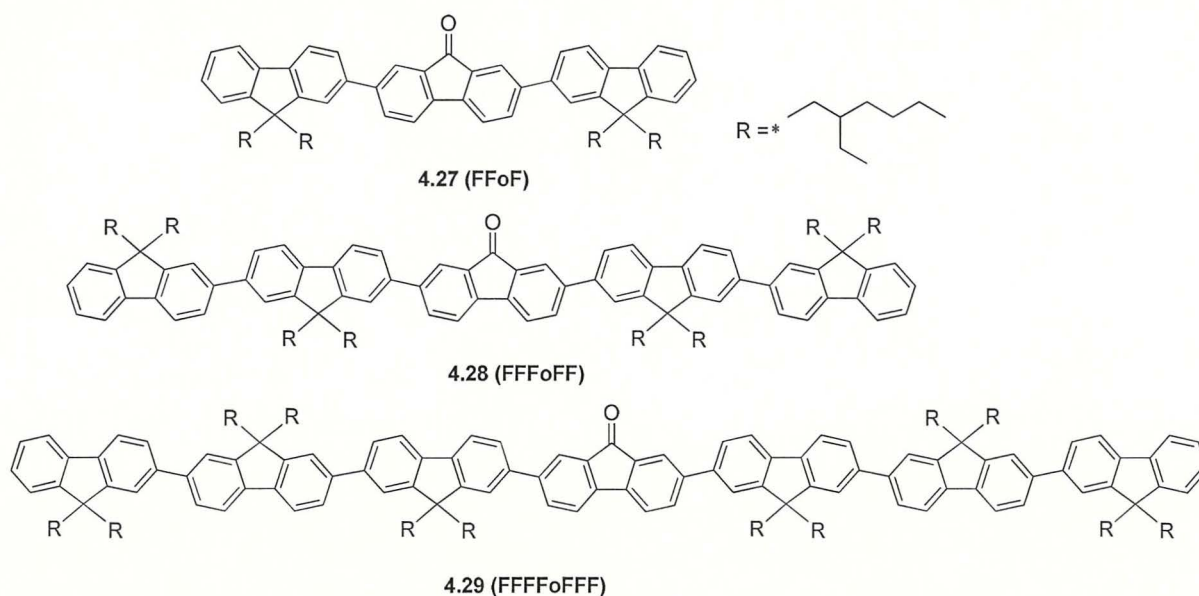


Fig. 4.3 Plot of $1/\lambda_{\max}$ vs. $1/n$ for oligo(9,9-dihexylfluorenes) in tetrahydrofuran, n is number of fluorene units.²¹

Oligofluorenes with one fluorenone unit in the centre such as **4.27 (FFoF)** and **4.28 (FFFoFF)** serve as model compound to understand the origin of keto-defect (low-energy emission band, 2.3 eV) in the photoluminescence and electroluminescence spectra of some polyfluorene.^{24,25,26} Cyclic voltammetry studies of the oligofluorenes with fluorenone units at centre (**4.27** trimer, **4.28** pentamer, **4.29** heptamer, shown in Fig 4.4) shows that HOMO decreases with extension of chain length from 5.73 eV for trimer **4.27 (FFoF)** to 5.52 eV for heptamer **4.29 (FFFFoFFF)**, whereas LUMO remains unchanged at around 3.13 eV. This observation implies that LUMO is strongly confined to fluorenone unit. This trend is consistent with theoretical calculation results.



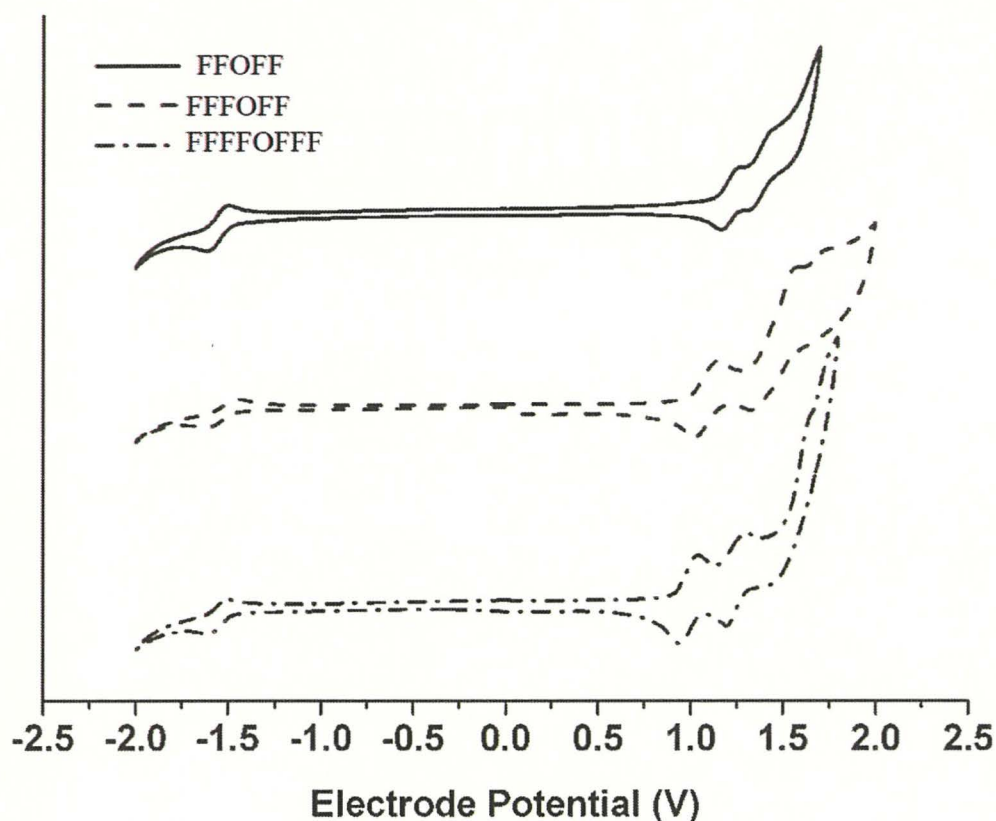


Fig 4.4 Cyclic voltammetry curves of oligo(fluorenes-*co*-fluorenone) **4.27**, **4.28**, **4.29**.²⁴

Furthermore, the position of the low-energy absorption and the green emission of oligofluorenes having central fluorenone unit is independent of the chain length of oligomers. This verifies that the $n-\pi^*$ state and CT $\pi-\pi^*$ states are localized on the fluorenone units. Oligofluorenes with fluorenone units exhibit strong green emission with monoexponential decay behaviour. This monoexponential decay remains independent on the concentrations, which rules out the possibility that the green emission band originates from aggregates.²⁴ The long wavelength emission from such oligomers is originated from excimer formation associated with the fluorenone unit, as it was independently established by different group.^{24,25,26} As an illustration, in support of this assertion, the effect of solution concentrations on the fluorescence intensity of trimer **4.30** (Fig 4.5) indicates that the intensity of emission at longer wavelength (552 nm) decreases relatively to shorter wavelength (400 nm) with a decreasing the solution concentration.²⁵

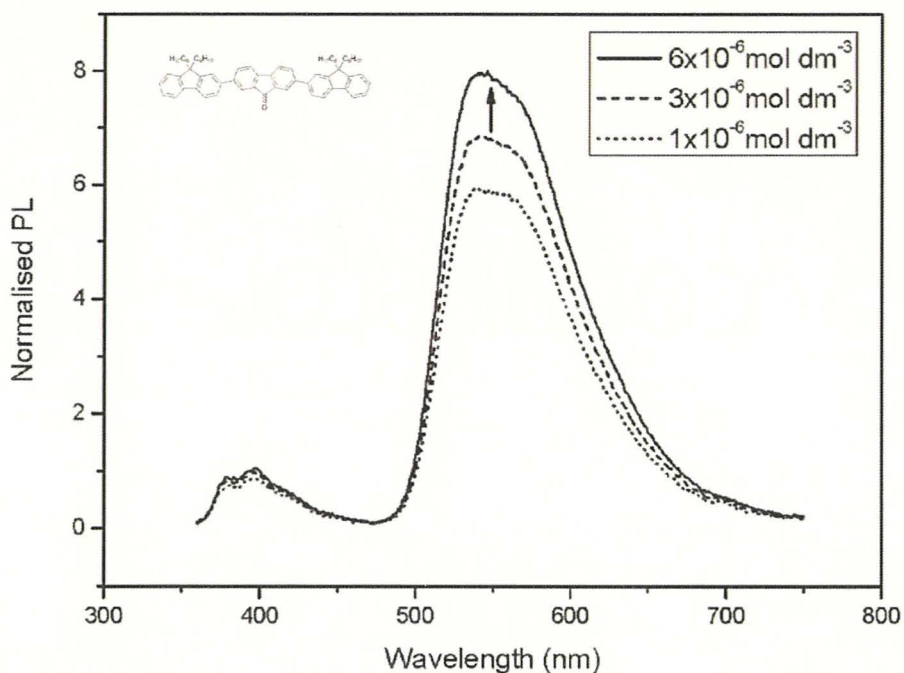
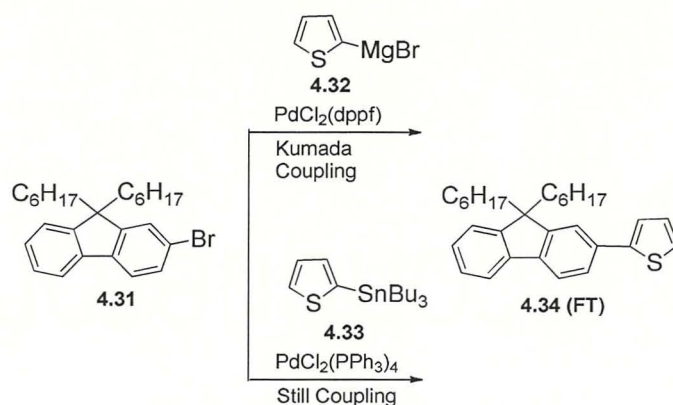


Fig. 4.5 Normalised PL emission of **4.30** (structure as insert) at different concentration under excitation at 350 nm.²⁵

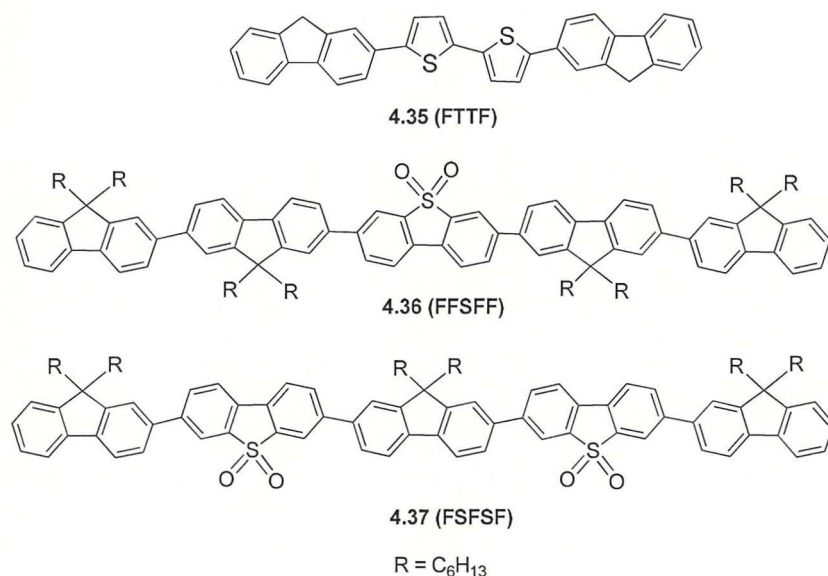
4.1.2 Fluorene-based co-oligomers: Synthesis and Properties

In general, fluorene co-oligomers are synthesised by Pd catalysed C–C bond forming reactions.⁹ Pd catalysed Suzuki reaction is generally used,²³ but is not always feasible when sensitive functional groups are involved. Pd catalysed Kumada coupling reaction between aryl Grignard reagent (such as **4.32**) and halofluorenes (such as **4.31**) provides a good alternative to Pd catalysed Suzuki reaction (as an example is illustrated in Scheme 4.3).²⁷ Stille coupling²⁸ is preferably used for incorporation of thiophene unit because of easy access to organotin-thiophene (such as **4.33**) which react readily with halofluorenes (as an example is shown in Scheme 4.3).²⁹ In addition, colour tuneable electroluminescent materials based on oligo(fluorene-thiophene) which are synthesised by Suzuki type coupling have been reported.³⁰



Scheme 4.3 Example of Kumada and Still coupling between fluorene and thiophene units.^{27,28}

Fluorene-based co-oligomers have been investigated for various applications e.g. OFET, lasers and OLED. For instance, oligothiophene consider have been consider as attractive materials for OFET but suffer from stability against oxidation. In contrast, fluorene-thiophene co-oligomers [such as **4.35 (FTTF)**] showed better stability against oxidation.³¹ Similarly, incorporation of dibenzothiophene-*S,S*-dioxide units into the conjugated oligomers of fluorene [such as **4.36 (FFSFF)**, **4.37 (FSFSF)**] were reported as stable high-efficient blue emitters with an improved electron affinity.³²



4.2 Results and Discussion

Consider the energy level diagrams of 9,9-diethylfluorene (**F**), dibenzothiophene-*S,S*-dioxide (**S**) and 9,9-diethyl-4,5-diazafluorene (**D**) obtained by the DFT calculation at B3LYP/6-31G(d) level of theory as shown in Fig. 4.6. The energy gaps (E_g , 4.96, 4.86, 4.88 eV) are similar within 0.1 eV differences, however, there is substantial difference in the individual LUMO

(-0.77, -1.81, -1.35 eV) and HOMO (-5.73, -6.66, -6.23) energy levels, which are of about 1 eV among **F**, **S** and **D** units. Therefore, incorporation of **S** and **F** units into **D** causes perturbation in HOMO and LUMO energy level which in turn may lead to interesting electronic properties such as improve electron transport ability. To study the effect of incorporation of **S** and **F** units into the backbone of **D** units a series of their co-oligomer has been synthesised and studied their photo-physical properties is discussed in the next section. Topologically similar to fluorene, homologous rod type 4, 5-diazafluorene based oligomers represent a novel class of electron deficient conjugated organic material, which may be useful for optoelectronic application and to our knowledge; they have not been reported elsewhere. In the following, synthesis of new monodisperse oligomers of **D** upto pentamer along with co-oligomers with **S** and **F** units are reported. Their photophysical properties have been studied together with DFT calculation. The synthesised oligomers have been fully characterised by $^1\text{H-NMR}$, $^{13}\text{C-NMR}$ and MS spectroscopy prior to study of their photophysical and electrochemical properties.

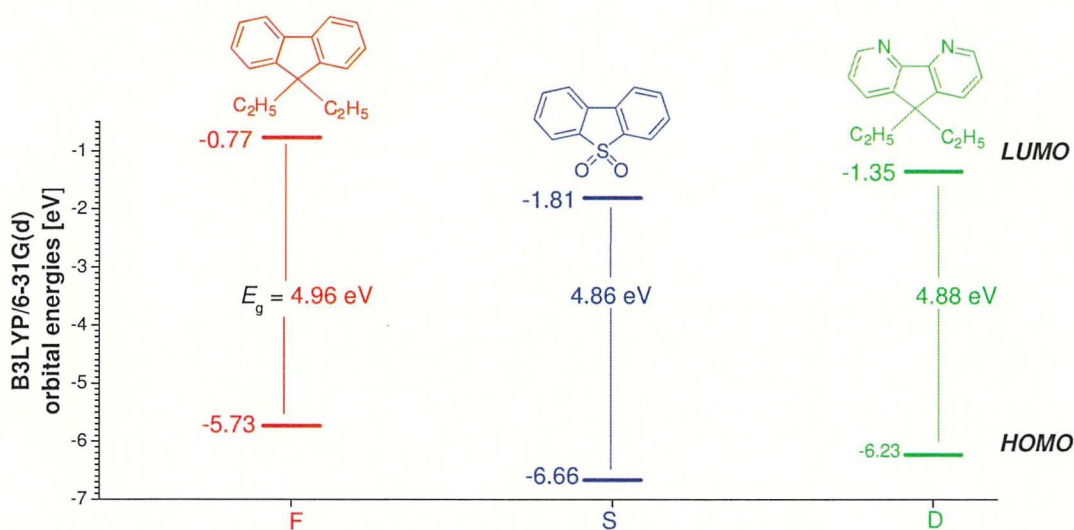
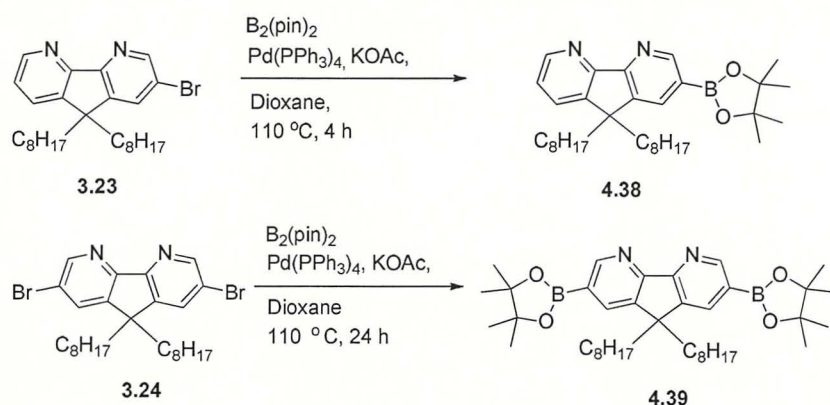


Fig. 4.6 DFT/B3LYP/6-31G(d) energy levels for 9,9-diethylfluorene (**F**), dibenzothiophene-*S,S*-dioxide (**S**) and 9,9-diethyl-4,5-diazafluorene (**D**).

4.2.1 Synthesis of 4,5-Diazafluorene-based Oligomers

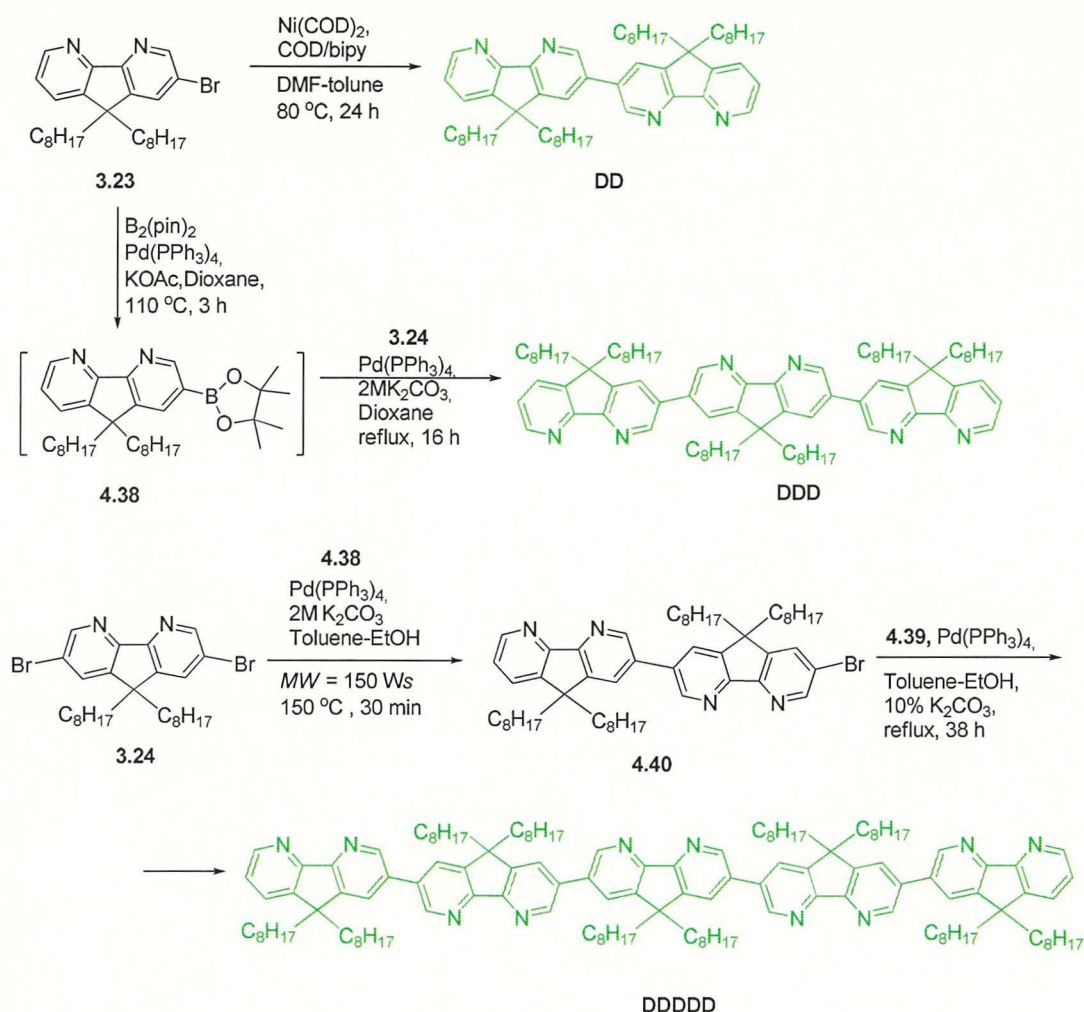
For the synthesis of homologous 4,5-diazafluorene oligomers, borolane-DAF **4.38** and diborolane-DAF **4.39** have been synthesised as monomer units shown in Scheme 4.4. Borolane-DAF **4.38** and diborolane-DAF **4.39** was synthesised by refluxing monobromo-DAF **3.23** and dibromo-DAF **3.24** in separate reactions with bis(pinacolato)diboron

[B₂(pin)₂] in dry dioxane with potassium acetate and tetrakis(triphenylphosphine)palladium [Pd(PPh₃)₄] under inert atmosphere (Scheme 4.4). The monobromo-DAF **3.23** and dibromo-DAF **3.24** were synthesised similar to literature with modified procedure described in Chapter 3.³³ Synthesised borolanes **4.38** and **4.39** was found to be multiple spots on TLC and could only be partially purified by column chromatography on silica gel with moderate yields (ca. 30%).



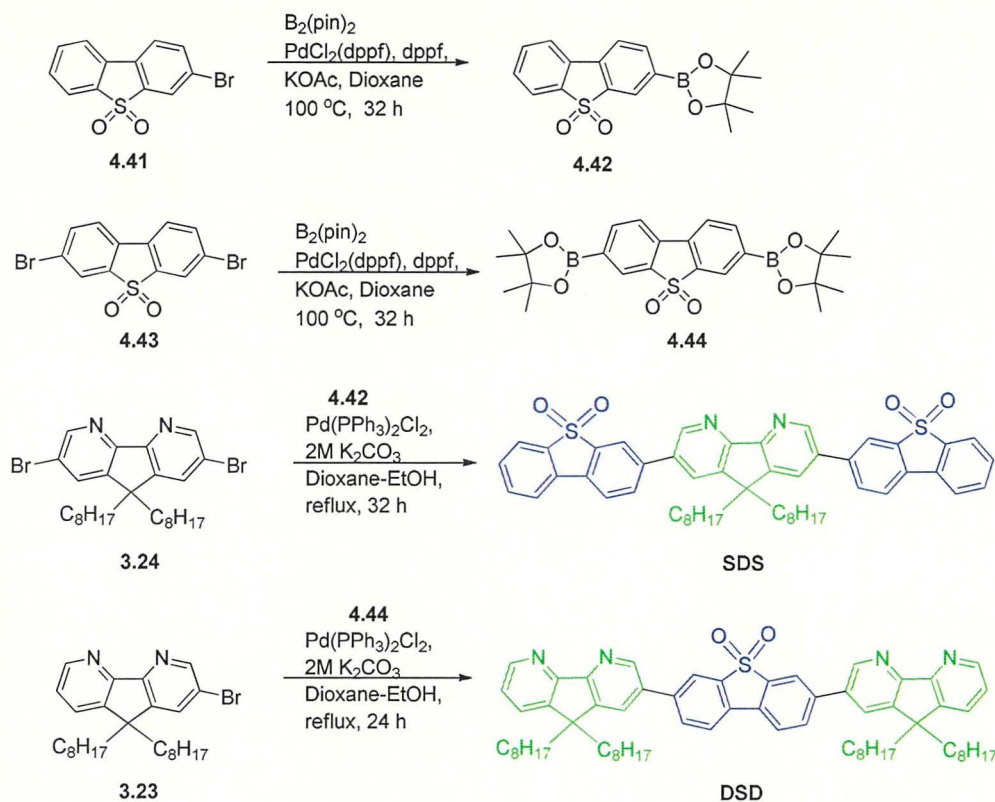
Scheme 4.4 Synthesis of borolane derivatives of 4,5-diazafluorene.

The homologous 4,5-diazafluorene based oligomers having octyl group at 9 position up to pentamer **DDDDD** have been synthesised (Scheme 4.5). The shortest oligomers in this category is the dimer **DD**, which was synthesised by a Ni-mediated homocoupling (Yamamoto reaction) giving good yields (64 %) after column chromatography. Trimer **DDD** was synthesised as one pot synthesis involving two steps; first Miyaura reaction followed by Suzuki cross coupling reaction. Miyaura coupling reaction to form monoboronate-DAF **4.38** was performed by refluxing the monobromo-DAF **3.23**, Pd(PPh₃)₄ and bis(pinacolato)diborolane in dioxane for 4 hours under anhydrous condition. The mixture was then subjected to Suzuki reaction, without isolating the monoborate **4.38**, by adding dibromo-DAF **3.24**, potassium carbonate solution and Pd catalyst and refluxing for another 16 hours under inert atmosphere. The crude product was purified by column chromatography on silica gel affording pure product **DDD** as yellow solid in low yield (26%). Bromo substituted dimer **4.40** was prepared by reacting an excess amount dibromo-DAF **3.24** with borolane-DAF **4.38**, in a microwave-assisted Suzuki coupling reaction (**3.24**→**4.40**), in good yield (39%) after column chromatography. Pentamer **DDDDD** was then synthesised by employing the Suzuki reaction involving diborate DAF **4.39** and bromo substituted dimer **4.40**; the crude was purified by recrystallisation in methanol followed by column chromatography on silica gel to afford pure product in good yield (35%).



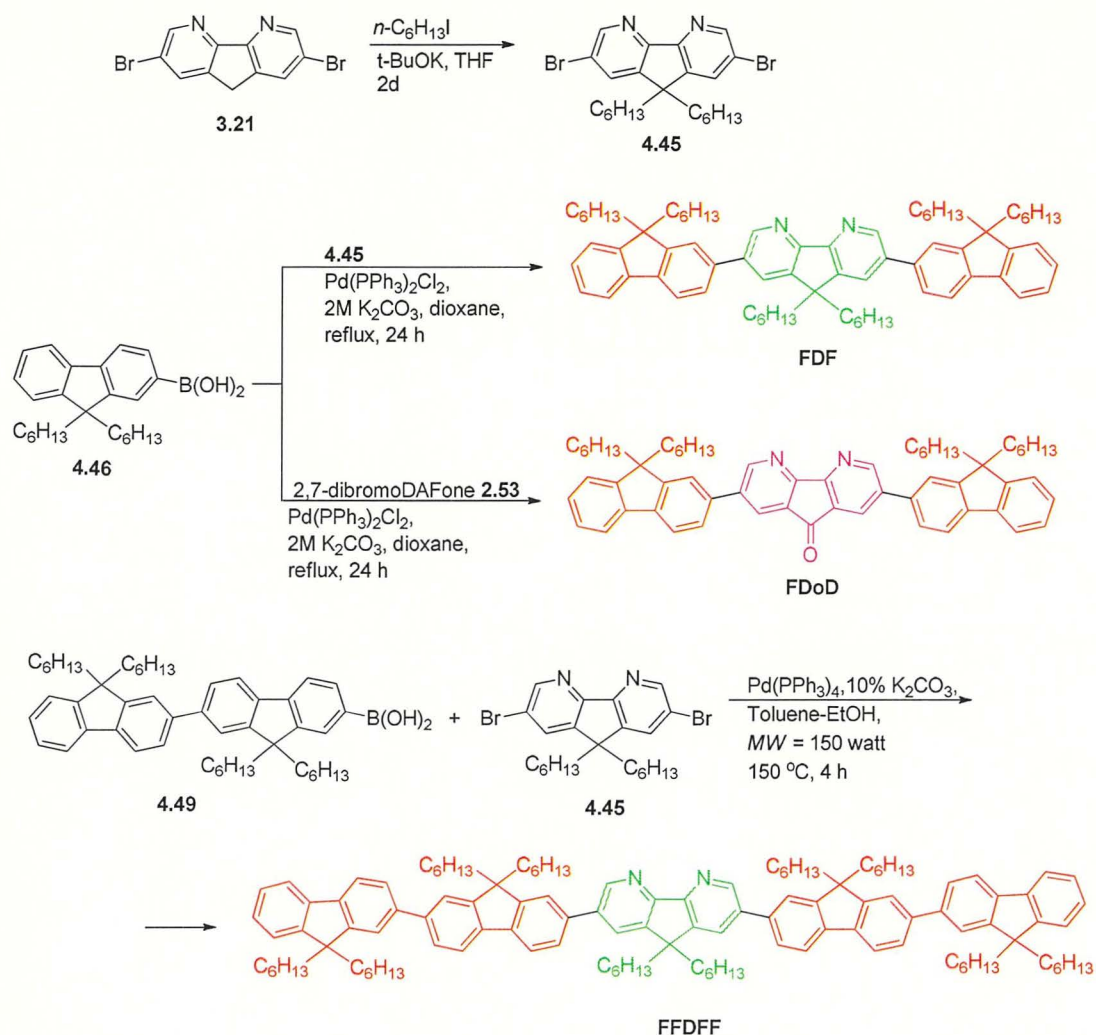
Scheme 4.5 Synthesis of homologous oligo(9,9-dioctyl-4,5-diazafluorenes).

Compounds **4.41** and **4.43** were synthesised by previously known literature procedures.³² Borolane derivative of dibenzothiophene-*S,S*-dioxide (**4.42**, **4.44**) were synthesised in excellent yields (> 80%) using Miyaura coupling involving PdCl₂(dppf)·DCM and ligand dppf as catalyst (Scheme 4.6). This developed procedure is a better option than the known literature procedure where the reported yield of **4.44** is about 26%.³⁴ Incorporation of dibenzothiophene-*S,S*-dioxide into the diazafluorene unit (**DSD**, **SDS**) was performed by similar Pd catalysed Suzuki reaction and purified by column chromatography on silica gel in good yields (26%, 59%) (Scheme 4.6). In general, for elaboration / optimisation the reaction conditions, most of the Pd catalysed reactions described here, were first tested in a small scale (< 50 mg) using microwave-assisted reaction conditions (allowing to keep the reaction time to be low in these trials), and then the optimised conditions were employed in conventional heating conditions for scaled up reactions (> 500 mg scale).



Scheme 4.6 Synthesis of 4,5-diazafluorene co-oligomers with dibenzothiophene-*S,S*-dioxide.

Hexyl-substituted DAF **4.45** was synthesised from dibromo-DAF **3.21** by a nucleophilic substitution reaction, using *n*-hexyliodide and *t*-BuOK as a base in THF under anhydrous conditions, in good yield (69%). It may be mentioned here that the synthesis of similar product, with longer alkyl groups in a side chain, namely octyl-substituted DAF **3.24**, was performed with octyl bromide using aqueous NaOH as a base and a phase transfer catalyst in DMSO (discussed in Chapter 3), which is easier to carry out and takes less reaction time. Co-oligomers of 4,5-diazafluorene with fluorene have been synthesised in similar fashion using Suzuki type coupling reactions (Scheme 4.7). Trimers (**FDF**) and (**FDoF**) have been synthesised with conventional heating while the pentamer (**FFDFF**) was prepared using microwave assisted reaction (irradiated with 150 watt at 150 °C) in good yields (61%) (Scheme 4.7). The boronic acid derivatives of fluorene (**4.46**, **4.49**) were synthesised by literature procedure.^{24,32}



Scheme 4.7 Synthesis of 4,5-diazafluorene and 4,5-diazafluorenone co-oligomers with fluorene.

4.2.2 Absorption and emission properties of 4,5-diazafluorene-based oligomers

The absorption and emission spectra of all the DAF based oligomers have been measured in both solution (degassed HPLC grade dichloromethane) and solid state (spin-coated films on quartz windows) at room temperature. The important photophysical data are compiled in Table 4.1.

4.2.2.1 Absorption

UV-Vis absorption spectra of all the oligomers both in solution (Fig. 4.7) as well as in film (Fig. 4.8) show strong bands between 300 nm to 400 nm attributed to spin allowed ($\pi\text{-}\pi^*$) transition; appearance of weak band around 450 nm in **FDoD** is attributed to spin forbidden ($n\text{-}\pi^*$) transition of the carbonyl group in DAFone unit. The absorption maxima of homologous oligomers shows a bathochromic shift of about 3 to 10 nm from solution to film

(Table 4.1), lowest red shift (3 nm) being for the longest oligomer **DDDDD**. Similar red shifted absorption maxima are observed for the co-oligomers, longest red shift (15 nm) being for the co-oligomer **DSD**.

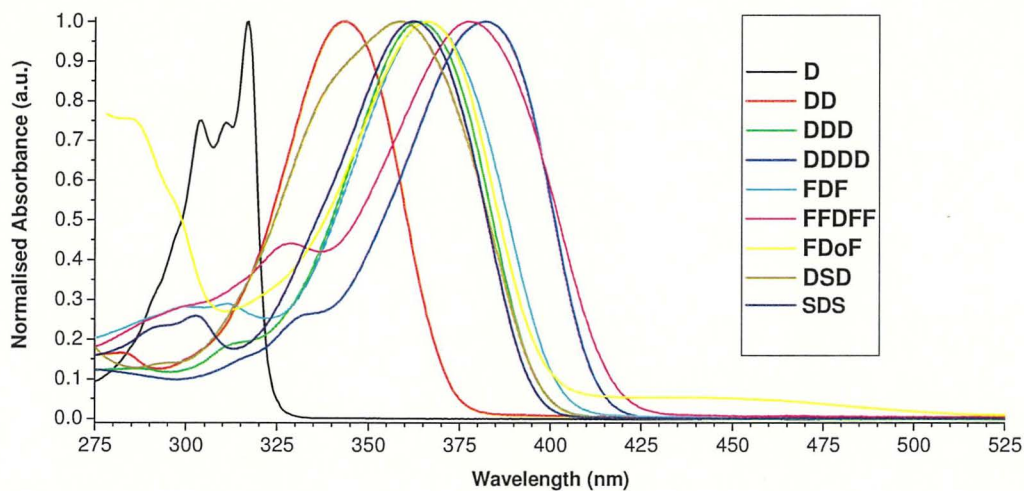


Fig. 4.7 Normalized UV-Vis absorption spectra of 4,5-diazafluorene oligomers and co-oligomers in dichloromethane.

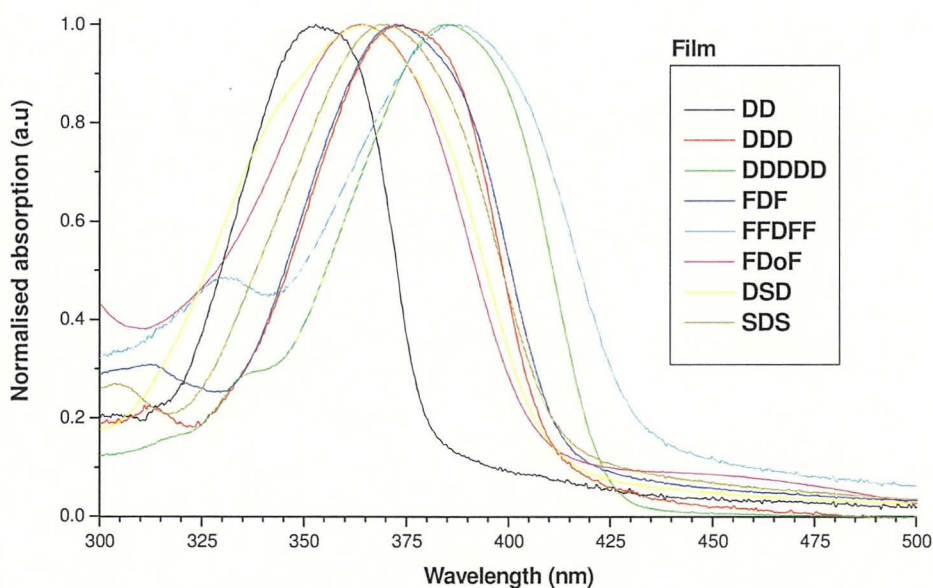


Fig. 4.8 Normalized UV-Vis absorption spectra of 4,5-diazafluorene oligomers and co-oligomers films spin coated film on quartz substrate

The optical energy gaps (E_g) were determined from the absorption edge of spin-coated films. They are in the range 2.44-3.27 eV and found to be decreasing with increase in conjugation length (**DD** to **DDDDD**) (3.27 to 2.93 eV). This decrease trend in band gap may improve the electron transport properties inherent to 4,5-diazafluorene molecule as demonstrated by Wang *et al.*^{35,36}

To determine the conjugation length in the linear π -system of oligo(4,5-diazafluorene), the longest wavelength absorption maxima of oligomers in dichloromethane (Table 4.1), is plotted against the reciprocal of monomer unit ($1/n$), and extrapolated to infinite chain length. This can be related to the conjugation length in the system investigated (Fig. 4.9).^{37,38} The resulting information on the so called effective conjugation length found to be 11-12 units for the homologous DAF oligomers. Therefore, the higher oligo(4,5-diazafluorene) or poly(4,5-diazafluorene) the absorption maximum may be predicted to be about 3.2 eV in DCM corresponding to 11–12 monomer units.³⁹ This value is close to the conjugation length observed for oligofluorenes reported in literature (see section 4.1.1).^{21,23}

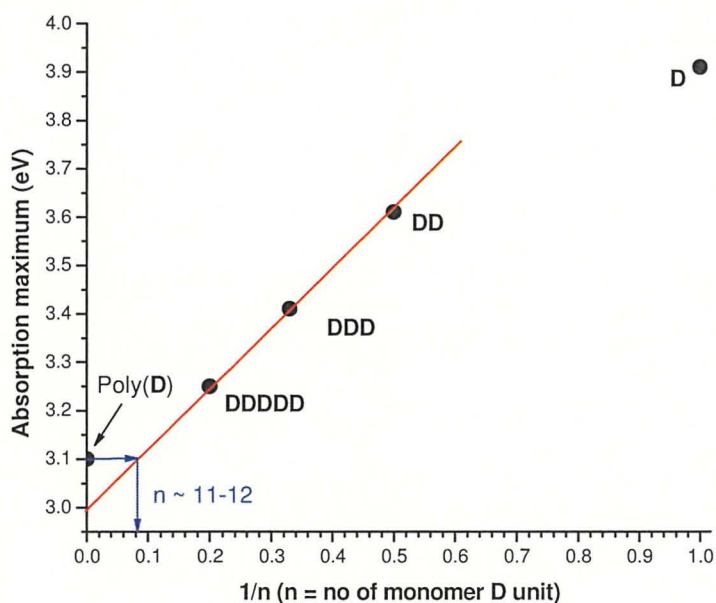


Fig. 4.9 Plot of absorption maxima (eV) *versus* $1/n$ for oligo(9,9-dioctyl-4,5-diazafluorenes) in dichloromethane, where n is the number of repeating **D** units in the oligomers (**D** = 9,9-dioctyl-4,5-diazafluorene). Extrapolated to Poly(**D**) in chloroform absorption maximum (data from chapter 5).

4.2.2.2 Emission

Emission spectra of all oligomers were measured in degassed HPLC grade dichloromethane at room temperature, with an excitation at 350 nm (except **FDoF**, which was excited at 370 nm) (Fig. 4.10). They exhibit vibronic emission in the blue region (375-429 nm), except for **FDoF** which emits broadly at 579 nm attributed to the presence of carbonyl group as reported in literature for **FfO**.^{24,25} Photoluminescence spectra of films measured at room temperature (Fig. 4.11) exhibit broad featureless emission in the range (415-440 nm). A red shift of about 25 nm from dimer (**DD**) to trimer.

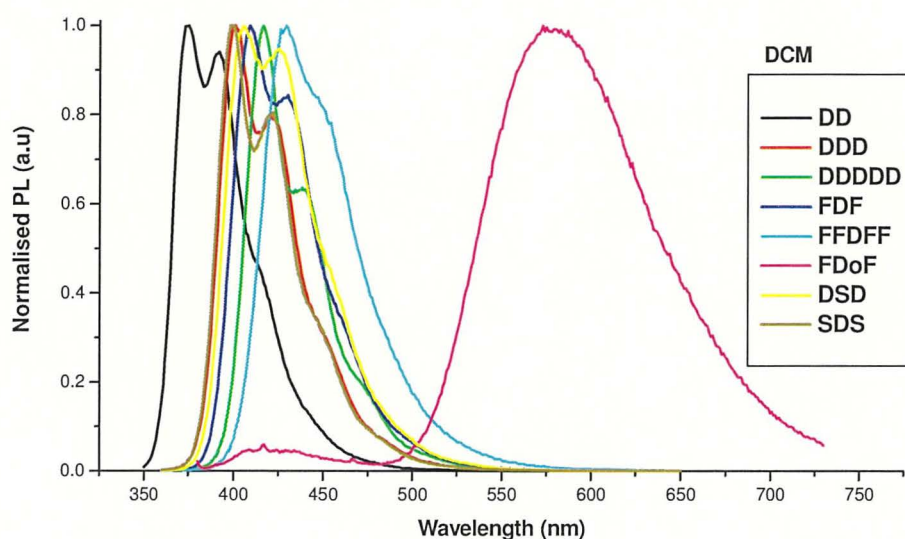


Fig. 4.10 Normalized photoluminescence spectra of 4,5-diazafluorene oligomers and co-oligomers in degassed dichloromethane. $\lambda_{\text{ex}} = 350$ nm (for **FDoF**, $\lambda_{\text{ex}} = 370$ nm).

DDD) and 42 nm from dimer (**DD**) to pentamer (**DDDDD**) compared to solution was observed in films. **FDF** exhibit largest red shifted emission of 68 nm in films with the emission maxima centered at 477 nm. A large red shifted emission maximum was observed for **FDF** (477) and a low red shift for **SDS** (435) compared to **DDD** (430 nm) in films. This may be attributed to fact that the fluorene units are better electron donor than the dibenzothiophene-*S,S*-dioxide units.

4.2.2.3 Photoluminescence quantum yields

For all the oligomers, photoluminescence quantum yields (PLQYs) were estimated both in solution and in film (Table 4.1). The PLQYs in solution using 9,9-diphenylanthracene as standard reference found to be high in the range 85-100% . In films, the absolute PLQYs are

in the range 15–40%. For homologous oligomers (**DD** to **DDDDD**) substantial quenching of PLQYs was observed in film compared to solution (from 80–100% in solution down to 12–15% in films). The co-oligomers of 4,5-diazafluorene with dibenzothiophene-*S,S*-dioxide (**SDS**, **DSD**) and fluorene (**FDF**, **FFDFF**) showed an improve photoluminescence quantum yields in film (24–42%) compared to homologous oligo-4,5-diazafluorenes. This phenomenon may be attributed to formation of aggregates or excimer in excited state.⁴⁰

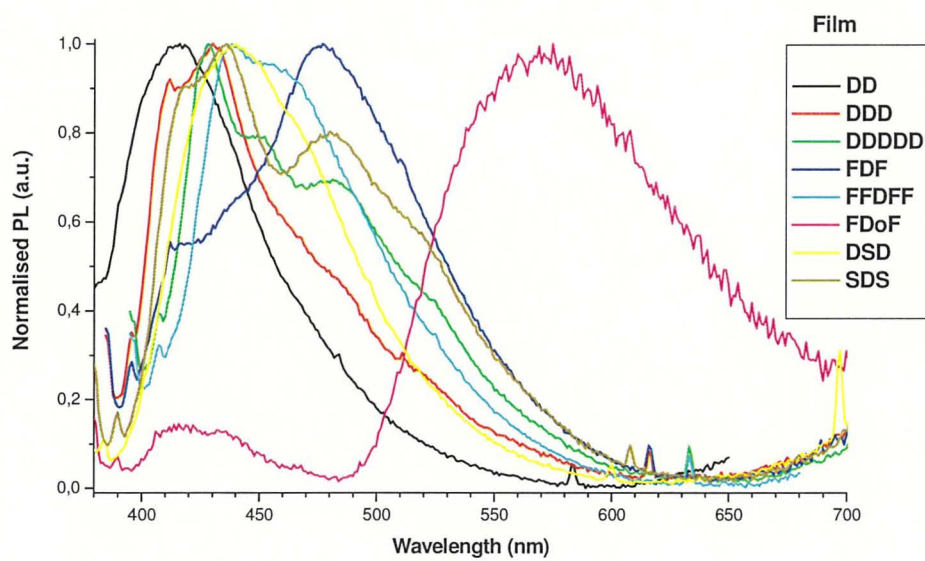


Fig. 4 11 Normalized PL spectra of 4,5-diazafluorene oligomers and co-oligomers films spin coated film on quartz substrate.

Incorporation of 9-diazafluorenone in between fluorene units (**FDoF**) results in green emission both in solution and in film similar to known oligofluorenone reported.⁴¹ The quantum yields for **FDoF** in film as well as in solution is considerably lower compared to other oligomers; similar trend is observed for fluorene-fluorenone systems that are reported in literature.²⁰

Table 4.1. Absorption photoluminescence maxima of 4,5-diazafluorene-based oligomers in solution and in the solid state, their photoluminescence quantum yields and optical energy gaps.

Compound	λ_{abs} (nm) CH ₂ Cl ₂	λ_{abs} (nm) Film	λ_{PL} (nm) CH ₂ Cl ₂	λ_{PL} (nm) Film	$\Phi_{\text{PL}}/\%$, ($\lambda_{\text{ex}}/\text{nm}$), ^a CH ₂ Cl ₂	$\Phi_{\text{PL}}/\%$, ($\lambda_{\text{ex}}/\text{nm}$), ^b Film	E_{g} (eV) ^c
D (3.22) ^d	317, 305	N.D.	(no emission)	N.D.	–	–	–
DD	343	353	375, 392 (sh)	415	86 (350)	15 (355)	3.27
DDD	364	374	400, 421 (sh)	430	101 (350)	13 (375)	3.04
DDDDD	382	385	417, 442 (sh)	427, 451 (sh), 481 (sh)	92 (350)	12 (385)	2.93
FDF	366	373	409, 428 (sh)	477	93 (350)	35 (350)	3.09
FFDF	377, 325 (sh)	386	429, 453 (sh)	440, 456 (sh)	84 (350)	42 (385)	2.92
FD_oF	360, 450(br)	364, 464 (br)	579 (br),	569 (br)	1 (370)	8 (370)	2.44
DSD	343 (sh), 350	365	405, 426 (sh)	440	89 (350)	24 (365)	3.02
SDS	362, 289, 303	370	398, 419	435, 480 (sh)	101 (350)	30 (370)	2.99

^aPhotoluminescence quantum yields estimated using 9,10-diphenylanthracene in degassed cyclohexane as a reference ($\Phi_{\text{PL}} = 0.90$)⁶¹, (excitation wavelengths in nm are in brackets).

^bAbsolute photoluminescence quantum yields in the solid state determined using an integrating sphere for spin coated films on a quartz substrate. ^cOptical energy (HOMO–LUMO) gap determined from the absorption onset of spin coated films on quartz substrate.

^dSynthesis of monomer unit **D (3.22)** is described in Chapter 3.

4.2.3 Cyclic voltammetry study of 4,5-diazafluorene-based oligomers

In order to evaluate n-doping and p-doping properties of the synthesised DAF based oligomers, electrochemical properties were investigated by cyclic voltammetry (CV) measurement (Fig. 4.12). The HOMO and LUMO energy level were derived from oxidation and reduction potential measured by CV using the equation (1) and (2) (the data are compiled in Table 4.2), assuming internal reference ionisation potential of Fc/Fc⁺ is 4.8 eV below the vacuum.^{42,43}

$$E_{\text{HOMO}} = - (E_{\text{p[ox vs. Fc+/Fc]}} + 4.8) \text{ (eV)} \dots\dots\dots(1)$$

$$E_{\text{LUMO}} = - (E_{1/2[\text{red vs. Fc+/Fc}]} + 4.8) \text{ (eV)} \dots\dots\dots(2)$$

As shown in Fig. 4.12a, the homologous oligomers of DAF show reversible reduction peaks in THF and quasireversible oxidation peaks in DCM. With increase in chain length from dimer **DD** to pentamer **DDDDD**, there is decrease in electrochemical energy gap (E_g , difference in HOMO and LUMO energy) of about 0.3 eV. Similar pattern in oxidation and reduction potentials was reported for structurally similar oligofluorenes.⁴⁴ The reduction potentials of the pentamers (**DDDDD** and **FFDFF**) were found difficult to measure, perhaps due to lower solubility of higher oligomers in THF and/or slower electrochemical kinetics. Two well-separated reduction peaks were observed for **FDoF** co-oligomer (Fig. 4.12b), which are positively shifted compared to the other oligomers. HOMO energy level of **FDoF** (-6.17 eV) is comparable to the other oligomers while substantially lower LUMO energy level (-3.44 eV) was observed. This can be attributed due to the keto group (contributes largely to LUMO orbital, see Fig. 4.15) at the central unit of **FDoF**. Incorporation of dibenzothiophene-*S,S*-dioxide (**S**) on DAF oligomers (**DSD** compared to **DDD**) (**D**) bring positive shift in reduction potential ($E_{1/2}^{\text{red1}}$) by ca. 0.1V and negative shift in oxidation potential by ca. 0.04V, signifying lower LUMO level of **DSD** compared to **DDD**. On the other hand, incorporation of fluorene units into backbone of **DAF** increases the oxidation potential and decreases the reduction potential. For instance, oxidation potential of **FDf** is 1.08 eV while that of **DDD** is 1.06 eV. It can be seen from Table 4.2, that for different oligomers, LUMO energy levels differs considerably compared to HOMO levels. Since the electronic properties of the conjugated system are largely associated with the first excited state transition (HOMO→LUMO), the photophysical properties of these oligomers are governed largely by the LUMO. Such materials are considered good candidate as electron transporting material. Moreover, the trend of electrochemical energy gap E_g (Table 4.2) obtained by CV measurement correlates well with optical energy gaps estimated from the absorption spectra edges of spin-coated thin films (Table 4.1). The energy gaps obtained from both methods are in the range of 2.5–3.1 eV.

Materials with such energy gap (2.5–3.1 eV) can be viewed as a potential semiconductor material for electronic applications.

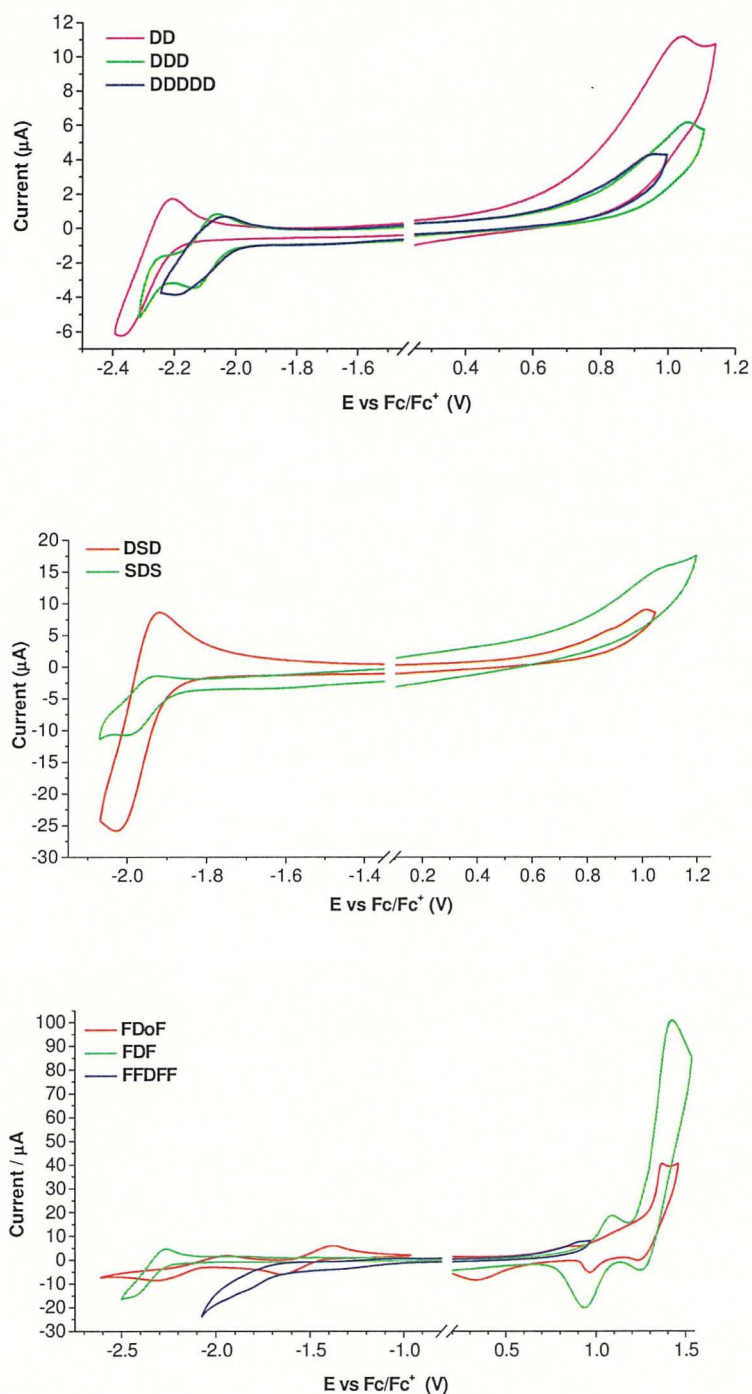


Fig. 4.12 Cyclic voltammograms of (a) monodisperse oligomers of 4,5-diazafluorene (b) **D/S** co-oligomer (c) and **F/D** co-oligomers. Reduction scan are in THF and oxidation scan in DCM at room temperature, scan rate of 100 mV/s, 0.2 M Bu_4NPF_6 as supporting electrolyte, Ag/Ag^+ as reference electrode and Pt as working electrode.

Table 4.2. Redox potentials of oligomers determined by cyclic voltammetry.

Samples	E_p^{ox} (V)	$E_{1/2}^{red1}$ (V)	$E_{1/2}^{red2}$ (V)	E_{HOMO} (eV)	E_{LUMO} (eV)	E_g^{CV} (eV)
DD	1.05	-2.31		-5.85	-2.49	3.35
DDD	1.06	-2.10		-5.86	-2.71	3.15
DDDDD	0.96	-2.12		-5.76	-2.69	3.06
FDF	1.08	-2.11		-5.88	-2.69	3.19
FFDFF	0.91	-1.69 ^a		-5.71	-3.11	2.60
FDoF	1.37	-1.36	-1.98	-6.17	-3.44	2.73
DSD	1.02	-1.96		-5.82	-2.84	2.98
SDS	1.07	-1.97		-5.87	-2.83	3.04

Potentials are recalculated vs Fc/Fc⁺ couple (0.19-0.22 V) as internal reference. $E_{HOMO} = -E_{p[ox vs. Fc+/Fc]} + 4.8$, $E_{LUMO} = -E_{1/2[red vs. Fc+/Fc]} + 4.8$, except for **FFDFF** where onset potential has been used. $E_g^{CV} = -(E_{HOMO} - E_{LUMO})$. ^aFirst half wave oxidation potential ($E_{1/2}^{ox}$). ^aOnset potentials. Reduction scans are in THF and oxidation scans are in DCM at room temperature; scan rate of 100 mV/s, 0.2 M Bu₄NPF₆ as supporting electrolyte, Ag/Ag⁺ quasi-reference electrode reference electrode and Pt as working electrode. E_p^{ox} is the peak potential of oxidation process. $E_{1/2}^{red1}$ is first half wave reduction potential and $E_{1/2}^{red2}$ is the second half wave potential.

4.2.4 Computational studies of 4,5-diazafluorene-based oligomers

In this section, a study of the structures of oligomers of DAF with fluorene and dibenzothiophene-*S,S*-dioxide units to determine the electronic properties: HOMO–LUMO energies and frontier orbital distribution have been presented. All these properties are important for application in optoelectronic devices point of view. All the computational studies were performed in Gaussian 09⁴⁵ using the density functional theory method (DFT) as applied in that computational package. The hybrid functional B3LYP, which combines Becke's exchange and Lee, Yang, Paar's correlation functional with 6-31G(d) basis set, were used for quantum-chemical calculation. Such model has been widely used for geometry optimization and determining the electronic properties for closed-shell organic compounds.^{46,47} It may be noted, all the oligomers geometry have been calculated with ethyl substituent at the 9 position of DAF and fluorene instead of octyl substituent so as to save calculation time, which in general does not affect the outcome of results. Here, **D** = 9,9-diethyl-4,5-diazafluorene, **Do** = 4,5-diazafluoren-9-one, **F** = 9,9-diethylfluorene, **Fo** = fluoren-9-one, **S** = dibenzothiophene-*S,S*-dioxide.

4.2.4.1 Geometry of diazafluorene-based oligomers

The geometries of conjugated oligomers **DDD**, **FDF**, **SDS** and **FDoF** have been optimized by density functional theory method (DFT) at B3LYP/6-31G(d) level of theory (Fig. 4.13) and an electronic structure of these oligomers have been calculated at the same level of theory using Gaussian 09 package of programs.⁴⁵ The force constants and vibrational frequency for stationary points have been calculated after optimization to check that they were true minima. The consecutive monomer units of the respective oligomers structure are arranged in slightly twisted manner with the substituent at 9-position (two alkyl chains) being opposite with respect to the plane of molecule (Fig. 4.13). For all the oligomers, the dihedral angles between the rings are similar and close to 38 degree. The inter-ring bond distances are about 1.48 Å for all the oligomers calculated from optimised geometry.

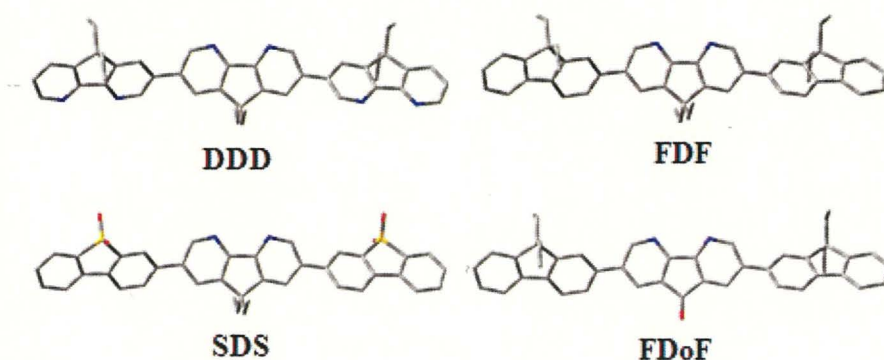


Fig. 4.13 Optimised structures of conjugated oligomers. Calculated at DFT/B3LYP/6-31G(d) level. For simplicity, H atoms are omitted and tube framework used with colours blue = nitrogen, red = oxygen, and yellow = sulphur atoms using GaussView 05 software.⁴⁵

4.2.4.2 Frontier Molecular Orbitals of diazafluorene-based oligomers

The highest occupied molecular orbitals (HOMO) and lowest unoccupied molecular orbitals (LUMO) of conjugated oligomers provide reasonable qualitative indication of their electronic properties and the ability of electron or hole transport. In addition, the HOMO–LUMO gap of oligomers provides an indication as potential semiconductor. Here, the frontier orbitals, HOMO and LUMO, of DAF-based oligomers are calculated and analysed.

The contour plots of the HOMO and LUMO of trimer such as **DDD**, **FDF**, **DSD**, **SDS** and **FDoF** are shown in Fig. 4.14. For all the oligomers, the frontier orbitals are distributed over the whole π -conjugated backbone with different contribution from the different part of the oligomer chain. There is antibonding between the bridge atoms of the inter-ring in HOMO while it is bonding in LUMO. In the same manner, there is bonding between the bridge

carbon atom and its conjoint atom of intra-ring in the HOMO while antibonding in the LUMO. This may explain the non-planarity of the optimised structure in ground state of oligomers as shown in Fig. 4.13. For these types of oligomers, the first excitation is almost exclusively between the HOMO and LUMO.^{32,47,48} This implies that the singlet-excited state is more planar than the ground state geometry.

As shown in Fig. 4.12, the oligomers **DDD**, **FDF**, and **SDS** show the same type of distribution of HOMO and LUMO. However, for **FDoF** the LUMO is concentrated at the central subunit while HOMO is spread all over the π -conjugated backbone. This may explain the experimental long wave emission (green emission, 579 nm, Table 4.1) and low reduction potential ($E_{1/2}^{\text{red1}} = -1.358$ V, Table 4.2) observed for **FDoF**. Similar long wave emission has been reported for structurally similar **FFoF** oligomers while investigating the 'keto defects'.^{24,25,26}

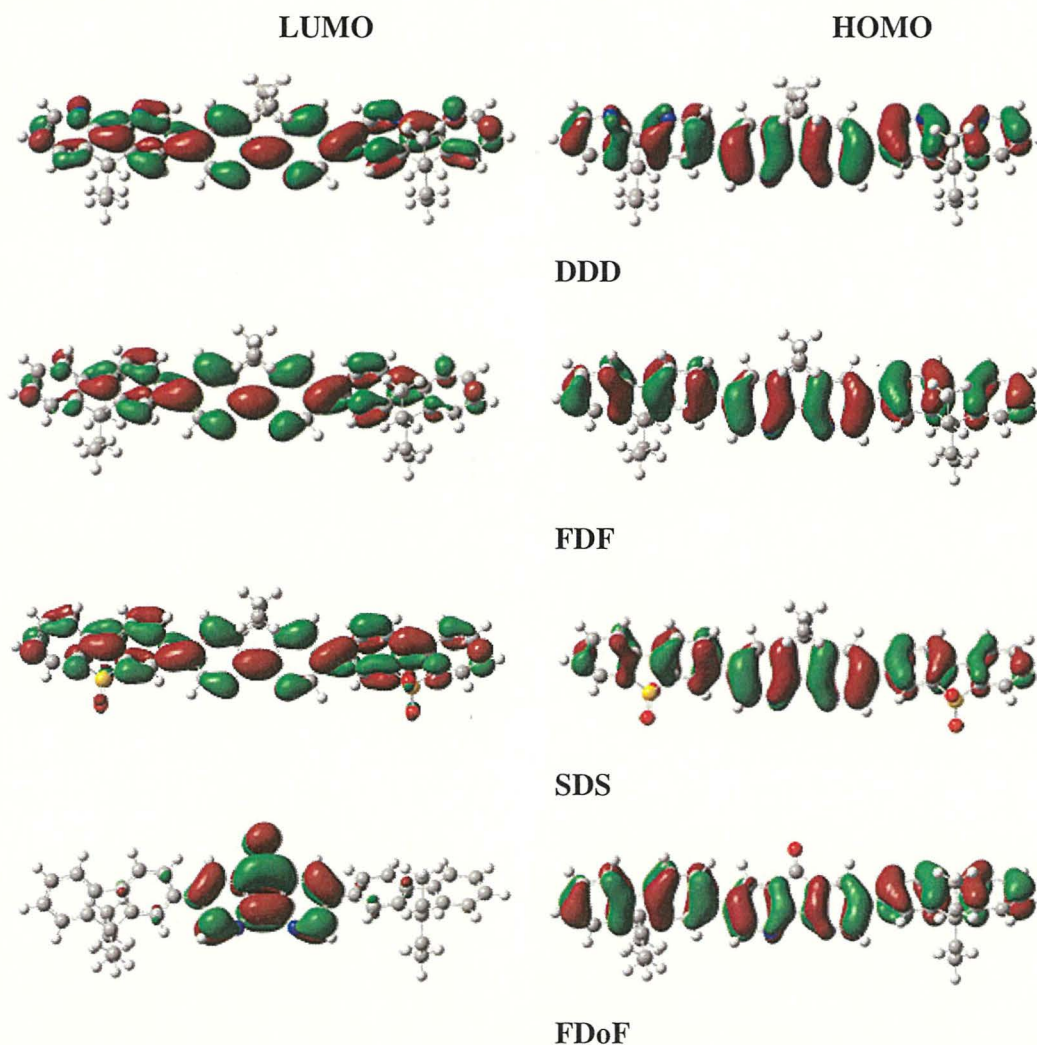


Fig. 4.14 HOMO and LUMO orbitals of DAF based oligomers DFT/B3LYP/6-31G(d) calculation (isovalue = 0.02).

In the experiment, the HOMO and LUMO energies are obtained from oxidation and reduction peaks of respective oligomers measured by cyclic voltammetry (Table 4.2). The similar HOMO and LUMO energies obtained by DFT/B3LYP/6-31G(d) calculation for oligomers are compiled in Table 4.3. Some additional model oligomers are also included for this study. The trend of increase and decrease of HOMO and LUMO energies of the respective oligomers can be explained in terms of electron accepting dibenzothiophene-*S,S*-dioxide (**S**) and electron donating fluorene (**F**) ability in comparison to 9,9-diethyl-4,5-diazafluorene (**D**) subunit. This trend of increase and decrease of HOMO and LUMO energies by DFT calculations correlate well with the experimental results obtained by cyclic voltammetry. For example, the LUMO energies of **SDS**, **FDf** and **DDD** obtained by DFT calculations are -2.339, -1.688 and -2.017 eV respectively (Table 4.3b) and those obtained by cyclic voltammetry are -2.832, -2.693 and -2.705 eV, respectively (Table 4.3), which clearly follows the same trend. The absolute values of orbital energies obtained by cyclic voltammetry measurements in solutions are higher than DFT calculated for a gas phase by ca. 0.5–1 eV.

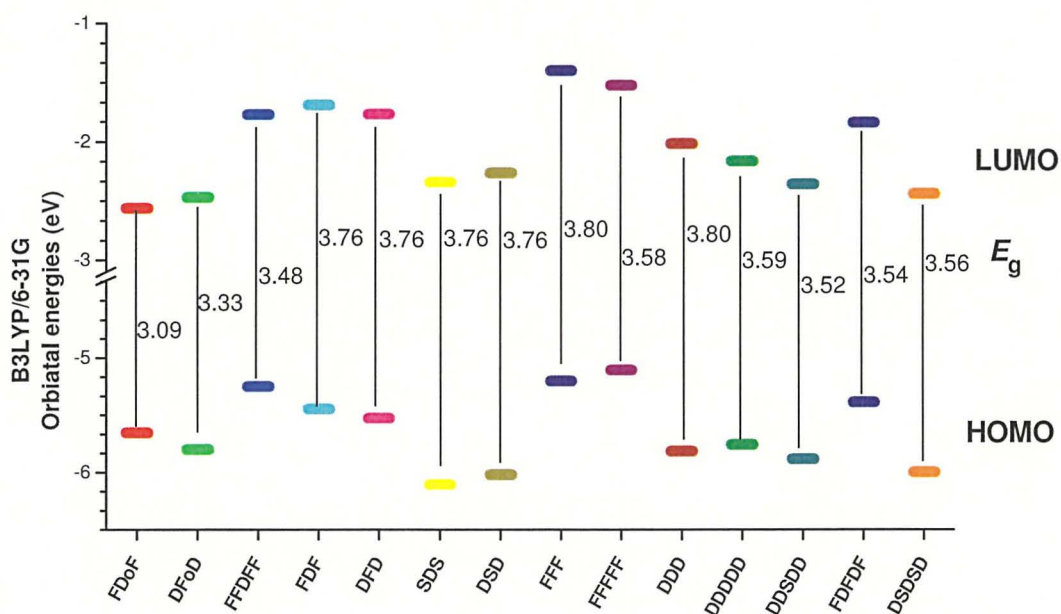


Fig. 4.15 HOMO and LUMO orbitals energies of oligomers by B3LYP/6-31G(d) calculation.

Table 4.3 HOMO and LUMO energy levels of 4,5-diazafluorene-based oligomers. Calculated at DFT/B3LYP/6-31G(d) level in a gas phase.

Oligomers	E_{HOMO} (eV)	E_{LUMO} (eV)	E_g^a (eV)
FDoF	-5.652	-2.560	3.09
DFoF	-5.798	-2.468	3.33
FFDFF	-5.250	-1.773	3.48
FDF	-5.446	-1.688	3.76
DFD	-5.527	-1.769	3.76
SDS	-6.103	-2.339	3.76
DSD	-6.018	-2.261	3.76
FFF	-5.201	-1.402	3.80
FFFFF	-5.106	-1.525	3.58
DDD	-5.813	-2.017	3.80
DDDDD	-5.754	-2.164	3.59
DDSDD	-5.882	-2.361	3.52
FDFDF	-5.386	-1.840	3.54
DSDSD	-5.994	-2.439	3.56

^aHOMO–LUMO energy gap, $E_g = E_{\text{LUMO}} - E_{\text{HOMO}}$.

Compared to oligofluorenes, **D/S** based oligomers result in narrower HOMO–LUMO gap. The experimental results of lower optical energy gap of **DSD** ($E_g = 3.02$ eV) compared to **DDD** ($E_g = 3.04$ eV) correlates well with that of DFT calculation results. DFT calculation up to octamer with ethyl substituent at the 9 positions of both **F** and **D** is carried out and are represented in Fig. 4.16. The HOMO–LUMO gap energies becomes similar for higher oligomers which is merely differ by 0.01 eV for **FFFFF** compared to **DDDDD**. Therefore, increasing chain length beyond 6–7 subunits will not bring observable changes in HOMO–LUMO gap. In the experiment, the conjugation length extrapolated to be about 12 units for DAF-based homologous oligomer (Fig. 4.8). Thus from synthetic point of view, homologous oligomers up to pentamer are good enough for understanding the physical properties related with chain length. The HOMO and LUMO energies of 4,5-diazafluorene oligomers are about 0.64 eV lower than that for fluorene oligomers (compared up to octamer). The effect of further increase in chain length DAF oligomers including polymeric behaviour will be discussed in Chapter 5.

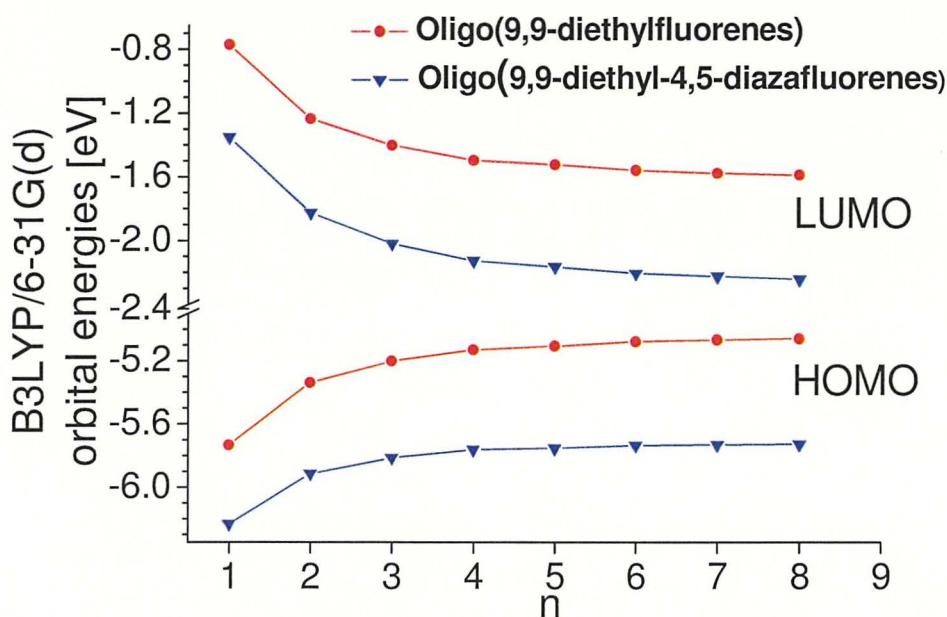


Fig. 4.16 Diagram of B3LYP/6-31G(d) frontier orbital energy levels vs. n (n is a number of monomer units) for oligo(9,9-diethylfluorenes) and oligo(9,9-diethyl-4,5-diazafluorenes).

4.4.5 Study of FDF oligomer as optical sensor for metal ions

As mention previously in Chapter 2, 4,5-diazafluorene derivatives have the potential to be used as sensors for metal ions because of presence of two nitrogen atoms, which can bind to metal ions. Therefore, careful design and synthesis of 4,5-diazafluorene derivatives may lead to novel sensors for metal ions. Fluorescent techniques are widely employed for detection of a variety of analytes.^{49,50,51,52} In general, metal coordination with organic chromophore results in change of their photophysical and/or electrochemical properties which are quantified as a signal for applications in sensing and detecting metal ions. Fluorescent probe is fast emerging field of research in biological and environmental science of detecting, sensing and imaging and is considered as one of the best detection technique due to the low detection limit, high sensitivity, commercial availability and fast measurement time.^{49,50} Most of the fluorescent probes for metal ions are based on metal coordination with organic chromophore resulting in a change in emission intensity, lifetime or wavelength of the organic chromophore. Various approaches are used in design of fluorescent probes for metal ions exploiting e.g. photo induced electron transfer (PET),⁵³ photo induced charge transfer (PCT)⁵⁴, fluorescence resonance energy transfer (FRET) or photo induced excimer/exciple formation.^{49,50}

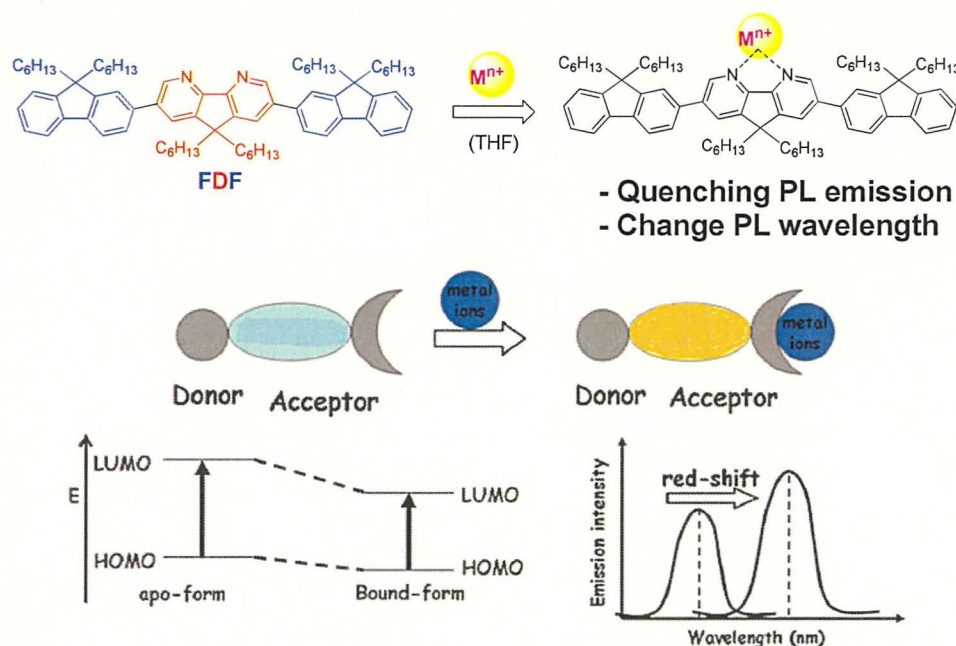


Fig. 4.17 PCT fluorescent probe for metal cation and their sensing mechanism.⁵⁴

The through-bond intramolecular charge transfer (ICT) occurs efficiently in donor-acceptor (**D-A**) systems in which the **D** and **A** units are separated by a π -conjugated linker.⁴⁹ Such **D-A** systems are normally characterised by a large Stokes shift, visible light excitability and metal-coordination induced emission shift.^{49,50,51} **FDF** oligomer represent a **D-A** system separated by σ -bond spacer in which **D** is the fluorene unit and **A** is the 4,5-diazafluorene unit. The photophysical properties of **FDF** has been studied in the solution as well as in the solid state and discussed in previous section. Photoluminescence spectrum of **FDF** oligomer showed some vibronic feature with two distinct bands at 409 nm and 429 nm (blue emission) in dichloromethane (Fig. 4.10). In films its photoluminescence is red-shifted to give a structureless emission peaked at 477 nm (Fig. 4.11). High photoluminescence quantum yield in solution 93% (in dichloromethane) as well as in solid state 35% (spin coated film) was recorded for **FDF** (Table 4 1). Cyclic voltametric study showed reversible reduction wave with $E_{1/2}^{\text{red}} = -2.11$ V and quasi-irreversible oxidation peaked at $E_p^{\text{ox}} = -1.08$ V (Table 4.2) which indicates good redox stability in solution.

The emission spectra of **FDF** showed dependence on the solvent polarity. As seen in Fig. 4.18, broadening of emission bands of **FDF** and their significant bathochromic shifts are observed upon increasing the solvent polarity (hexane \rightarrow toluene \rightarrow acetonitrile \rightarrow ethanol). Such a solvent dependence of emission indicates that ICT occur efficiently between **D** and **F** unit in the excited state. The peak absorption wavelengths of **FDF** were only slightly

dependent on the solvent polarity (Fig. 4.18) which indicates very low interaction between **D** and **F** in the ground state. Such process suggests fast PET fluorescence probe mechanism.^{49,50,51}

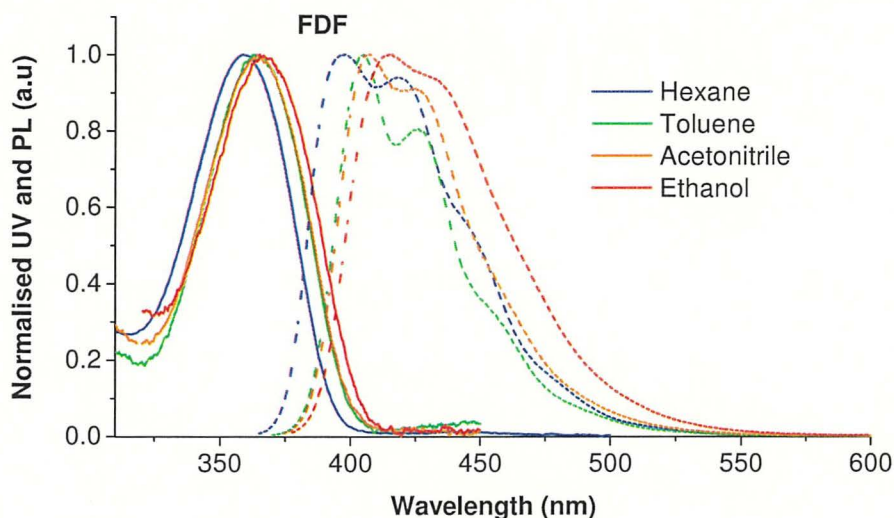


Fig. 4.18 Normalised absorption (solid line) and emission spectra (dashed line, excited at absorption maxima) of **FDF** in hexane (blue), toluene (green), acetonitrile (orange) and ethanol (red).

The combined photophysical properties of **FDF** together with chelating ability implies that DAF-based emissive D–A type oligomers can be good candidates for developing sensors for metal ions. In this section, preliminary studies using UV-Vis and fluorescence spectroscopy to understand the interaction of various metal salts with the **FDF** oligomer is discussed.

4.4.5.1 Effect of various metal ions on UV-Vis and PL spectra of FDF

The metal salts used in these studies were NaClO₄, Ba(ClO₄)₂, LiClO₄, Mg(ClO₄)₂, Ni(NO₃)₂, Hg(ClO₄)₂, Cu(BF₄)₂, Fe(ClO₄)₃, Pb(ClO₄)₂ and AgClO₄. Absorption spectra of **FDF** and its 1:1 mixture solutions with various metal salts in THF are shown in Fig. 4.19-4.20 and corresponding emission spectra are shown in Fig. 4.21-4.22. Marginal decrease in absorption intensity of **FDF** was observed upon addition of excess amount of Cu²⁺, Mg²⁺, Na⁺, Li⁺ and Ba²⁺ ions with no changes in absorption maxima (less than 1 nm). In contrast to the behaviour of the above cations, Hg²⁺ and Fe³⁺ showed pronounced decrease in the absorption intensity with pronounced red shift of absorption maxima of about 38 nm and 52 nm respectively. Furthermore, among all the studied metal ions, Hg²⁺ and Fe³⁺ led to a significant red shift of emission of about 100 nm and high degree of photoluminescence quenching.

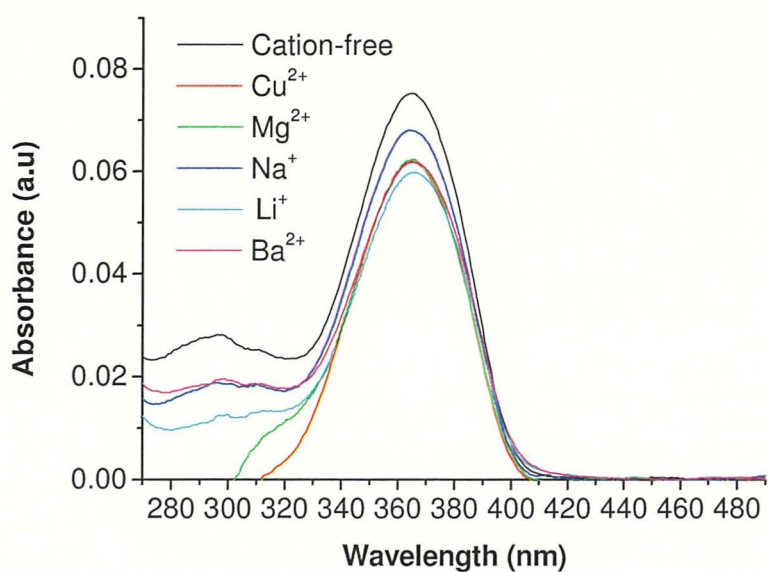


Fig. 4.19 The absorption spectrum of 1.37 μM oligomer (**FDF**) in THF solutions with different metal cation.

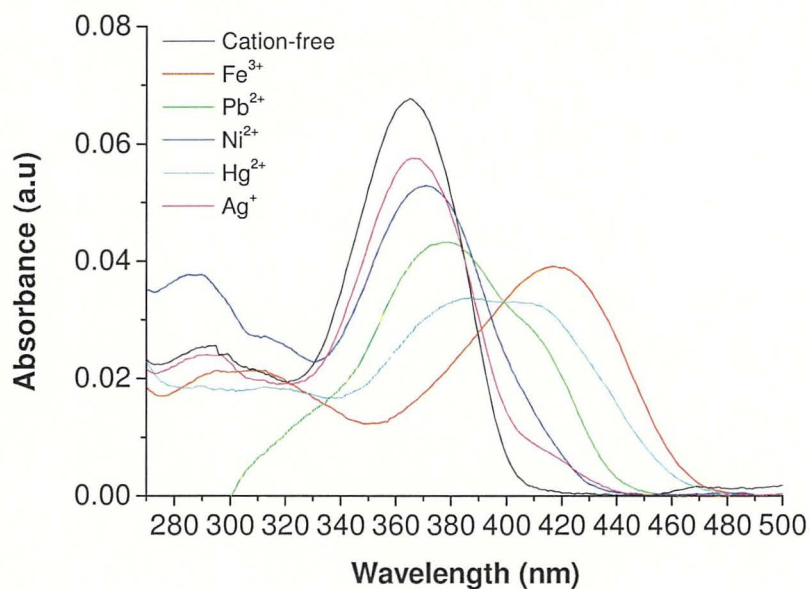


Fig. 4.20 The absorption spectrum of 1.37 μM oligomer (**FDF**) in THF solutions with different metal cations.

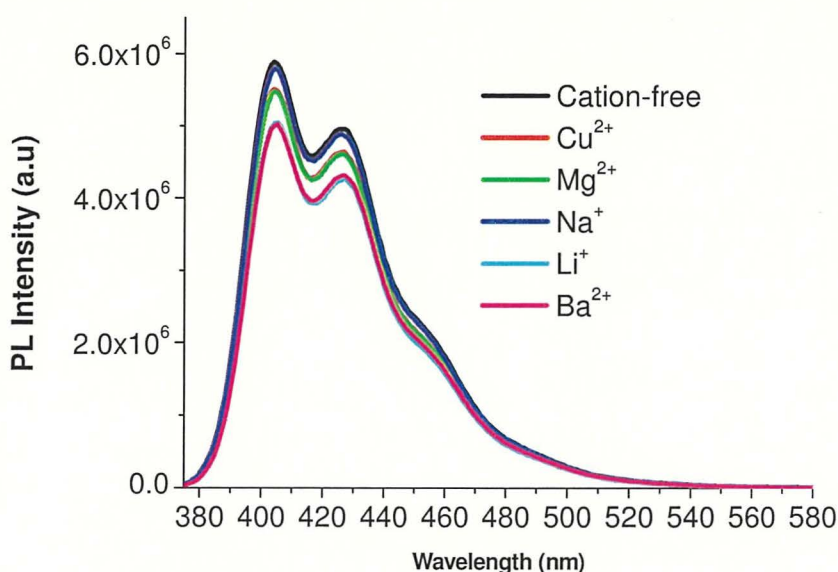


Fig. 4.21 Fluorescence spectra of 1.37 μM oligomer **FDF** in THF solutions (excited at 365 nm) in the absence of metal cations and in presence of 13.7 μM different metal cations (Cu^{2+} , Mg^{2+} , Na^+ , Li^+ , Ba^{2+}) excited at 365 nm.

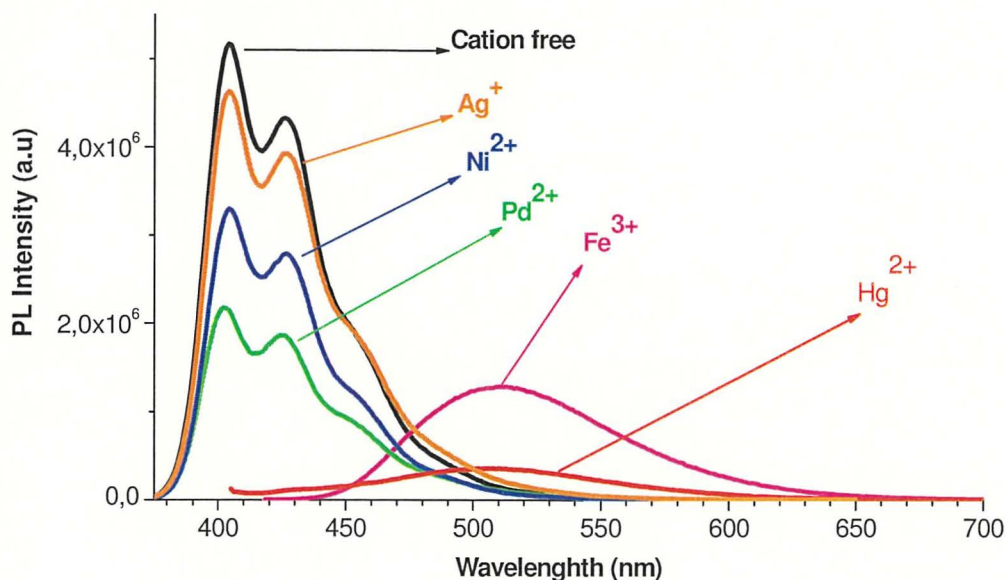
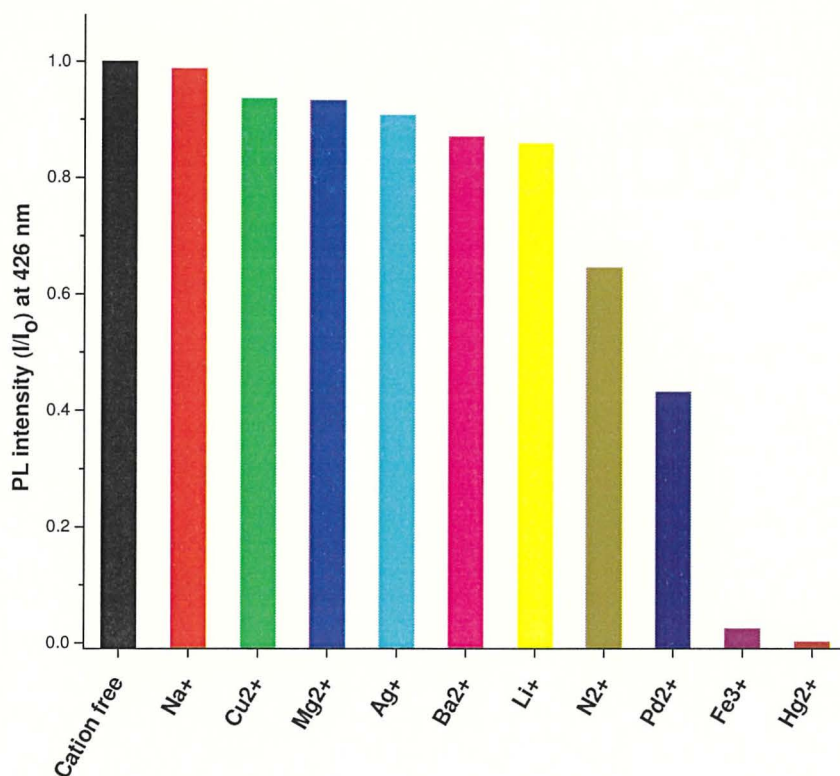


Fig. 4.22 Fluorescence spectra of oligomer **FDF** (1.37 μM) in THF solutions (excited at 365 nm) in the absence of metal cations and in presence of 13.7 μM of Hg^{2+} (excited at 403 nm), Fe^{3+} (excited at 417 nm), Ag^+ (excited at 367 nm), Pb^{2+} (excited at 379 nm) and Ni^{2+} (excited at 371 nm).

These initial results indicate that **FDF** oligomer chelates strongly with Fe^{3+} and Hg^{2+} cations and as a result, such metal coordination induces the changes in absorption and emission spectra. Graph 4.1 depicts the efficiency of the photoluminescence quenching upon addition

of various metal ions demonstrating particularly efficient process for Hg^{2+} which led to nearly 100% quenching of the emission when excited at 426 nm.



Graph 4.1: Fluorescence intensity responses (I/I_0) at 426 nm of the oligomer (**FDF**) before and after adding the metal cation, excited at absorption maximum (365–417 nm), I_0 is the fluorescence intensity of cation free and I is the fluorescence intensity of with metal ion.

The possible PCT mechanism for the red shift observed in the emission spectrum of the oligomer **FDF** upon coordination with the metal ion is illustrated in Fig.4.17. Further, metal coordination with the acceptor of ICT chromophore (that is bound **FDF**) led to decrease in HOMO and LUMO energy level compared to unbound **FDF** and results in red shifted emission.

FDF oligomer shows good binding ability towards both Hg^{2+} and Fe^{3+} as evident from corresponding changes in its absorption and emission spectra upon complexation. The normalised absorption and emission spectra of **FDF** are shown in Fig 4.23 for more clear illustration. Both Hg^{2+} and Fe^{3+} caused red shifts (41 and 53 nm, respectively) of absorption maximum centred at 405 and 417 nm in THF, respectively. Absorption maximum upon addition of Fe^{3+} is about 12 nm more red shifted compared to that of Hg^{2+} (Fig. 4.23b).

Moreover, about 100 nm red shifted structureless emission maximum centred at 502 nm was observed for both Hg^{2+} and Fe^{3+} when excited at 415 nm (Fig 4.23b). Development of sensor for mercury ions is highly sought after as it is one of the most toxic metal ion causing environment and water pollution.^{55,56,57} We focused our studies on Hg^{2+} detection, since the development of sensors for mercury ions is a big challenge due to the high toxicity of mercury and the associated issues of water contamination and environmental pollution by mercury compounds.

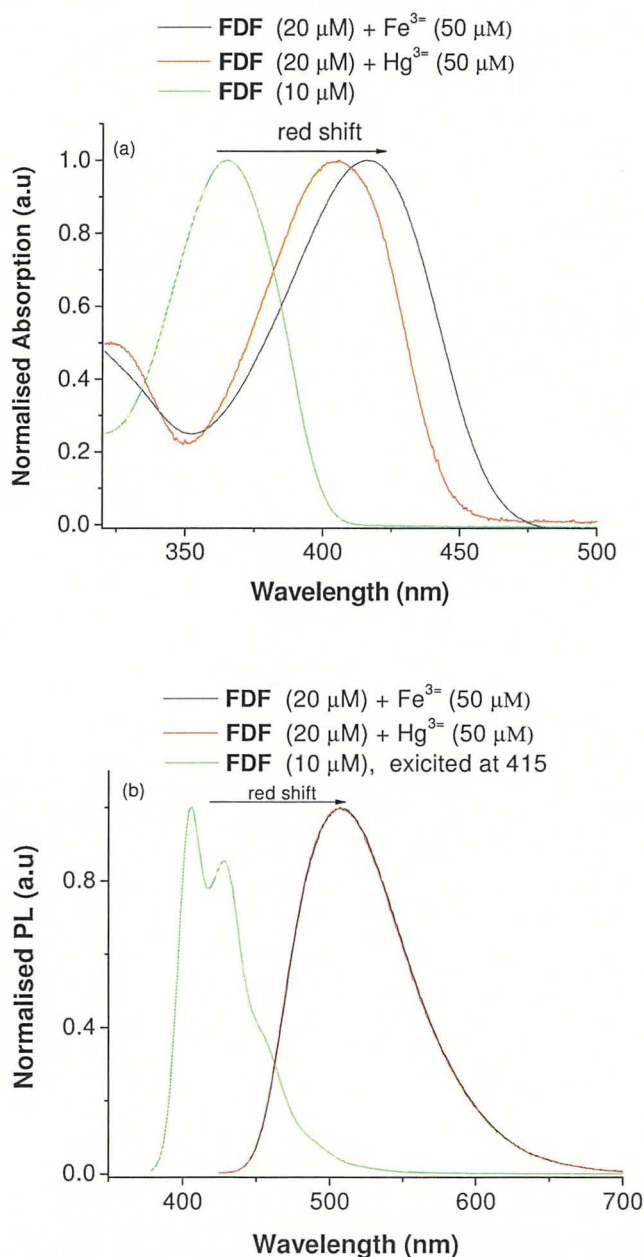


Fig. 4.23 Normalised absorption spectra (a) and PL spectra (b) of **FDF** (10 μM) and 1:1 mixture solution of **FDF** (20 μM) with HgClO_4 (50 μM) and FeClO_4 (50 μM) in THF.

4.4.5.1 Effect of Hg^{2+} ions concentrations on absorption and emission spectra of *FDF*

Effect of increase in concentration of Hg^{2+} (1 to 50 μM) into **FDF** (20 μM) solution in THF on emission, excited at 365 and 415 nm is shown in Fig. 4.24. When excited at 365 nm, with an increase in concentration of Hg^{2+} upto 40 μM follows a trend of increase in the quenching of emission. The quenching of emission becomes nearly 100% at 50 μM concentration of Hg^{2+} . At excitation wavelength of 415 nm, about 40 times enhancement of the emission intensity along with 99 nm red shift centred at 507 nm was observed. This may be attributed as a result of chelation enhanced fluorescence phenomena. The maximum enhancement of emission intensity occurs when concentration of Hg^{2+} is about double then that of **FDF**. The corresponding effect of increase concentration of Hg^{2+} (1 to 50 μM) into **FDF** (20 μM) solution in THF on absorption is shown in Fig. 4.24b. Gradual red shifted (up to 41 nm) absorption maximum of **FDF** was observed as a result of increase in concentration of Hg^{2+} upto 40 μM . As shown in Fig 4.24a, the formed complex is emissive and emits at longer wavelength (507 nm, green emission). Therefore, this gives rise to the possibility of detecting Hg^{2+} through both quenching of blue emission of **FDF** ("ON \rightarrow OFF") when excited at 365 nm and formation of complex **FDF**: Hg^{2+} which results in emit green light when excited at 415 nm ("OFF \rightarrow ON").

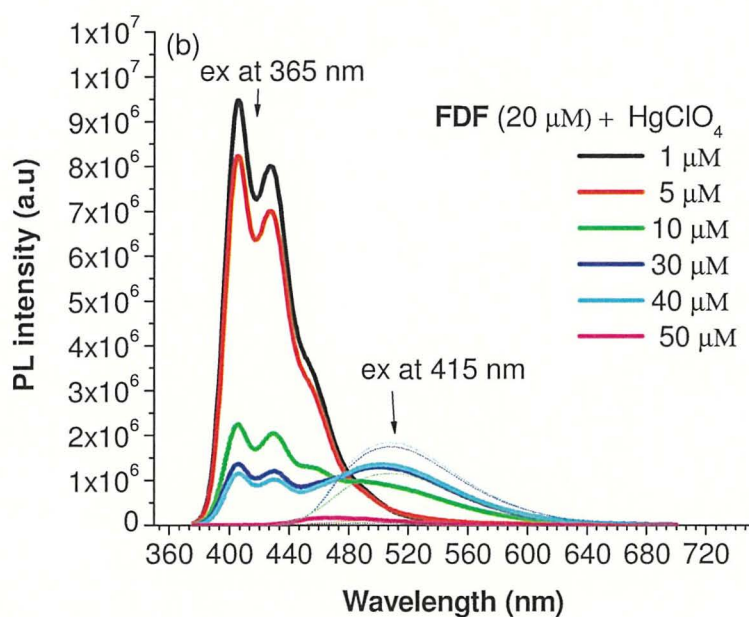
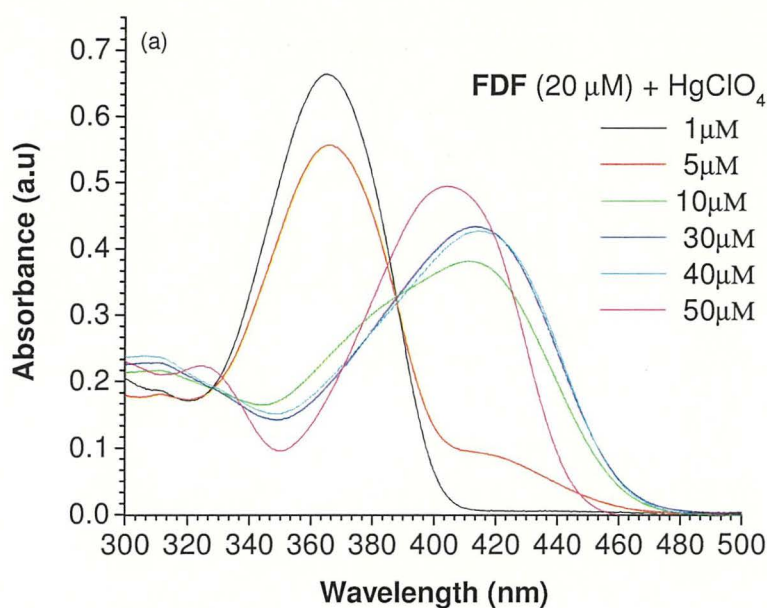


Fig. 4.24 The absorption (a) and PL spectra (b) of **FDF** (20 μM) in THF with increased concentration of $\text{Hg}(\text{ClO}_4)_2$: 1, 5, 10, 30, 40, 50 μM (solutions were prepared as in a 1:1 mixtures). For PL spectra (b), the THF solutions were excited at 365 nm (solid lines) and 415 nm (dashed lines), respectively.

4.4.5.2 Determination of stoichiometry of the complex between FDF and Hg^{2+} , and detection limit of Hg^{2+}

Binding stoichiometry of the coordination complex can be determined using Job's method.^{58,59} The absorption and photoluminescence spectra for titration of **FDF** with HgClO_4 are shown in Fig. 4.25. The corresponding Job's plot using both fluorescence and absorption intensity (Fig. 4.26) reveal 2:1 (**FDF**: Hg^{2+} , mole ratio) stoichiometry for the [**FDF**- Hg^{2+}] adduct. The corresponding structure of the possible complex formation is depicted in Fig. 4.27.

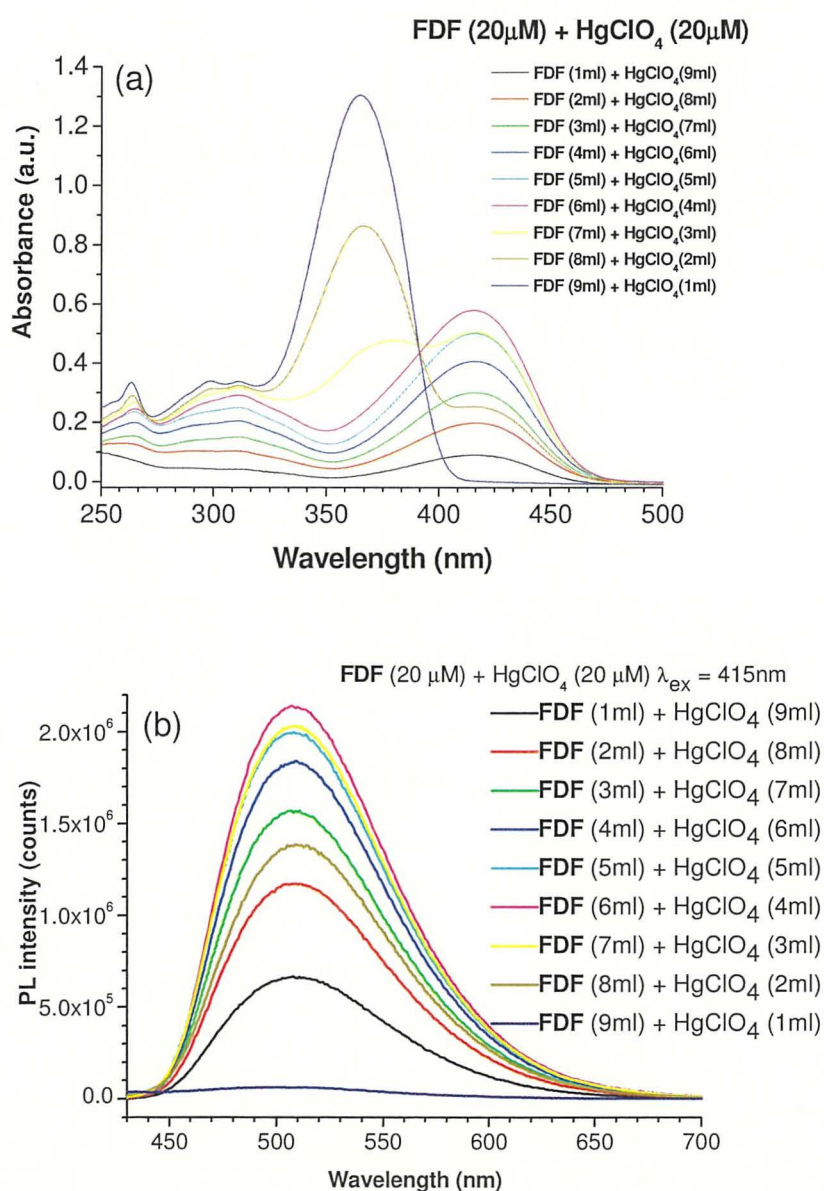


Fig. 4.25 UV-Vis absorption (a) and emission spectra (b) of mixtures of equal concentrations (20 μM each) of **FDF** and $\text{Hg}(\text{ClO}_4)_2$ in different ratios, in THF.

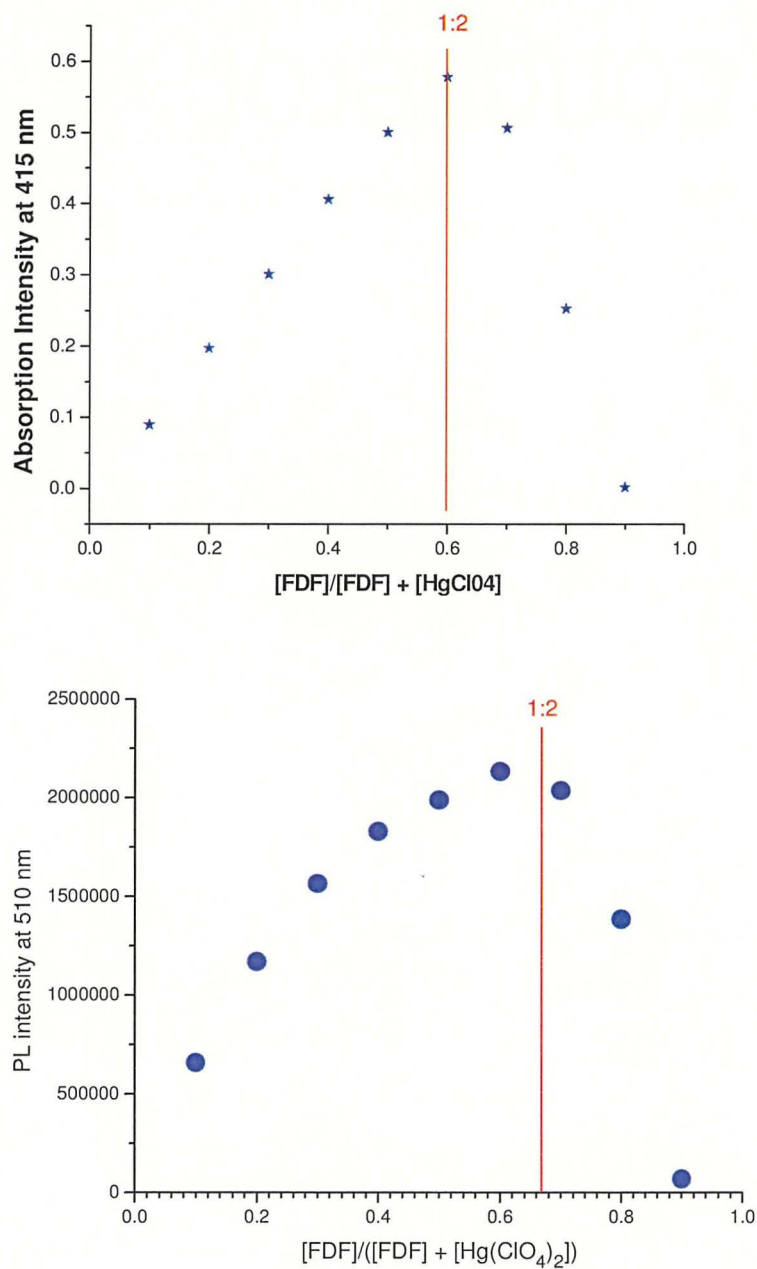


Fig. 4.26 Job's plots for the mixtures of **FDF** (20 μM) and $\text{Hg}(\text{ClO}_4)_2$ (20 μM) at different ratios in THF for stoichiometry determination of the complex. (a) Absorption intensity at 415 nm and (b) PL intensity at 510 nm ($\lambda_{\text{ex}} = 415$ nm).

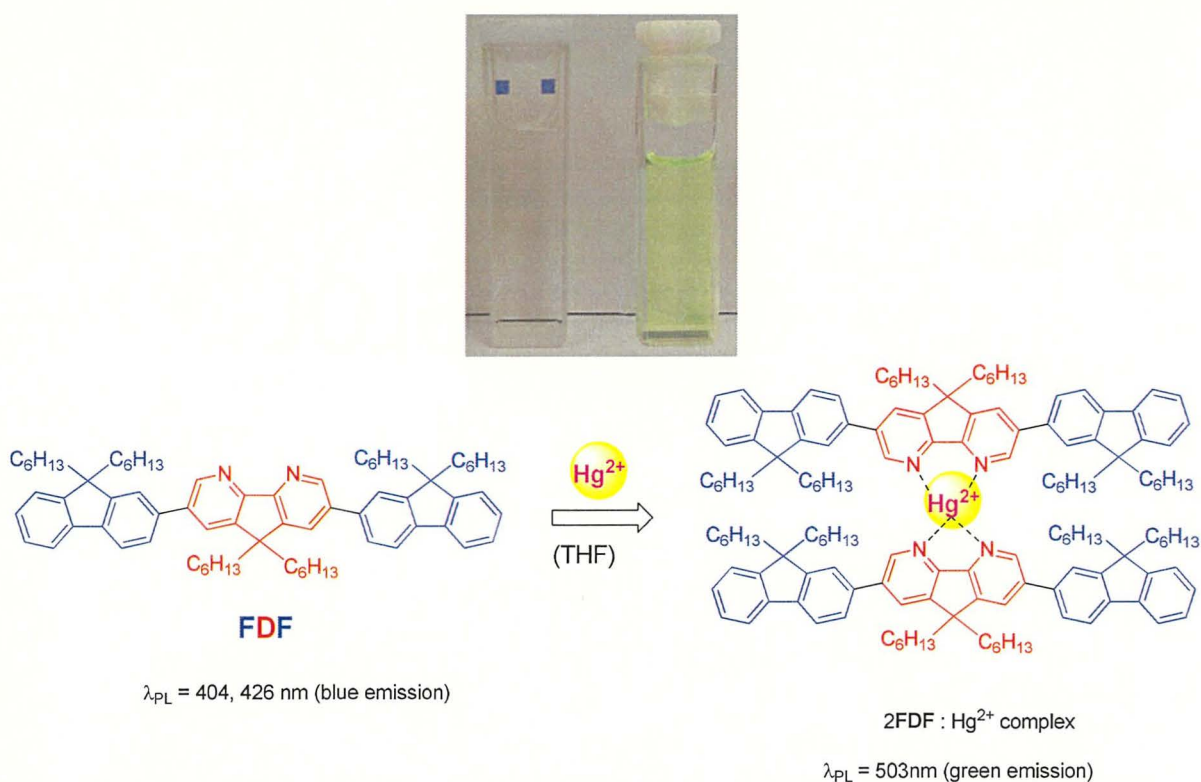


Fig. 4.27 Formation of possible 2:1 ratio **FDF**: Hg^{2+} complex in THF and change in the emission characteristics on complexation. Photograph depicting the colourless **FDF** solution in THF turn greenish upon addition of Hg^{2+} in day light.

Measurements of known concentrations of **FDF**: Hg^{2+} complex emission intensity can be used to determine the unknown concentration of Hg^{2+} in a given sample by plotting calibration graph of the emission intensity vs concentration. Photoluminescence titration of **FDF** with Hg^{2+} ions showed that an intensity of the long wavelength emission band at 507 nm of **FDF**- Hg^{2+} complex gradually increased with an increase of Hg^{2+} ions up to certain limit (Fig.4.28). Measurable increase in fluorescence intensity with an increase of Hg^{2+} concentration added into **FDF** solution in THF could be observed which allowed to estimate the detection limit to be about 3×10^{-7} M. The formation of complex of Hg^{2+} with **FDF** could be visible in naked eyes with change in colour from nearly colourless solution of **FDF** in THF to light green colour when Hg^{2+} is added (Fig. 4.27).

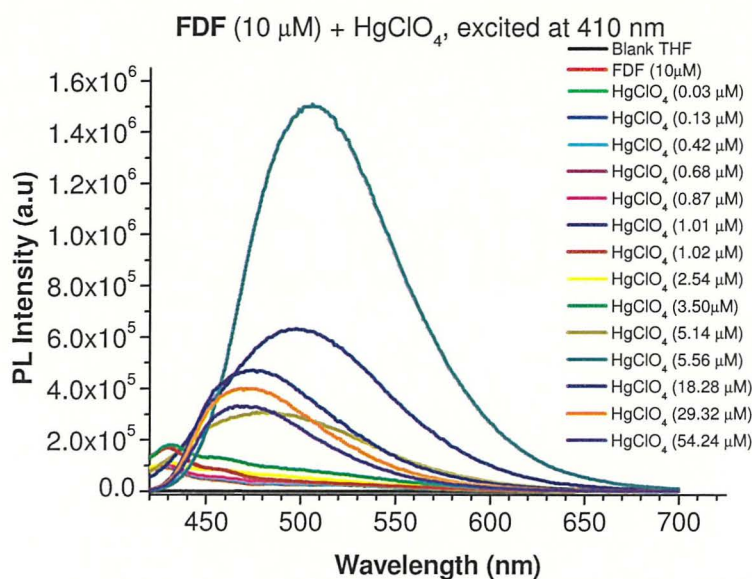


Fig. 4.28 The photoluminescent spectra of **FDF** (10 μ M) titrated with increased concentration **HgClO₄** (0-54.25 μ M) in THF excited at 410 nm.

4.3 Conclusion

We have synthesised novel monodisperse rigid rod type oligomers of based on 4,5-diazafluorene monomer unit, up to pentamer, along with its co-oligomers with fluorene and dibenzothiophene-*S,S*-dioxide moieties in good yields (25–70%) and carried out their photophysical and electrochemical studies. All the oligomers were purified using column chromatography and fully characterized using NMR and MS spectroscopy prior to physical studies. Homologous rigid rod type oligomers of 4,5-diazafluorene (**DD** to **DDDDD**) can serve as model to understand the behaviour of π -conjugated polymers of this class of compounds.

The absorption maxima in solution (343–382 nm) as well as in films (353–385) for DAF homo-oligomers undergo red shift with an increase of the chain length (by 20 nm from dimer **DD** to pentamer **DDDDD**). In addition, there is some red shift of absorption maxima (~10 nm) from solutions to films. The optical HOMO–LUMO energy gap determined from absorption edge in films was found to be decreased with an increase of the main chain length (**DD**, $E_g = 3.27$ eV to **DDDD**, $E_g = 2.93$ eV), indicating possibility of further decrease in band gap with increase in chain length. The electrochemical band gap determined by cyclic voltammetry for homologous 4,5-diazafluorene oligomers follows the similar trend. The emission maxima for this class of oligomers are in deep blue region of the spectrum (375–417

nm) in solution and somewhat red shifted by ca. 10–40 nm in films (415–427 nm). Introduction of fluorene and dibenzothiophene-*S,S*-dioxide into the backbone of 4,5-diazafluorene to construct co-oligomers such **FDf**, **SDS** allowed us to further change in physical properties. For example, the electrochemical band gap of **FDf** ($E_g = 3.53$ eV) is more while **SDS** ($E_g = 3.04$ eV) is less when compared to **DDD** ($E_g = 3.15$ eV). This demonstrated that electrochemical properties of this class of compounds can be tuned by the means of co-oligomer formation.

The emission spectra of **FDf** showed dependence on the solvent polarity with the broadening of emission bands that underwent significant bathochromic shifts upon increasing the solvent polarity (hexane, toluene, acetonitrile and ethanol). This solvent dependence of emission indicates that an ICT occur efficiently between **D** and **F** unit in excited state. All the oligomers show high PLQY in solution (80–100%), which are decreased in films but still keep reasonably high (for solid states) efficiency of 12–40 % (except of **FDof**, in which quenching the emission is very strong due to presence of carbonyl group that facilitates singlet-triplet transition). The optical energy gaps (2.4–3.3 eV) estimated from absorption edges of the films and electrochemical HOMO–LUMO gaps (2.7–3.5 eV) estimated from cyclic voltammetry are in good agreement and characterise the oligomers as high band gap semiconductors. All the oligomers frontier orbitals and geometry along with some model similar compounds were investigated by DFT method at B3LYP/6-31G level of theory. The experimental results of HOMO–LUMO gaps and that of the DFT calculations showed good correlation. Their use as new class of organic semiconducting materials for optoelectronic applications can be expected from these studies.

Studies of **FDf** oligomer as sensor for metal ions have been carried out. **FDf** oligomer exhibited selective chelation of Hg^{2+} ions in THF. Both fluorescence 'turn on' and 'turn off' probe for Hg^{2+} ion using **FDf** have been demonstrated highlighting the potential of DAF derivatives as highly emissive materials for using as fluorescent sensors. We have studied the effect of complexation of **FDf** with metal cations (Li^+ , Na^+ , K^+ , Ag^+ , Mg^{2+} , Ba^{2+} , Cu^{2+} , Ni^{2+} , Pb^{2+} , Hg^{2+} , Fe^{3+} ; perchlorates or nitrates) on its absorption and emission spectra. Adding metal ions decreases absorption intensity, with some red shift for some ions (40 nm for Hg^{2+}). An emission intensity is also decreased but quenching the emission substantially depends on the nature of the cation: (i) only weak quenching was observed by mono-valent metals, as well as for Mg^{2+} , Ba^{2+} and Cu^{2+} ; (ii) moderate quenching was observed by Ni^{2+} , Pb^{2+} and Fe^{3+} cations; (iii) extremely strong quenching has been demonstrated by Hg^{2+} cations. Job's plots

confirm formation of $\mathbf{FDF}:\text{Hg}^{2+} = 2:1$ complex and the detection limit was estimated as low as 3×10^{-7} M of Hg^{2+} . Another important observation was that the formed complex is emissive showing photoluminescence at longer wavelength, in green region (507 nm), and as such complexation can be monitored at two wavelengths (“ON→OFF” for blue emission of \mathbf{FNF} and “OFF→ON” for green emission of $(2\mathbf{FNF}:\text{Hg}^{2+})$). Thus, there is the possibility of fabricating a sensor, which can be selective for Hg^{2+} in presence of other metal ions.

4.4 Experimental

Instrumentation

NMR detail given in Chapter 2. Mass spectra of synthesised compounds were determined using microTOF LC Bruker Daltronics mass spectrometer. Microwave assisted syntheses were performed on a CEM Discover SP microwave reactor. Spin coated films were prepared on spin coater Laurel Technologies, Model WS-650Mz-23NPP/LITE. Some of the synthesised products were purified using Telydyne Isco automatic flash chromatograph model Combiflash Rf 200 using Biotage disposable PTFE columns, hand-filled with silica gel LC60 (40–60 μM).

Absorption and emission spectra

Absorption and emission spectra in solution were measured HPLC grade solvent in 10 mm path length quartz cells and solid state measurement by spin coated film prepared on 12.5 mm circular quartz substance, using Shimadzu UV-3600 UV-Vis-NIR spectrophotometer and Horiba Yvon Fluoromax-4 spectrofluorometer at room temperature. The films were prepared by spin coating at 3000-4000 rpm of oligomer solutions (1-3 mg dissolved in 1 mL of dichloromethane). Photoluminescence quantum yields (PLQY, Φ_{PL}) in solutions for all oligomers were measured in HPLC grade dichloromethane at room temperature according to literature described method.⁶⁰ The values of Φ_{PL} were calculated according to the following formula:⁴⁹

$$\Phi_{\text{PL}} = \Phi_r \times (A/A_r) \times (OD_r/OD) \times (n^2/n_r^2)$$

Where Φ_{PL} is the quantum yield, A is the integrated intensity, OD is the optical density, and n is the refractive index. The subscript r refers to the reference fluorophore of known quantum yield. 9,10-diphenylanthracene (DPA) dilute solution in cyclohexane ($\Phi_r = 90\%$) was used as fluorophore standard. The solutions were bubbled by argon for about 10 minutes to avoid

quenching by dissolved oxygen. Corrected emission and absorption spectrum was used to calculate quantum yields and the results are within 10% accuracy.

Table 4.4 Determination of photoluminescence quantum yields (PLQY, Φ_{PL}) of oligomers in degassed dichloromethane.

Compound	Integral intensity A ($\lambda_{ex} = 350$ nm) (S_{1C}/R_{1C})	Optical density OD	PLQY, Φ_{PL} (%)
9,10-DPA ^a	7.52727×10^7	0.04858	
FDoF ^b	9.75347×10^5	0.05337	1
FFDF	1.04318×10^8	0.07172	84
FDF	1.12848×10^8	0.06955	93
SDS	1.20848×10^8	0.06876	101
DSD	8.53682×10^7	0.0552	89
DDDD)	1.19948×10^8	0.07447	92
DDD	7.76534×10^7	0.04419	101
DD	6.80422×10^7	0.04544	86

^a In degassed cyclohexane, ^b $\lambda_{ex} = 370$ nm, DPA dilute solution in cyclohexane ($\Phi_r = 90\%$) was used as fluorophore standards.⁶¹

PLQY of spin coated film prepared in chloroform on quartz substrate were determined using integrating sphere on Horiba Yvon Fluoromax-4 spectrofluorometer at room temperature. Absolute PLQY values were measured for spin-coated films on quartz substrates using an integrating sphere on Horiba Yvon Fluoromax-4 spectrofluorometer at room temperature.

Cyclic voltammetry

Cyclic voltammetry experiments were conducted in a standard three-electrode configuration, using Metrohm Autolab PGSTAT-302N potentiostat / galvanostat, with iR drop compensation. Platinum disk electrode (d = 1.5 or 2 mm) and platinum wire (d = 0.2 mm) were used as the working and counter electrodes, respectively. The reference electrode was Ag/Ag⁺ (silver wire immersed in mixture of 0.1 M AgNO₃ and 0.1 M Bu₄NPF₆ in acetonitrile, separated from the solution by a Vycor frit). Potentials are referenced with respect to half-wave potential ($E_{1/2}$) of ferrocene, which was used as an internal standard. The average $E_{1/2}$ potentials for Fc/Fc⁺ were 0.20-0.22 V in DCM and 0.19–0.21 V in THF. Oxidation scans were performed in DCM

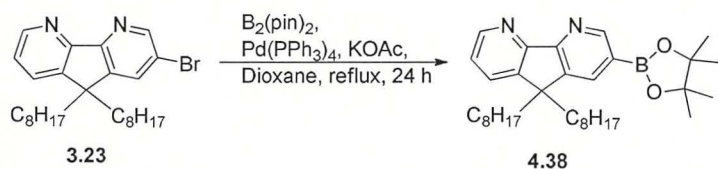
containing 0.2 M Bu₄NPF₆, reduction scans were carried out in freshly distilled THF containing 0.2 M Bu₄NPF₆, under argon.

Synthesis

General procedure for reaction involving Pd-catalysed reaction: under inert atmosphere, flame heated three-neck flask fitted with nitrogen inlet was charged with borate component, halogenated component, base and degassed solvents. The mixture were degassed with argon for 15 minutes before adding Pd-catalyst and degassed again for another 15–20 minutes. The degassed mixture was stirred under reflux for a certain period depending on the substrate. After cooling, the solvent was removed under reduce pressure on rotavapor. The residue was dissolved in EA/DCM, washed with water, dried over MgSO₄, and evaporated to afford the crude product, which was then purified by flash chromatography on silica gel eluting with appropriate solvent (basing on preliminary TLC tests).

9,9-Dioctyl-2-(4,4,5,5-tetramethyl-1,3,2-dioxaborolan-2-yl)-4,5-diazafluorene (4.38)

Exp: SG-065

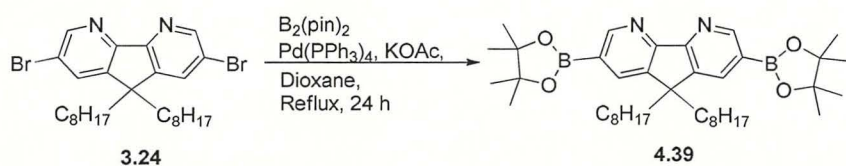


Under nitrogen, a three-neck flask was charged with 9,9-dioctyl-2-bromo-4,5-diazafluorene (**3.23**) (1.02 g, 2.11 mmol), bis(pinacolato)diborolane (1.03 g, 4.22 mmol), Pd(PPh₃)₄ (243 mg, 10 mol %), potassium acetate (620 mg, 6.11 mmol) and anhydrous dioxane (20 mL, freshly distilled over Na) at room temperature. The mixture was degassed by bubbling with nitrogen for 15 minutes and then was stirred under reflux (oil bath, 115 °C) for 4 hours under nitrogen atmosphere. The mixture was cool down to room temperature, filtered through short silica gel layer, which was then washed with ethyl acetate (50 mL). The combined filtrates were evaporated on a rotary evaporator to afford the crude product (1.81 g) as brown oil. The crude product was purified by flash chromatography on silica gel eluting with PE:EA (gradually increasing the ratio from 4:1 to 1:1) to afford product **4.38** (321 mg, 29.8 %) as a brown oil. ¹H NMR purity ca. 80%. The partially pure product was used in the next step without further purification.

¹H NMR (500 MHz, CDCl₃): δ (ppm) 9.05 (1H, d, *J* = 1.4 Hz), 8.69 (1H, dd, *J* = 4.8, 1.4 Hz), 8.04 (1H, d, *J* = 1.4 Hz), 7.71 (1H, dd, *J* = 7.7, 1.5 Hz), 7.29 (1H, dd, *J* = 7.6, 4.8 Hz), 2.03–1.96 (4H, m, CH₂C₇H₁₅), 1.24 (12H, s, CH₃ borolane), 1.23–0.99 (20H, m, (CH₂)₂(CH₂)₅CH₃), 0.81 (6H, t, *J* = 7.2 Hz, CH₃ octyl), 0.68–0.57 (4H, m, CH₂CH₂C₆H₁₃).

9,9-Dioctyl-2,7-bis(4,4,5,5-tetramethyl-1,3,2-dioxaborolan-2-yl)-4,5-diazafluorene (4.39)

Exp:SG-149



Under nitrogen, a two-neck flask was charged with 9,9-dioctyl-2,7-dibromo-4,5-diazafluorene (**3.24**) (202 mg, 0.365 mmol), bis(pinacolato)diboron (370 mg, 1.46 mmol), dry potassium acetate (107 mg, 1.10 mmol), Pd(PPh₃)₄ (21 mg, 0.018 mmol) and dry dioxane (10 mL, freshly distilled over Na). The mixture was degassed with nitrogen for 15 minutes and then reflux (oil bath 115 °C) with stirring for 24 hours under nitrogen atmosphere. After cooling, the mixture was evaporated on rotavapor, the residue was dissolved in ethyl acetate (30 mL), washed with brine (20 mL) followed by water (3 × 20 mL), dried over anhydrous MgSO₄, filter off and evaporated on rotavapor to afford the crude product (289 mg) as brown oil. The crude product was purified by flash chromatography on silica gel eluting with PE: EA (gradient ratio of 9:1 to 1:1) to afford the two fractions: analytically pure product **4.39** (36 mg, 15.2%) as a white solid and less pure product **4.39** (189 mg, 79.1%) as a yellowish semi solid.

¹H NMR (400 MHz, CDCl₃): δ (ppm) 9.06 (2H, d, *J* = 2.3 Hz), 8.05 (2H, d, *J* = 2.2 Hz), 2.03–1.99 (4H, m, CH₂C₇H₁₅), 1.40–1.02 (44H, m, (CH₂)₂(CH₂)₅CH₃ + CH₃ borolane), 0.81 (6H, t, *J* = 7.0 Hz, CH₃ octyl), 0.65–0.53 (4H, m, CH₂CH₂C₆H₁₃).

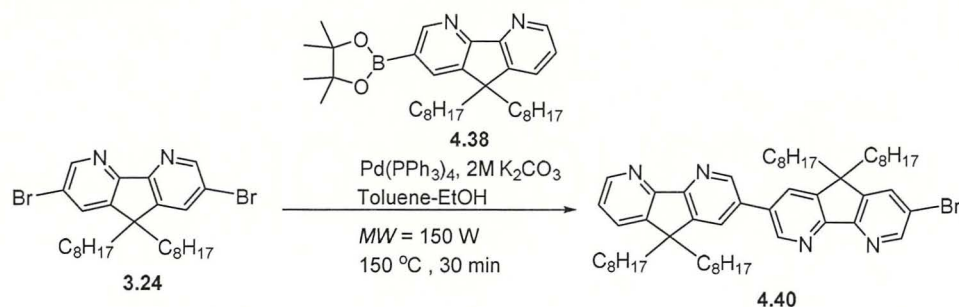
¹³C NMR (100 MHz, CDCl₃): δ (ppm) 160.71, 155.77, 144.62, 136.39, 123.38, 84.27, 51.57, 39.06, 31.71, 29.79, 29.09, 24.92, 23.86, 22.56, 14.04.

DEPTQ NMR (100MHz, CDCl₃): δ (ppm) 160.76 (CH), 155.81, 144.61 (CH), 136.38, 84.27, 51.58 (C-9), 39.06, 31.71, 29.80, 29.08, 24.93 (CH₃ borolane), 23.87, 22.56, 14.05 (CH₃ octyl).

MS (ESI⁺) *m/z*: 645.50 ([M+H]⁺, 80%). Calcd. for C₃₉H₆₂B₂N₂O₄: 644.49.

7-Bromo-5,5,5',5'-tetraoctyl-5H,5'H-3,3'-bi(cyclopenta[1,2-b:5,4-b']dipyridine) (5)

Exp.SG-108



Under argon, in a thick walled 30 mL MW reactor pyrex tube, 9,9-dioctyl-2-(4,4'-5,5'-tetramethyl-1,3,2-dioxaborolanyl)-4,5-diazafluorene (**4.38**) (251 mg, 0.482 mmol) and 9,9-dioctyl-2,7-dibromo-4,5-diazafluorene (**3.24**) (794 mg, 1.45 mmol), 10% aqueous K₂CO₃ (2 mL, 1.4 mmol) was added into solution of toluene (12 mL) and ethanol (2 mL). The mixture was degassed for 15 minutes before Pd(PPh₃)₄ (11 mg, 2 mol%) was added and degassed for another 20 minutes. The mixture was stirred at 150 °C in a microwave reactor (max irradiating power being 150 W) for 30 minutes. After cooling, the mixture was diluted with water (30 mL) and extracted with ethyl acetate (2 × 20 mL). The combined organic layers were washed with water (2 × 20 mL), dried over anhydrous MgSO₄, filtered off and evaporated to afford the crude product as brown oil (833 mg). The crude product was purified by flash chromatography on silica gel eluting with PE:EA (gradient from 9:1 to 1:1) to afford pure product **4.40** (164 mg, 39 %) as a white solid, along with unreacted starting dibromide **3.24** (472 mg) recovered as a white solid.

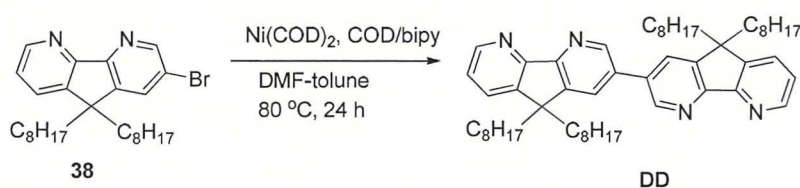
¹H NMR (500 MHz, CDCl₃): δ (ppm) 8.98 (2H, d, *J* = 1.9 Hz), 8.79 (1H, dd, *J* = 2.1, 0.7 Hz), 8.75 (1H, dd, *J* = 4.6, 1.7 Hz), 7.95 (2H, d, *J* = 1.8 Hz), 7.88 (1H, dd, *J* = 2.0, 0.7 Hz), 7.77 (1H, d, *J* = 7.5 Hz), 7.35 (1H, dd, *J* = 4.9, 2.2 Hz), 2.10–2.01 (8H, m), 1.24–1.10 (40H, m), 0.82–0.78 (12H, m) 0.77–0.72 (8H, m).

¹³C NMR (100 MHz, CDCl₃): δ (ppm) 158.58, 157.94, 157.31, 156.56, 150.89, 149.83, 148.90, 148.59, 147.20, 145.47 (2 × C), 145.36, 133.74, 133.55, 133.07, 130.78, 128.84, 128.75, 123.22, 120.69, (51.78, 51.60), (39.19, 39.10), 31.69, (29.85, 29.80), 29.14, (29.12, 29.09), 24.13, 22.55, 14.03. DEPTQ NMR (100 MHz, CDCl₃): δ (ppm) 158.58, 157.94, 157.31, 156.56, 150.89 (CH), 149.83 (CH), 148.90 (CH), 148.59 (CH), 147.20, 145.47 (2×C), 145.36, 133.74 (CH), 133.55, 133.07, 130.78 (CH), 128.84 (CH), 128.74 (CH), 123.22 (CH), 120.69, [51.78, 51.60 (C-9)], [39.19, 39.10 (CH₂)], 31.69 (CH₂), [29.85, 29.80 (CH₂)], [29.14,

29.12 (CH₂), 29.09 (CH₂), 24.13 (CH₂), 22.55 (CH₂), 14.03 (CH₃). MS (ESI⁺) *m/z*: 861.37 ([M+H]⁺, 100%, ⁷⁹Br), 863.36 ([M+H]⁺, 98%, ⁸¹Br). Calcd. for C₅₄H₇₇BrN₄: 860.53.

Di(9,9-dioctyl-4,5-diazafluorene) (DD)

Exp.: SG-092



Under argon atmosphere, in a two-neck flask bis(1,5-cyclooctadiene)nickel(0) (38 mg, 0.138 mmol), 1,5-cyclooctadiene (15 mg, 0.138 mmol) and 2,2'-bipyridine (22 mg, 0.138 mmol) in dry DMF (0.5 mL) were stirred at 80 °C for 30 min, resulting in a blue colour solution of the complex. To this, a solution of 2-bromo-9,9-dioctyl-4,5-diazafluorene (**3.23**) (22 mg, 0.046 mmol) in dry degassed toluene (50 mL) was added and the mixture was stirred at 80 °C for 24 hours. After cooling to room temperature, the mixture was filtered through the Celite 521 pad, which was then washed with PE (50 mL). The combined filtrates were evaporated on a rotavapor to afford the crude product (100 mg) as a brown oil. The crude product was purified by flash chromatography on silica gel eluting with PE:EA in the ratio 9:1 to afford pure dimer **DD** (27 mg, 64%) as a light yellow solid.

¹H NMR (500 MHz, CDCl₃): δ (ppm) 8.98 (2H, d, *J* = 2.0 Hz, H-6,6'), 8.74 (2H, dd, *J* = 4.9, 1.4 Hz, H-3,3'), 7.97 (2H, d, *J* = 2.0 Hz, H-8,8'), 7.76 (2H, dd, *J* = 7.7, 1.3 Hz, H-1,1'), 7.34 (2H, dd, *J* = 7.6, 4.6 Hz, H-2,2'), 2.10–2.06 (8H, m, CH₂C₇H₁₅), 1.21–1.17 (40H, m, (CH₂)₂(CH₂)₅CH₃), 0.80 (12H, t, *J* = 7.0 Hz, CH₃), 0.77–0.74 (8H, m, CH₂CH₂C₆H₁₃).

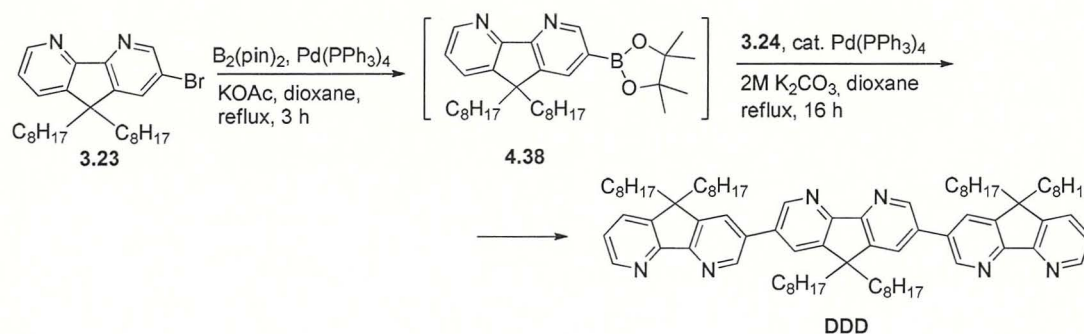
¹³C NMR (100 MHz, CDCl₃): δ (ppm) 158.42, 158.02, 149.79, 148.60, 145.46 (× 2), 133.33, 130.77, 128.77, 123.17, 51.60 (C-9), 39.22, 31.70, 29.87, 29.15, 29.09, 24.13, 22.56, 14.04 (CH₃).

MS (ESI⁺) *m/z*: 783.55 ([M+H]⁺, 100%).

GC-MS (TOF, EI⁺) *m/z*: 782.80 ([M]⁺, 100%) Calcd. for C₅₄H₇₈N₄: 782.62.

Tri(9,9-dioctyl-4,5-diazafluorene) (DDD)

Exp: SG-064



Under nitrogen, a two-neck flask was charged with 9,9-dioctyl-2-bromo-4,5-diazafluorene (**3.23**) (300 mg, 0.633 mmol), bis(pinacolato)diboron (301 mg, 1.18 mmol), $Pd(PPh_3)_4$ (75 mg, 10 mol%), dry potassium acetate (180 mg, 1.83 mmol) and anhydrous dioxane (10 mL, freshly distilled from Na). The mixture was degassed with nitrogen for 15 min and then reflux (oil bath 115 °C) with stirring for 3 hours under nitrogen atmosphere. The mixture was allowed to cooled down to room temperature and then 9,9-dioctyl-2,7-dibromo-4,5-diazafluorene (**3.24**) (100 mg, 0.182 mmol), 2M aqueous K_2CO_3 (2 mL, 4 mmol) and $Pd(PPh_3)_4$ (33 mg, 5 mol%) were quickly added under continuous nitrogen flow. The mixture was reflux again for next 16 hours under nitrogen atmosphere. After cooling to room temperature, the mixture was evaporated to dryness under reduced pressure, the residue was dissolved in ethyl acetate (100 mL), washed with water (3×50 mL), dried over anhydrous $MgSO_4$, filtered off and evaporated on a rotavapor to afford the crude product as a yellow solid (230 mg). The crude product was purified by flash chromatography on silica gel (3×15 cm sized column) eluting first with DCM and then with DCM:MeOH mixture (gradient from 100:1 to 100:2) to afford pure trimer **DDD** (54 mg, 26%) as a yellow solid.

1H NMR (400 MHz, $CDCl_3$): δ (ppm) 9.01 (4H, dd, $J = 8.4, 1.9$ Hz), 8.75 (2H, dd, $J = 4.8, 1.2$ Hz), 7.99 (4H, dd, $J = 11.7, 2.0$ Hz), 7.77 (2H, dd, $J = 7.7, 1.3$ Hz), 7.33 (2H, dd, $J = 7.6, 4.8$ Hz), 2.20–2.16 (4H, m), 2.12–2.67 (8H, m), 1.25–1.03 (60H, m), 0.87–0.74 (30H, m).

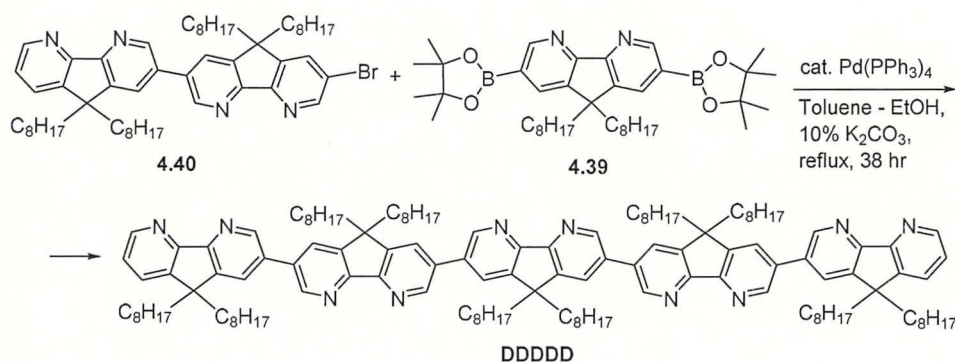
^{13}C NMR (100 MHz, $CDCl_3$): δ (ppm) 158.54, 157.97, 157.84, 149.83 (CH), 148.88 (CH), 148.64 (CH), 145.96, 145.49 ($\times 2$), 133.61, 133.21, 130.80 (CH), 128.90 (CH), 128.79 (CH), 123.23 (CH), (52.84, 51.61), 39.21 ($\times 2$), (32.71, 31.68.), (29.87, 29.71), 29.16 ($\times 2$), 29.11 ($\times 2$), (24.26, 24.16), (22.57, 22.55), (14.04, 14.02, CH_3).

DEPTQ NMR (100MHz, CDCl₃): δ (ppm) 158.56, 158.00, 157.85, 149.84 (CH), 148.89 (CH), 148.65 (CH), 145.94, 145.47 (×2), 133.61, 133.21, 130.78 (CH), 128.89 (CH), 128.78 (CH), 123.21 (CH), (51.84, 51.62), 39.22 (×2), (31.72, 31.68), (29.87, 29.71), 29.16 (×2), 29.11 (×2), (24.26, 24.16), 22.57 (×2), (14.04, 14.02, CH₃).

MS (ESI⁺) *m/z*: 1174.92 (([M+H]⁺, 100%) Calcd. for C₈₁H₁₁₆N₆: 1172.93.

Penta(9,9-dioctyl-4,5-diazafluorene) (DDDDD)

Exp.: SG-150



In a two-neck flask, 9,9-dioctyl-2,5-bis(4,4'-5,5'-tetramethyl-1,3,2-dioxaborolane)-4,5-diazafluorene (32 mg, 0.050 mmol) (**4.39**), 2-bromo-9,9,9',9'-tetraoctyl-7,7'-bis(4,5-diazafluorene) (**4.40**) (91 mg, 0.104 mmol) and 10 w% aqueous K₂CO₃ (1.5 mL, 1.1 mmol) was added into a solution of toluene (4 mL) and ethanol (1 mL). The mixture was degassed with argon for 15 minutes before Pd(PPh₃)₄ (3 mg, 5 mol%) was added and degassed again for another 20 minutes. The mixture was reflux (oil bath 115 °C) with stirring for 38 hours under nitrogen atmosphere. After cooling to room temperature, excess solvent was removed under reduced pressure on a rotavapor until dryness. The yellowish residue was stirred with a mixture of diethyl ether (5 mL) and PE (5 mL) for 20 minutes. The precipitate was collected by filtration, which was washed with water (2 × 5 mL) and dried *in vacuo* to afford the crude product as a light greenish-yellow solid (98 mg). The crude product was recrystallised from methanol (15 mL) to afford the product as a gray solid (41 mg). It was further purified by column chromatography on silica gel eluting with DCM:MeOH in the ratio 95:5 to afford pure pentamer **DDDDD** as a light yellow solid (34 mg, 35%).

¹H NMR (400 MHz, CDCl₃): δ (ppm) 9.06–9.02 (8H, m), 8.76 (2H, d, *J* = 4.0 Hz), 8.04–7.99 (8H, m), 7.78 (2H, d, *J* = 7.3 Hz), 7.37–7.35 (2H, m), 2.25–2.06 (20H, m, CH₂C₇H₁₅), 1.25–1.04 (100H, m, (CH₂)₂(CH₂)₅CH₃), 0.94–0.71 (50H, m, CH₂CH₂(CH₂)₅CH₃).

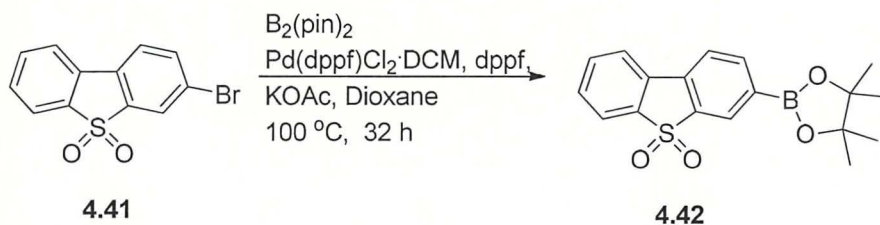
^{13}C NMR (100 MHz, CDCl_3): δ (ppm) 158.58, 157.97 ($\times 2$), 157.91, 157.78, 149.84 (CH), 148.93 [$\times 2$ (CH)], 148.64 (CH), 146.04, 146.01 ($\times 2$), 145.51 ($\times 2$), 133.68, 133.54, 133.46, 133.19, 130.80 (CH), 128.93 [$\times 3$ (CH)], 128.79 (CH), 123.24 [$\times 2$ (CH)], (51.87, 51.62), 39.22 ($\times 2$), (31.72, 31.70), 29.86 ($\times 2$), 29.17 ($\times 2$), 29.10 ($\times 2$), (24.29, 24.16), 22.57 ($\times 2$), 14.03 ($\times 2$).

DEPTQ NMR (100MHz, CDCl_3): δ (ppm) 158.57, 157.96, 157.91, 157.77, 149.84 (CH), 148.92 (CH), 148.63 (CH), 146.02, 145.99, 145.49, 133.67, 133.53, 133.45, 133.17, 130.79 (CH), 128.92 (CH), 128.79 (CH), 123.24, (51.86, 51.62), 39.22 ($\times 2$), (31.71, 31.69), 29.85 ($\times 2$), 29.16 ($\times 2$), 29.10 ($\times 2$), (24.28, 24.15), 22.56 ($\times 2$), 14.03 ($\times 2$).

MS (MALDI-TOF) m/z : 1954.83 ($[\text{M}+\text{H}]^+$, 100%). Calcd. for $\text{C}_{135}\text{H}_{192}\text{N}_{10}$: 1953.53.

3-(4,4,5,5-Tetramethyl-1,3,2-dioxaborolan-2-yl)dibenzothiophenes-*S,S*-dioxide (4.43)

Exp: SG143



Under argon, in a two necked flask (100 mL) charged with 3-bromodibenzothiophene-*S,S*-dioxide **4.41** (1.01 g, 3.39 mmol), bis(pinacolato)diboron (1.29 g, 5.08 mmol), anhydrous KOAc (1.25 g, 0.01 mol), 1,1'-bis(diphenylphosphino)ferrocene (dppf) (70 mg, 0.13 mmol) and dry dioxane (50 mL) were degassed with argon for 15 minutes before $\text{Pd}(\text{dppf})\text{Cl}_2 \cdot \text{DCM}$ (104 mg, 3 mol%) added and degassed for another 15 minutes. The mixture was heated at $100\text{ }^\circ\text{C}$ for 32 hours under argon atmosphere. After cooling to room temperature, the solvent dioxane was removed under reduced pressure and the residue was diluted with water (50 mL). The aqueous solution was then extracted with dichloromethane ($2 \times 50\text{ mL}$), washed with water ($2 \times 20\text{ mL}$), dried over anhydrous MgSO_4 . The dichloromethane solution (black colour) was then passed through a short silica gel bed eluting with DCM (100 mL) to give a clear solution which was concentrated to afford the product **4.42** as an off white solid (1.05 g, 91%). ^1H NMR purity ca. 80% with the main other component being the unreacted excess bis(pinacolato)diboron. The product was used in the next step reaction without further purification.

$^1\text{H NMR}$ (400 MHz, CDCl_3): δ (ppm) 8.28 (1 H, s), 8.05 (1 H, dd, $J = 7.7, 0.7$ Hz), 7.80 (3 H, m), 7.64 (1 H, td, $J = 7.7, 1.0$ Hz), 7.54 (1H, td, $J = 7.6, 0.8$ Hz), 1.36 (12 H, s).

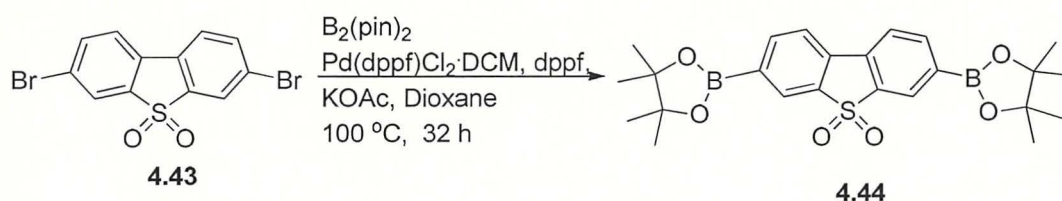
$^{13}\text{C NMR}$ (101 MHz, CDCl_3): δ (ppm) 140.12, 138.10, 137.13, 133.81, 133.80, 132.03(br.), 131.54, 130.75, 128.34, 122.16, 121.93, 120.75, 84.56, 24.87.

DEPTQ NMR (101 MHz, CDCl_3): δ (ppm) δ 140.12(CH), 138.10, 137.13, 133.81(CH), 131.54, 130.75(CH), 128.35(CH), 122.17(CH), 121.93(CH), 120.75(CH), 83.50, 24.87(CH₃).

$\text{MS (EI}^+)$ m/z : 341.99 ($[\text{M}]^+$, 100%). (Calcd. for $\text{C}_{18}\text{H}_{19}\text{BO}_4\text{S}$: 342.11).

3,7-Bis(4,4,5,5-tetramethyl-1,3,2-dioxaborolan-2-yl)dibenzothiophene-*S,S*-dioxide (4.44)

Exp: SG-144



Under nitrogen, in a two-necked flask (100 mL) charged with 3,8-dibromodibenzothiophene-*S,S*-dioxide **4.43** (1.01 g, 2.70 mmol), bis(pinacolato)diboron (1.49 g, 5.88 mmol), anhydrous KOAc (1.57 g, 15.99 mmol), dppf (89 mg, 0.16 mmol) and dry dioxane (50 mL) were degassed with argon for 15 minutes before $\text{Pd}(\text{dppf})\text{Cl}_2 \cdot \text{DCM}$ (131 mg, 0.16 mmol) was added and degassed for another 15 minutes. The mixture was heated at $100\text{ }^\circ\text{C}$ for 32 hours under argon atmosphere. After cooling to room temperature, the solvent dioxane was removed under reduced pressure and the residue was diluted with water (50 mL). The aqueous solution was extracted with dichloromethane (2×50 mL), washed with water (2×20 mL), dried with anhydrous MgSO_4 . The dichloromethane solution (black colour) was then passed through a short silica gel bed eluting with dichloromethane (100 mL) to give a clear solution which was concentrated to afford the product **4.44** as an off white solid (1.01 g, 85%).

$^1\text{H NMR}$ (400 MHz, CDCl_3): δ (ppm) 8.28 (1H, s), 8.05 (1H, d, $J = 8.1$ Hz), 7.80 (1H, d, $J = 7.7$ Hz), 1.36 (12H, s).

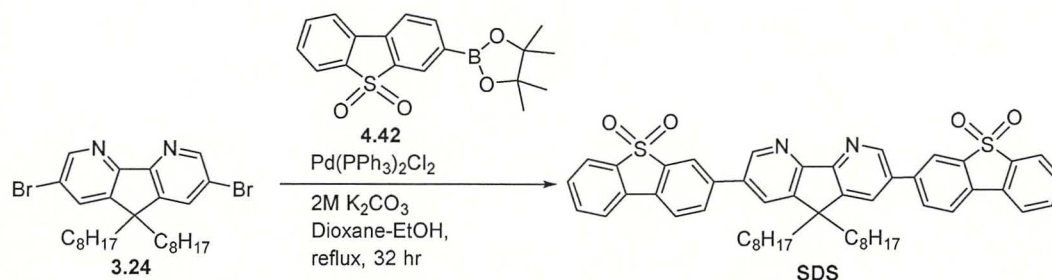
$^{13}\text{C NMR}$ (101 MHz, CDCl_3): δ (ppm) 140.05 (CH), 137.50, 133.73, 132.37 (br.), 128.33 (CH), 121.09 (CH), 84.56, 24.87 (CH₃).

DEPTQ NMR (101 MHz, CDCl₃): δ (ppm) (101 MHz, CDCl₃) 140.05 (CH), 137.49, 133.73, 128.33 (CH), 121.09 (CH), 84.56, 24.87 (CH₃).

MS (EI⁺) m/z : 468.12 ([M]⁺, 100%). (Calcd. for C₂₄H₃₀B₂O₆S: 468.19).

2,7-Bis(dibenzothiophene-*S,S*-dioxide-3-yl)-4,5-diazfluorene (SDS)

Exp: SG-145



In a three-necked flask (50 mL), charged with 2,7-dibromo-9,9-dioctyl-4,5-diazafluorene (**3.24**) (150 mg, 0.272 mmol), 3-(4,4,5,5-tetramethyl-1,3,2-dioxaborolan-2-yl)dibenzothiophene-*S,S*-dioxide (**4.42**) (373 mg, 0.290 mmol), 2M aqueous K₂CO₃ (4 mL, 8 mmol), dioxane (20 mL) and ethanol (4 mL) were degassed with argon for 15 minutes before adding Pd(PPh₃)₂Cl₂ (6 mg, 0.008 mmol) and degassed again for another 15 minutes. The mixture was reflux (oil bath 115 °C) with stirring for 32 hours under nitrogen atmosphere. After cooling to room temperature, the mixture was diluted with water (15 mL) and then extracted with DCM (2 × 100 mL). The combined DCM layers were washed with water (2 × 20 mL), dried with anhydrous MgSO₄, filtered off and evaporated on a rotavapor to afford the crude product as a brown oil (580 mg). The crude product was purified by flash chromatography on silica gel eluting with DCM: MeOH mixture (gradient ratio of 100:1 to 100:2) to afford pure oligomer **SDS** as an off yellow solid (60 mg, 26%).

¹H NMR (400 MHz, CDCl₃): δ (ppm) 9.03 (2H, d, $J = 1.9$ Hz), 8.15 (2H, d, $J = 1.12$ Hz), 8.00–7.95 (6H, m), 7.89 (4H, d, $J = 8.0$ Hz), 7.72 (2H, t, $J = 7.5$ Hz), 7.60 (2H, t, $J = 7.6$ Hz), 2.16–2.12 (4H, m, CH₂C₇H₁₅), 1.28–1.11 (20H, m, C₂H₄(CH₂)₅CH₃), 0.79 (6H, t, $J = 6.0$ Hz, C₇H₁₄CH₃), 0.78–0.71 (4H, m, CH₂CH₂C₆H₁₃).

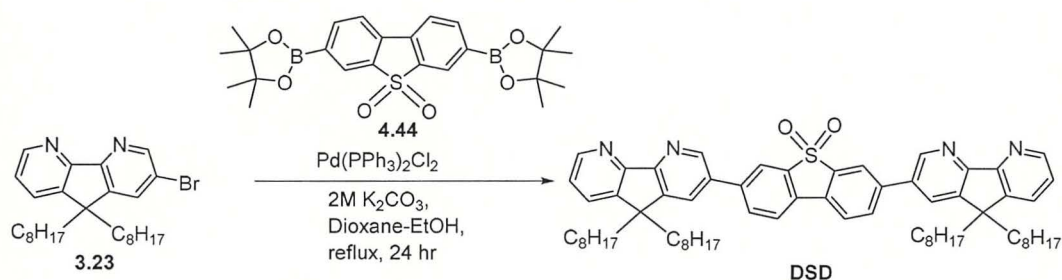
^{13}C NMR (100MHz, CDCl_3): δ (ppm) 158.14, 148.50 (CH), 146.13, 140.72, 138.92, 137.92, 134.15, 134.12 (CH), 132.69 (CH), 131.22, 131.18, 130.68 (CH), 128.78 (CH), 122.41(CH), 122.34 (CH), 121.87 (CH), 120.91 (CH), 51.94, 39.39 (CH_2), 31.63 (CH_2), 29.92 (CH_2), 29.19 (CH_2), 29.16 (CH_2), 24.30 (CH_2), 22.57 (CH_2), 14.04 (CH_3).

DEPTQ NMR (100MHz, CDCl_3): δ (ppm) 158.14, 148.50 (CH), 146.13, 140.73, 138.92, 137.92, 134.16, 134.12 (CH), 132.70 (CH), 131.19, 130.69 (CH), 128.79 (CH), 122.42 (CH), 122.33 (CH), 121.86 (CH), 120.92 (CH), 51.94, 39.39 (CH_2), 31.70 (CH_2), 29.92 (CH_2), 29.19 (CH_2), 29.17 (CH_2), 24.29 (CH_2), 22.57 (CH_2), 14.04 (CH_3).

MS (ESI $^+$) m/z : 843.39 ($[\text{M}+\text{Na}]^+$, 100%). Calcd. for $\text{C}_{51}\text{H}_{52}\text{N}_2\text{O}_4\text{S}_2$: 820.34.

3,7-Bis(9,9-dioctyl-4,5-diazafluoren-2-yl)dibenzothiophene-*S,S*-dioxide (DSD)

Ex. No. SG-146



In a three-necked flask, charged with 2-bromo-9,9-dioctyl-4,5-diazafluorene (**3.23**) (402 mg, 0.854 mmol), 3,7-bis(4,4,5,5-tetramethyl-1,3,2-dioxaborolan-2-yl)dibenzothiophene-*S,S*-dioxide (**4.44**) (200 mg, 0.427 mmol), 2M aqueous K₂CO₃ (4 mL, 8 mmol), 1,4-dioxane (20 mL) and ethanol (2 mL) were degassed with argon for 15 minutes before Pd(PPh₃)₂Cl₂ (10 mg, 0.014 mmol) added and degassed again for another 15 minutes. The mixture was reflux (oil bath, T= 115 °C) with stirring for 24 hours under nitrogen atmosphere. After cooling to room temperature, the solvent was evaporated under reduced pressure on a rotavapor. The residue was dissolved in ethyl acetate (100 mL), washed with water (2 × 50 mL), dried over anhydrous MgSO₄, filtered off and evaporated to afford the crude product as a brown oil (788 mg). The crude product was purified by flash chromatography on silica gel eluting with PE:EA (gradient from 1:1 to 1:9) to afford pure oligomer **DSD** as a yellow solid (152 mg, 59%).

$^1\text{H NMR}$ (400 MHz, CDCl_3): δ (ppm) 9.00 (2H, d, $J = 2.0$ Hz), 8.74 (2H, dd, $J = 4.8, 1.2$ Hz), 8.16 (2H, d, $J = 0.8$), 8.05–7.99 (4H, m), 7.95 (2H, d, $J = 2.0$ Hz), 7.76 (2H, dd, $J = 7.6, 1.2$ Hz), 7.33 (2H, dd, $J = 7.6, 4.8$ Hz), 2.10–2.06 (8H, m, $\text{CH}_2\text{C}_7\text{H}_{15}$), 1.25–1.08 (40H, m, $\text{C}_2\text{H}_4(\text{CH}_2)_5\text{CH}_3$), 0.79 (12H, t, $J = 7.2$ Hz, $\text{C}_7\text{H}_{14}\text{CH}_3$), 0.72–0.66 (8H, m, $\text{CH}_2\text{CH}_2\text{C}_6\text{H}_{13}$).

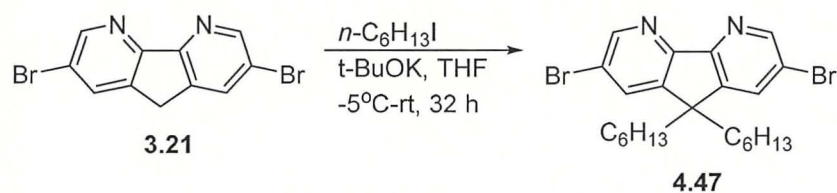
$^{13}\text{C NMR}$ (100MHz, CDCl_3): δ (ppm) 159.01, 157.78, 149.88 (CH), 148.18 (CH), 145.64, 145.55, 141.17, 139.00, 133.65, 132.87 (CH), 130.79, 130.65 (CH), 128.69 (CH), 123.37 (CH), 122.52 (CH), 121.03 (CH), 51.66 (C-9), 39.31 (CH_2), 31.72 (CH_2), 29.90 (CH_2), 29.18 (CH_2), 29.14 (CH_2), 24.16 (CH_2), 22.58 (CH_2), 14.05 (CH_3).

DEPTQ NMR (100 MHz, CDCl_3): δ (ppm) 159.01, 157.82, 149.91 (CH), 148.20 (CH), 145.61, 145.52, 141.19, 138.98, 133.63, 132.86 (CH), 130.76, 130.64 (CH), 128.66 (CH), 123.35 (CH), 122.51 (CH), 121.03 (CH), 51.66 (C-9), 39.31 (CH_2), 31.72 (CH_2), 29.18 (CH_2), 29.14 (CH_2), 24.16 (CH_2), 22.57 (CH_2), 14.05 (CH_3).

MS (ESI $^+$) m/z : 1020.42 ($[\text{M}+\text{Na}]^+$, 100%). Calcd. for $\text{C}_{66}\text{H}_{84}\text{N}_4\text{O}_2\text{S}$: 996.63.

2,7-Dibromo-9,9-dihexylfluorene-4,5-diazafluorene (4.45)

Exp. AS211B



Under nitrogen, to a stirred mixture of 2,7-dibromo-9,9-dihexyl-4,5-diazafluorene (**3.21**) (1.0 g, 3.06 mmol) and dry THF (20 mL) was added n -iodohexane (0.95 mL, 6.44 mmol) at -5°C . Then a solution of potassium tert-butoxide (720 mg, 6.44 mmol) in dry THF (15 mL) was added over a period of 50 min at -5°C . After addition, the reaction mixture was allowed to warm up slowly to room temperature and continued stirring for 32 hours at room temperature. The solvent was removed on rotavapour. The residue was purified via column chromatography on silica gel (column size = 2×20 cm) eluting with isooctane:EA in the ratio 10:1 to afford product (1.2 g) as a yellow solid (1.2 g). The product was further purified by recrystallisation with the solution (25 mL) of isopropanol and water in the ratio 5:1 to yield **4.45** as a light yellow solid (1.04g, 69%).

$^1\text{H NMR}$ (400 MHz, CDCl_3): δ (ppm) 8.75 (2H, d, $J = 2.0$ Hz), 7.84 (2H, d, $J = 2.0$ Hz), 2.06–1.87 (4H, m, $\text{CH}_2\text{C}_5\text{H}_{11}$), 1.22–0.97 (12H, m, $\text{C}_2\text{H}_4(\text{CH}_2)_3\text{CH}_3$), 0.79 (6H, t, $J = 7.1$ Hz, $\text{C}_5\text{H}_{10}\text{CH}_3$), 0.73–0.60 (4H, m, $\text{CH}_2\text{CH}_2\text{C}_4\text{H}_9$).

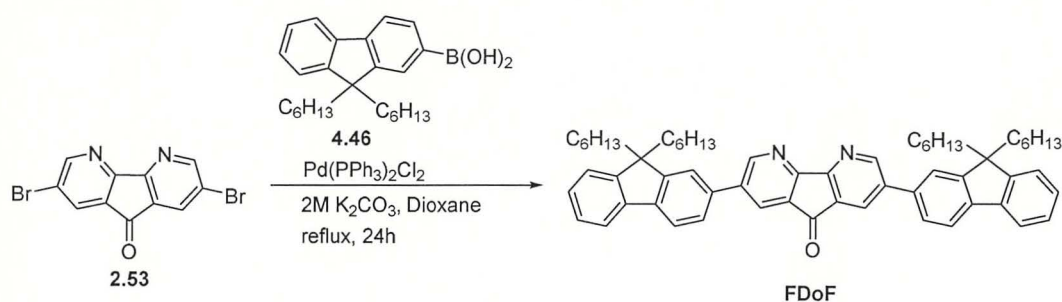
$^{13}\text{C NMR}$ (101 MHz, CDCl_3): δ (ppm) 155.93, 150.93, 146.59, 133.50, 120.79, 51.56, 39.01, 31.35, 29.45, 24.01, 22.49, 13.93.

DEPTQ NMR (101 MHz, CDCl_3): 156.04, 150.93 (CH), 146.59, 133.50 (CH), 120.79, 51.70 (C-9), 39.01 ($\text{CH}_2\text{C}_5\text{H}_{11}$), 31.35 ($\text{C}_2\text{H}_4\text{CH}_2\text{C}_3\text{H}_7$), 29.45 ($\text{C}_3\text{H}_6\text{CH}_2\text{C}_2\text{H}_5$), 24.01 ($\text{CH}_2\text{CH}_2\text{C}_4\text{H}_9$), 22.49 ($\text{C}_4\text{H}_8\text{CH}_2\text{CH}_3$), 13.93 ($\text{C}_5\text{H}_{10}\text{CH}_3$).

$\text{MS (ESI}^+) m/z$: 491.97 ($[\text{M}+\text{H}]^+$, 50%, ^{79}Br , ^{79}Br), 494.00 ($[\text{M}+\text{H}]^+$, 100%, ^{79}Br , ^{81}Br), 495.92 ($[\text{M}+\text{H}]^+$, 51%, ^{81}Br , ^{81}Br). Calcd. for $\text{C}_{23}\text{H}_{30}\text{Br}_2\text{N}_2$: 492.08

3,7-Bis(9,9-dihexylfluoren-2-yl)-4,5-diazafluoren-9-one (FDoF)

Exp: SG-005



Under nitrogen, in three-necked flask 2,7-dibromo-4,5-diazafluoren-9-one (**2.53**) (201 mg, 0.58 mmol), 9,9-dihexylfluoren-2-boronic acid (**4.46**) (453 mg, 1.20 mmol) and Pd(PPh₃)₂Cl₂ (9 mg, 2 mol%), degassed 2M aqueous K₂CO₃ (4 mL, 8 mmol) and 1,4-dioxane (10 mL) were added via a syringe. The reaction mixture was stirred under reflux (oil bath 110 °C) for 24 hours under nitrogen, with protection from sunlight. The reaction mixture was cool down to room temperature and the resulting slurry was poured into 5% NaCl aqueous solution. The product was extracted with dichloromethane (50 mL), the organic layer was washed with water until pH = 7, dried over anhydrous MgSO₄, filtered off and the solvent was evaporated to afford the crude product (405 mg, 79%) as yellow solid. The crude product was purified by flash chromatography on silica gel, eluting first with PE and then with PE:DCM mixture (gradient from 1:1 to 1:4 v/v ratio) to yield pure product **FDoF** (252 mg, 49%) as a yellow solid.

$^1\text{H NMR}$ (400 MHz, CDCl_3): δ (ppm) 9.12 (2H, d, $J = 2.1$ Hz), 8.28 (2H, $J = 2.1$ Hz, s), 7.83 (2H, d, $J = 7.9$ Hz), 7.77–7.75 (2H, m), 7.65 (2H, dd, $J = 7.8, 1.5$ Hz), 7.60 (2H, d, $J = 1.2$ Hz), 7.40–7.34 (6H, m), 2.06–2.02 (8H, m , $\text{CH}_2\text{C}_5\text{H}_{11}$), 1.13–1.02 (24H, m , $\text{C}_2\text{H}_4(\text{CH}_2)_3\text{CH}_3$), 0.77 (12H, t, $J = 6.8$ Hz, CH_3), 0.67–0.61 (8H, m , $\text{CH}_2\text{CH}_2\text{C}_4\text{H}_9$).

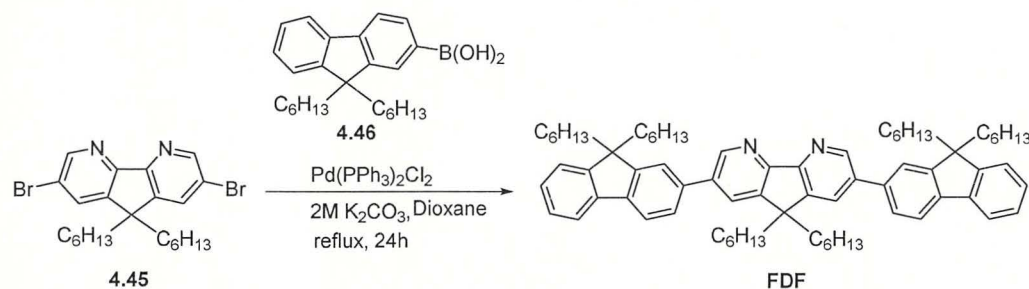
$^{13}\text{C NMR}$ (100MHz, CDCl_3): δ (ppm) 190.18 (CO), 161.71, 153.77 (CH), 152.08, 151.07, 142.18, 140.15, 138.50, 135.23, 130.02, 129.65 (CH), 127.72 (CH), 126.98 (CH), 125.95 (CH), 123.00 (CH), 121.27 (CH), 120.48 (CH), 120.11 (CH), 55.38 (C-9), 40.39, 31.49, 29.66, 23.79, 22.56, 13.99 (CH_3).

DEPTQ NMR (100MHz, CDCl_3): δ (ppm) 161.73, 153.79 (CH), 152.09, 151.08, 142.18, 140.16, 138.51, 135.25, 130.03, 129.66 (CH), 127.72 (CH), 126.99 (CH), 125.95 (CH), 123.01 (CH), 121.28 (CH), 120.48 (CH), 120.11 (CH), 55.39 (C-9), 40.40, 31.49, 29.67, 23.79, 22.57, 14.00 (CH_3).

$\text{MS (ESI}^+)$ m/z : 847.55 ($[\text{M}+\text{H}]^+$, 100%). Calcd. for $\text{C}_{61}\text{H}_{70}\text{N}_2\text{O}$: 846.55.

3,7-Bis(9,9-dihexylfluoren-2-yl)-9,9-dihexyl-4,5-diazafluorene (FDF)

Exp: SG-002



Under nitrogen, to a mixture of 2,7-dibromo-9,9-dihexyl-4,5-diazafluorene (**4.45**) (245 mg, 0.49 mmol), 9,9-dihexylfluorene-2-boronic acid (**4.46**) (382 mg, 1.01 mmol) and Pd(PPh₃)₂Cl₂ (7 mg, 2 mol%), degassed 2M aqueous K₂CO₃ (4 mL, 8 mmol) and 1,4-dioxane (10 mL) were added via syringe. The mixture was stirred under nitrogen with heating at 110 °C (oil bath) for 24 hours with protection from the sunlight. The mixture was cool down to room temperature and the resulting slurry was poured into 5% NaCl aqueous solution (50 mL). The precipitate was collected by filtration, washed with water (3 × 20 mL), dried *in vacuo* to afford the crude product (448 mg, 88%) as brown solid. The crude product was purified by column chromatography on silica gel, eluting first with PE to remove by-products and then with PE:EA mixture, with gradual increase of EA contents from 2% to 6%, to yield product **FDF** (353 mg, 70.5%) as a light yellow solid.

¹H NMR (500 MHz, CDCl₃): δ (ppm) 9.01 (2H, d, *J* = 1.9 Hz), 7.93 (2H, d, *J* = 2.0 Hz), 7.83 (2H, d, *J* = 7.8 Hz), 7.78–7.76 (2H, m), 7.67–7.63 (4H, m), 7.40–7.34 (6H, m), 2.16–2.12 (4H, m), 2.08–2.03 (8H, m), 1.18–1.09 (36H, m), 0.89–0.82 (4H, m), 0.83–0.66 (26H, m).

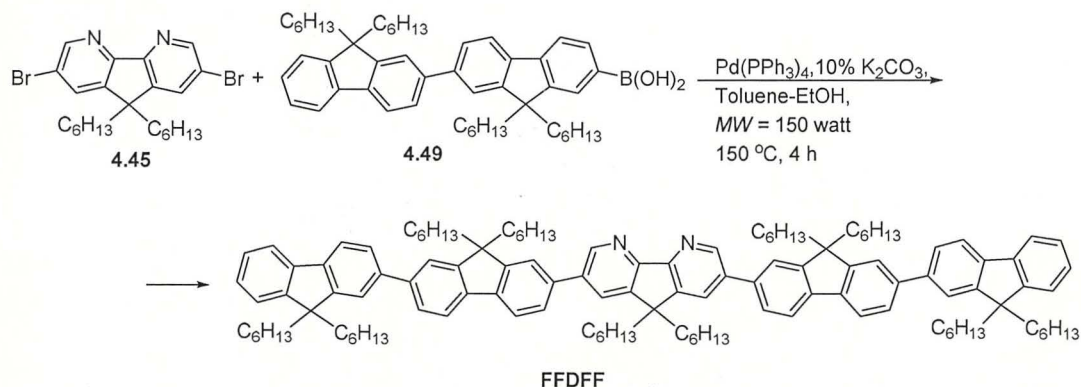
¹³C NMR (100 MHz, CDCl₃): δ (ppm): 151.99, 151.13, 148.45 (CH), 145.80, 141.53 (× 2), 140.43 (× 2), 136.84, 128.99 (CH), 127.52 (CH), 126.98 (CH), 126.39 (CH), 123.08 (CH), 121.60 (CH), 120.33 (CH), 119.11 (CH), 56.39, 51.70, 40.36, 40.29, 31.51, 31.42, 29.69, 29.59, 24.19, 22.84, 22.58, 22.52, 14.04, 13.99.

DEPTQ NMR (100 MHz, CDCl₃): δ (ppm) 151.87, 151.05, 145.48 (CH), 141.32, 140.42, 137.05, 136.52, 128.66 (CH), 127.40 (CH), 126.90 (CH), 126.32 (CH), 123.01 (CH), 121.53 (CH), 120.24 (CH), 119.94 (CH), 55.31, 40.30, 39.29, 31.46, 31.39, 29.64, 29.56, 24.13, 23.78, 22.54, 22.48, 14.00, 13.96.

MS (ESI⁺) *m/z*: 1001.76 ([M + H]⁺, 100%). Calcd. for C₇₃H₉₆N₂: 1000.76).

9,9-Dihexyl-2,7-bis(9,9,9',9'-tetrahexyl-9H,9'H-[2,2'-bifluoren]-7-yl)-9H-4,5-diazafluorene (FFDFF)

Exp: SG-185



Under nitrogen, to a mixture of 2,7-dibromo-9,9-dihexyl-4,5-diazafluorene **4.45** (10 mg, 0.020 mmol), 9,9,9',9'-tetrahexyl-[2,2'-bifluoren]-7-yl-boronic acid **4.49** (41 mg, 0.057 mmol) and Pd(PPh₃)₄ (3 mg, 10 mol%), 10% K₂CO₃ aqueous solution (0.5 mL, 0.4 mmol), ethanol (0.5 mL) and toluene (3 mL) were added into a reaction tube. The reaction mixture was degassed for 15 minutes with Argon and then irradiated with microwave (150 watt) at the 150 °C in microwave reactor for 4 hours. The reaction mixture was cooled down to room temperature and evaporated to remove solvent. The resulting slurry was poured into 5% NaCl aqueous solution, the product was extracted with chloroform (2 × 15 mL), the combined organic layer was washed with water until pH = 7, dried over anhydrous magnesium sulphate and the solvent was evaporated to afford the crude product (45 mg) as yellowish solid. The crude product was purified by flash chromatography on silica gel, eluting first with PE, then

with gradient increase to PE:EA, 4:1 to yield pure product **FFDFF** (21 mg, 61%) as a light yellow solid.

¹H NMR (400 MHz, CDCl₃): δ (ppm) 9.04 (2H, d, *J* = 1.8 Hz), 7.96 (2H, d, *J* = 1.8 Hz), 7.89–7.63 (20H, m), 7.39–7.26 (6H, m), 2.18–1.98 (20H, m), 1.22–1.08 (60H, m), 0.92–0.64 (50H, m).

¹³C NMR (101 MHz, CDCl₃) δ 157.22, 152.20, 151.84, 151.52, 151.02, 148.73, 145.55, 141.05, 141.01, 140.76, 140.45, 140.37, 139.57, 137.02, 136.55, 128.68, 127.05, 126.81, 126.44, 126.28, 126.07, 122.95, 121.61, 121.59, 121.46, 120.32, 120.20, 119.92, 119.75, 55.48, 55.19, 51.51, 40.38, 40.29, 39.32, 31.48, 31.44, 31.41, 29.70, 29.61, 29.58, 24.16, 23.85, 23.79, 22.57, 22.54, 22.50, 14.02, 13.98.

DEPTQ NMR (101 MHz, CDCl₃) δ 157.21, 152.20, 151.84, 151.52, 151.02, 148.73 (CH), 145.55, 141.05, 141.01, 140.76, 140.45, 140.37, 139.57, 137.02, 136.55, 128.68 (CH), 127.05 (CH), 126.81 (CH), 126.44 (CH), 126.27 (CH), 126.07 (CH), 122.95 (CH), 121.60 (CH), 121.59 (CH), 121.46 (CH), 120.32 (CH), 120.20 (CH), 119.92 (CH), 119.75 (CH), [55.48, 55.19 (C-9)], 51.51 (CH₂) [40.38, 40.29, 39.32 (CH₂)], [31.48, 31.44, 31.41 (CH₂)], [29.70, 29.61, 29.58 (CH₂)], [24.16, 23.85, 23.79 (CH₂)], [22.57, 22.54, 22.50 (CH₂)], [14.02, 13.98 (CH₃)].

MS (MALDI TOF) *m/z*: 1666.81 ([M + H]⁺, 100%). Calcd. for C₁₂₃H₁₆₀N₂: 1665.26.

References

- 1 (a) A. R. Murphy and J. M. Fréchet, *Chem. Rev.*, **2007**, *107*, 1066; (b) A. N. Sokolov, B. C.-K. Tee, C. J. Bettinger, J. B.-H. Tok, and Z. Bao, *Acc. Chem. Res.*, **2012**, *45*, 361.
- 2 (a) S. R. Forrest, *Nature*, **2004**, *428*, 911; (b) S. B. Zhao and S. Wang, *Chem. Soc. Rev.*, **2010**, *39*, 3142; (c) M. C. Gather, A. Kohnen, and K. Meerholz, *Adv. Mater.*, **2011**, *23*, 233.
3. (a) B. Walker, C. Kim, and T.-Q. Nguyen, *Chem. Mater.*, **2011**, *23*, 470; (b) Y. Sun, G. C. Welch, W. L. Leong, C. J. Takacs, G. C. Bazan, and A. Heeger, *Nature Mater.*, **2012**, *11*, 44.
- 4 S. C. Lo and P. L. Burn, *Chem. Rev.*, **2007**, *107*, 1097.
- 5 C. Wang, H. Dong, W. Hu, Y. Liu, and D. Zhu *Chem. Rev.*, **2012**, *112*, 2208.
- 6 A. Geng, D. Trajkovska, J. J. Katsis, J. J. Ou, S. W. Culligan, and S. H. Chen, *J. Am. Chem. Soc.*, **2002**, *124*, 8337.
- 7 A. L. Kanibolotsky, I. F. Perepichka, and P. J. Skabara, *Chem. Soc. Rev.*, **2010**, *39*, 2695.
- 8 (a) A. C. Grimsdale, K. Müllen, *Adv. Polym. Sci.*, **2006**, *199*, 1; (b) M. Leclerc, *J. Polym. Sci. A, Polym. Chem.*, **2001**, *39*, 2867; (c) W. Y. Wang, *Coord. Chem. Rev.*, **2005**, *249*, 971.
- 9 J. U. Wallace and S. H. Chen, in: *Polyfluorenes, Advances in Polymer Science – Vol. 212*, U. Scherf and D. Neher (Eds.), Springer-Verlag, **2008**, pp. 145–180.
- 10 Y. Geng, S. W. Culligan, A. Trajkovska, J. U. Wallace, and S. H. Chen, *Chem. Mater.*, **2003**, *15*, 542.

-
- 11 X. Gong, P. K. Iyer, D. Moses, G. C. Bazan, A. J. Heeger, and S. S. Xiao, *Adv. Funct. Mater.*, **2003**, *13*, 325.
 - 12 M. Gaal, E. J. List, and U. Scherf, *Macromolecules*, **2003**, *36*, 4236.
 - 13 Y. Geng, A. Trajkovska, D. Katsis, J. J. Ou, S. W. Culligan, and S. H. Chen, *J. Am. Chem. Soc.*, **2002**, *124*, 8337.
 - 14 E. Somma, B. Loppinet, C. Chi, G. Fytas, and G. Wegner, *Phys. Chem. Chem. Phys.*, **2006**, *8*, 2773.
 - 15 J. Salbeck, M. Schorner, and T. Fuhrman, *Thin Solid Films*, **2002**, 417, 20.
 - 16 J. Locking, D. Li, S. C. D. Mannsfeld, E. J. Borkent, H. Meng, R. Advincula, and Z. Bao, *Chem. Mater.*, **2005**, *17*, 3366.
 - 17 Y. Geng, D. Katsis, S. W. Culligan, J. J. Ou, S. H. Chen, and L. J. Rothberg, *Chem. Mater.*, **2002**, *14*, 463.
 - 18 D. Katkis, Y. H. Geng, J. J. Ou, S. W. Culligan, A. Trajkovska, S. H. Chen, and L. J. Rothberg, *Chem. Mater.*, **2002**, *14*, 1332.
 - 19 R. Anemian, J.-C. Mulatier, C. Andraud, O. Stephan, and J.-C. Vial, *Chem. Commun.*, **2002**, 1608.
 - 20 P. Robert, A. Bolduc, and W. G. Skene, *J. Phys. Chem. A*, **2012**, *116*, 9305.
 - 21 G. Klaener and R. D. Miller, *Macromolecules*, **1998**, *31*, 2007.
 - 22 Y. Koizumi, S. Seki, A. Achyara, A. Saeki, and S. Tagada, *Chem. Lett.*, **2004**, *33*, 1290.
 - 23 J. Jo, C. Chi, S. Hoger, G. Wegner, and D. Y. Yoon, *Chem. Eur. J.*, **2004**, *10*, 2681.
 - 24 C. Chi, C. Im, V. Enkelmann, A. Ziegler, G. Lieser, and G. Wegner, *Chem. Eur. J.*, **2005**, *11*, 6833.
 - 25 F. J. -Isaza and M. L. Turner, *J. Mater. Chem.*, **2006**, *16*, 83.
 - 26 X.-H. Zhou, Y. Zhang, Y.-Q. Xie, Y. Cao, and J. Pei, *Macromolecules*, **2006**, *39*, 3830.
 - 27 T. Hayashi, M. Konishi, Y. Kobori, M. Kumada, T. Higuchi, and K. Hirotsu, *J. Am. Chem. Soc.*, **1984**, *106*, 158.
 - 28 J. K. Stille, *Angew. Chem. Int. Ed. Engl.*, **1986**, *25*, 508.
 - 29 Y. Geng, A. C. A. Chen, J. J. Ou, S. H. Chen, K. Klubek, K. M. Vaeth, and C. W. Tang, *Chem. Mater.*, **2003**, *15*, 4352.
 - 30 J. Khunchalee, R. Tarsang, N. Prachumrak, S. Jungsuttiwong, T. Keawin, T. Sudyoasuk, and V. Promarak, *Tetrahedron*, **2012**, *68*, 8416.
 - 31 H. Meng, Z. Bao, A. J. Lovinger, B.-C. Wang, and A. M. Mujsce, *J. Am. Chem. Soc.*, **2001**, *123*, 9214.
 - 32 I. I. Perepichka, I. F. Perepichka, M. R. Bryce, and L.-O. Pålsson, *Chem. Commun.*, **2005**, 3397.
 - 33 W.-J. Li, B. Liu, Y. Qian, L.-H. Xie, J. Wang, S.-B. Li, and W. Huang *Polym. Chem.*, **2013**, *4*, 1796.
 - 34 K. C. Moss, K. N. Bourdakos, V. Bhalla, K. T. Kamatekar, M. R. Bryce, M. A. Fox, H. L. Vaughan, F. B. Dias, and A. P. Monkman, *J. Org. Chem.*, **2010**, *75*, 6771.
 - 35 K. T. Wong, R. T. Chen, F. C. Fang, C. C. Wu, and Y. T. Lin, *Org. Lett.*, **2005**, *7*, 1979.
 - 36 K. T. Wong, R. T. Chen, and F. C. Fang, *Org. Lett.*, **2006**, *8*, 3501.
 - 37 J. Roncali, *Chem. Rev.*, **1997**, *97*, 173.
 - 38 J. Gierschner, J. Cornil, and H.-J. Egelhaaf, *Adv. Mater.*, **2007**, *19*, 173.
 - 39 K. Müllen and G. Wegner (Eds.), *Electronic Materials: The Oligomer Approach*, Wiley-VCH, **1998**.
 - 40 (a) A. Charas, J. Morgado, J. M. G. Martinho, L. Alcácer, and F. Cacialli, *Chem. Commun.*, **2001**, 1216; (b) A. Charas, J. Morgado, J. M. G. Martinho, A. Fedorov, L. Alcácer, and F. Cacialli, *J. Mater. Chem.*, **2002**, *12*, 3523.

-
- 41 (a) E. J. W. List, R. Guentner, P. S. de Freitas, and U. Scherf, *Adv. Mater.*, **2002**, *14*, 374; (b) M. Gaal, E. J. W. List, and U. Scherf, *Macromolecules*, **2003**, *36*, 4236; (c) L. Romaner, A. Pogantsch, P. S. de Freitas, U. Scherf, M. Gaal, E. Zojer, and E. J. W. List, *Adv. Funct. Mater.*, **2003**, *13*, 597; (d) X. Gong, P. K. Iyer, D. Moses, G. C. Bazan, A. J. Heeger, and S. S. Xiao, *Adv. Funct. Mater.*, **2003**, *13*, 325.
- 42 C. M. Cardona, W. Li, A. E. Kaifer, D. Stockdale, and G. C. Bazan, *Adv. Mater.*, **2011**, *23*, 2367.
- 43 N. G. Connelly and W. E. Geiger, *Chem. Rev.*, **1996**, *96*, 877.
- 44 (a) A. L. Kanibolotsky, R. Berridge, P. J. Skabara, I. F. Perepichka, D. D. C. Bradley, and M. Koeberg, *J. Am. Chem. Soc.*, **2004**, *126*, 13696; (b) J.-P. Choi, K.-T. Wong, Y.-M. Chen, J.-K. Yu, P.-T. Chou, and A. J. Bard, *J. Phys. Chem. B*, **2003**, *107*, 14407.
- 45 M. J. Frisch, G. W. Trucks, H. B. Schlegel, G. E. Scuseria, M. A. Robb, J. R. Cheeseman, G. Scalmani, V. Barone, B. Mennucci, G. A. Petersson, H. Nakatsuji, M. Caricato, X. Li, H. P. Hratchian, A. F. Izmaylov, J. Bloino, G. Zheng, J. L. Sonnenberg, M. Hada, M. Ehara, K. Toyota, R. Fukuda, J. Hasegawa, M. Ishida, T. Nakajima, Y. Honda, O. Kitao, H. Nakai, T. Vreven, J. A. Montgomery, Jr., J. E. Peralta, F. Ogliaro, M. Bearpark, J. J. Heyd, E. Brothers, K. N. Kudin, V. N. Staroverov, R. Kobayashi, J. Normand, K. Raghavachari, A. Rendell, J. C. Burant, S. S. Iyengar, J. Tomasi, M. Cossi, N. Rega, J. M. Millam, M. Klene, J. E. Knox, J. B. Cross, V. Bakken, C. Adamo, J. Jaramillo, R. Gomperts, R. E. Stratmann, O. Yazyev, A. J. Austin, R. Cammi, C. Pomelli, J. W. Ochterski, R. L. Martin, K. Morokuma, V. G. Zakrzewski, G. A. Voth, P. Salvador, J. J. Dannenberg, S. Dapprich, A. D. Daniels, O. Farkas, J. B. Foresman, J. V. Ortiz, J. Cioslowski, and D. J. Fox, Gaussian, Inc., Wallingford CT, **2009**, Gaussian 09, Revision A.02,
- 46 R. M. Gutiérrez-Pérez, N. R. Flores-Holguin, D. Glossman-Mitnik, and L. M. Rodríguez-Valdez, *J. Mol. Model.*, **2011**, *17*, 1963.
- 47 N. A. Sánchez-Bojorge, L. M. Rodríguez-Valdez, and N. F.-Holguin, *J. Mol. Model.*, **2013**, *19*, 3542.
- 48 L. Yang, A.-M. Ren, J.-K. Feng, and J.-F. Wang, *J. Org. Chem.*, **2005**, *70*, 3009.
- 49 J. R. Lakowicz, *Principles of Fluorescence Spectroscopy*, Kluwer/Plenum, 2nd edn, **1999**.
- 50 B. Valeur, *Molecular Fluorescence: Principles and Applications*, Wiley-VCH, **2001**.
- 51 Z. Liu, W. He, and Z. Guo, *Chem. Soc. Rev.*, **2013**, *42*, 1568.
- 52 H. Kobayashi, M. Ogawa, R. Alford, P. L. Choyke, and Y. Urano, *Chem. Rev.*, **2010**, *110*, 2620.
- 53 B. Valeur and I. Leray, *Coord. Chem. Rev.*, **2000**, *205*, 3.
- 54 P. J. Jiang and Z. J. Guo, *Coord. Chem. Rev.*, **2004**, *248*, 205.
- 55 T. W. Clarkson and L. Magos, *Crit. Rev. Toxicol.*, **2006**, *36*, 609.
- 56 E. L. Que, D. W. Domaille, and C. J. Chang, *Chem. Rev.*, **2008**, *108*, 1517.
- 57 M. A. Palacios, Z. Wang, V. A. Montes, G. V. Zyryanov, and P. J. Anzenbacher, *J. Am. Chem. Soc.*, **2008**, *130*, 10307.
- 58 C. Y. Huang, *Methods in Enzymology*, **1982**, *87*, 509.
- 59 P. Job, *Annali di Chimica Applicata*, **1928**, *9*, 113.
- 60 (a) Y. Yang, Q. Pei, and A. J. Heeger, *J. Appl. Phys.*, **1996**, *79*, 934; (b) J. Stampfl, S. Tasch, G. Leising, and U. Scherf, *Synth. Met.*, **1995**, *71*, 2125.
- 61 S. Hamai and F. Hirayama, *J. Phys. Chem.*, **1983**, *87*, 83.

Chapter 5

4,5-Diazafluorene-Based Polymers

5.1 Introduction

Conjugated polymers and co-polymers as active layers in polymer OLEDs offer the technology of simple processable material from solution and the low cost production method with easy tunable properties of emission through chemical modifications. The success in this relies, largely, on the clever design and efficient synthesis of new materials with particular structures and properties. Linear rigid-rod oligo- and polyfluorenes (PFs) are among the most prominent organic semiconductors attracting intense research effort due to their unique properties (e.g. high photo- and electroluminescence quantum yields, high charge mobilities, good thermal and photochemical stabilities) and consequently great potential applications in electronic devices, such as OLEDs, field-effect transistors, photovoltaic cells, optical switches and lasers etc.^{1,2} Several classes of conjugated dibenzoheterole polymers topologically similar to polyfluorenes (Fig. 5.1) when C-9 carbon atom in the fluorene moiety replaced by N, S or Si heteroatoms (e.g. dibenzosiloles,³ carbazoles,⁴ dibenzothiophenes⁵ and dibenzothiophene-*S,S*-dioxides⁶) have been synthesised and recognized as promising materials for OLED and other application in organic electronics. Search for new polymers with improved properties for organic electronics is considered a fast growing discipline of active research in both academia and industries.

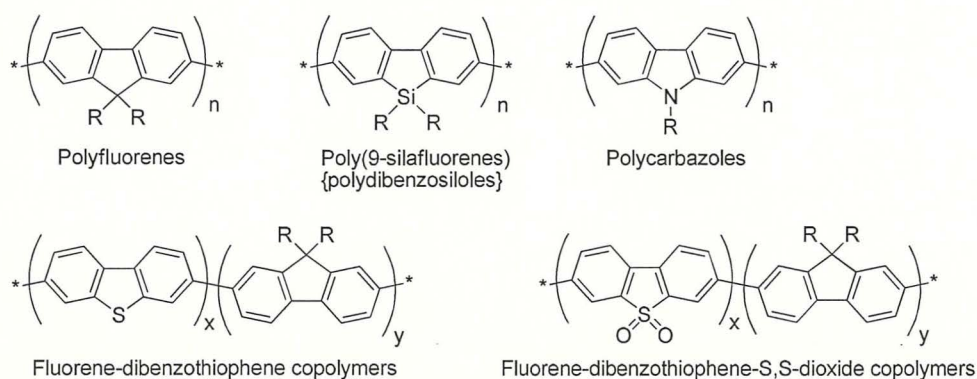
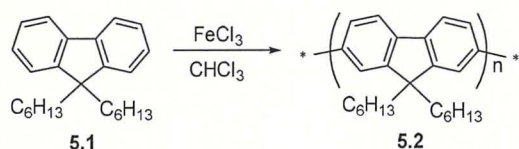


Fig. 5.1 Conjugated polymers with Si, N and S heteroatoms.

As part of this Thesis work, synthesis and study of novel materials, topologically similar to poly(fluorene)s but containing electron deficient nitrogen atoms is poly(4,5-diazafluorene)s for potential applications in organic electronics is presented in the Results and Discussion Section of this Chapter. Also, a brief discourse on the synthesis and properties of well-known polyfluorenes as materials for organic electronics is included.

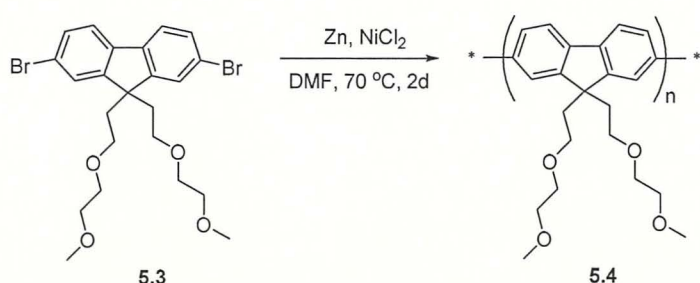
5.1.1 Synthesis and properties of polyfluorenes

Polyfluorenes (PFs) is the simplest class of stepladder-type polyphenylene. Unsubstituted polyfluorene was synthesised for the first time electrochemically by anodic oxidation of fluorene in 1985⁷ and subsequently various 9-substituted polyfluorene was synthesised electrochemically. The first chemical synthesis of poly(9,9-dihexylfluorene) (**5.2**) using 9,9-dihexylfluorene (**5.1**) as monomer unit was performed by Yoshino *et al.* in 1989 via an oxidative coupling using anhydrous ferric chloride in chloroform and low molecular weight polymer **5.2** with a number average molecular weight (M_n) up to 5000 was obtained (Scheme 5.1).⁸



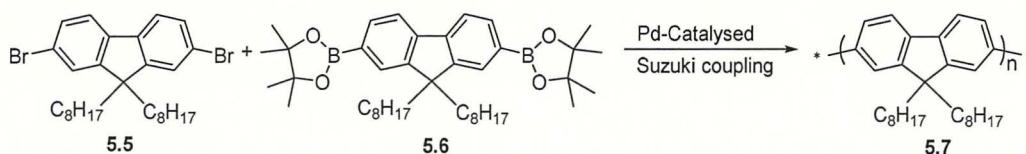
Scheme 5.1 Synthesis of poly(9,9-dihexyl)fluorene (**5.2**) by oxidative coupling.⁸

Molecular weight up to 5,000 (determined by GPC analysis) was obtained using above procedure was rather low for device application. High molecular weight PFs ($M_w = 94,000$) was reported for the first time by Pie and Yang in 1996⁹ for poly[9,9-bis(3,6-dioxaheptyl)fluorene] (**5.4**), which was synthesised by the Yamamoto coupling using $NiCl_2$ as coupling agent shown in Scheme 5.2.



Scheme 5.2 First Yamamoto synthesis of poly[9,9-bis(3,6-dioxaheptyl)fluorene] (**5.4**).⁹

Most of the high molecular weight polyfluorenes are synthesised either by Pd-catalysed Suzuki reaction or by Yamamoto reaction using Ni(COD)₂ as coupling agent. For example, researcher at Dow Chemical reported high molecular weight ($M_w > 100,000$) polymer **5.7** by Suzuki coupling between fluorene monomer units **5.5** and **5.6** as shown in Scheme 5.3.¹⁰



Scheme 5.3 Synthesis of Poly(9,9-dioctyl)fluorene (**5.7**) by Suzuki coupling.¹⁰

PFs derivatives are most widely investigated for optoelectronic good application due to their, bright blue emission, high photoluminescence quantum efficiency and thermal stability. Moreover, fluorene monomers for construction of fluorene-based polymers are easy to synthesise with high yields that offer a wide range of different type of PFs derivatives possible to make, so as to establish structure property relationship for targeted device application.¹¹ The emission from alkylated PFs is well known to be in violet-blue region of the spectrum with maxima at ca. 425 nm and 440 nm. For illustration, the photoluminescence and absorption spectra of poly(9,9-dioctylfluorene) and poly[9,9-di-(2-ethylhexyl)fluorene] in thin films reported by Moses *et al.*¹² are shown in Fig. 5.2. In addition, PFs show the optimum HOMO–LUMO energy level and excellent charge-transport properties. PFs are, therefore, widely investigated for device applications, that can be inferred from the number of review articles published.^{1a,13,14,15}

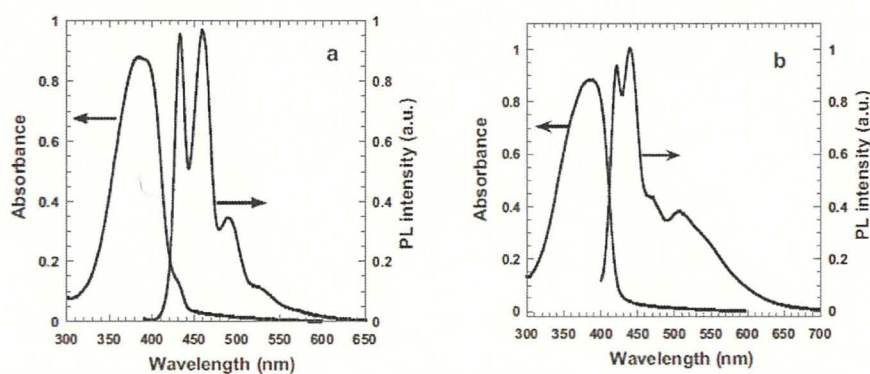
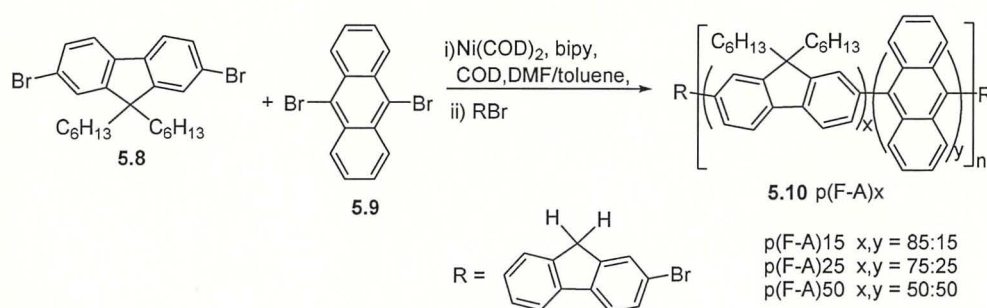


Fig. 5.2 Photoluminescence and absorption spectra in thin films of (a) poly(9,9-dioctylfluorene) and (b) poly[9,9-di-(2-ethylhexyl)fluorene].¹²

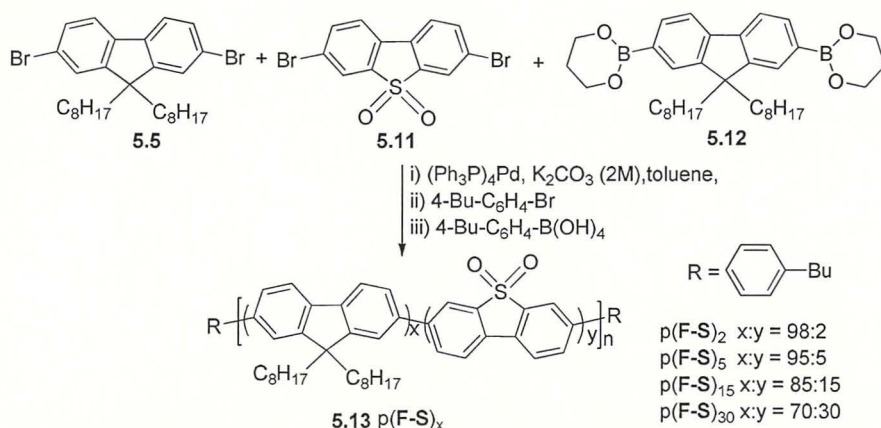
5.1.2 Synthesis and properties of fluorene based copolymer

Copolymer synthesis is an important method to control or tune the optoelectronic properties required for a particular application. In order to improve the photophysical properties of fluorene-based material, a variety of fluorene-based copolymers are synthesised and reported in last decades for potential application in oelectronic devices.¹ In general, Yamamoto-type coupling^{16,17,18} and Suzuki-type coupling^{6,19,20} are used to synthesise fluorene-based copolymers. As an example, Yamamoto type coupling between fluorene and anthracene monomers reported by Miller *et al.*¹⁶ is shown in Scheme 5.4. The copolymers **5.10** p(F-A)_x displayed stable blue-light emission in light-emitting devices. Interestingly, incorporation of anthracene into the polyfluorene backbone completely suppressed the formation of troublesome excimer, which is a key drawback for polymers with planar π -system.¹⁶



Scheme 5.4 Synthesis of poly(fluorene-*co*-anthracene) via Yamamoto type coupling.¹⁶

As an example, Suzuki-type copolymerisation involving incorporation of dibenzothiophene-*S,S*-dioxide (S) moiety into the polyfluorenes backbone to afford p(F-S)_x copolymers is depicted in Scheme 5.5.⁶



Scheme 5.5 Synthesis of poly(fluorene-*co*-dibenzothiophene-*S,S*-dioxide) **5.13** via Pd-catalysed Suzuki coupling co-polymerisation.⁶

When comparing to polymer **PFO (5.7)**, under similar condition of measurement, copolymers $p(\mathbf{F-S})_x$ (**5.13**) showed improved electron injection, balanced mobility and marked improve device performance. The reported absorption and photoluminescence spectra of the copolymers $p(\mathbf{F-S})_x$ (**5.13**) in toluene solution is shown in Fig. 5.3. The absorption spectra showed progressive small red shifts and some broadening with an increasing **S** loading while somewhat larger red shifts in emission spectra. Also, the copolymers $p(\mathbf{F-S})_x$ displayed broad emission throughout the visible spectrum resulting from dual-fluorescence process, giving efficient single polymer WLEDs with broadened emission.⁶

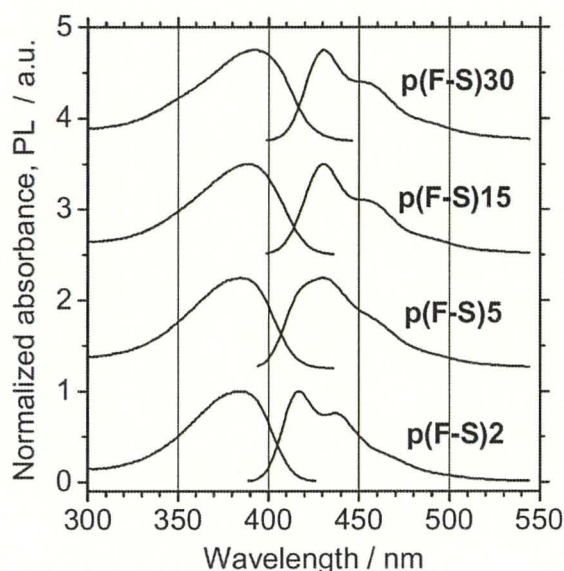


Fig. 5.3 Absorption and photoluminescence spectra of the copolymer $p(\mathbf{F-S})_x$ (**5.13**) in toluene solution.⁶

5.1.3 Defects in polyfluorenes: keto defects

Polyfluorenes and polyfluorenes-type co-polymers are widely investigated and are emerging as a leading class of the emitter materials for applications as polymeric blue light-emitting diodes, PLED. However, a major setback of polyfluorene-based PLED is the degradation of emitting material upon device operation leading to unwanted green emission band at $\sim 2.2\text{--}2.4$ eV (520–530 nm).^{12,21} As an illustration, an additional green emission and reduced efficiency were observed during annealing the thin film of **PFO (5.7)** in the air is shown in Fig. 5.4. This is a longtime known fact in polyfluorene photophysics, but in earlier studies, despite a great deal of exertion by the scientific community, the origin of this low energy band was considered controversial and attributed mainly due to aggregates or excimers, or direct emission from chemical defects ("keto-defect").²²

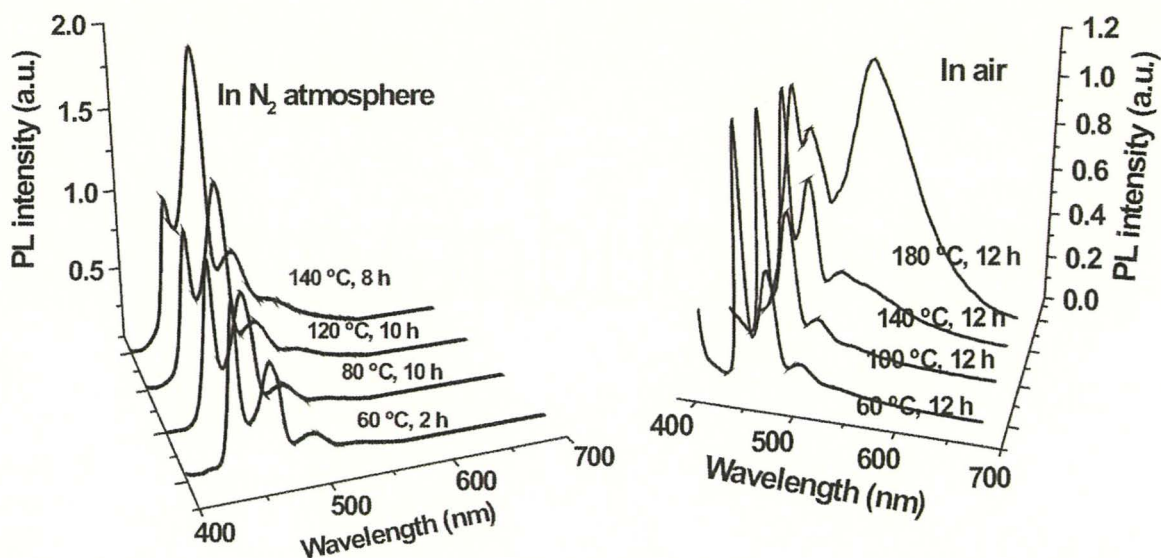
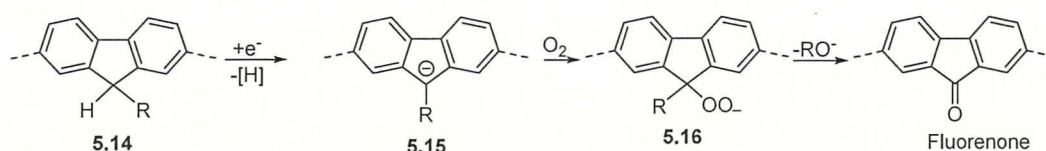


Fig. 5.4 The PL spectra of the PFO (5.7) thin film annealed (a) in nitrogen atmosphere and (b) in air; new green emission band is progressively developed on annealing the film in air.¹²

In recent times, keto-defect sites are generally accepted concept of the origin of the low-energy emission in polyfluorene supported by experimental results^{23,24,25,26,27} and quantum chemical calculations.^{28,29} From chemist's line of thought, the keto-defect sites may be formed during polymer synthesis as a result of incomplete monomer alkylation at C-9 as well as due to photo-, electro-, or thermal oxidative degradation processes after polymer synthesis. The formation of keto-defects during polymer synthesis can be interpreted by a mechanism proposed by Scherf group (Scheme 5.6).^{21a} In the proposed mechanism, the process starts from the reduction of monoalkylated fluorene 5.14 generating the fluorenyl anions 5.15, which undergoes an aerial oxidation to form hydro peroxide anion 5.16. Thereafter, the hydro peroxide anion 5.16 undergoes rearrangement to generate fluorenone moieties. It is known that even smallest traces of fluorenone species in polyfluorenes may cause severe change in photophysical properties of polyfluorenes.³⁰ Therefore, very high purity dialkylated monomers are generally require for synthesis of polyfluorenes to minimise the formation of keto defects and to improve the stability of the polymers.^{31,32}



Scheme 5.6 Proposed mechanism for the formation of keto defects at monoalkylated sites of poly(dialkylfluorene).^{21a}

As an illustration, formation of keto defects during device operation in polyfluorene-based PLED and change in emission is shown in Fig. 5.5.^{1b} It has been established that the effect of Keto-defect on the emission is more pronounced in electroluminescence process when compared to photoluminescence.

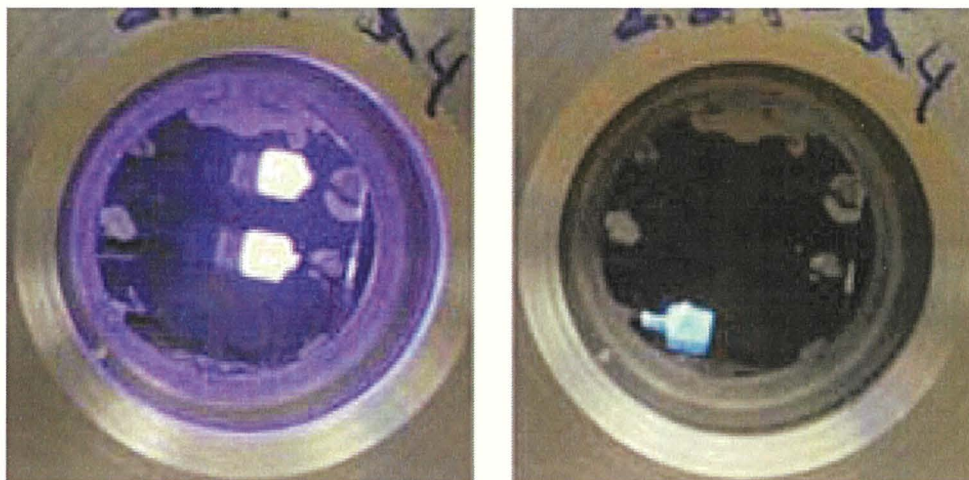
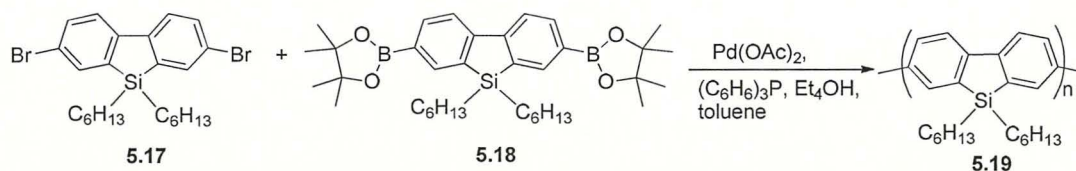


Fig. 5.5 Electroluminescence of a polyfluorene-type PLED, the initial emission of the device (left) and the emission after device operation (right). [from ref 1b, p. 295].

To overcome this drawback of low energy emission in polyfluorenes several strategies have been applied, such as i) the thorough purification of the fluorene monomers,³⁰ ii) copolymerization with other moieties,^{6,34} iii) replacing linear alkyl solubilising side groups at C-9 with more bulky substituents.^{33,34,35} However, these strategies do not provide a complete solution of problem associated with the degradation process at C-9 position of polyfluorenes. A noble approach reported by Holmes group did overcome this effect whereby replacing CH₂ bridge of fluorene to silicon atom. They synthesised poly(9,9-dihexyl-2,7-dibenzosiloles) **5.19** via Suzuki cross-coupling (Scheme 5.7), which, when compared to polyfluorenes exhibit extremely high emission stability.³⁶



Scheme 5.7 Synthesis of poly(9,9-dihexyl-2,7-dibenzosiloles) **5.19** via Suzuki cross-coupling polymerisation.³⁶

Thereafter, some other groups followed this approach and reported the syntheses and properties of similar silafluorene polymers as novel blue-emitting materials.^{37,38,39} Likewise, an active area of research has been focused on the synthesis and properties of similar new polyfluorenes type material with prolonged blue emission stability. One of the aim of the current Thesis work is to investigate whether 4,5-diazafluorene type polymers have stability better than polyfluorenes, so that degradation processes associated with keto defect is eliminated or minimised, and can be considered as a stable blue PLED material (Section 5.2).

Poly(9,9-dioctylfluorene) (**PFO**, **5.7**) and poly(9,9-dihexylfluorene) (**5.2**) are the well-known conjugated polymers among the poly(9-alkylfluorenes) studied as an active material for OLEDs.^{40,41} The rigid-rod polyfluorenes are known to form a nematic type arrangement in bulk, which facilitates chain aggregation leading to red-shifted emission and reduce emission efficiency.⁴² The common phase associated with PFs is the amorphous phase with an average torsional angle (ϕ) of backbone chain of 135° and the other one, so called β -phase, with more planar backbone with the torsional angle of 160° .⁶⁵ The β -phase is exclusively found in **PFO** and considered important because it leads to interesting specific physical properties such as an efficient energy transfer from amorphous phase, high charge mobility and improved device performance.^{1a,64,65} The formation of β -phase depends on specific condition and can be probed by characteristic peak around 435 nm in the UV-vis absorption spectra. For example, β -phase is formed in **PFO** film was prepared from DCM solution, whereas only amorphous phase is formed when **PFO** film was prepared from toluene solution is shown in Fig. 5.6.

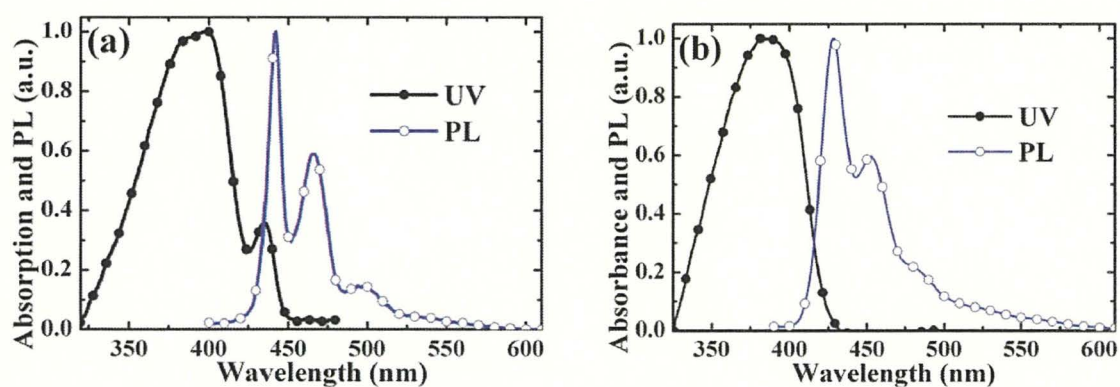


Fig. 5.6 Normalised UV-vis and PL spectra of PFO film (a) β -phase, film prepared with DCM (b) amorphous phase, film prepared with toluene.⁶⁵

The β -phase of **PFO** films exhibits characteristic well-define sharp vibronic replicas in the PL spectrum with almost no storkes shift. Moreover, β -phase acts as self-dopant, that enhances

blue emission and colour purity of **PFO**. Formation of similar β -phase behaviour in 4,5-diazafluorene based polymer is investigated as a part of this Thesis work and is presented in the Result and Discussion Section of this Chapter.

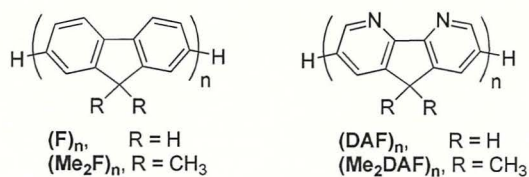
In order to improve the photophysical properties of **PFO**, several strategies have been applied, such as synthesis of alternating or statistical copolymers of **PFO** having kink linkage with carbazole,⁴³ dibenzophenazine,⁴⁴ polyphenylene dendrimer substituents,⁴⁵ pyridine,⁴⁶ end-capping⁴⁷ to allow control over conjugation length and blue emission. Also, donor-acceptor type copolymers of **PFO**, containing electron rich and electron deficient groups results in an intermolecular charge transfer (ICT) complexes and improves photophysical properties such as charge-injection and charge-transport properties.⁴⁸

5.2 Results and discussion

5.2.1 Computational study of polyfluorene and poly(4,5-diazafluorene)

Computational studies on the electronic structures of the polymers provides a valuable contribution towards rationalization of the properties of known polymers and for prediction of those yet unknown polymer^{49,50,51,52} The frontier orbitals (HOMO and LUMO) provides useful information about the applicability of polymers as semiconductor material.

To model and estimate the properties of 4,5-diazafluorene-based polymers and to compared them with corresponding polyfluorenes, we have performed comparative calculations of frontier orbital energy levels for oligomers of the fluorene and 4,5-diazafluorene series by DFT B3LYP/6-31G(d) method as implemented in Gaussian 09 package of programs.⁵³ Similar calculations have already been described for some shorter oligomers (up to $n = 8$) in Chapter 4. Herein computations have been performed in a gas phase and 9-unsubstituted [(**F**)_n, (**DAF**)_n], or 9,9-dimethylated oligofluorenes and oligo-4,5-diazafluorenes [(**Me₂F**)_n, (**Me₂DAF**)_n] have been chosen that allowed (for such a high-level method) to perform calculations up to $n = 20$, the value which is higher than the conjugation length in fluorene-type polymers ($n \sim 12$). While we understood that these computations might be not in a good agreement with experimental energy levels, for the same level of theory, systematic errors (due to the selected method, computations for a gas phase etc.) for two topologically similar structures of the **F** and **DAF** should be near the same. As such, these calculations should describe well the evolutions of HOMO/LUMO energies due to insertion of nitrogen atoms and due to methylation of oligomers.



Dependences of HOMO and LUMO energy levels, and HOMO-LUMO gaps versus number of repeating monomer units (n) are shown in Fig. 5.7a,c. An increase of the lengths of the oligomers results in an increase of HOMO and decrease of LUMO energy levels, as well as the HOMO-LUMO gaps, demonstrating saturation of the values for $n > 12-14$, in good agreement with experimental data for oligofluorenes^{54,55,56} (see Chapter 4). Methylation of oligofluorenes (and of polyfluorene) $[(\mathbf{F})_n \rightarrow (\mathbf{Me}_2\mathbf{F})_n]$ has a smaller effect on their orbital energy levels, with somewhat larger effect on LUMO (decreased by 30 meV, for $n = 18$) than on HOMO (increased by 16 meV). In contrast, for **DAF** series, substitution of hydrogens at position 9 by methyl substituents $[(\mathbf{DAF})_n \rightarrow (\mathbf{Me}_2\mathbf{DAF})_n]$ does not change LUMO energies at all, whereas the main effect is observed in HOMO levels (increased by 60 meV, for $n = 20$). Overall, methylation of **F** and **DAF** units' results in quite small changes of HOMO/LUMO energies, and further increase of the length of the side alkyl chain to ethyl has an even lower effect (Chapter 4, Fig. 4.16). Thus, for octamers $(\mathbf{DAF})_8 \rightarrow (\mathbf{Me}_2\mathbf{DAF})_8 \rightarrow (\mathbf{Et}_2\mathbf{DAF})_8$, HOMO is changed by 54 and 49 meV, respectively, and LUMO is changed by 4 and -1 meV, respectively (for octamers $(\mathbf{F})_8 \rightarrow (\mathbf{Me}_2\mathbf{F})_8 \rightarrow (\mathbf{Et}_2\mathbf{F})_8$ these changes are 16 and -11 meV for HOMO and -25 and -26 meV for LUMO).

An insertion of electronegative nitrogen atoms into benzene rings of oligofluorenes has a drastic effect on the frontier orbital energies, showing similar evolutions of HOMO and LUMO energies. Thus, for "methylated" oligomers, $(\mathbf{Me}_2\mathbf{F})_n$ and $(\mathbf{Me}_2\mathbf{DAF})_n$ series, this results in decreasing the HOMO and LUMO by 0.71 eV and 0.69 eV, respectively, when passing on from $n = 2$ to $n = \infty$ extrapolated value), i.e. an effect of nitrogen atoms is near the same for HOMO and LUMO orbitals (Fig. 5.7a,b). As a result, the HOMO-LUMO gaps for **F** and **DAF** series are very similar: extrapolated values for $(\mathbf{Me}_2\mathbf{F})_n$ and $(\mathbf{Me}_2\mathbf{DAF})_n$ to $n = \infty$ are 3.420 eV and 3.435 eV, so the difference is of 15 meV only (Fig. 5.7c,d). Thus, poly(4,5-diazafluorenes) are expected to absorb and emit the light in the same region as corresponding polyfluorenes. On the other hand, predicted lowering HOMO and LUMO energy levels for 4,5-diazafluorene polymer compared to parent polyfluorene should improve the electron transporting properties of **DAF**-based polymers and decrease the electron injection barrier in

the case of its use as material for OLED. This justifies an interest in the preparation and studies of electrochemical/photophysical properties of 4,5-diazafluorene based polymers.

To estimate the HOMO/LUMO levels, the transition energy (and parameters related to them) of a polymer from energies obtained for the corresponding oligomers, the latter are usually plotted as a function versus $1/n$ (where n is a number of repeating monomer units or number of double bonds along the conjugated chain).^{57,58,59} This allows linearization the graphs simplifying the analysis and such a linearization was confirmed by numerous publications for experimental and calculated data.⁵⁷ Presentation of our data (Fig. 5.7a,c) for oligomers of **F** and **DAF** series as “energy vs. $1/n$ ” (Fig. 5.7b,d) demonstrates reasonably good linear dependences for $n \sim 2-10$. For longer oligomers, some deviations with “saturation effect” is observed, that becomes more and more evident with the growing length of the polymer chain. Thus a real band gap of polymers and their HOMO energies are always lower (and LUMO is higher) than their linearly extrapolated values from “E vs. $1/n$ ” graphs. This fact is well known from the literature and it relates to the conjugation length of the polymer. There is also the theoretical background explaining this effect, because relationship vs. $1/n$ is a simplification of more complex physical description of the phenomenon.⁵⁷

From the plots of HOMO and LUMO energies and HOMO–LUMO gaps versus $1/n$, shown on Fig. 5.7b, d one can see such a deviation from linear dependences for longer oligomers ($n > 12$), where only very small changes in energies are observed for oligomers with $n = 12-20$ (< 20 meV). While they are not negligible for computed values, these correspond to $\sim 1-2$ nm spectral differences and thus can be considered as unimportant.

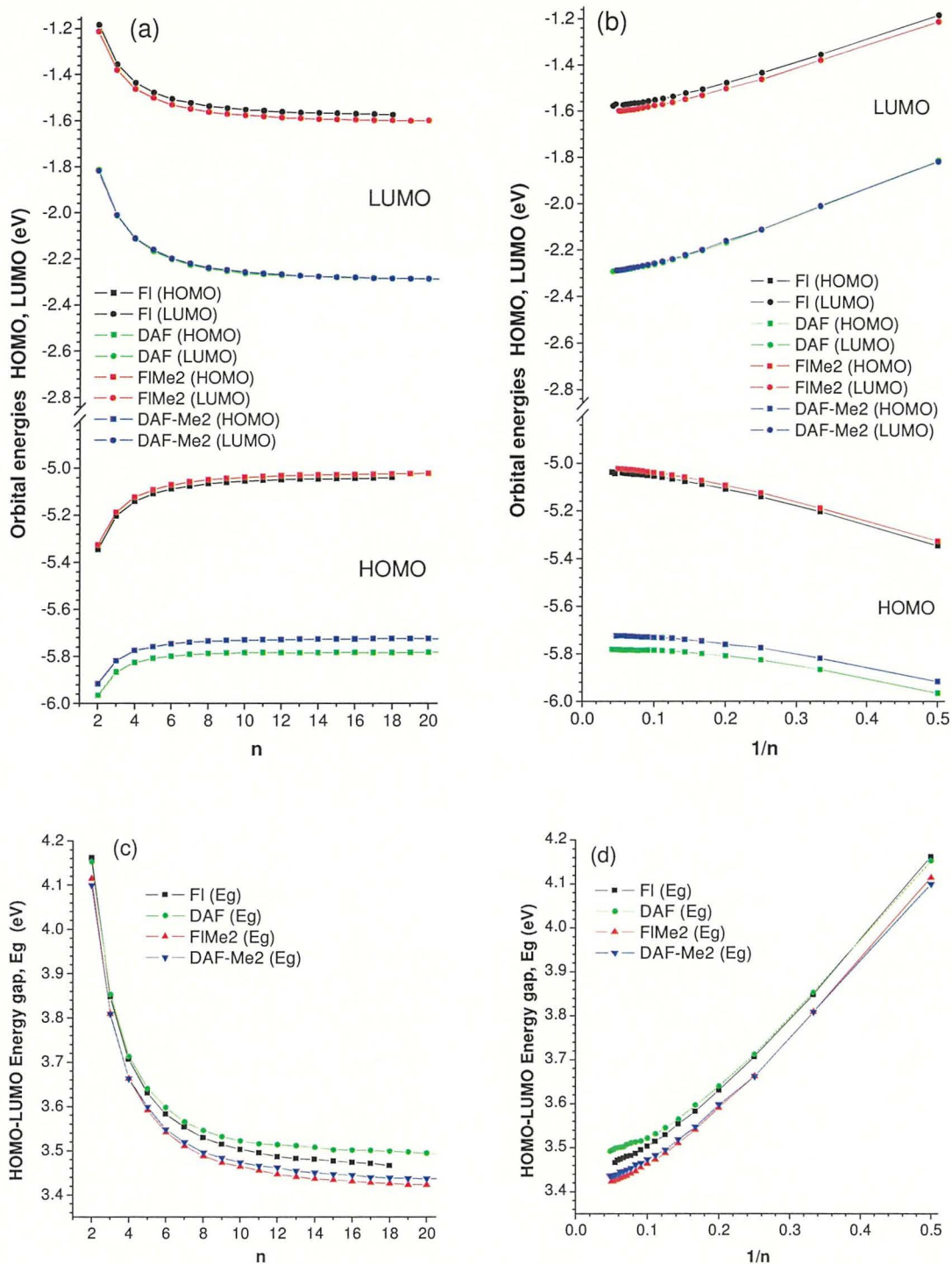


Fig. 5.7 B3LYP/6-31G(d) frontier orbital energy levels and HOMO–LUMO gaps versus n (a,c) and $1/n$ (b,d) (n is a number of monomer units) diagrams for fluorene [(F) $_n$], 4,5-diazafluorene [(DAF) $_n$], 9,9-dimethylfluorene [(Me₂F) $_n$] and 9,9-dimethyl-4,5-diazafluorene [(Me₂DAF) $_n$] oligomers with up to 20 repeating units.

As an example, to demonstrate the delocalisation of HOMO and LUMO orbitals in 4,5-diazafluorene polymer along the main chain, the contour diagrams of HOMO and LUMO orbitals of the trimer $(\text{Me}_2\text{DAF})_3$ and the octamer $(\text{Me}_2\text{DAF})_8$ are shown in Fig. 5.8. The adjacent **DAF** subunits are bonding in LUMO while antibonding in HOMO. The HOMO and LUMO orbitals are spread over the whole molecules for small chain length oligomer $(\text{Me}_2\text{DAF})_3$. With the chain length grows $[(\text{Me}_2\text{DAF})_8]$, the HOMO and LUMO orbitals are localised in the middle part of the chain, as an increase in the chain length results in a decrease of their energies due to delocalisation and end fluorene units are less involved in this process.

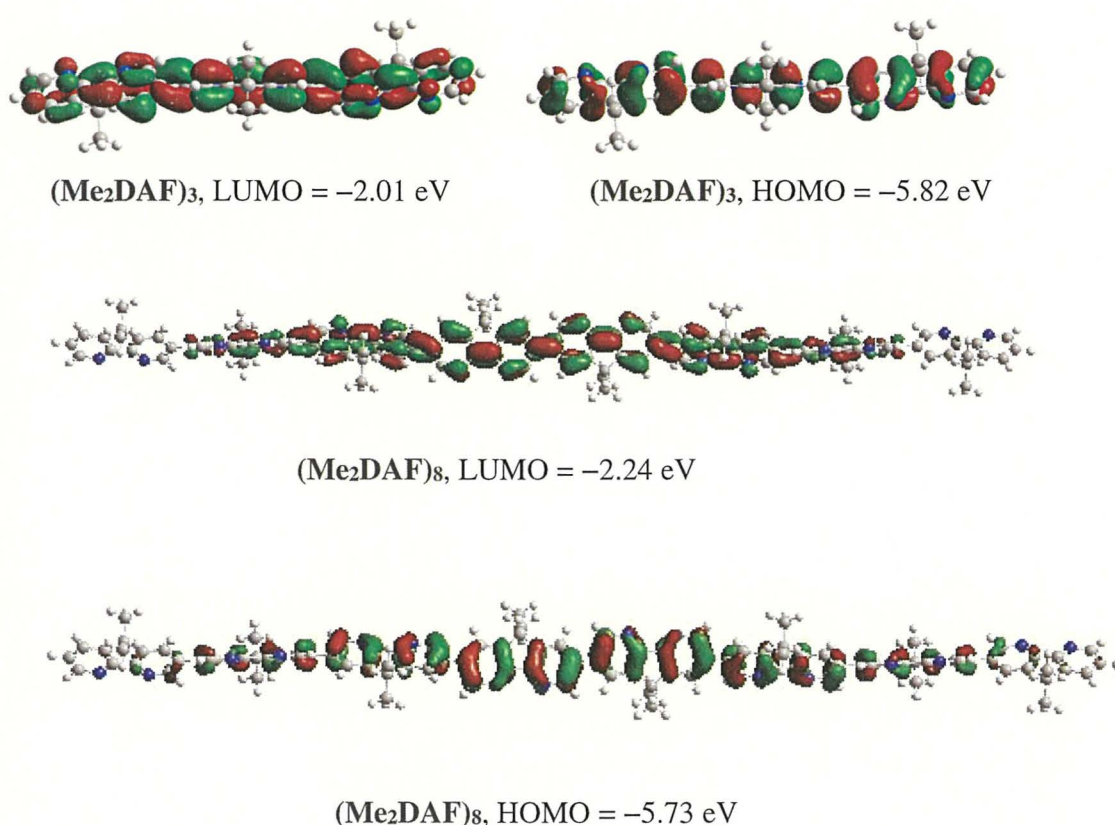


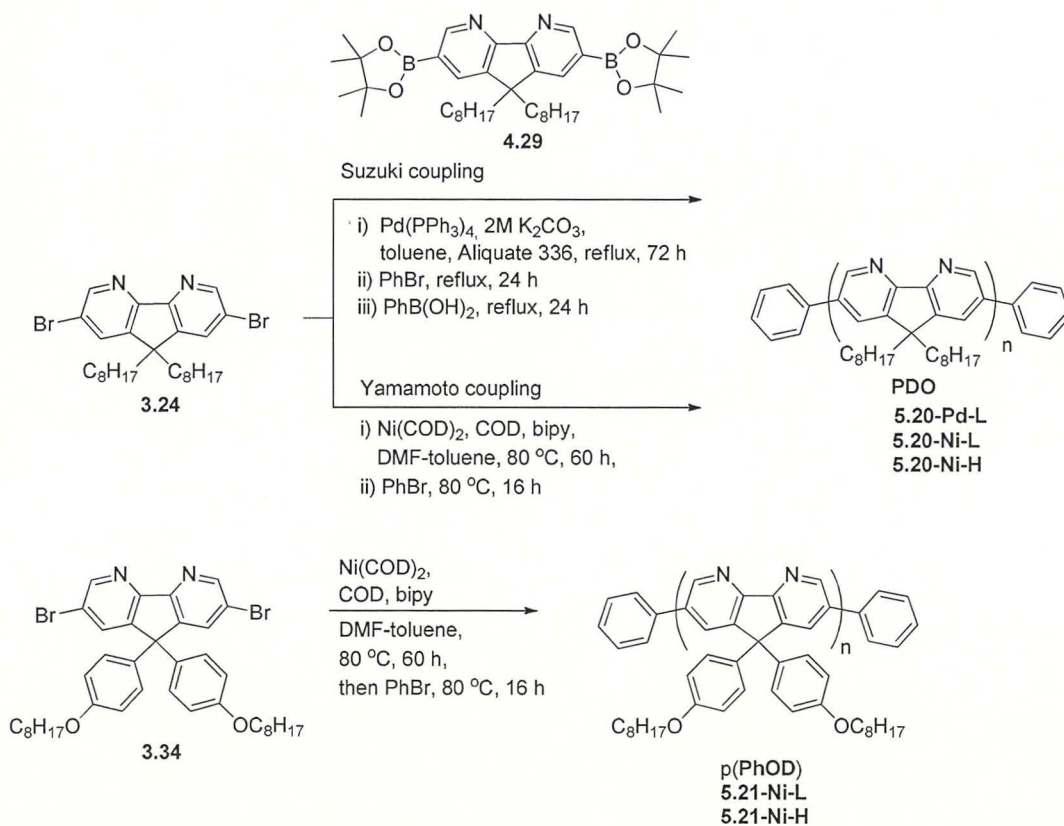
Fig. 5.8 Isocontour plots (0.02 e bohr^{-3}) of HOMO and LUMO orbital coefficients of the trimer $(\text{Me}_2\text{DAF})_3$ and octamer $[(\text{Me}_2\text{DAF})_8]$ for DFT B3LYP/6-31G(d) optimised geometries (visualised by GaussView 05 program)

In the next section, synthesis and study of physical properties of 4,5-diazafluorene based polymers have been described.

5.2.2 Synthesis and characterisation of 4,5-diazafluorene-based homopolymers

Synthesis of conjugated rigid rod type two novel homopolymers, poly(9,9-dioctyl-4,5-diazafluorene) (**PDO 5.20**) and poly[9,9-di(4-octyloxyphenyl)-4,5-diazafluorene] [**p(PhOD) 5.21**] from 4,5-diazafluorene monomer units (**3.24**, **4.29** and **3.34**) are shown in Scheme 5.8. Synthesis of monomer units **3.24** and **3.34** has been described in Chapter 3 and monomer unit **4.29** in Chapter 4. The polymer **PDO** was synthesised by two methods (Scheme 5.8). First method involved Pd-catalysed Suzuki coupling polymerisation between bifunctional monomers dibromo-DAF **3.24** and diborolane-DAF **4.29** in toluene with 2M K₂CO₃ and aliquat 336 under reflux for three days in argon atmosphere, followed by end-capping of the polymer with bromobenzene and benzenboronic acid to obtained a low molecular weight polymer **5.20-Pd-L** in a moderate yield (46%).

The second used method was based on Yamamoto coupling; performed under an inert condition with Schlenk-flask where the monomer unit dibromo-DAF **4.29** was mixed with Ni(COD)₂, cyclooctadiene, bipyridine in DMF-toluene solution and heated at 80 °C for nearly three days. This was followed by addition of end capper phenyl bromide and kept at 80 °C for another 16 hours to obtain somewhat higher molecular weight polymer **5.20-Ni-L** in good yield (56%).



Scheme 5.8 Synthesis of homopolymers **PDO** and **p(PhOD)** based on 4,5-diazafluorene.

In order to obtain high molecular weight polymer, the second method was repeated at more controlled conditions; taking into account of very hygroscopic nature and sensitivity to air of Ni(COD)₂, using glove box for weighing all the components, carefully keeping the reaction vessel from air/water during polymerisation. This polymerisation in a carefully controlled conditions resulted in a high molecular weight polymer **5.21-Ni-H** ($M_w = 109,900$, Table 5.1) obtained in a moderate yield of 31% (after purification). For both methods, crude products were purified by a Soxhlet extraction with acetone to remove low molecular weight fractions, followed by extraction with chloroform and then reprecipitation into methanol. Average molecular weight (M_w), number average molecular weight (M_n) was determined using GPC analysis of the respective polymers with polystyrene as the standard reference in chloroform (Table 5.1). It was found that polymer **PDO** prepared by Yamamoto coupling method with controlled conditions gave much higher average molecular weight ($M_w = 109,900$, PDI = 3.90) compared to Suzuki coupling polymerisation ($M_w = 6,100$, PDI = 2.69). End-capping (phenyl group) is well noticeable in the ¹H NMR spectrum of the low molecular weight polymer **5.20-Pd-L** shown in Fig. 5.9. This allowed us to reasonably estimate its molecular weight from ¹H NMR peak intensity integral⁶⁰ to be ($M_n = 2500$) corresponding to repeating units ($n = 6$), which is close to the value obtained by GPC analysis ($M_n = 2300$).

The homopolymer poly[9,9-di(4-octyloxyphenyl)-4,5-diazafluorene] (**5.21**) was synthesised in similar manner to the second method; by Yamamoto coupling of monomer unit **3.34** using Ni(COD)₂, cyclooctadiene, bipyridine in DMF-toluene solution and heated at 80 °C for nearly three days followed by end-capping with bromobenzene and kept at 80 °C for another 16 hours to obtain polymer **5.21-Ni-L** in good yields (46). In more controlled conditions as mention before giving higher molecular weight polymer **5.21-Ni-H** in good yields (56%).

Both the homo polymers are thermally stable with thermal decomposition temperature $T_d = 403$ °C and 350 °C (Fig. 5.10), respectively for polymers **5.20-Ni-L** and **5.21-Ni-L** (T_d determine by TGA, Table 5.1). Spectral stability of the polymers is discussed in section 5.2.3.4. Both the polymers (**5.20** and **5.21**) are highly soluble in chloroform, toluene and partly in tetrahydrofuran. Good solubility of synthesised homopolymers allowed a comprehensive study of their physical properties. Structures of synthesised polymers were characterised by ¹H NMR and ¹³C NMR. The ¹H NMR spectrum of both the polymers (**5.20** and **5.21**) found to be similar to the monomer unit with about 0.5-0.1 ppm up field shifted and broaded peak intensities.

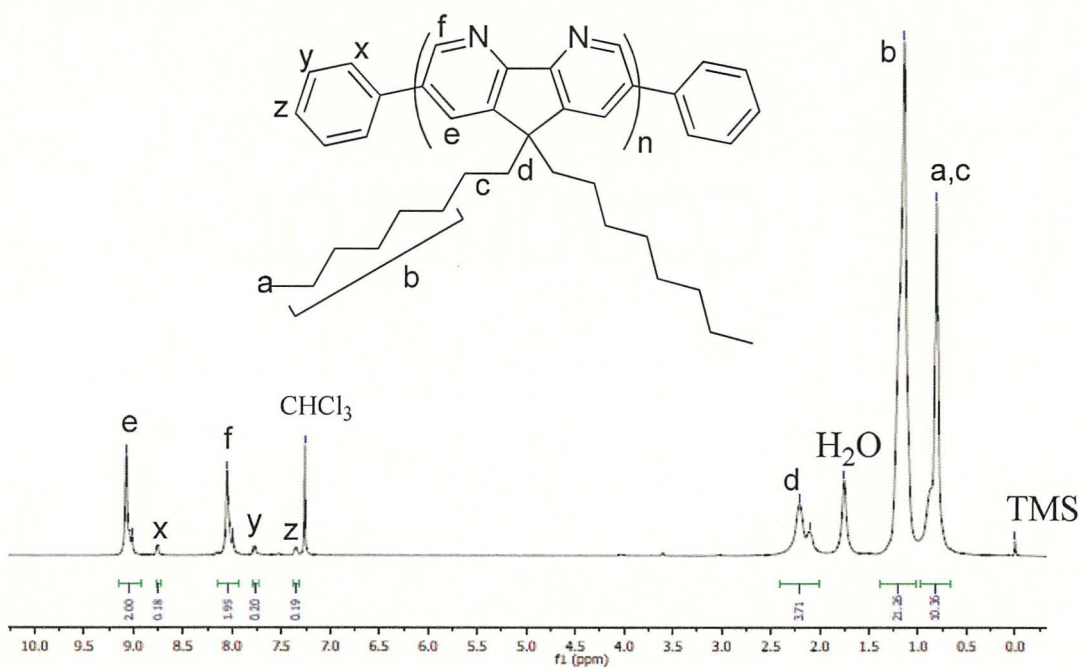


Fig. 5.9 ¹H NMR spectrum of homopolymer PDO (5.20-Pd-L).

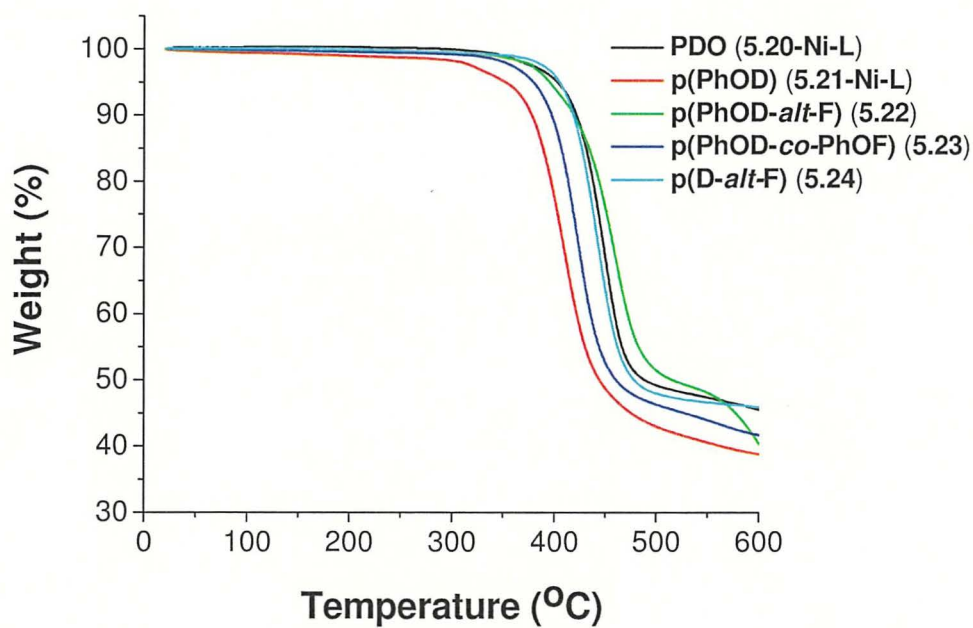


Fig. 5.10 TGA curves for polymers 5.20–5.24 under nitrogen; heating rate 5 °C min⁻¹.

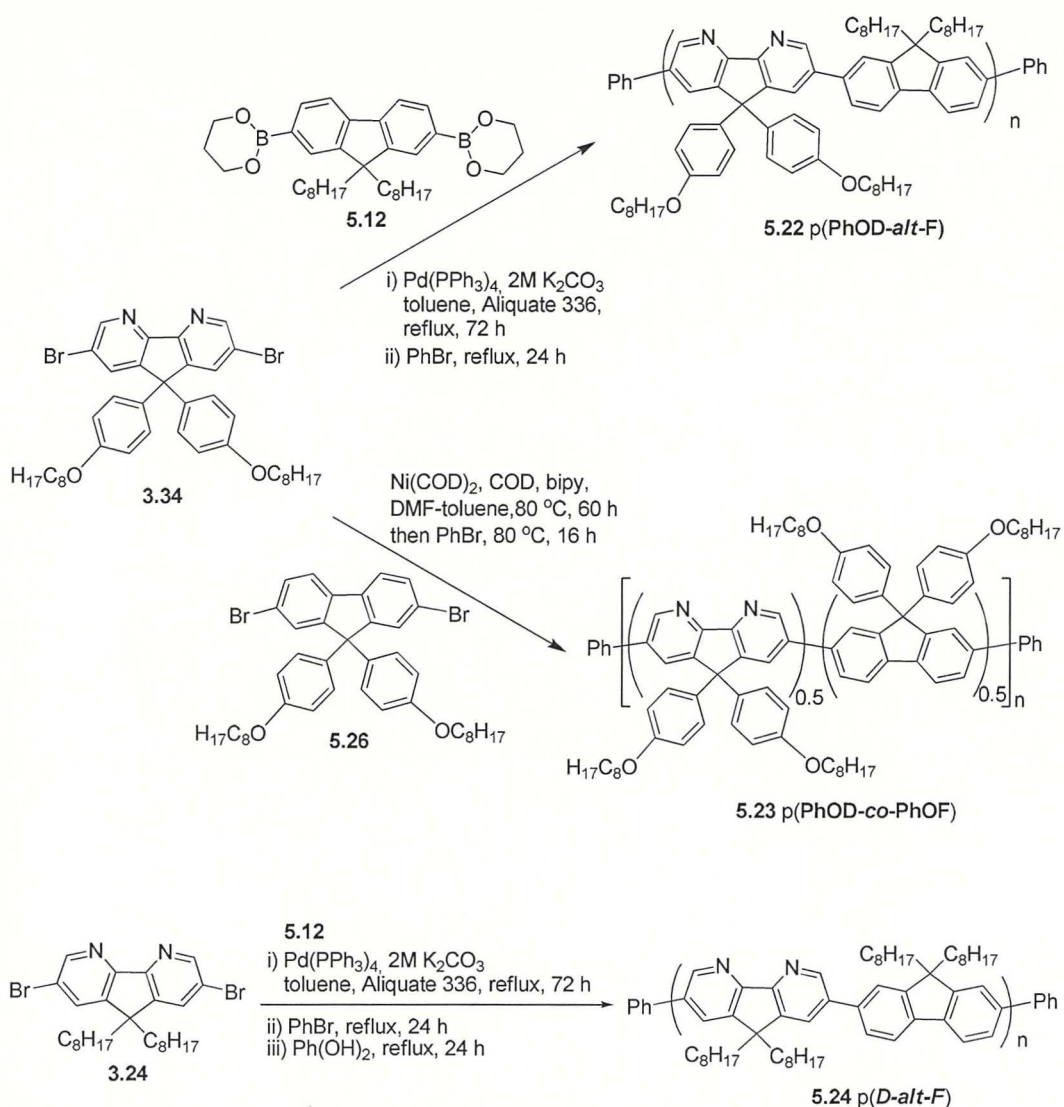
Table 5.1 GPC and TGA data for polymers **5.20–5.24** and **PFO**.

Polymers	M_n	M_w	PDI	T_d (°C) ^d
PDO (5.20-Pd-L)	2,300	6,100 ^a	2.69	–
PDO (5.20-Ni-L)	3,600	23,200 ^a	6.53	403
PDO (5.20-Ni-H)	28,200	109,900 ^a	3.90	–
p(PhOD) (5.21-Ni-L)	1,530	4,050 ^a	2.64	350
p(PhOD) (5.21-Ni-H)	71,600	206,800 ^a	2.89	–
p(PhOD-<i>alt</i>-F) (5.22)	11,700	28,900 ^b	2.48	394
p(PhOD-<i>co</i>-PhOF) (5.23)	15,100	39,900 ^b	2.64	379
p(D-<i>alt</i>-F) (5.24)	4,200	21,900 ^b	5.17	405
PFO^e	53,400	194,100 ^a	3.63	385 ^c

^aPerformed with polystyrenes as standard references in chloroform. ^bPerformed with polystyrenes as standard references in tetrahydrofuran. ^cDatum taken from ref. 24. ^dThermal decomposition temperature determined by TGA at 5% weight loss under nitrogen heating rate 5 °C min⁻¹. ^eThis sample of high molecular weight **PFO** has been synthesised in Prof. U. Scherf group.

5.2.3 Synthesis and properties of 4,5-diazafluorene-based copolymers

Three different copolymers of 4,5-diazafluorene with fluorene (**5.22**, **5.23**, **5.24**) was successfully prepared (Scheme 5.9). A regioregular copolymer **p(PhOD-*alt*-F) (5.22)**, consisting of 1:1 ratio of 9,9-bis(octyloxyphenyl)-4,5-diazafluorene to 9,9-dioctylfluorene unit was synthesized by employing Suzuki coupling between monomer units **3.34** and **5.12** in a good yield (66%). Similarly, another regioregular copolymer **p(D-*alt*-F) (5.24)** was synthesised in the ratio 1:1 of 9,9-dioctyl-4,5-diazafluorene and 9,9-dioctylfluorene unit by Pd-catalysed Suzuki reaction in good yield (51%). When this work was underway, Huang *et al.* reported synthesis of similar statistical co-polymers **5.24** with different ratio of diazafluorene and fluorene units using similar method.⁶¹ A master student in our group of research has synthesised polymer similar to **5.24** with the ratio 90:10 = fluorene:diazafluorene units and used it for studying metal sensing property.⁶² Metal sensing ability of polymer **5.24** with the ratio 90:10 = fluorene:diazafluorene units was found to follow similar trend as that of the **FDF** oligomer described in Chapter 4. A random polymer **p(PhOD-*co*-PhOF) (5.23)** of 9,9-bis(octyloxyphenyl)-4,5-diazafluorene and 9,9-bis(octyloxyphenyl)fluorene units was synthesised by Yamamoto coupling using Ni(COD)₂ as reductive transition metal-based coupling agent followed by end capping with bromobenzene in good yield (77%).



Scheme 5.9 Synthesis of fluorene–4,5-diazafluorene copolymers **5.22–5.24**.

The ratio between the monomer units was estimated by the peak intensity of ¹H-NMR spectrum confirming 1:1 ratio. Weight average molecular weight (M_w), number average molecular weight (M_n) and polydispersity index (M_w/M_n) was determined by GPC analysis in THF with polystyrene standard (Table 5.2). Average molecular weight of random copolymer **5.23** was found to be higher compared to alternate copolymers **5.24** and **5.22**, suggesting better polymerization result from Yamamoto coupling. Thermal properties were estimated by TGA measurements. TGA analysis reveals excellent thermal stabilities for both homo- and copolymers **5.20-5.24** under nitrogen. Thermal decomposition temperature (5% weight loss) (Table 5.1) found to be highest for copolymer **5.24** ($T_d = 405$ °C) compared to copolymer **5.23** ($T_d = 379$ °C) and **5.22** ($T_d = 394$ °C). These decompositions at > 400 °C with initial mass loss of ~ 50–60% correspond to a thermal cleavage of C–C bond at C-9 carbon atom with an

abstraction of side solubilising groups. DSC studies of polymers **5.20-5.24** under nitrogen did not show glass transition points.

5.2.4 Electrochemical properties of the 4,5-diazafluorene based polymers

To determine the n-doping and p-doping character of the polymers, the oxidation and reduction potentials of the polymer films were investigated by cyclic voltammetry (CV). Cyclic voltammograms of polymers **5.20–5.24** are shown in Fig. 5.11 and their oxidation and reduction potentials ($E_{\text{onset}}^{\text{ox}}$, $E_{\text{onset}}^{\text{red}}$) determined from onsets of the electrochemical p-doping and n-doping are summarised in Table 5.2.

The p- and n-doping are assigned to the oxidation and reduction of π -conjugated systems. The polymers exhibit irreversible or partly reversible redox waves in both n-doping and p-doping processes. The HOMO and LUMO levels derived from the oxidation and reduction potential of DAF based homopolymer **PDO (5.20-Ni-L)** are -5.74 eV and -2.54 eV, respectively. These values are close to the DFT calculated values of **(Me₂DAF)_n** in gas phase (-5.72 eV and -2.30 eV, obtained by extrapolation, Fig 5.14 b). Thus, a good correlation was seen between the experimental and the calculated values of HOMO and LUMO levels of DAF based polymer **PDO**.

From Table 5.2, it can be seen that the band gaps (E_g) of the polymers **5.20–5.24** (3.20–3.36 eV) are close, but slightly lower than literature values for the homopolymer **PFO** (3.61 eV),⁴⁶ The main reason of this differences is that the LUMO levels of polymers **5.20–5.24** (ca. -2.4 eV) are lower while HOMO levels (ca. -5.7 eV) are close to that of **PFO** (HOMO = -2.16 eV, LUMO = -5.77 eV). The polymers **5.20–5.24**, therefore, are expected to exhibit improved charge injection from cathode and electron transporting properties compared to homopolymer **PFO**. Thus, electron deficient diazafluorene moiety gives polymers with slightly reduced band gap. The main effect of electronegative atoms in polymers is in decreasing of LUMO orbital energies with only slight changes of HOMO energies

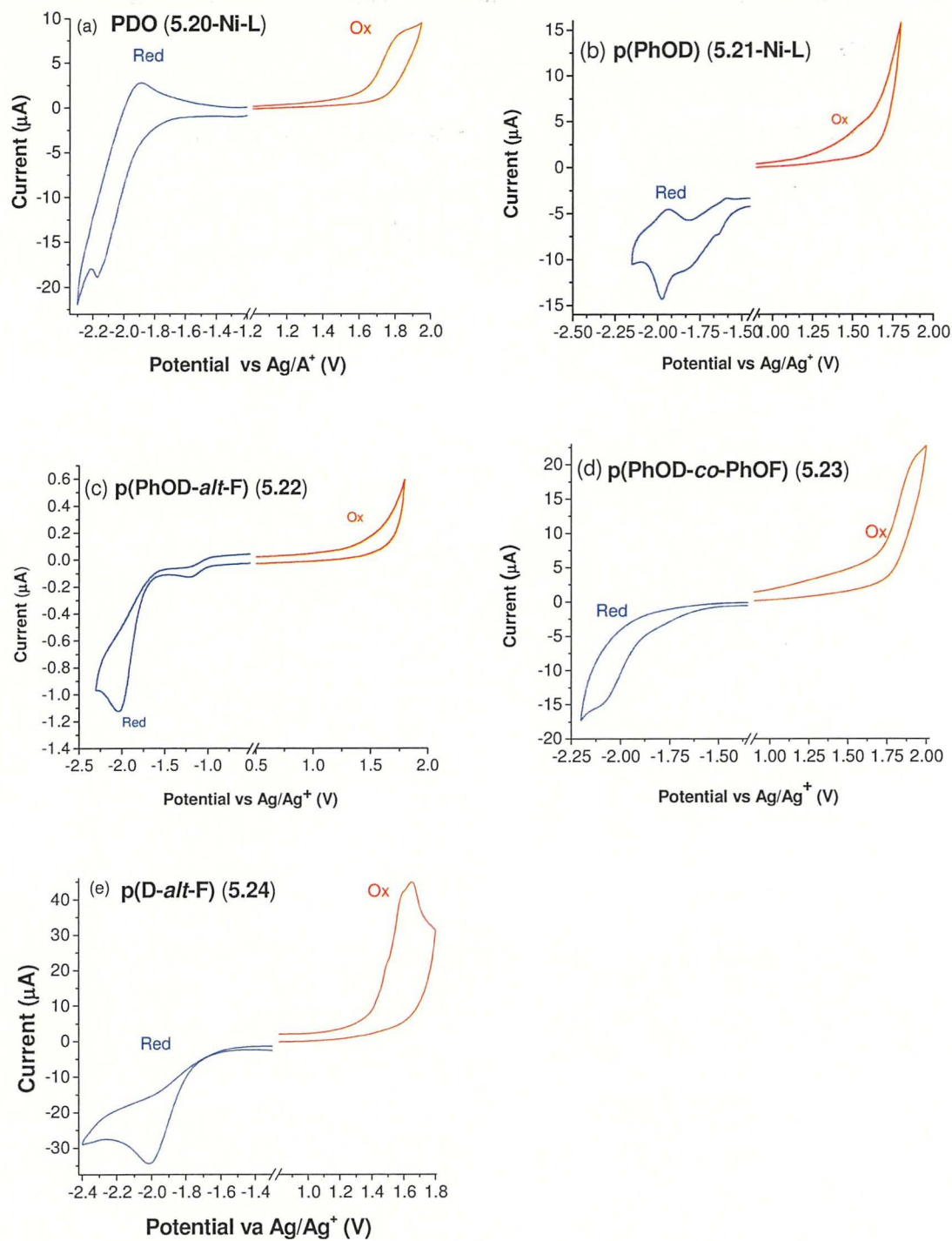


Fig. 5.11 Cyclic voltammograms of polymers 5.20–5.24 in films; scan rate 50 mV/s, acetonitrile, supporting electrolyte 0.1 M Bu₄NPF₆, reference electrode Ag/Ag⁺.

Table 5.2 Redox potentials, HOMO, LUMO energy levels and band gap for polymers **5.20–5.24** in films, from cyclic voltammetry measurements.^a

Polymer	$E_{\text{onset}}^{\text{ox}}$ (V)	$E_{\text{onset}}^{\text{red}}$ (V)	E_{HOMO} (eV)	E_{LUMO} (eV)	E_{g}^{CV} (eV) ^a
PDO (5.20-Ni-L)	1.45	-1.75	-5.74	-2.54	3.20
p(PhOD) (5.21-Ni-L)	1.46	-1.81	-5.75	-2.48	3.27
p(PhOD-<i>alt</i>-F) (5.22)	1.45	-1.86	-5.74	-2.43	3.31
p(PhOD-<i>co</i>-PhOF) (5.23)	1.48	-1.88	-5.77	-2.41	3.36
p(D-<i>alt</i>-F) (5.24)	1.43	-1.89	-5.72	-2.40	3.32
PFO ⁴⁶	1.36	-2.24	-5.77	-2.16	3.61

^aScan rate = 50 mV/s, acetonitrile, 0.1 M Bu₄NPF₆, glassy carbon electrode (2 mm disk), Ag/Ag⁺ quasi-reference electrode; potentials are recalculated vs Fc/Fc⁺ as an internal standard. ^a $E_{\text{g}}^{\text{CV}} = E_{\text{HOMO}} - E_{\text{LUMO}}$.

5.2.5 Optical properties of the 4,5-diazafluorene based polymers

The optical properties of synthesised homopolymers and copolymers have been investigated both in the solution and in the solid state. The films of the polymers for solid state measurements have been prepared by spin-coating of chloroform solutions on quartz plates. UV-Vis absorption spectra and photoluminescence spectra of polymers **5.20–5.24** in chloroform solution and as spin-coated films on quartz substrate are shown in Fig. 5.12 and Fig. 5.13 and the data are summarised in Table 5.1.

The absorption spectra in solution are characterised by structureless bands with absorption maxima in the range of $\lambda_{\text{abs}} = 395\text{--}404$ nm that can be assigned to $\pi\text{-}\pi^*$ transition of the conjugated backbone. Compared to polyfluorene homopolymer **PFO** ($\lambda_{\text{abs}} = 386\text{--}389$ nm^{43,46,63}), **DAF**-based homopolymers **5.20** ($\lambda_{\text{abs}} = 399$ nm) and **5.21** ($\lambda_{\text{abs}} = 396$ nm) show small bathochromic shifts by $\sim 6\text{--}13$ nm, while copolymers **5.22–5.24** demonstrate a further bathochromic shift by $\sim 1\text{--}9$ nm (Table 5.1). Similarly, to polyfluorene **PFO**, **DAF**-based homopolymers **5.20–5.21** and copolymers **5.22–5.23** do not show substantial differences between their absorptions in solution and the solid state: the differences are of $\sim 0\text{--}3$ nm only (copolymer **5.24** shows the slight blue shift by 7 nm in the film compared to the solution).

Optical band gaps determined from the absorption edges of polymers in the solid state are in the range of 2.73–2.88 eV (Table 5.1). Recently, Huang *et al.* reported synthesis of polymer **5.24** and spectral data is consistent with what we observed.⁶¹

Photoluminescence maximum is in the blue region of the spectrum in chloroform, in the range 421–428 nm with two distinct bands, while in film shows red shifted and broad emission (Fig.

5.12, Fig. 5.13, right). This broadening and red shifted emission in film compared to solution may be attributed to intermolecular interactions in the solid state as observed before for other conjugated polymers, including polyfluorenes. Photoluminescence quantum yields (PLQY) in a solution have been determined in chloroform using 9,10-diphenylanthracene as a standard and absolute quantum yields for the solid state have been measured using a calibrated integrating sphere. Photoluminescence quantum yields of 4,5-diazafluorene-based homopolymers and copolymers **5.20-5.24** were found to be 62–68% in solution 15–17% in films (Table 5.1). This dropdown of quantum yields from solution to solid state may be attributed to the formation of aggregates in the solid state.

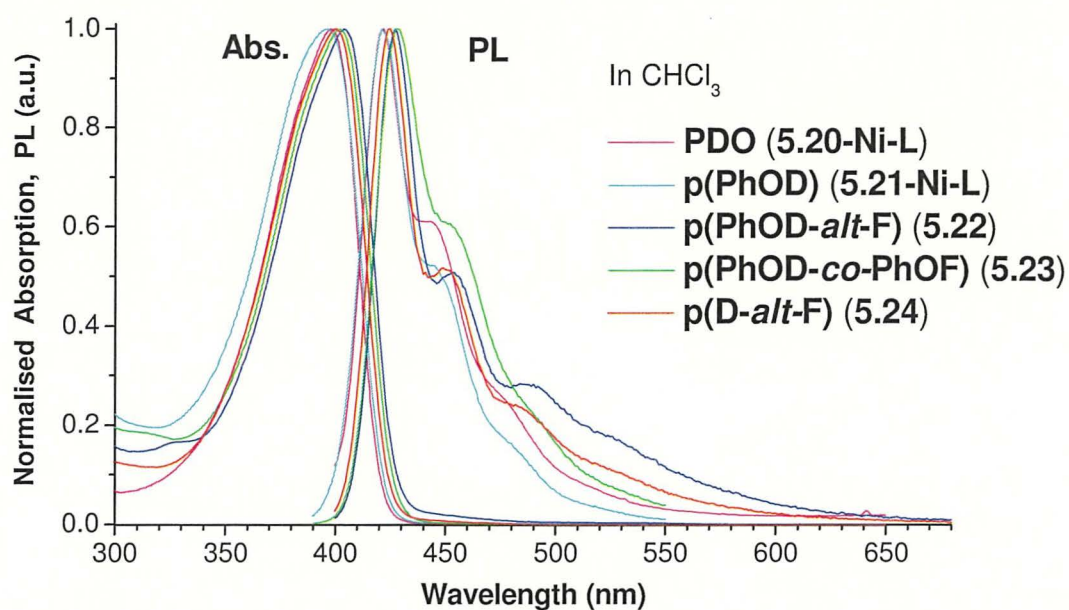


Fig. 5.12 Normalised absorption and emission spectra of polymers (5.20-5.24) in chloroform.

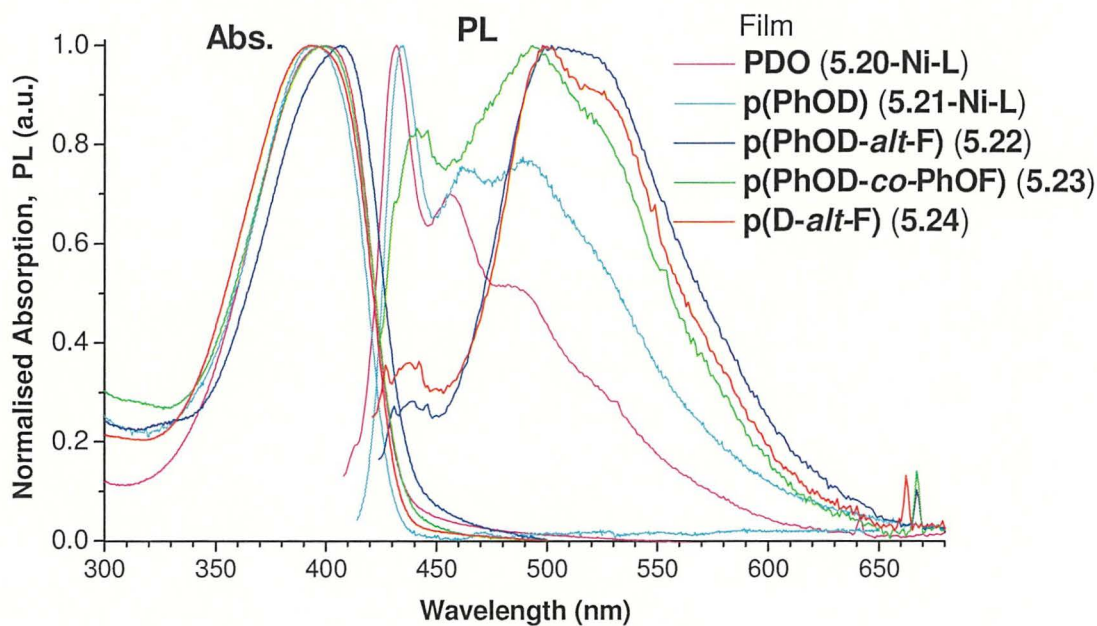


Fig. 5.13 Normalised absorption and photoluminescence spectra of polymers 5.20-5.24 as spin coated films on quartz windows.

Table 5.3 Absorption and photoluminescence, band gap, and PLQY of polymers.

Polymers	λ_{abs}	λ_{PL}	Φ_{PL}	λ_{abs}	λ_{PL}	Φ_{PL}	$E_{\text{g}}^{\text{opt}}$ (eV) ^c
	(nm) CHCl ₃	(nm) CHCl ₃	(%) ^a CHCl ₃	(nm) Film	(nm) Film	(%) ^b Film	
PDO (5.20-Pd-L)	399	421, 445sh, 482sh	65 (390)	400	431, 455sh, 489sh	16 (400)	2.73
p(PhOD) (5.21-Ni-L)	395	421	68 (380)	395	435, 463sh, 493sh	15 (395)	2.79
p(PhOD-<i>alt</i>-F) (5.22)	404	427	62 (390)	407	502, 438sh 524br	16 (407)	2.83
p(PhOD-<i>co</i>- PhOF) (5.23)	401	428	67 (380)	400	443 sh, 493	16 (400)	2.86
p(D-<i>alt</i>-F) (5.24)	400	425	66 (390)	393	500, 435sh, 530sh	17 (406)	2.87
PFO^d				401	441, 467sh, 503br	37 (390)	2.71
PFO⁴⁶	386	443		391	422		2.76
PFO⁶³	387 (tol)	414	85	389	435		
PFO⁴³	389	417, 439	78	383	425, 447, 520	40	

^aPLQY measured in chloroform using 9,10-diphenylanthracene in degassed cyclohexane as standard ($\Phi_{\text{PL}} = 90\%$). ^bAbsolute PLQY for spin-coated films measured in an integrating sphere (excitation wavelengths, λ_{ex} , are given in brackets). ^c $E_{\text{g}}^{\text{opt}}$ is the optical band gap estimated from the absorption edge of the polymer film. ^dThis sample of high molecular weight **PFO** has been synthesised in Prof. U. Scherf group.

5.2.6 Thermal annealing studies of the 4,5-diazafluorene based polymers

To study the spectral stability polymer in film, thermal annealing in air experiments was performed on polymers **5.20**, **5.21** and **5.24**. Also, in order to investigate whether similar g-band appear (commonly associated with PFs) in our newly synthesis poly(9,9-dioctyl-4,5-diazafluorene) (**PDO**, **5.20-Ni-L**) which is topologically similar to poly(9,9-dioctylfluorene) (**PFO**) we did thermal annealing at various temperature for fixed time interval of 1 hour in air and measure their PL spectrum and absorption spectrum for both the polymer (**PDO** and **PFO**) as shown in Fig. 5.14-5.15.

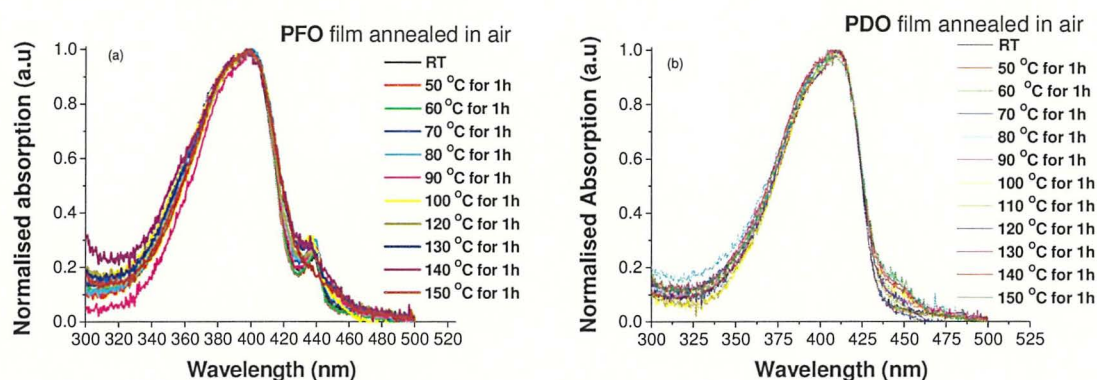


Fig. 5.14 Effect of thermal annealing on absorption spectrum of **PFO** (a) and **PDO** (b) spin coated film upon thermal anneal in air.

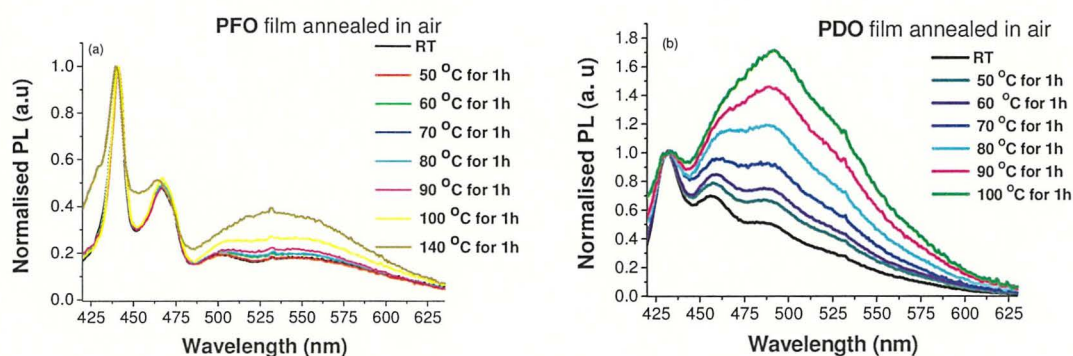


Fig. 5.15 Effect of thermal annealing in air on photoluminescence spectra for poly(9,9-dioctylfluorene) (**PFO**) (a) and **PDO** (**5.20-Ni-L**) (b).

It can be seen from the emission spectrum (Fig. 5.15), that upon thermal annealing, g-band appear to increase with increase in temperature above 70 °C for **PFO**. A similar effect was also observed for the polymer **PDO** (Fig. 5.16), but the increase in band at about 510 nm (broad emission, may be called g-band) starts at a lower temperature of 50 °C. It can be

inferred that **PDO** also shows g-band as that exhibited by **PFO** and their spectral stability is comparable to **PFO** under thermal annealing in air. Normalised absorption spectra of both polymers (**PFO** and **PDO**) (Fig. 5.15) do not show any significant changes upon thermal annealing, however, a decrease in intensity of the absorption maximum with increase in temperature in their unnormalised absorption spectrum was observed.

Small band at 435 nm in the absorption spectrum of **PFO** in spin coated film is assigned to its β -phase.^{1a,64} As mentioned before, β -phased **PFO** exhibit improved device performance compared to amorphous phase **PFO**.⁶⁵ Under similar conditions of preparing film **PDO** do not show the formation of β -phase at room temperature. It is not clear about the reason for more disorder morphology in **PDO** compared to **PFO**. For comparison, normalise UV and PL spectrum of **PDO** and **PFO** at room temperature is shown in Fig. 5.16. Absorption maximum for both the polymers is about 400 nm. PL maximum show slight blue shift of about 10 nm for **PDO** compared to **PFO** implying a deeper blue emitter. The optical band gap of **PDO** (2.73 eV) measured from the adsorption edge in films found to be about 0.04 eV lower than that of **PFO** (2.76 eV).⁴⁶

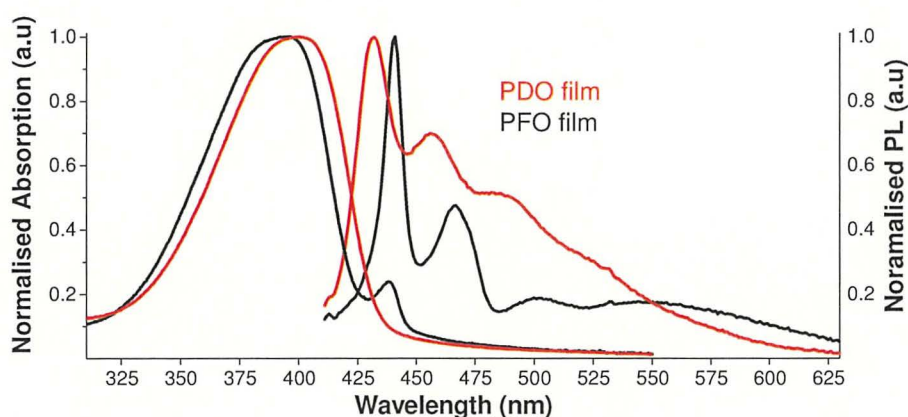


Fig. 5.16 Normalised PL and UV spectra for poly(9,9-dioctyl-4,5-diazafluorene) (**PDO**, **5.20-Ni-L**) and poly(9,9-dioctylfluorene) (**PFO**) in spin coated films.

The homopolymer **p(PhOD)** (**5.21-Ni-L**) and copolymer **p(D-alt-F)** (**5.24**) shows a similar trend as observed in **PDO** (**5.20-Ni-L**) upon thermal annealing in air. The absorption and emission spectrum of polymer **5.21-Ni-L** upon thermal anneal in the air at 150 °C (2 hours), 180 °C (1.5 hours) and 200 °C (2 hours) is shown in Fig. 5.17. The absorption spectra do not show any significant changes upon thermal annealing. The spectral stability of **p(PhOD)** (**5.21**) is somewhat better than **PDO** (**5.21**), since emission peak at 430 nm changes less at

higher temperatures of heating for **p(PhOD)**. Also, the vibronic structure of the emission in the region 480-540 nm remain intact while heating upto 180 °C (1.5 hours) which further indicates better stability in comparison to **PFO**.

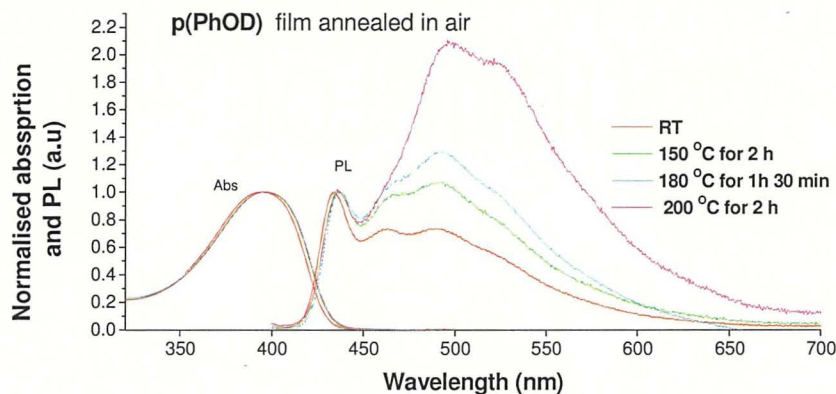


Fig. 5.17 Effect of thermal annealing of poly(9,9-dioctyloxyphenyl-4,5-diazafluorene) **5.21** film in air atmosphere on its absorption and emission spectra.

The absorption and emission spectrum of polymer **5.24** upon thermal annealing in air at 150 °C (2 hours), 180 °C (1.5 hours) and 200 °C (2 hours) is shown in Fig. 5.18. The normalised absorption spectra remain unchanged. The g-band is noticeable even at room temperature for the copolymer **5.24** which gradually increases upon annealing at higher temperature. The vibronic structure of the emission in the region 480-540 becomes single broad structureless emission beyond 150 °C (2 hours) of annealing in air. This suggests a better stability compared to **PFO**.

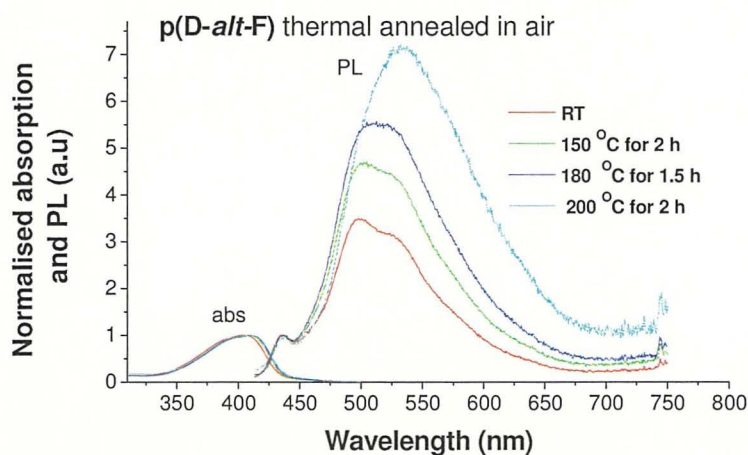


Fig. 5.18 Effect of thermal annealing of **p(D-alt-F)** (**5.24**) film in an air atmosphere on its absorption and emission spectra.

5.3 Conclusion

We have performed a comparative calculations of frontier orbital energy levels for oligomers of the fluorene and 4,5-diazafluorene series by DFT B3LYP/6-31G(d) method in the gas phase. The 9-unsubstituted [(**F**)_n, (**DAF**)_n], or 9,9-dimethylated oligofluorenes and oligo-4,5-diazafluorenes [(**Me₂F**)_n, (**Me₂DAF**)_n] have been chosen that allowed to perform calculations up to $n = 20$, the value which is higher than the conjugation length in fluorene-type polymers ($n \sim 12$). It was found that with an increase of the lengths of the oligomers results in an increase of HOMO and decrease of LUMO energy levels, as well as the HOMO–LUMO gaps. This demonstrated the saturation of the values for $n > 12$ –14. Methylation of **F** and **DAF** units' results in quite small changes of HOMO/LUMO energies, and further increase of the length of the side alkyl chain to ethyl has an even lower effect. For “methylated” oligomers, (**Me₂F**)_n and (**Me₂DAF**)_n series, this results in decreasing the HOMO and LUMO by 0.71 eV and 0.69 eV, respectively, when passing on from $n = 2$ to $n = \infty$ extrapolated value), i.e. an effect of nitrogen atoms is near the same for HOMO and LUMO orbitals (Fig. 5.7a,b). The HOMO–LUMO gaps for **F** and **DAF** series are very similar: extrapolated values for (**Me₂F**)_n and (**Me₂DAF**)_n to $n = \infty$ are 3.420 eV and 3.435 eV, so the difference is about 15 meV only (Fig. 5.7c,d). The predicted lowering HOMO and LUMO energy levels for 4,5-diazafluorene polymer compared to parent polyfluorene implied an improve in the electron transporting properties of **DAF**-based polymers with decrease in the electron injection barrier in the case of its use as material for OLED. A deviation from linear dependences for longer oligomers ($n > 12$) was observed Fig. 5.7b. The HOMO and LUMO orbitals are mainly localised in the middle part of the chain for higher chain length oligomers.

Novel polymers of 4,5-diazafluorene **5.20**–**5.24** were synthesised by either Yamamoto or Suzuki coupling reactions of the respective monomer units. Method for synthesis of high molecular weight, rigid rod type DAF based homo polymers [**PDO** (**5.20-Ni-H**; $M_w = 109,900$), **p(PhOD)** (**5.21-Ni-H**; $M_w = 206,800$)] were developed, using Yamamoto coupling reaction in good yields (31%, 56%). A regioregular copolymer **p(PhOD-*alt*-F)** (**5.22**), consisting of 1:1 ratio of 9,9-bis(octyloxyphenyl)-4,5-diazafluorene to 9,9-dioctylfluorene unit was synthesised by employing Suzuki coupling between monomer units **3.34** and **5.12** in a good yield (66%). Similarly, a regioregular copolymer **p(D-*alt*-F)** (**5.24**) was synthesised in the ratio 1:1 of 9,9-dioctyl-4,5-diazafluorene and 9,9-dioctylfluorene unit by Pd-catalysed Suzuki reaction in good yield (51%) and a random polymer **p(PhOD-co-PhOF)** (**5.23**) of 9,9-bis(octyloxyphenyl)-4,5-diazafluorene and 9,9-bis(octyloxyphenyl)fluorene units was synthesised by Yamamoto coupling using Ni(COD)₂

as reductive transition metal-based coupling agent in good yield (77%). All the polymers were end-capped with phenyl group using bromobenzene/benzene boronic acid after polymerisation reaction time. The crude polymers were purified by Soxhlet extraction with acetone followed by re-precipitation in methanol to afford yellowish solids. Average molecular weight (M_w), number average molecular weight (M_n) was determined by GPC analysis of the respective polymers (Table 5.1). For lower molecular weight polymers (**5.20-Pd-L**, **5.20-Ni-L**, **5.21-Ni-L**), the end-capped group (phenyl group) peaks was observed in their $^1\text{H-NMR}$ spectrum. The ratio between the monomer units of copolymer (**5.22-5.24**) was estimated by the integral of the peak intensity of their $^1\text{H-NMR}$ spectrum confirming expected feed ratio of 1:1. Thermal properties, estimated by TGA analysis (Fig 5.17, Table 5.1), reveals excellent thermal stabilities for both the homo- and copolymers **5.20-5.24**. The thermal decomposition temperature (T_d) is in the range 350-405 °C similar to polyfluorene.

The polymers **5.20-5.24** exhibit irreversible or partly reversible redox waves in both n-doping and p-doping processes determined by cyclic voltammetry. A good correlation of HOMO and LUMO levels determined by the cyclic voltammetry measurement of polymer **PDO** (**5.20-Ni-L**, -5.74 eV and -2.54eV, Table 5.1) and the DAF calculated values of $(\text{Me}_2\text{DAF})_n$ in gas phase (-5.72 eV and -2.30, extrapolated from Fig 5.14 b). The polymers **5.20-5.24** exhibit slightly lower level of band gap (3.20-3.36 eV) compared to literature known value of **PFO** (3.61 eV) by CV measurement (Table 5.2). In addition, the LUMO levels are found to be comparatively lower than the HOMO levels. This has been attributed to the electron withdrawing nitrogen atoms of diazafluorene units. The polymers **5.20-5.24** are, therefore, expected to exhibit improved exhibit improved charge injection from cathode compared to homopolymer **PFO**.

The absorption spectra in solution as well in film of polymers **5.20-5.24** are characterised by structureless bands with absorption maxima at nearly the same region in the range $\lambda_{\text{abs}} = 395\text{--}404$ nm. Their photoluminescence maximum is in the blue region of the spectrum in chloroform, in the range 421-428 nm with two distinct bands, while in film shows red shifted and broad emission in the range 431-500 nm (Fig. 5.12, Fig. 5.13). They exhibit a good photoluminescent quantum yield in the solution (ca. 70%) and in the film (ca. 16%) (Table 5.3).

The polymers (**5.20-Ni-L**, **5.21-Ni-L**, **5.24**) showed spectral stability upon thermal annealing in air of their films, comparable to **PFO**. Among them, the spectral stability of **p(PhOD)**

(**5.21-Ni-L**) found to be more stable, since the vibronic emission peak in the region 430-530 nm changes less with the increase in temperatures of annealing in air. Overall, the polymers **5.20-5.24** exhibit good thermal and spectral stability as emissive material. Potential application of these polymers is as deep blue emissive material in PLED, electron transport material and sensor.

5.4 Experimental

Chemicals

All chemicals were purchased from Aldrich and Alfa Aesar chemical companies and were used without any further purification. The solvents THF, toluene and dioxane were dried by reflux over Na metal under nitrogen, and distilled off directly before use. The catalyst Pd(PPh₃)₄ was synthesised according to the literature procedure.⁶⁶ Synthesis of key starting 2,7-dibromo-4,5-diazafluorene monomers **3.24-3.34** are described in Chapter 2. All the polymerization reactions were performed under argon atmosphere.

Instrumentation

NMR details are given in Chapter 2. The weight-average molecular weights (M_w) and polydispersity indices (M_w/M_n) of the polymers were measured on a PL-GPC model 50 chromatograph at room temperature using THF or CHCl₃ as eluents and standard polystyrenes as references. Absorption and emission spectra in solution were measured using HPLC grade solvent in 10 mm path length quartz cells and solid-state measurement by spin coated film prepared on 12.5 mm circular quartz substance, using Shimadzu UV-3600 UV-Vis-NIR spectrophotometer and Horiba Yvon Fluoromax-4 spectrofluorometer at room temperature. TGA and DSC were measured on TA SDTQ600.

Photoluminescence quantum yields (PLQY, Φ_{PL}) of all the polymers were measured in HPLC grade chloroform at room temperature, which were carefully purged with argon prior to measurements, according to previously described method.⁶⁷ The photoluminescence quantum yields were calculated according to the following formula:⁶⁸

$$\Phi = \Phi_r(A/A_r)(OD_r/OD)(n^2/n_r^2)$$

Where Φ is the quantum yield, A is the integrated intensity, OD is the optical density, and n is the refractive index. The subscript r refers to the reference fluorophore of known quantum

yield. 9,10-diphenylanthracene (9,10-DPA) dilute solution in cyclohexane ($\Phi_r = 90\%$) was used as fluorophore standards. The solutions were bubbled by argon for about 10 minutes to avoid quenching by dissolved oxygen.

General procedure used for thermal annealing experimentation: Circular quartz cell (diameter =125 mm) was used to prepare film by spin coating at 300 rpm with the respective polymer solution (1mg dissolved in 1 mL of chloroform). The spin-coated films were annealed in an oven over a certain period of time. After cooling to room temperature, the film was measured for absorption and emission spectrum. After measurement, the films was subsequently annealed at different temperature and measured absorption and emission spectrum.

Cyclic voltammetry experiments were conducted in a standard three-electrode configuration, using Metrohm Autolab PGSTAT-302N potentiostat / galvanostat, with iR drop compensation. A glassy carbon electrode coated with thin film by drop cast method from the chloroform solution of polymer was used as working electrode and platinum wire (d = 1 mm) as counter electrodes, respectively. Ag/AgNO₃ (0.1M in ACN) reference electrode was used (separated from the solution by a Vycor frit) and the potentials are quoted versus ferrocene half wave potential. Oxidation and reduction scans were performed in acetonitrile containing 0.1 M Bu₄NPF₆, under argon at room temperature with a scanning of 50 mV/s. HOMO and LUMO are calculated according to the empirical formula:

$$E_{\text{HOMO}} = - (E_{[\text{ox vs. Fc}^+/\text{Fc}]} + 4.4) \text{ (eV)},$$

$$E_{\text{LUMO}} = - (E_{[\text{red vs. Fc}^+/\text{Fc}]} + 4.4) \text{ (eV)},$$

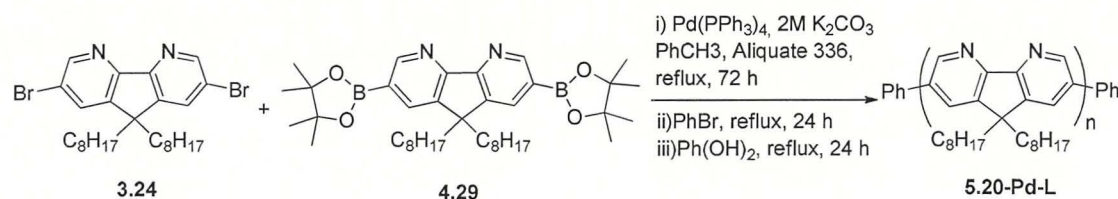
Where -4.4 eV represents the absolute energy level of Fc⁺/Fc redox couple below the vacuum in energy diagram.^{69,70,71}

Synthesis of 4,5-diazafluorene-containing polymers

Poly(9,9-dioctyl-4,5-diazafluorene) (PDO)

A) Pd-Catalysed Suzuki coupling polymerization method:

Exp: SG-189 Low molecular weight polymer, 5.20-Pd-L



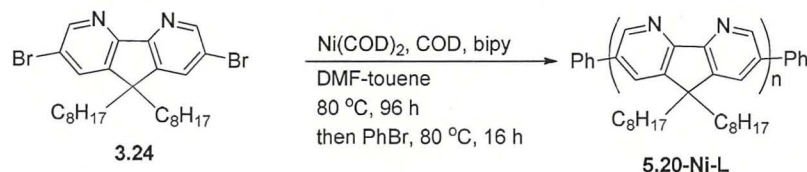
A three-neck flask was charged with 2,7-dibromo-9,9-dioctyl-4,5-diazafluorene **3.24** (80.0 mg, 0.146 mmol), 9,9-dioctyl-2,7-bis(4,4,5,5-tetramethyl-1,3,2-dioxaborolan-2-yl)-4,5-diazafluorene **4.29** (94.1 mg, 0.146 mmol), $\text{Pd}(\text{PPh}_3)_4$ (8 mg, 5 mol %) were vacuum evacuated and refilled with argon three times. Added via syringe a degassed mixture of 10% K_2CO_3 solution (2.0 mL, 1.4 mmol), aliquat 336 (1 drops, ca. 36 mg), toluene (8 mL) and ethanol (1 mL). The mixture was vigorously stirred at 85 °C (oil bath) with protection from light for 72 h under argon atmosphere. Bromobenzene (12 mg, 0.07 mmol) was added, stirring was continued at 85 °C (oil bath) for 16 h before benzenboronic acid (9 mg, 0.07 mmol) was added, and stirring continued at 115 °C (oil bath) for 16 h. After cooling, the gray mixture was concentrated to a small volume (ca. 2 mL) on rotavapor and then added slowly to stirring methanol (100 mL) for 30 minutes to precipitate the crude polymer as gray powder. The precipitate was filtered off, washed sequentially with methanol (10 mL), water (10 mL) and acetone (10 mL), and dried to afford the crude polymer as a gray powder (109 mg). The crude polymer was re-dissolved in toluene (20 mL), aqueous solution of *N,N*-diethyldithiocarbamic acid trihydrate (1g in 10 mL water) was added, and the mixture was stirred at 65 °C for 16 h. The layers were separated, and the aqueous phase was extracted with toluene. The combined organic layers were washed with diluted HCl solution (10%, 10 mL), sodium acetate solution (10%, 10 mL), and water (2 × 10 mL). The organic phase was filtered through a Celite 521 plug eluting first with toluene (20 mL) and then with chloroform (100 mL) to yield a clear yellow solution. The combined solutions were concentrated until it became brownish semi-solid, re-dissolved in chloroform (5 mL) and poured drop wise into stirred methanol (100 mL) to precipitate the polymer as yellowish gray solid. The precipitate was collected by filtration, washed with methanol and dried *in vacuo* to afford product **5.20-Pd** (24 mg, 42%) as a yellowish gray solid. Note: Further purification was not performed as the yield was low, and the reaction gave rather low molecular weight polymer.

¹H NMR (400 MHz, CDCl₃): δ (ppm) 9.07–9.02 (2H, br. s), 8.05–7.99 (2H, br. s), 2.21–2.11 (4H, m), 1.41–1.00 (20H, m), 0.95–0.84 (4H, m), 0.82 (6H, br. t, *J* = 6.4 Hz).

GPC (CHCl₃): *M*_w = 6,100, *M*_n = 2,300, PDI = 2.69.

B) Ni-Mediated Yamamoto coupling polymerisation method:

Exp: SG-184: Low molecular weight polymer, 5.20-Ni-L



Under argon, a three-neck flask (50 mL) fitted with argon inlet was charged with bis(1,5-cyclooctadiene)nickel(0) [$\text{Ni}(\text{COD})_2$] (380 mg, 1.39 mmol), 2,2'-bipyridyl (bpy) (216 mg, 1.39 mmol), 1,5-cyclooctadiene (COD) (150 mg, 1.39 mmol) and anhydrous DMF (8 mL) stirred at 80 °C (oil bath) for 30 min to produce a dark violet solution. To this, a solution of 2,7-dibromo-9,9-dioctyl-4,5-diazafluorene (**3.24**) (506 mg, 0.923 mmol) in anhydrous toluene (20 mL, degassed with nitrogen) was added via septum through syringe and stirred at 80 °C for 96 h. Bromobenzene (426 mg, 2.769 mmol) was added as end capper and stirred at 80 °C for 16 h. After cooling, the solution was poured into a stirred solution of methanol:acetone: 10% HCl = 1:1:1 (v/v) (150 mL) and stirred for 20 minutes. The yellowish aqueous-organic layer was extracted with toluene (3 × 20 mL) and then the combined toluene layers were stirred with ammonium hydroxide solution (35%, 20 mL) for 20 minutes. The organic layer was separated, washed with water (2 × 30 mL) and evaporated at reduced pressure. The residue was dissolved in chloroform (5 mL) and poured drop wise into methanol (50 mL) under vigorous stirring, resulting in yellow precipitates. Precipitates were collected by filtration, washed with acetone (50 mL), and dried *in vacuo* to afford the crude product (335 mg) as a light yellow solid. The crude product was purified by Soxhlet extraction with acetone (50 mL) for 16 hours to remove oligomers followed by extraction with chloroform (50 mL) for 1 hours. The chloroform was concentrated into a small volume (~3–5 mL) and re-precipitated into methanol (100 mL), collected by filtration and dried *in vacuo* to afford the polymer **5.20-Ni-L** (202 mg, 56%) as a yellow floppy solid.

¹H NMR (400 MHz, CDCl₃): δ (ppm) 9.18–9.01 (2H, br.s), 8.25–7.95 (2H, br.s), 2.21–2.11 (4H, m, CH₂C₇H₁₅), 1.28–1.05 (20H, m, CH₂CH₂(CH₂)₅CH₃), 0.95–0.84 (4H, m, CH₂CH₂C₆H₁₃), 0.82 (6H, br. t, *J* = 6.84 Hz, CH₃).

¹³C NMR (100 MHz, CDCl₃): δ (ppm) 158.02, 148.95, 146.04, 133.50, 128.94, 53.42, 51.89, 39.22, 31.70, (29.87, 29.19), 29.11, 24.29, 22.57, 14.04.

GPC (CHCl₃): *M_w* = 23,200, *M_n* = 3,600, PDI = 6.53.

TGA (5% weight loss, heating @ 5 °C/min): *T_d* = 403 °C.

Exp: SG-191: High molecular weight polymer, 5.20-Ni-H

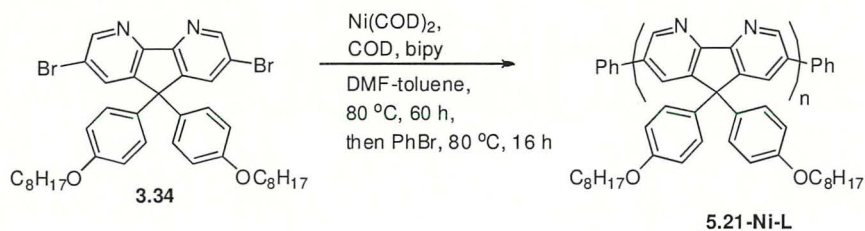
Under argon, a two-neck schlenk flask (25 mL) with argon inlet was charged with Ni(COD)₂ (226 mg, 0.821 mmol), bpy (128 mg, 0.821 mmol), COD (89 mg, 0.821 mmol) and anhydrous DMF (degassed with argon) (1.5 mL) stirred at 80 °C (oil bath) for 30 min to produce a dark violet solution. (Note: glove box using nitrogen inlet was used for weighing all the compounds). To this, a solution of 2,7-dibromo-9,9-dioctyl-4,5-diazafluorene (**3.24**) (251 mg, 0.456 mmol) in anhydrous toluene (4.7 mL) (freshly distilled from Na metal + benzophenone) was added via the septum through a syringe and stirred at 80 °C for 96 h. Bromobenzene (140 mg, 0.912 mmol) was added as end capper and stirred at 80 °C for 16 h. After cooling, the greenish mixture was poured into a stirred solution of methanol:acetone: 10% HCl = 1:1:1 (v/v) (100 mL) and stirred for 20 minutes. The yellowish aqueous-organic layer was extracted with toluene (3 × 20 mL) and then the combined toluene layers were stirred with ammonium hydroxide solution (35%, 20 mL) for 15 minutes. The organic layer separated, washed with water (2 × 30 mL) and evaporated at reduced pressure. The residue was dissolved in chloroform (2 mL) and poured drop wise into methanol (100 mL) under vigorous stirring, resulting in yellow precipitate. Precipitates was collected by filtration, washed with acetone (50 mL), and dried *in vacuo* to afford the crude product (141 mg, 79 %) as a light yellow solid. The crude product was purified by Soxhlet extraction with acetone (100 mL) for 16 hours to remove oligomers followed by extraction with chloroform (25 mL) for 1 hours which was concentrated into small volume (3-5 mL) and re-precipitated into methanol (100 mL), collected by filtration and dried *in vacuo* to afford the polymer **5.20-Ni-H** (54 mg, 31%) as a yellow floppy solid.

¹H NMR (400 MHz, CDCl₃): δ (ppm) 9.18–9.01 (2H, br.s), 8.25–7.95 (2H, br.s), 2.21–2.11 (4H, m, CH₂C₇H₁₅), 1.28–1.05 (20H, m, CH₂CH₂(CH₂)₅CH₃), 0.95–0.85 (4H, m, CH₂CH₂C₆H₁₃), 0.82 (6H, br. t, *J* = 6.84 Hz, CH₃).

GPC (CHCl₃): $M_w = 109,900$, $M_n = 28,200$, PDI = 3.90.

Poly(9,9-dioctyloxyphenyl-4,5-diazafluorene) [p(PhOD)]

Exp: SG-081: Low molecular weight polymer, 5.21-Ni-L



Under argon, a two-neck schlenk flask (25 mL) with argon inlet charged with Ni(COD)₂ (113 mg, 0.409 mmol), bpy (63mg, 0.409 mmol), COD (44 mg, 0.409 mmol) and anhydrous DMF (1 mL) were stirred at 80 °C (oil bath) for 30 min to produce a dark violet solution. To this, a solution of 2,7-dibromo 9,9-bis(4-octyloxyphenyl)-4,5-diazafluorene (**3.34**) (200 mg, 0.273 mmol) in anhydrous toluene (5 mL) was added via septum through syringe and stirred at 80 °C for 60 h. Then bromobenzene (126 mg, 0.819 mmol) was added as end capper and stirred at 80 °C for 10 h. After cooling, the solution was poured into a stirred solution of methanol:acetone:10% HCl = 1:1:1 (v/v) (120 mL) and stirred for 20 minutes. The aqueous-organic layer was extracted with toluene (3 × 50 mL) and the combined toluene layers was washed with water (2 × 50 mL) and evaporated at reduced pressure. The residue was dissolved in chloroform (5 mL) and poured drop wise into methanol (50 mL) under vigorous stirring. Precipitate was collected by filtration followed by washing with acetone (50 mL) and then dried *in vacuo* to afford product **5.21-Ni-L** (70 mg, 45%) as yellow powder.

¹H NMR (400 MHz, CDCl₃): δ (ppm) 9.09–8.75 (2H, br. m), 8.04–7.72 (2H, br. m), 7.15–7.06 (4H, m, C₆H₄), 6.88–6.66 (4H, m, C₆H₄), 4.31–3.37 (4H, m, OCH₂), 1.87–1.65 (4H, m, CH₂CH₂C₆H₁₃), 1.51–1.37 (4H, m, CH₂CH₂CH₂C₅H₁₁), 1.36–1.11 (16H, m, CH₂CH₂CH₂(CH₂)₄CH₃), 0.86 (6H, br. t, *J* = 8.3 Hz, CH₃).

GPC (CHCl₃): $M_w = 4,050$, $M_n = 1,530$, PDI = 2.64.

TGA (5% weight loss, heating @ 5 °C/min): T_d = 350 °C.

Exp: SG-192: High molecular weight polymer, 5.21-Ni-H

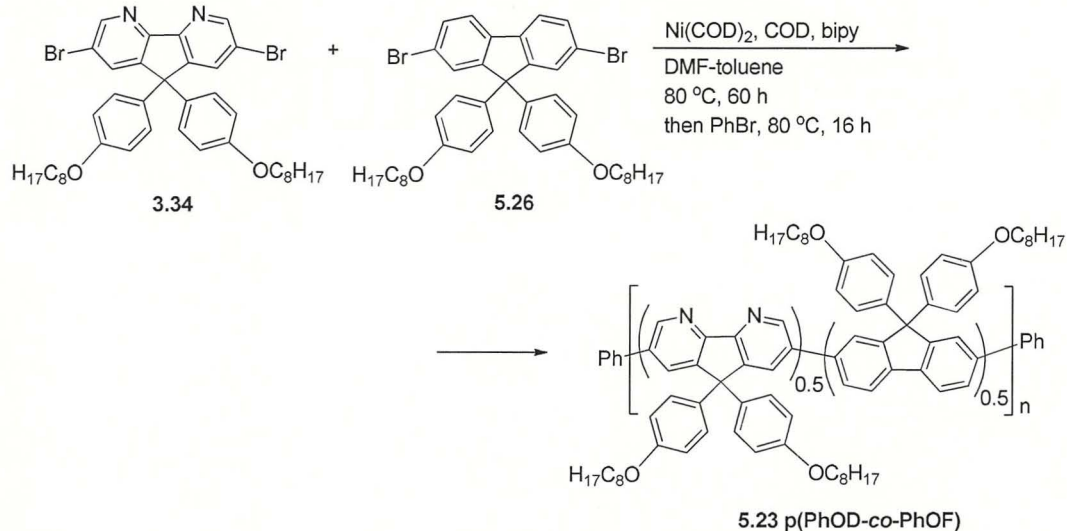
Under argon, bis(1,5-cyclooctadiene)nickel(0) (182 mg, 0.664 mmol), 2,2'-bipyridyl (103 mg, 0.664), 1,5-cyclooctadiene (71 mg, 0.664 mmol) and anhydrous DMF (1.2 mL) were added to Schlenk tube (10 cm long) fitted with argon inlet(note: the compounds were weight inside plastic glove box under nitrogen). The blue-violet mixture was stirred at 80 °C (oil bath) for 30 min to produce a dark violet solution. To this, 2,7-dibromo 9,9-bis(4-octyloxyphenyl)-4,5-diazafluorene (**3.34**) (271 mg, 0.369 mmol) dissolved in anhydrous toluene (3.8 mL, degassed, freshly distilled over Na) was added via septum through syringe and stirred at 80 °C for 96 h under argon atmosphere. Bromobenzene (113 mg, 0.738 mmol) was added as end capper and stirred at 80 °C for 24 h. After cooling, the solution was poured into a stirred solution of methanol:acetone: 10%. HCl = 1:1:1 (v/v) (120 mL) and stirred for 20 minutes. The aqueous- organic layer was extracted with toluene (3 × 50 mL) and the combine toluene layer was washed with ammonium hydroxide solution (35%, 25 mL) followed by water (2 × 50 mL) and evaporated at reducing pressure. The residue was re-dissolved in chloroform (3 mL) and poured drop wise into methanol (100 mL) under vigorous stirring. Precipitate was collected by filtration, washed with acetone (50 mL), and dried *in vacuo* to afford the crude product (243 mg) as yellow powder. The crude product was purified by Soxhlet extraction with acetone (100 mL) for 16 hours to remove oligomers followed by extraction with chloroform (25 mL) for 3 hours, which was concentrated into small volume (3-5 mL) and re-precipitated into methanol (100 mL). Precipitate was collected by filtration followed by washing with acetone (50 mL) and then dried *in vacuo* to afford product **5.21-Ni-H** (156 mg, 74 %) as a yellow solid.

¹H NMR (400 MHz, CDCl₃): δ (ppm) 9.09–8.75 (2H, br. s), 8.04–7.72 (2H, br. s), 7.15-7.06 (4H, m, *J* = 8.4 Hz, C₆H₄), 6.88–6.66 (4H, br d, *J* = 8.4 Hz, C₆H₄), 4.31–3.37 (4H, br. s, OCH₂), 1.87–1.65 (4H, br.s, CH₂CH₂C₆H₁₃), 1.51–1.37 (4H, br.s, CH₂CH₂CH₂C₅H₁₁), 1.36–1.11 (16H, m, CH₂CH₂CH₂(CH₂)₄CH₃), 0.86 (6H, br. t, *J* = 8.3 Hz, CH₃).

GPC (CHCl₃): *M*_w = 206,800, *M*_n = 71,600, PDI = 2.89.

Poly(9,9-dioctyloxyphenyl-4,5-diazafluorene-co-9,9-dioctyloxyphenylfluorene) (5.23)

Exp: SG-084



Under argon, $\text{Ni}(\text{COD})_2$ (240 mg, 0.871 mmol), COD (95 mg, 0.87 mmol), bpy (136 mg, 0.874 mmol) and anhydrous DMF (3 mL) were stirred at 80 °C (oil bath) for 30 min to produce a dark violet solution. To this, a solution of 9,9-bis(4-octyloxyphenyl)-2,7-dibromo-4,5-diazafluorene (**3.34**) (200 mg, 0.273 mmol) and 2,7-dibromo-9,9-(4-octyloxyphenyl)fluorene (**5.25**) (200 mg, 0.273 mmol) in anhydrous toluene (15 mL) was added via the septum through a syringe and stirred at 80 °C for 60 h. Bromobenzene (168 mg, 1.09 mmol) was added as end capper and stirred at 80 °C for 10 h. After cooling, the solution was poured into a stirred solution of methanol:acetone:conc. HCl = 1:1:1 (v/v) and stirred for 20 minutes. The aqueous organic layer was extracted with toluene (3×50 mL) and the combine toluene layer was washed with water (2×50 mL) and evaporated at reducing pressure. The residue was dissolved in chloroform (5 mL) and poured drop wise into methanol (300 mL) under vigorous stirring resulted in yellowish precipitate. The precipitate was collected by filtration, washed with acetone (50 mL), and dried *in vacuo* to afford the crude product (222 mg) as yellow solid. The crude product was dissolved in toluene (50 mL) and stirred with ammonium hydroxide solution (35%, 20 mL) for 20 minutes. The organic layer was separated and washed with water (3×30 mL) and evaporated at reduced pressure to obtain yellowish residue. The yellowish residue was dissolved in chloroform (10 mL) and poured drop wise into methanol (150 mL) and stirred for 30 minutes to afford yellow precipitate which was collected by filtration and dried *in vacuo* to afford product polymer **5.23** (155 mg, 55%) as a yellow powder.

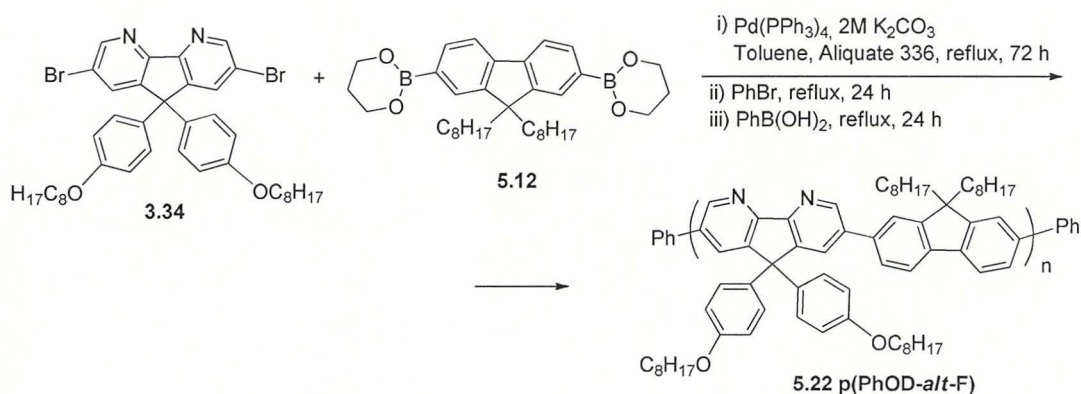
$^1\text{H NMR}$ (500 MHz, CDCl_3): δ (ppm) 8.99–8.89 (2H, br. s), 7.93–7.73 (4H, m), 7.61–7.49 (4H, br. m), 7.21–7.08 (8H, m), 6.85–6.71 (8H, m), 4.08–3.82 (8H, m), 1.79–1.69 (8H, m), 1.47–0.99 (40H, m), 0.92–0.79 (12H, br. t).

GPC (THF): $M_w = 39,800$, $M_n = 15,100$, $\text{PDI} = 2.64$.

TGA (5% weight loss, heating @ $5\text{ }^\circ\text{C}/\text{min}$): $T_d = 379\text{ }^\circ\text{C}$.

Poly (9,9-dioctyloxyphenyl-4,5-diazafluorene-co-9,9-dioctylfluorene) (5.22)

Exp: SG-078)



A flask was charged with 2,7-dibromo-9,9-bis(4-octyloxyphenyl)-4,5-diazafluorene (**3.34**) (100 mg, 0.136 mmol), 9,9-dioctylfluorene-2,7-diboronic acid bis(1,3-propanediol) ester (**5.12**) (76 mg, 0.136 mmol, purity 99.5%), $2\text{M K}_2\text{CO}_3$ solution (2 mL, 4 mmol), aliquat 336 (1 drops, ca. 18 mg) and toluene (15 mL). The mixture was degassed for 15 min before $\text{Pd}(\text{PPh}_3)_4$ (3 mg, 2 mol %) was added, and degassing was continued for 15 min, the mixture was vigorously stirred at $115\text{ }^\circ\text{C}$ (oil bath) with protection from light for 72 h. Bromobenzene (63 mg, 0.409 mmol) was added, stirring was continued at $115\text{ }^\circ\text{C}$ (oil bath) for 24 h before benzenboronic acid (53 mg, 0.437 mmol) was added, and stirring was continued at $115\text{ }^\circ\text{C}$ (oil bath) for 24 h. After cooling, the blue mixture was added slowly to a stirring methanol (150 mL) over a period of 10 minutes and then stirred at room temperature for 30 minutes to induce precipitate of the crude polymer as gray fibers. The fibers were filtered and washed sequentially with methanol (10 mL), water (10 mL), and acetone (10 mL). The polymer was re-dissolved in toluene (50 mL), an aqueous solution of *N,N*-diethyldithiocarbamic acid trihydrate (1.0 g in 10 mL water) was added, and the mixture was stirred at $65\text{ }^\circ\text{C}$ for 16 h. The organic layer was separated, and the aqueous layer was extracted with toluene. The combined organic layers were washed with 10% diluted HCl solution, 10% aqueous sodium acetate solution, water ($2 \times 20\text{ mL}$) and filtered through a Celite 521 plug which was washed

with toluene (20 mL). Obtained clear yellow solution was concentrated until it became viscous (~ 4 mL) and was poured drop wise into vigorously stirred methanol (200 mL) to precipitate the polymer as yellow fibers. These fibers were isolated by filtration, washed with methanol and dried *in vacuo* to afford the crude polymer (146 mg) as a yellow floppy solid. The polymer was further purified by Soxhlet extraction with acetone (50 mL) for 16 hours to remove short oligomers followed by extraction with chloroform (50 mL) for 3 hours, which was concentrated, re-precipitated into methanol (100 mL) and dried *in vacuo* to afford polymer **5.22** (100 mg, 65.5%) as a yellow floppy solid.

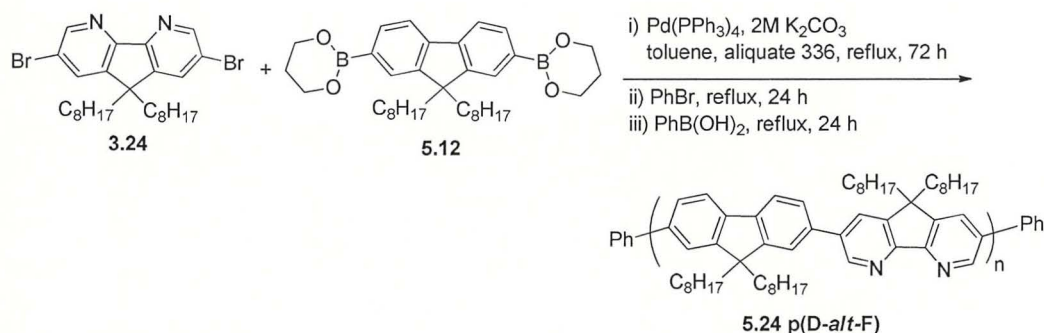
¹H NMR (500 MHz, CDCl₃): δ (ppm) 9.22–9.00 (2H, br.s), 8.08–7.96 (2H, br.s), 7.88–7.76 (2H, br.s), 7.65–7.52 (6H, br.s), 7.24 (4H, d, *J* = 8.4 Hz), 6.85(4H, d, *J* = 8.6 Hz), 4.00–3.74 (4H, br), 3.24–2.79 (4H, m), 2.24–1.92 (4H, m), 1.83–1.68(4H, m), 1.48–1.37 (4H, m), 1.30–0.95 (32H, m), 0.87 (6H, t, *J* = 7.15 Hz), 0.78 (6H, t, *J* = 7.15 Hz) 0.74–0.64 (4H, m).

GPC in THF: *M*_w = 28,900, *M*_n = 11,700, PDI = 1.92.

TGA (5% weight loss, heating @ 5 °C/min): T_d = 394 °C.

Poly(9,9-dioctyl-4,5-diazafluorene-co-9,9-dioctylfluorene) (5.24)

Exp: SG-073



A flask was charged with 2,7-dibromo-9,9-dioctyl-4,5-diazafluorene (**3.24**) (200 mg, 0.366 mmol), 9,9-dioctylfluorene-2,7-bis(trimethyleneborate) (**5.12**) (204 mg, 0.366 mmol, Aldrich, purity 99.5%), 2 M K₂CO₃ solution (2.0 mL, 4 mmol), aliquat 336 (2 drops, ca. 36 mg) and toluene (15 mL). The mixture was degassed for 15 min before Pd(PPh₃)₄ (8 mg, 2 mol %) was added, and degassing continued for 15 min, the mixture was vigorously stirred at 115 °C (oil bath) with protection from light for 72 h. Bromobenzene (25 mg, 0.160 mmol) was added, stirring was continued at 115 °C (oil bath) for 24 h. Subsequently benzenboronic acid (25 mg, 0.205 mmol) was added while stirring continued at 115 °C (oil bath) for another 24 h.

Heating stopped and after cooling the gray mixture was added slowly to a stirring methanol (150 mL) for 30 minutes to precipitate the crude polymer as gray fibers. The gray fibers were filtered off and washed sequentially with methanol (10 mL), water (10 mL), and acetone (10 mL) and dried *in vacuo*. The dried polymer was re-dissolved in toluene (20 mL) and then mixed with aqueous solution of *N,N*-diethyldithiocarbamic acid trihydrate (1g in 10 mL water). The mixture was stirred at 65 °C for 16 h. The organic layer was separated, and the aqueous layer was extracted with toluene (20 mL). The combined organic phases were washed with a diluted HCl solution (10%, 10 mL), sodium acetate solution (10%, 10 mL), and water (2 × 10 mL). The organic layer was filtered through a Celite 521 plug eluting first with toluene (20 mL) and then with chloroform (100 mL) to yield a clear yellow solution. The combine solution was concentrated until it became brownish semi-solid, re-dissolved in chloroform (5 mL) and poured dropwise to a stirred methanol (250 mL) to precipitate the polymer as yellow fibers. The precipitate was collected by filtration, washed with methanol and dried *in vacuo* to afford the crude polymer (220 mg) as yellow fluffy solid. The crude polymer was further purified by Soxhlet extraction with acetone (50 mL) for 16 hours, to remove low-molecular weight oligomers. Then it was extracted with chloroform (50 mL) for 1 hour, the extract was concentrated to a small volume (~4 mL, viscous liquid) and poured dropwise into vigorously stirred methanol (150 mL). The precipitate was collected by filtration, washed with methanol and dried *in vacuo* to afford product **5.24** (145 mg, 51%) as a yellow floppy solid.

¹H NMR (500 MHz, CDCl₃): δ (ppm) 9.14–9.06 (2H, br.s), 8.06–8.02 (2H, br.s), 7.98–7.95 (2H, m), 7.76–7.65 (4H, m), 2.61–2.07 (8H, m), 1.32–1.03 (40H, m), 0.94–0.69 (20H, m).

GPC (THF): *M*_w = 21,900, *M*_n = 4,200, PDI = 5.17.

TGA (5% weight loss, heating @ 5 °C/min): T_d = 394 °C.

References

- 1 (a) U. Scherf and E. J. W. List, *Adv. Mater.*, **2002**, *14*, 477; (b) U. Scherf and D. Neher (Eds.), *Polyfluorenes, Advances in Polymer Science – Vol. 212*, Springer-Verlag, Berlin, **2008**.
- 2 W. Y. Lai, R. Xia, D. D. C. Bradley, and W. Huang, *Chem. Eur. J.*, **2010**, *16*, 8471.
- 3 L. Chan, M. J. McKiernan, C. R. Towns, and A. B. Holmes, *J. Am. Chem. Soc.*, **2005**, *127*, 7662.
- 4 J. Li and A. C. Grimsdale, *Chem. Soc. Rev.*, **2010**, *39*, 2399.
- 5 F. B. Dias, S. King, A. P. Monkman, I. I. Perepichka, M. A. Kryuchkov, I. F. Perepichka, and M. R. Bryce, *J. Phys. Chem. B*, **2008**, *112*, 6557.
- 6 S. M. King, I. I. Perepichka, I. F. Perepichka, F. B. Dias, M. R. Bryce, and A. P. Monkman, *Adv. Funct. Mater.*, **2009**, *19*, 586.
- 7 J. Rault-Berthelot and J. Simonet, *J. Electrochem. Soc.*, **1985**, *182*, 187.

-
- 8 M. Fukuda, K. Sawada, and K. Yoshino, *J. Polym. Sci. A: Polym. Chem.*, **1993**, *31*, 2465.
- 9 Q. Pie and Y. Yang, *J. Am. Chem. Soc.*, **1996**, *118*, 7416.
- 10 M. Inbasekaran, W. Wu, and E. P. Woo, *US Patent US005777070A*, **1998**.
- 11 (a) M. T. Bernius, M. Inbasekaran, J. O'Brien, and W. Wu, *Adv. Mater.*, **2000**, *12*, 1737; (b) M. Leclerc, *J. Polym. Sci. A: Polym. Chem.*, **2001**, *39*, 2867; (c) U. Scherf, E. J. W. List, *Adv. Mater.*, **2002**, *14*, 477; (d) D. F. Perepichka, I. F. Perepichka, H. Meng, and F. Wudl, in: *Organic Light-Emitting Materials and Devices*, Z. R. Li and H. Meng (Eds.), CRC Press, Boca Raton, FL, 2006, Chapter 2, pp. 45–293; (e) L.-H. Xie, C.-R. Yin, W.-Y. Lai, Q.-L. Fan, and W. Huang, *Prog. Polym. Sci.*, **2012**, *37*, 1192.
- 12 X. Gong, P. K. Iyer, D. Moses, G. C. Bazan, A. J. Heeger, and S. S. Xiao, *Adv. Func. Mater.*, **2003**, *13*, 325.
- 13 A. C. Grimsdale and K. Müllen, *Adv. Polym. Sci.*, **2006**, *199*, 1.
- 14 M. Leclerc, *J. Polym. Sci. A: Polym. Chem.*, **2001**, *39*, 2867.
- 15 W. Y. Wang, *Coord. Chem. Rev.*, **2005**, *249*, 971.
- 16 G. Klärner, M. H. Davey, W.-D. Chen, J. C. Scott, and R. D. Miller, *Adv. Mater.* **1998**, *10*, 993.
- 17 M. Kreyenschmidt, G. Klärner, T. Fuhrer, J. Ashenurst, S. Karyenschmidt, G. Klärner, T. Fuhrer, J. Ashenurst, S. Karg, W.-D. Chen, V. Y. Lee, J. C. Scott, and R. D. Miller, *Macromolecules*, **1998**, *31*, 1099.
- 18 U. Asawapirom and U. Scherf, *Macromol. Rapid Commun.*, **2001**, *22*, 746.
- 19 M. Redecker, D. D. C Bradley, M. Inbasekaran, W. Wu, and E. Woo, *Adv. Mater.*, **1999**, *11*, 241.
- 20 M. Redecker, D. D. C Bradley, K. Baldwin, D. Smith, M. Inbasekaran, W. Wu, and E. Woo, *J. Mater. Chem.*, **1999**, *9*, 2151.
- 21 (a) E. J. W. List, R. Güntner, P. Scanducci de Freitas, and U. Scherf, *Adv. Mater.*, **2002**, *14*, 374; (b) J. M. Lupton, M. R. Craig, E. W. Meijer, *Appl. Phys. Lett.*, **2002**, *80*, 4489; (c) M. Gaal, E. J. W. List, and U. Scherf, *Macromolecules*, **2003**, *36*, 4236.
- 22 (a) K. Becker, J. M. Lupton, J. Feldmann, B. S Nehls, F. Galbrecht, D. Q. Gao, and U. Scherf, *Adv. Funct. Mater.*, **2006**, *16*, 364; (b) R. Grisorio, G. Allegretta, P. Mastorilli, and G. P. Suranna, *Macromolecules*, **2011**, *44*, 7977.
- 23 C. Li and Z. Bo, *Polymer*, **2010**, *51*, 4273.
- 24 L. Romaner, A. Pogantsch, P. Scanducci de Freitas, U. Scherf, M. Gaal, E. Zojer, and E. J. W. List, *Adv. Funct. Mater.*, **2003**, *13*, 597.
- 25 W. Zhao, T. Cao, and J. M. White, *Adv. Funct. Mater.*, **2004**, *14*, 783.
- 26 Y. H. Kim and D. A. V. Bout, *Appl. Phys. A*, **2009**, *95*, 241.
- 27 X. Chen, H. Wan, H. Li, F. Cheng, J. Ding, B. Yao, Z. Xie, L. Wang, and J. Zhang, *Polymer*, **2012**, *53*, 3827.
- 28 W. Z. Liang, Y. Zhao, J. Sun, J. Song, S. Hu, and J. Yang, *J. Phys. Chem. B*, **2006**, *110*, 9908.
- 29 I. Franco and S. Tretiak, *Chem. Phys. Lett.*, **2003**, *372*, 403.
- 30 M.R. Craig, M. M. de Kok, J. W. Hofstraat, A. P. H. J. Schenning, and E. W. Meijer, *J. Mater. Chem.*, **2003**, *13*, 2861.
- 31 R. Grisorio, G. Allegretta, P. Mastorilli, and G. Paola Suranna, *Macromolecules*, **2011**, *44*, 7977.
- 32 M. R. Craig, M. M. de Kok, J. W. Hofstraat, A. P. H. J. Schenning, and E. W. Meijer, *J. Mater. Chem.*, **2003**, *13*, 2861.

-
- 33 J.-Hoon and D.-Hoon Hwang, *Chem. Comm.*, **2003**, 2836
- 34 J. Liu, J.H Zou, W. Yang, H. B. Wu, C. Li, B. Zhang, J. B. Peng, and Y. Cao, *Chem. Mater.*, **2008**, *20*, 4499
- 35 C. W. Huang, K.Y. Peng, C.Y. Liu, T. H. Jen, N. J. Yang, and S.A. Chen, *Adv. Mater.*, **2008**, *20*, 3709.
- 36 K. L. Chan, M. J. McKiernan, C. R. Towns, and A. B. Holmes, *J. Am. Chem. Soc.*, **2005**, *127*, 7662.
- 37 D. Yan, J. Mohsseni-Ala, N. Auner, M. Bolte, and J. W. Bats, *Chem.- Eur. J.*, **2007**, *13*, 7204.
- 38 Y. Yabusaki, N. Ohshima, H. Kondo, T. Kusamoto, Y. Yamanoi, and H. Nishihara, *Chem.- Eur. J.*, **2010**, *16*, 5581.
- 39 J. Wang, C. -qing Zhang, C.-mei Zhang, S.-jun Hu, X.-yi Chang, Y. Qi Mo, X. Chen, and H.-bin Wu, *Macromolecules*, **2011**, *44*, 17
- 40 A. Farcas, S. Janietz, V. Harabagiu, P. Guegan, and P. H Aubert, *J. Polym. Sci. A: Polym. Chem.*, **2013**, *51*, 1672.
- 41 W. D. Huang, Y. S. Wu, Y. C. Hsu, H. C. Lin, J. T. Lin, *Polymer*, **2009**, *47*, 3651
- 42 V. N. Bliznyuk, S. A. Carter, J. C. Scott, G. Klarnar, R. D Miller, and D. C. Miller, *Macromolecules*, **1999**, *32*, 361.
- 43 C. Xia and R. C. Advincula, *Macromolecules*, **2001**, *34*, 5854.
- 44 Y. Zhu, M. Gibbons, A. P. Kulkarni, and S. A. Jenekhe, *Macromolecules*, **2007**, *40*, 804.
- 45 S. Setayesh, A. C. Grimsdale, T. Weil, V. Enkelmann, K. Müllen, F. Meghdadi, E. J. W. List, and G. J. Leising, *J. Am. Chem. Soc.*, **2001**, *123*, 946.
- 46 W. Yang, J. Huang, C. Liu, Y. Niu, Q. Hou, R. Yang, and Y. Cao, *Polymer*, **2004**, *45*, 865.
- 47 T. Miteva, A. Meisel, W. Knoll, H. G. Nothofer, U. Scherf, D. C. Muller, K. Meerholz, A. Yasuda, and D. Neher, *Adv. Mater.*, **2001**, *13*, 565.
- 48 P.-T. Wu, F. S. Kim, R. D. Champion, and S. A. Jenekhe, *Macromolecules*, **2008**, *41*, 7021.
- 49 J. Ma, S. H. Li, and Y.-S. Jiang, *Macromolecules*, **2002**, *35*, 1109.
- 50 M. A. De Oliveira, H. A. Duarte, J. M. Pernaut, and W. B. De Almeida, *J. Phys. Chem. A*, **2002**, *104*, 8256.
- 51 N. A. Sánchez-Bojorge, L. M. Rodríguez-Valdez, and N. F.-Holguin, *J. Mol. Model.*, **2013**, *19*, 3542.
- 52 R. M Gutiérrez-Pérez, N. R. Flores-Holguin, D. Glossman-Mitnik, and L. M. Rodríguez-Valdez, *J. Mol. Model.*, **2011**, *17*, 1963.
- 53 M. J. Frisch, G. W. Trucks, H. B. Schlegel, G. E. Scuseria, M. A. Robb, J. R. Cheeseman, G. Scalmani, V. Barone, B. Mennucci, G. A. Petersson, H. Nakatsuji, M. Caricato, X. Li, H. P. Hratchian, A. F. Izmaylov, J. Bloino, G. Zheng, J. L. Sonnenberg, M. Hada, M. Ehara, K. Toyota, R. Fukuda, J. Hasegawa, M. Ishida, T. Nakajima, Y. Honda, O. Kitao, H. Nakai, T. Vreven, J. A. Montgomery, Jr., J. E. Peralta, F. Ogliaro, M. Bearpark, J. J. Heyd, E. Brothers, K. N. Kudin, V. N. Staroverov, R. Kobayashi, J. Normand, K. Raghavachari, A. Rendell, J. C. Burant, S. S. Iyengar, J. Tomasi, M. Cossi, N. Rega, J. M. Millam, M. Klene, J. E. Knox, J. B. Cross, V. Bakken, C. Adamo, J. Jaramillo, R. Gomperts, R. E. Stratmann, O. Yazyev, A. J. Austin, R. Cammi, C. Pomelli, J. W. Ochterski, R. L. Martin, K. Morokuma, V. G. Zakrzewski, G. A. Voth, P. Salvador, J. J. Dannenberg, S. Dapprich, A. D. Daniels, O. Farkas, J. B. Foresman, J. V. Ortiz, J. Cioslowski, and D. J. Fox, Gaussian, Inc., Wallingford CT, **2009**, Gaussian 09, Revision A.02.
- 54 G. Klaener and R. D. Miller, *Macromolecules*, **1998**, *31*, 2007.
- 55 Y. Koizumi, S. Seki, A. Achyara, A. Saeki, and S. Tagada, *Chem. Lett.*, **2004**, *33*, 1290.

-
- 56 J. Jo, C. Chi, S. Hoger, G. Wegner, and D. Y. Yoon, *Chem. Eur. J.*, **2004**, 10, 2681.
- 57 J. Gierschner, J. Cornil, and H.-J. Egelhaaf, *Adv. Mater.*, **2007**, 19, 173.
- 58 G. Zeng, W.-L. Yu, S.-J. Chua, and W. Huang, *Macromolecules*, **2002**, 35, 6907.
- 59 K.-T. Wong, C.-F. Wang, C. H. Chou, Y. O. Su, G.-H. Leem and S.-M. Peng, *Org. Lett.*, **2002**, 4, 4439.
- 60 J. U. Izunobi and C. L. Higginbotham, *J. Chem. Educ.*, **2011**, 88, 1098.
- 61 W.-J. Li, B. Liu, Y. Qian, L.-H. Xie, J. Wang, S.-B. Li, and W. Huang, *Polym. Chem.*, **2013**, 4, 1796.
- 62 A. S. Alghunaim, MSc Thesis, **2011**, Bangor Univeristy.
- 63 Y. Zhu, K. M. Gibbons, A. P. Kulkarni and S. A. Jenekhe, *Macromolecules*, **2007**, 40, 804.
- 64 H. H. Lu, C. Y. Liu, C. H. Chang, and S. A. Chen, *Adv. Mater.*, **2007**, 19, 2574.
- 65 X. Zhang, Q. Hu, J. Lin, Z. Lei, X. Guo, L. Xie, W. Lai and W. Huang, *Appl. Phys. Lett.*, **2013**, 03, 153301.
- 66 P. Fitton and J. E. McKeon, *J. Chem. Soc. Chem. Commun.*, **1968**, 4.
- 67 (a) Y. Yang, Q. Pei, and A. J. Heeger, *J. Appl. Phys.*, **1996**, 79, 934; (b) J. Stampf, S. Tasch, G. Leising, and U. Scherf, *Synth. Met.*, **1995**, 71, 2125.
- 68 J. R. Lakowicz, *Principles of Fluorescence Spectroscopy*, Springer, 3rd Ed., **2006**, Chapter 2, p.53.
- 69 J. L Bredas, R. Silbey, D. S. Boudreaux, R. R. Chance, *J. Am. Chem. Soc.*, **1983**, 105, 6555.
- 70 C. M. Cardona, W. Li, A. E. Kaifer, D. Stockdale, and G. C. Bazan, *Adv. Mater.*, **2011**, 23, 2367.
- 71 B. Liu, W. L. Yu, Y. H. Lai, and W. Huang, *Chem. Mater.*, **2001**, 13, 1984.

Appendix-NMR and MS spectra

See attached CD as supplementary data

A.1 NMR and MS spectra of Chapter 2

A.2 NMR and MS spectra of Chapter 3

A.3 NMR and MS spectra of Chapter 4

A.4 NMR spectra of Chapter 5.